Single B cell antibody technology and high-throughput immune repertoire sequencing as complementary tools to better understand central nervous system (CNS) inflammation and treatment effects

Inaugural dissertation

for the attainment of the title of doctor
in the Faculty of Mathematics and Natural Sciences
at the Heinrich Heine University Düsseldorf

presented by

Sumanta Barman
from Shariatpur, Bangladesh

Düsseldorf, March 2021

Single B cell antibody technology and high-throughput immune repertoire sequencing as complementary tools to better understand central nervous system (CNS) inflammation and treatment effects

Inaugural dissertation

for the attainment of the title of doctor
in the Faculty of Mathematics and Natural Sciences
at the Heinrich Heine University Düsseldorf

presented by

Sumanta Barman
from Shariatpur, Bangladesh

Düsseldorf, March 2021

from the Department of Neurology, Medicine Faculty,
Heinrich Heine University Düsseldorf

Published by permission of the
Faculty of Mathematics and Natural Sciences at
Heinrich Heine University Düsseldorf

Supervisor: Professor Dr. Norbert Goebels
Co-supervisor: Professor Dr. Philipp Lang

Date of the oral examination: 28/09/2021

Dedication

This dissertation is dedicated to my parents-

Ashit Kumar Barman
and
Ila Barman

Contents

Summary ..... I-II

Graphical summary III

1. Introduction 1-14

1.1 Background

1.1.1 Immune receptors and repertoires

1.1.2 Generation of TCR and antibody diversity

1.1.3 Multiple sclerosis

1.1.4 Autoimmune encephalitis and associated autoantibodies

1.1.5 Anti-N-methyl-d-aspartate (NMDA) receptor encephalitis

1.1.6 Myelin oligodendrocyte glycoprotein (MOG) specific autoantibodies

1.2 Technical approaches and outcomes

1.2.1 Single B cell antibody technology and development of recombinant antibodies

1.2.1.1 Development of anti-NMDAR-specific recombinant monoclonal antibody

1.2.2 Murine organotypic cerebellar slice cultures (OSC) as an ex vivo model of the immune-CNS interface

1.2.3 High-throughput immune repertoire sequencing and understanding of treatment effects in multiple sclerosis

1.2.3.1 High-throughput sequencing of immune repertoire

1.2.3.2 Disease-modifying therapies in multiple sclerosis and assessment of immune repertoire

1.3 References

2. Manuscript I…..…… 15-107

"Reprogramming the immune system" with alemtuzumab in multiple sclerosis (MS) patients: Cell type specific longitudinal immune repertoire dynamics and emergence of secondary autoimmunity

3. Published scientific article I …….. 108-145

NMDAR encephalitis: passive transfer from man to mouse by a recombinant antibody

4. Published scientific article II …… 146-156

An assay to determine mechanisms of rapid autoantibody-induced neurotransmitter receptor endocytosis and vesicular trafficking in autoimmune encephalitis

5. Published scientific article III …….. 157-165

N-Methyl-D-Aspartate receptor antibodies in autoimmune encephalopathy alter oligodendrocyte function

6. Published scientific article IV ……... 166-185

Dose-dependent inhibition of demyelination and microglia activation by IVIG

7. Curriculum Vitae …….. 186-188

8. Financial support …….. 189

9. Acknowledgements ……... 190

10. Declaration …….. 191

Summary

Common denominator of this cumulative dissertation is the interaction between the immune system and the central nervous system (CNS), with a focus on chronic CNS inflammation. Although the CNS is partially protected from major influences of the periphery by a semi selective blood brain barrier (BBB), activated T and B lymphocytes are able to enter the CNS compartment in health and disease. In chronic CNS inflammation, triggered by infectious agents (e.g. herpes simplex virus (HSV) - encephalitis, Neuroborreliosis) or autoimmune/paraneoplastic immunity (e.g. multiple sclerosis (MS), autoimmune encephalitis (AIE) syndromes) often "oligoclonal immunoglobulins" (also known as "oligoclonal bands", OCB), produced by CNS resident plasma cells, are detectable by diagnostic isoelectric focusing electrophoresis. While their target specificity has not been conclusively identified in multiple sclerosis, characteristic CSF +/- serum antibody signatures of presumably pathogenic relevance have been described in autoimmune encephalitis. This thesis addressed aspects ranging from pathogenesis to treatment of these diseases.

Single B cell antibody technology is a dynamic strategy to develop recombinant monoclonal antibody based on the direct amplification of immunoglobulin heavy chain (IgH) and matching light-chain (IgL) variable region encoding genes from single human B cells. In order to recover the typical intrathecal antibody signature in recombinant form, a human monoclonal antibody SSM5 was cloned and expressed from clonally expanded intrathecal plasma cells from a patient with anti N-Methyl-D-aspartic acid (NMDA) receptor encephalitis. We reproduced NMDAR epitope specificity and key pathogenic features of the human disease *in vitro* and *in vivo*. Moreover, we showed that, internalization of the recombinant NMDAR-autoantibody complex into endosomes and lysosomes increases the pH-rhodamine fluorescence. Furthermore, we revealed that reduction of NMDAR-mediated responses in oligodendrocytes is mediated by patient derived recombinant human monoclonal SSM5 antibody.

High-throughput immune repertoire sequencing is a powerful approach for characterizing adaptive immune responses. We did immune repertoire analysis to characterize longitudinal evolutions in the clonal compositions of patients' peripheral lymphocyte repertoires before and during alemtuzumab (LEMTRADA®) treatment, and to better understand the beneficial properties and potential side effects of this drug. Immune repertoire sequencing data showed that alemtuzumab has distinctive effects on T cell and B cell repertoires. Moreover, post-alemtuzumab T and B cell repertoires are more diverse than pre-treatment repertoires

predominantly in non-secondary autoimmunity patients, in contrast, secondary autoimmunity patients had reduced T cell repertoire diversity, particularly in post-secondary autoimmunity repertoires. Importantly, secondary autoimmunity patients showed significantly increased persistence and expansion of T cell clones already after the first alemtuzumab infusion and a delayed expansion of memory B cell clones after the second infusion, which provides a novel mechanistic explanation for development of secondary autoimmunity combining current B or T cell-related hypotheses.

Additionally, we applied a recombinant humanized monoclonal antibody specific for myelin oligodendrocyte glycoprotein (MOG) to induce, together with complement, demyelination in murine organotypic cerebellar slice cultures (OSC) as an *ex vivo* model of the immune-CNS interface. Using transgenic mice expressing GFP in myelin allowed us to investigate the effects of potentially protective (in this case the commonly used immunomodulatory intravenous immunoglobulins (IVIG)) and/or remyelination promoting in OSC by live imaging.

Graphical summary

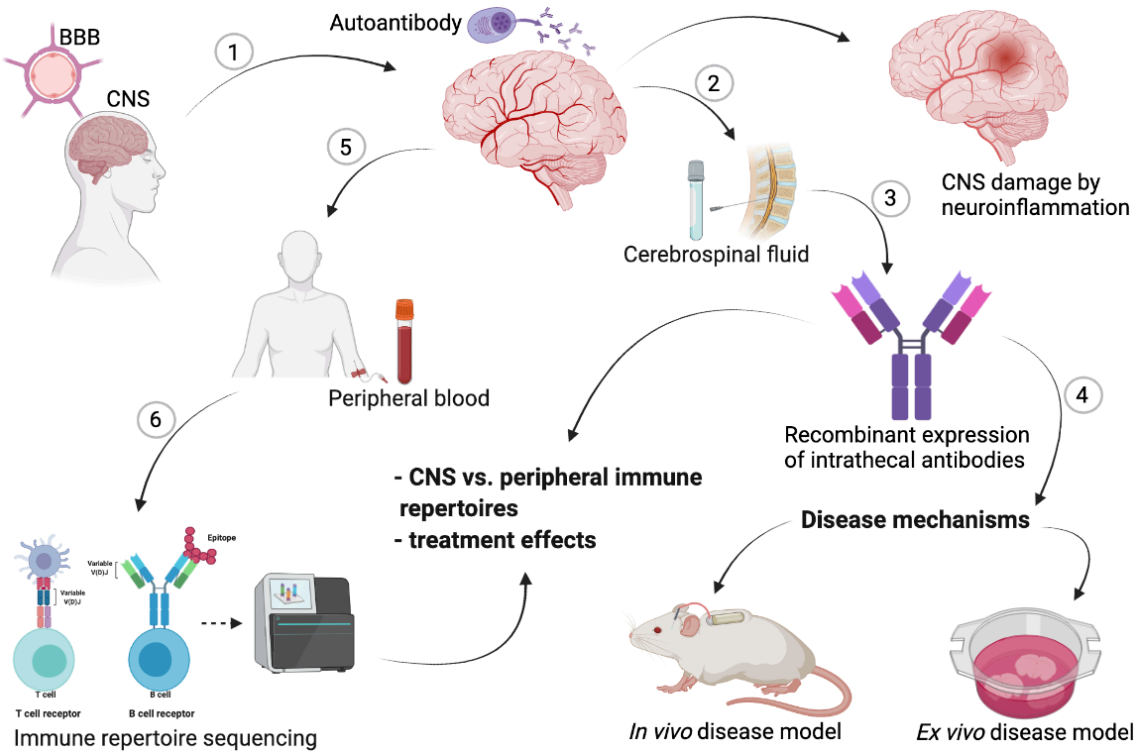

The blood-brain barrier (BBB) has an important function in protecting the central nervous system (CNS) from potentially harmful peripheral influences. However, activated, e.g. autoantigen reactive B and T cells can cross the BBB and partially survive and expand within the CSF compartment. (1) Autoantibody producing plasma cells may drive CNS inflammation, causing CNS damage in inflammatory autoimmune diseases e.g. autoimmune encephalitis (AIE), multiple sclerosis (MS) and others. (2) After collecting cerebrospinal fluid (CSF) from patients by lumbar puncture, single intrathecal plasma cells are isolated. (3) Using single B cell antibody technology, genetic information amplified from individual cells are used for constructing recombinant monoclonal antibodies. (4) After recovery of the intrathecal antibody signature in recombinant form they can be used in *in vivo* and *ex vivo* disease models to characterise their role in disease mechanisms of CNS inflammation (***Malviya et al., Amedonu et al., Matute et al., Winter et al.***). (5-6) Immune repertoire sequencing of peripheral blood T and B cells from patients with inflammatory CNS diseases is applied to compare CNS- and peripheral immune repertoires and to provide a better understanding of beneficial properties as well as potential side effects of current immune treatments (e.g. with alemtuzumab) (***Ruck et al. - under revision, Barman et al. - unpublished***). (Graphic is created with BioRender.com).

1.1 Background

The central nervous system (CNS) has traditionally been considered an "immune-privileged" site: The presence of the blood-brain barrier (BBB) protects the CNS from many adverse effects of soluble mediators and cellular components of the peripheral immune system. However, immune cells are increasingly recognized to access the CNS in both health and disease *(1)*. Leukocytes can express inflammatory cytokines, reactive oxygen species (ROS) and other enzymes that can assist their access to CNS compartment *(2)*. Lymphocytes can enter the CNS through several points, including the blood-brain barrier, the blood-meningeal barrier and the third, blood-cerebrospinal fluid barrier *(3, 4)*. In individuals with CNS inflammation, B lymphocytes number can increase by at least several orders of magnitude in the CNS parenchyma and perivascular spaces *(5)* and by severalfold in the cerebrospinal fluid (CSF) *(6)*. They can also enter the CSF in the subarachnoid space, either by extravasation across subpial venules of the blood-meningeal barrier or by crossing the stroma and epithelium of the choroid plexus (blood-CSF barrier) *(1)*. Autoimmunity in the CNS can manifest as the result of cellular or humoral immune responses to autoantigens, or both *(7)*. The manifestation of the cellular and humoral immune response triggers inflammation in the CNS. Inflammation and corresponding mediators contribute to many inflammatory autoimmune CNS diseases, e.g. multiple sclerosis (MS), autoimmune encephalitis (AIE) and others.

1.1.1 Immune receptors and repertoires

The adaptive immunity consists of two major components, cellular immunity and humoral immunity, which are highly specific to particular pathogens. T and B lymphocytes are two abundant and functionally important cell types that play pivotal roles to combat countless number of pathogens. The T cell receptor (TCR) is a molecule found on the surface of T lymphocytes, that is responsible for recognizing fragments of antigen, whereas the B cell receptor (BCR) is an immunoglobulin molecule forming a type I transmembrane protein on the surface of B cells *(8)*. The diversified TCRs can recognize and bind to the various peptides of the antigens presented by major histocompatibility complex (MHC) molecules of antigen presenting cells, thus forming a TCR-antigen-MHC structure complex. On the other hand, immunoglobulins can bind to antigens directly *(9)*. The totality of diverse antigen receptors of

T and B lymphocytes with distinct variable domains in a given individual is denoted as immune repertoire *(10)*.

1.1.2 Generation of TCR and antibody diversity

A powerful adaptive immune system relies on the generation of diversified T cell receptors (TCRs) and B cell receptors (BCRs) to recognize the enormous variety of antigens *(9)*. T and B cells recognize specific antigens through their antigen receptors. Both BCR and TCR share structural similarities, e.g. they comprise distinct pairs of chains which include two heavy and two light chains for the BCR, one α- and one β-chain for the αβ TCR and variable domains mediating the binding to antigens *(11)* ***(Figure 1)***. The human TCR alpha gene (TRA) locus is located on chromosome 14, beta chain gene (TRB) locus is positioned on chromosome 7, while the human IGH, IGL, and IGK genes are located on the chromosomes 14, 22, and 2, respectively *(9)*.

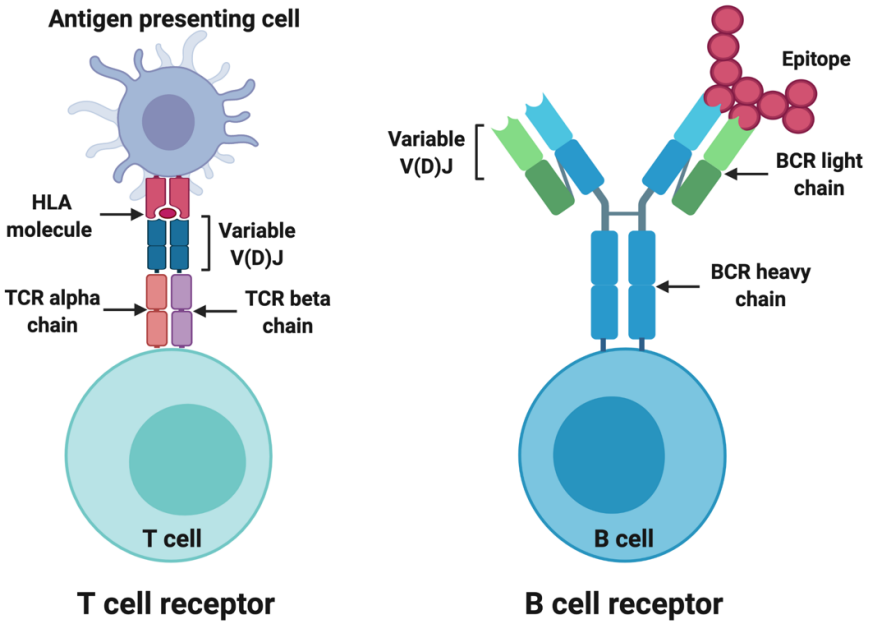

Figure 1: Structure of antigen receptors. *(a) T cell receptor (TCR) (b) B cell receptor (BCR) (graphic inspired by Lossius et al. and created with BioRender.com).*

During lymphocyte development the genes encoding the variable domains undergo somatic diversification ***(Figure 2)***. The gene segments: V (variable), D (diversity), J (joining), and C

(constant), determine the binding specificity and downstream applications of immunoglobulins (BCRs) and T cell receptors (TCRs). Three gene families, including Variable (V), Diversity (D), and Joining (J) genes encode the immunoglobulin heavy chain variable region, however, for light chains, only V and J gene families are involved in recombination *(9)*. Akin to the immunoglobulin heavy chain region, the TCR beta variable region is encoded by three gene families, including Variable (V), Diversity (D), and Joining (J) genes, whereas the TCR alpha variable region is encoded by two gene families known as Variable (V), and Joining (J) genes. In addition, nucleotides maybe randomly added or removed between the segments *(11)*. Upon encountering antigens, B cells can undergo additional rounds of diversification, typically in lymphoid germinal centres. This process involves the enzyme "activity-induced cytidine deaminase" and is known as somatic hypermutation *(10)*.

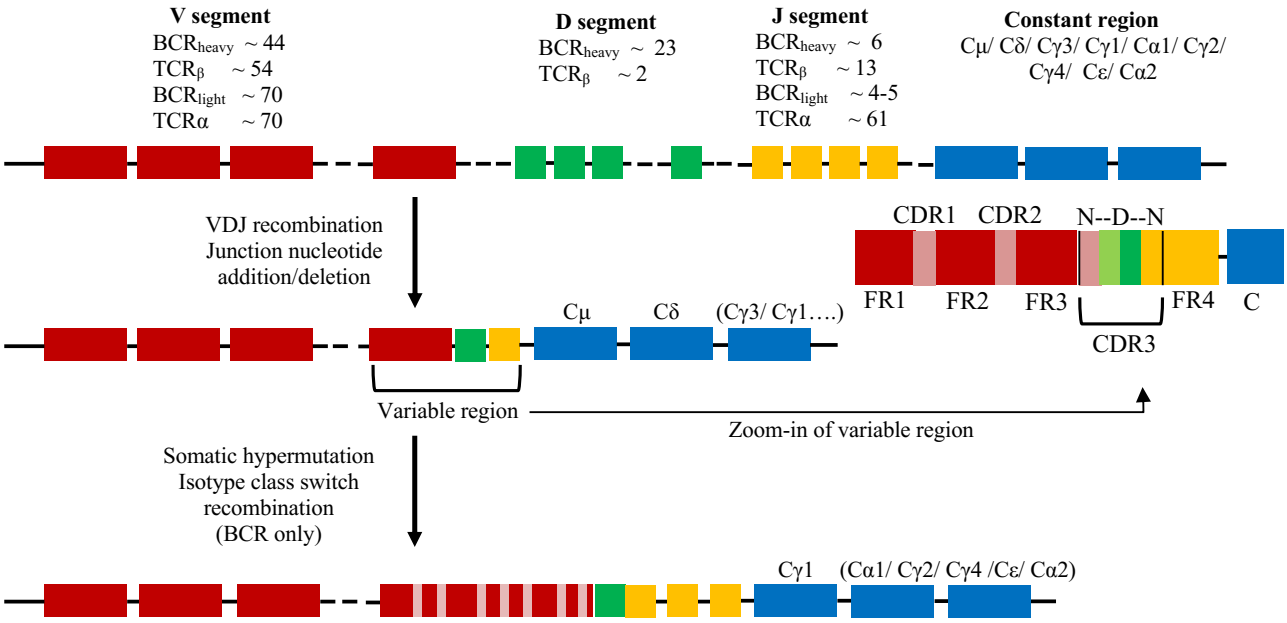

Figure 2: Antigen receptor diversification. *Antigen receptor repertoire diversity is primarily established during lymphocyte development, during which Variable-V (red), Diversity-D (green), and Joining-J (yellow) gene segments are rearranged through the process of V(D)J recombination. During the recombination process, random nucleotides may be added or deleted at segment junctions, contributing to additional sequence diversity ("N-region diversity"). B cell receptor (BCR)-specific secondary diversification may occur following antigen recognition. In somatic hypermutation processes, mutations (pink) are introduced throughout the variable region. Modified BCRs may be selected through affinity maturation. In class-switch recombination, gene segments encoding constant regions (blue) are rearranged, resulting in the production of antibodies with different isotypes and corresponding effector functions (12).*

Random V(D)J gene segments recombination in the bone marrow for B cells and in the thymus for T cells, generate an enormous number of variable regions to cope with different kinds of antigens. The greatest diversity is found within the complementarity determining regions (CDRs), specifically in CDR3, which contributes most to the specificity of the receptors *(11)*. Pairing of the receptor chains leads to additional divergence of the repertoire, and the possible diversity has been estimated to 10^{18} αβ TCRs and 5×10^{13} BCRs *(11)*. The third hypervariable domains (CDR3) of TCRs and BCRs can be used as molecular fingerprints to track lymphocytes of similar specificities *(11)*.

1.1.3 Multiple sclerosis

Multiple sclerosis (MS) is the most common chronic, inflammatory, demyelinating and neurodegenerative disease of the CNS, and characterized by inflammatory infiltrates, demyelination and axonal damage. Acute demyelination is displayed as clinical relapses that may fully or partially resolve, however, chronic demyelination and neuroaxonal injury lead to persistent and irreversible neurological symptoms, often progressing over time *(13)*. MS commonly affects young adults, with an onset between 20 and 40 years of age and has higher prevalence in female population *(14)*. Based on the predominance of episodic acute demyelinating events or of the chronic neurodegenerative process, the clinical course is defined either as relapsing-remitting (represents around 60% of prevalent cases) or as progressive MS. If progression starts from onset it is termed as primary progressive (PP), whereas, secondary progressive MS begins after a preceding relapsing-remitting phase *(13)*. Clinical onset for approximately 80-90% patients with MS is primarily marked by relapsing then remitting neurological deficits that is referred to as secondary progressive MS (SPMS), featured by disability acceleration in the absence of acute inflammation *(15)*. Rest 10-15% patients exhibit gradual worsening of neurological function evolving into primary progressive MS (PPMS) *(15)*.

1.1.4 Autoimmune encephalitis and associated autoantibodies

Autoimmune encephalitis (AIE) refers to a group of conditions where the body's immune system mistakenly attacks healthy brain cells, thus leading to an inflammation of the brain. In a substantial proportion this immunologic auto aggression is triggered by tumors expressing neuronal antigens. Patients with autoimmune encephalitis may have various neurologic and/or

psychiatric symptoms. Neurologic symptoms include impaired memory and cognition, abnormal movements, seizures, and/or problems with balance, speech, or vision while psychiatric symptoms can be manifested as psychosis, aggression, inappropriate sexual behaviours, panic attacks, compulsive behaviours, euphoria or fear *(16)*. At onset of the symptoms, CSF and serum analysis show a mild to moderate lymphocytic pleocytosis (< 100 cells/µl) in 60–80% of patients. More than 30% of patients display mild to moderate increased CSF protein concentration, while in 50% of patients oligoclonal bands can be detected *(17, 18)*.

AIE often is associated with the presence of autoantibodies specific for CNS antigens. Autoantibodies associated with AIE are classified in two groups: a) Antibodies against intracellular antigens and b) Antibodies against neuronal cell surface antigens.

a) Antibodies against intracellular antigens: Examples of these antibodies, which often are referred to as onconeuronal antibodies, include anti-Hu, anti-Glutamic Acid Decarboxylase (GAD), anti Ma2 and others. Since these antibodies are specific for intracellular antigens, they are commonly not thought to be pathogenic, yet may serve as disease markers, while CNS inflammation is thought to be mediated mostly by T cells *(19)*.

b) Antibodies against neuronal cell surface antigens: This antibodies are directed against distinct membrane antigens on pre- or post-synaptic sites of the neuron and are often associated with limbic encephalitis. The cognate targets of some of the antibodies have already been identified, including receptors for NMDA, AMPA, glycine, GABA and others, as well as the voltage gated potassium channel (VGKC) complex. These antibodies are thought to be involved in causing symptoms such as memory deficits, headache, irritability, sleep disturbance, delusions, hallucinations, agitation, seizures and psychosis in affected patients *(19, 20)*.

1.1.5 Anti-N-methyl-d-aspartate (NMDA) receptor encephalitis

Anti-N-methyl D-aspartate receptor (anti-NMDAR) encephalitis is among the most common AIE, first described in 2007 by Dalmau and colleagues, in which psychiatric and neurologic symptoms were found in women with ovarian teratomas *(21)*. It was reported that most paraneoplastic encephalitides have been associated with antibodies to intracellular onconeuronal proteins and cytotoxic T cells presumably against the same proteins. However,

they showed the patients' antibodies recognize epitopes exposed on the cell surface, which may have possible pathogenic role *(21)*. As such, anti-NMDA receptor encephalitis is associated with antibodies against NR1 subunits of the NMDA receptor. Encephalitis associated with anti-NMDAR antibodies can be triggered either by the presence of peripheral tumours *(22, 23)* or by preceding viral CNS infection or occur in the absence of such obvious events *(24, 25)*. It typically represents neurocognitive deficits that are variably accompanied by psychiatric symptoms, motor dysfunction, epileptic seizures, and disorders of movement and consciousness. Additionally, it is also associated in some cases with ovarian pathology, in particular teratomas *(26)*.

1.1.6 Myelin oligodendrocyte glycoprotein (MOG) specific autoantibodies

Myelin oligodendrocyte glycoprotein (MOG) is a quantitatively minor myelin protein, with an immunoglobulin (Ig)−like extracellular domain that is expressed in abundance on the outermost layer of myelin sheaths *(27)*. Autoantibodies against MOG have been shown to enhance demyelination in several EAE models *(28)*. Autoantibodies against a specific myelin protein mediate target membrane damage in CNS demyelinating disease *(29, 30)*. In both rodents and nonhuman primates antibodies against conformational epitopes of MOG seem to have a pathogenic role for destruction of the myelin whereas antibodies against MOG peptide have no direct link to demyelination. Therefore, recognition of conformational MOG epitopes by antibodies or B cells appears to be an important parameter for demyelinating pathogenicity *(31, 32)*.

1.2 Technical approaches and outcomes

1.2.1 Single B cell antibody technology and development of recombinant antibodies

To facilitate the identification of antigen specificity and pathogenicity of intrathecal antibody responses, we employed single B cell antibody technology. Whereas the CSF contains antibodies produced in the CNS compartment in a mixed and diluted form, this technology allows to reconstruct individual, patient derived antibody signatures in a monoclonal form and potentially unlimited quantities. Starting from the PCR amplification of the expressed of heavy-(VH) and corresponding light-chain (VL) region encoding genes from individual human B cells

and expression cloning of the resulting amplicons, corresponding recombinant antibodies are expressed in culture and purified *(33)*.

1.2.1.1 Development of anti-NMDAR-specific recombinant monoclonal antibody

Antibodies against NMDAR can be detected both in peripheral blood (PB) and CSF, and patients typically exhibit intrathecal synthesis of anti-NMDAR antibodies *(22)*. The intrathecal source of pathogenic antibodies in anti-NMDAR encephalitis has been suggested to originate from CD138+ plasma cells, which were identified in perivascular and interstitial spaces in biopsy and autopsy studies *(34, 35)*. The pathogenic relevance of anti-NMDA receptor antibodies has been suggested by passive transfer of patients' CSF in mice *in vivo*. Recently, a recombinant human anti-NMDAR monoclonal antibody was cloned from intrathecal B cells and showed pathogenic effects in *in vitro* systems and the observation was similar to those previously reported using CSF of patients *(36, 37)*. However, it was not investigated whether the GluN1-reactive human monoclonal antibody indeed exerted any pathogenic effects *in vivo*.

To analyse the intrathecal plasma cell repertoire, identify autoantibody-producing clones, and characterize their antibody signatures in recombinant form, we designed our experiments for developing anti-N-Methyl-D-aspartic acid (NMDA)-specific recombinant monoclonal antibody from clonally expanded intrathecal plasma cells of an anti-NMDAR encephalitis patient. Immunoglobulin (Ig) transcripts from single FACS sorted CSF plasma cells are amplified by single cell RT-PCR and sequenced. Matching Ig heavy (IgH) and light chain (IgL) variable gene regions of clonally expanded plasma cells (cePc) are cloned and expressed in recombinant form for the further characterization *in vitro* and *in vivo.*

In addition, we have further plan to study the peripheral immune repertoire of autoimmune encephalitis patients using next generation sequencing. From peripheral immune repertoire analysis it will be possible to characterize B and T lymphocytes repertoire in peripheral system and to learn about trafficking of autoantibody producing plasma cells from the periphery to the CNS or vice versa. Moreover, single-cell RNA sequencing and immune repertoire study will help to track the pathogenic clones in CNS and periphery, and to identify meaningful target of intrathecal immune response which permits further elucidation of disease mechanisms and development of targeted therapies in anti-NMDAR encephalitis.

1.2.2 Murine organotypic cerebellar slice cultures (OSC) as an *ex vivo* model of the immune-CNS interface

A large proportion of current MS research is currently performed in a model system called experimental autoimmune encephalomyelitis (EAE). For the induction of EAE, rodents or nonhuman primates are actively immunized with myelin antigens, thus inducing an inflammation of the CNS. This inflammation leads to a progressive paralysis of the animals before they eventually are sacrificed. While CNS inflammation can also be caused by adoptive transfer of MOG-reactive T cells alone, in rats and nonhuman primates antibodies are additionally required for the induction of demyelination. Likewise, deposits of immunoglobulin and complement can be detected in MS lesions supporting the role of immunoglobulins in MS pathogenesis. Although EAE has provided many valuable insights into the pathology of MS, it only partially reflects MS. Therefore it is difficult to discern the role of different arms of the immune system in respect of the induction of CNS damage. In order to overcome the difficulties pertaining to EAE model, we have therefore established an experimental model system using organotypic CNS slice cultures, in which the complex architecture of the CNS is maintained. Notably it allows the detailed investigation of interactions between the CNS and components of the immune system as well as mechanisms of CNS damage and repair thereof *(38)*. Using this organotypic cerebellar slice culture model system of inflammatory CNS injury, Sobottka and colleagues visualized axonal loss that can be accompanied with "collateral bystander damage" by auto-aggressive, myelin directed cytotoxic CD8+T cells *(39)*.

To understand the interaction between immune system and nervous system, we aimed to observe the immunomodulatory intravenous immunoglobulins (IVIG) effects on antibody mediated immune mechanisms. Thus, a recombinant humanized MOG-specific antibody is synthesized to induce, together with complement, demyelination in murine organotypic cerebellar slice cultures (OSC) as an *ex vivo* model of the immune-CNS interface.

1.2.3 High-throughput immune repertoire sequencing and understanding of treatment effects in multiple sclerosis

To characterize longitudinal changes in the clonal compositions of MS patients' peripheral lymphocyte repertoires before and during treatment and to better understand beneficial properties as well as potential side effects of treatment we are intended to perform high-

throughput immune repertoire sequencing of peripheral blood T and B cells from patients with multiple sclerosis.

1.2.3.1 High-throughput sequencing of immune repertoire

Sanger sequencing and CDR3 spectratyping have provided important insights on the clonality of intrathecal B- and T- cell repertoires, and promising tools for studies of the specificity of CSF and CNS B cells. However, conventional sanger sequencing and spectratyping have limitations to reveal the complete immune repertoire. Cloning and conventional sanger sequencing, nevertheless, only allows interrogation of a small fraction of the immune repertoire. CDR3 spectratyping, on the other hand, gives an "eagle eye" perspective, but does not provide information about the receptor specificity determining sequence *(40)*. These limitations have hampered an unbiased characterization of representative immune repertoires within immunological or anatomic compartments. Nevertheless, high-throughput sequencing overcomes these limitations and offers the best of both worlds. It enables sequencing of millions of short templates in parallel, capturing even infrequent or unique clones. The advent of immune repertoire sequencing of the BCR and TCR from different B and T lymphocyte populations has provided important insights into the clonal characteristics of B and T cells in the blood, CSF and CNS of patients with MS. Sequencing of IgG from MS lesions and CSF samples revealed clonally expanded antibodies with preferential use of certain variable heavy (VH) chain genes which strongly suggests antigen driven clonal expansion *(1)*. Moreover, it is also reported the strong sharing of expanded T-cells and IgG-expressing B cells clones between CNS and periphery *(41–43)*.

1.2.3.2 Disease-modifying therapies in multiple sclerosis and assessment of immune repertoire

Currently approved disease-modifying therapies (DMTs) are immunomodulatory or immunosuppressive drugs that significantly but variably reduce the frequency of attacks of the relapsing forms of the disease *(13)*. Currently DMTs for MS approved by the European Medicines Agency (EMA) and Food and Drug Administration (FDA) include injectable agents - interferon beta (IFNβ) 1-a and 1-b, glatiramer acetate (GA), mitoxantrone, natalizumab, alemtuzumab, ocrelizumab and oral agents - fingolimod, cladribine, teriflunomide, and dimethyl fumarate *(13)*. Some other disease modifying drugs are under investigation. All

mentioned agents act by modulating and/or suppressing the immune system at various levels and with different mechanisms of action. Treatment with DMTs has been shown to reduce relapse rates and slow progression of changes, progression of disability, and cognitive decline, but efficacy varies among products *(44)*. Moreover, along with these DMTs, a novel therapeutic approach like hematopoietic stem cell transplantation (HSTC) is also approved by FDA. For better understanding of beneficial properties as well as potential side effects of one of the current immune treatments (e.g. with alemtuzumab), we aimed to analyse immune repertoire of peripheral blood T and B cells from MS patients.

Alemtuzumab (LEMTRADA®) is a recombinant, humanized, monoclonal IgG1 kappa antibody targeting the cell-surface glycoprotein CD52. It induces antibody-dependent cellular cytotoxicity (ADCC) and complement-dependent cytotoxicity (CDC), and activates pro-apoptotic pathways on CD52-expressing cells *(45)*. Robust clinical and radiologic data, derived from clinical trials and long-term observational studies, indicate that alemtuzumab induces a marked immunomodulation, which is related to the depletion of circulating T and B lymphocytes *(45)*. Following alemtuzumab treatment, repopulation/reconstruction of T and B lymphocytes is assumed to lead to a rebalancing of the immune system *(46)*. Yet, during the period of repopulation of the immune cells, a significant percentage of patients experience secondary autoimmunity *(47)*. The recovery rate of lymphocytes varies where B cells recover faster than T cells. For B cells it takes 7.1 months while CD4+ and CD8+ T cells take 35 and 20 months respectively to reach baseline level *(48)*. A study focused on peripheral CD4 recovery suggests that it can be used to predict disease activity after alemtuzumab treatment in MS patient *(49)*. Autologous stem cell transplantation and the monoclonal antibody alemtuzumab are assumed to "reset/reprogramming" the immune system. To test this hypothesis in MS patients treated with stem cell transplantation, Muraro, Robins and colleagues followed the renewal of the T-cell repertoire applying high-throughput TCR β sequencing *(50)*. This allowed a comprehensive assessment of the regenerated CD4+ and CD8+ T-cell repertoires, including the impact of individual surviving clones on the newly reprogrammed repertoire. Interestingly, whereas the CD4+ T-cell repertoire after transplantation were largely composed of newly generated clones, the CD8+ T-cell repertoire was re-established from clones already present before treatment *(50)*. Less diverse T cell receptor (TCR) repertoires were associated with a poor response to stem cell transplantation *(51)*. These experimental results show that high-throughput sequencing may enable monitoring of T-cell clones following

therapies with fundamental effects on the immune system. However, for monitoring the repertoire changes following alemtuzumab treatment, no B- and T- cell receptor repertoire study in alemtuzumab treated MS patients with larger cohort is reported. Therefore, in order to track the TCR-β and the Ig-H clonal repertoire on the peripheral blood of alemtuzumab treated MS patients, untreated MS controls and healthy controls, we designed our experimental plan.

We hypothesized that alemtuzumab treatment leads to a beneficial "reprogramming" of the auto-aggressive immune system in MS. In an effort to better understand the beneficial properties and potential side effects of alemtuzumab, we aimed to investigate the longitudinal changes in the clonal compositions of patients' peripheral lymphocyte repertoires before and during the treatment. Moreover, we have future plan to analyse the intrathecal plasma cell repertoire for comparing treatment effects between CNS- and peripheral immune repertoires.

1.3 References

1. J. J. Sabatino, A.-K. Pramp, S. S. Zamvil, B cells in autoimmune and neurodegenerative central nervous system diseases, *Nat. Rev. Neurosci.* , doi:10.1038/s41583-019-0233-2.

2. C. Larochelle, J. I. Alvarez, A. Prat, How do immune cells overcome the blood-brain barrier in multiple sclerosis?, *FEBS Lett.* **585**, 3770–3780 (2011).

3. B. Engelhardt, P. Vajkoczy, R. O. Weller, The movers and shapers in immune privilege of the CNS*Nat. Immunol.* **18**, 123–131 (2017).

4. A. Louveau, B. A. Plog, S. Antila, K. Alitalo, M. Nedergaard, J. Kipnis, Understanding the functions and relationships of the glymphatic system and meningeal lymphatics*J. Clin. Invest.* **127**, 3210–3219 (2017).

5. J. Machado-Santos, E. Saji, A. R. Trö Scher, M. Paunovic, R. Liblau, G. Gabriely, C. G. Bien, J. Bauer, H. Lassmann, The compartmentalized inflammatory response in the multiple sclerosis brain is composed of tissue-resident CD8 + T lymphocytes and B cells, , doi:10.1093/brain/awy151.

6. M. C. Kowarik, V. Grummel, S. Wemlinger, D. Buck, M. S. Weber, A. Berthele, B. Hemmer, Immune cell subtyping in the cerebrospinal fluid of patients with neurological diseases, *J. Neurol.* **261**, 130–143 (2014).

7. J. E. Merrill, M. C. Graves, D. G. Mulder, in *Western Journal of Medicine*, (BMJ Publishing Group, 1992), vol. 156, pp. 639–646.

8. Kuby Immunology - Jenni Punt|Sharon Stranford|Patricia Jones|Judith A Owen - Macmillan International Higher Education (available at https://www.macmillanihe.com/page/detail/kuby-immunology/?k=9781319114701&loc=au&priceCode=au).

9. X. Liu, J. Wu, History, applications, and challenges of immune repertoire research, *Cell*

Biol. Toxicol. **34**, 441–457 (2018).

10. A. Lossius, J. N. Johansen, F. Vartdal, T. Holmøy, C. A. Lossius, High-throughput sequencing of immune repertoires in multiple sclerosis, *Ann. Clin. Transl. Neurol.* **3**, 295–306 (2016).

11. K. Murphy, *Janeway's Immunobiology* (Garland Science, New York, USA, ed. 8th).

12. J. J. A. Calis, B. R. Rosenberg, Characterizing immune repertoires by high throughput sequencing: strategies and applications, (2014), doi:10.1016/j.it.2014.09.004.

13. A. Gajofatto, M. D. Benedetti, Treatment strategies for multiple sclerosis: When to start, when to change, when to stop?, *World J. Clin. Cases* **3**, 545 (2015).

14. J. M. Greer, P. A. McCombe, Role of gender in multiple sclerosis: Clinical effects and potential molecular mechanisms, *J. Neuroimmunol.* **234**, 7–18 (2011).

15. S. Klineova, F. D. Lublin, Clinical Course of Multiple Sclerosis, *Cold Spring Harb. Perspect. Med.* **8**, a028928 (2018).

16. E. Lancaster, The Diagnosis and Treatment of Autoimmune Encephalitis., *J. Clin. Neurol.* **12**, 1–13 (2016).

17. F. Leypoldt, T. Armangue, J. Dalmau, Autoimmune encephalopathies, *Ann. N. Y. Acad. Sci.* **1338**, 94–114 (2015).

18. F. Graus, M. J. Titulaer, R. Balu, S. Benseler, C. G. Bien, T. Cellucci, I. Cortese, R. C. Dale, J. M. Gelfand, M. Geschwind, C. A. Glaser, J. Honnorat, R. Höftberger, T. Iizuka, S. R. Irani, E. Lancaster, F. Leypoldt, H. Prüss, A. Rae-Grant, M. Reindl, M. R. Rosenfeld, K. Rostásy, A. Saiz, A. Venkatesan, A. Vincent, K. P. Wandinger, P. Waters, J. Dalmau, A clinical approach to diagnosis of autoimmune encephalitis*Lancet Neurol.* **15**, 391–404 (2016).

19. R. Rössling, H. Prüss, SOP: antibody-associated autoimmune encephalitis, , doi:10.1186/s42466-019-0048-7.

20. E. Tüzün, L. Zhou, J. M. Baehring, S. Bannykh, M. R. Rosenfeld, J. Dalmau, Evidence for antibody-mediated pathogenesis in anti-NMDAR encephalitis associated with ovarian teratoma., *Acta Neuropathol.* **118**, 737–43 (2009).

21. J. Dalmau, E. Tüzün, H. Wu, J. Masjuan, J. E. Rossi, A. Voloschin, J. M. Baehring, H. Shimazaki, R. Koide, D. King, W. Mason, L. H. Sansing, M. A. Dichter, M. R. Rosenfeld, D. R. Lynch, Paraneoplastic anti-N-methyl-D-aspartate receptor encephalitis associated with ovarian teratoma., *Ann. Neurol.* **61**, 25–36 (2007).

22. J. Dalmau, A. J. Gleichman, E. G. Hughes, J. E. Rossi, X. Peng, M. Lai, S. K. Dessain, M. R. Rosenfeld, R. Balice-Gordon, D. R. Lynch, Anti-NMDA-receptor encephalitis: case series and analysis of the effects of antibodies., *Lancet. Neurol.* **7**, 1091–8 (2008).

23. M. J. Titulaer, L. McCracken, I. Gabilondo, T. Armangué, C. Glaser, T. Iizuka, L. S. Honig, S. M. Benseler, I. Kawachi, E. Martinez-Hernandez, E. Aguilar, N. Gresa-Arribas, N. Ryan-Florance, A. Torrents, A. Saiz, M. R. Rosenfeld, R. Balice-Gordon, F. Graus, J. Dalmau, Treatment and prognostic factors for long-term outcome in patients with anti-NMDA receptor encephalitis: an observational cohort study., *Lancet. Neurol.* **12**, 157–65 (2013).

24. H. Prüss, C. Finke, M. Höltje, J. Hofmann, C. Klingbeil, C. Probst, K. Borowski, G. Ahnert-Hilger, L. Harms, J. M. Schwab, C. J. Ploner, L. Komorowski, W. Stoecker, J. Dalmau, K. P. Wandinger, N-methyl-D-aspartate receptor antibodies in herpes simplex encephalitis, *Ann. Neurol.* **72**, 902–911 (2012).

25. T. Armangue, F. Leypoldt, I. Málaga, M. Raspall-Chaure, I. Marti, C. Nichter, J. Pugh, M. Vicente-Rasoamalala, M. Lafuente-Hidalgo, A. Macaya, M. Ke, M. J. Titulaer, R. Höftberger, H. Sheriff, C. Glaser, J. Dalmau, Herpes simplex virus encephalitis is a trigger of brain autoimmunity., *Ann. Neurol.* **75**, 317–23 (2014).

26. H. Barry, S. Byrne, E. Barrett, K. C. Murphy, D. R. Cotter, Anti-N-methyl-D-aspartate receptor encephalitis: Review of clinical presentation, diagnosis and treatment*Psychiatrist* **39**, 19–23 (2015).

27. C. Brunner, H. Lassmann, T. V Waehneldt, J. M. Matthieu, C. Linington, Differential ultrastructural localization of myelin basic protein, myelin/oligodendroglial glycoprotein, and 2',3'-cyclic nucleotide 3'-phosphodiesterase in the CNS of adult rats., *J. Neurochem.* **52**, 296–304 (1989).

28. H. Lassmann, C. Brunner, M. Bradl, C. Linington, Experimental allergic encephalomyelitis: the balance between encephalitogenic T lymphocytes and demyelinating antibodies determines size and structure of demyelinated lesions, *Acta Neuropathol.* **75**, 566–576 (1988).

29. C. P. Genain, B. Cannella, S. L. Hauser, C. S. Raine, Identification of autoantibodies associated with myelin damage in multiple sclerosis., *Nat. Med.* **5**, 170–5 (1999).

30. C. S. Raine, B. Cannella, S. L. Hauser, C. P. Genain, Demyelination in primate autoimmune encephalomyelitis and acute multiple sclerosis lesions: a case for antigen-specific antibody mediation., *Ann. Neurol.* **46**, 144–60 (1999).

31. H.-C. von Büdingen, S. L. Hauser, J.-C. Ouallet, N. Tanuma, T. Menge, C. P. Genain, Frontline: Epitope recognition on the myelin/oligodendrocyte glycoprotein differentially influences disease phenotype and antibody effector functions in autoimmune demyelination., *Eur. J. Immunol.* **34**, 2072–83 (2004).

32. J.-A. Lyons, M. J. Ramsbottom, A. H. Cross, Critical role of antigen-specific antibody in experimental autoimmune encephalomyelitis induced by recombinant myelin oligodendrocyte glycoprotein., *Eur. J. Immunol.* **32**, 1905–13 (2002).

33. T. Tiller, Single B cell antibody technologies*N. Biotechnol.* **28**, 453–457 (2011).

34. J.-P. Camdessanché, N. Streichenberger, G. Cavillon, V. Rogemond, G. Jousserand, J. Honnorat, P. Convers, J.-C. Antoine, Brain immunohistopathological study in a patient with anti-NMDAR encephalitis., *Eur. J. Neurol.* **18**, 929–31 (2011).

35. E. Martinez-Hernandez, J. Horvath, Y. Shiloh-Malawsky, N. Sangha, M. Martinez-Lage, J. Dalmau, Analysis of complement and plasma cells in the brain of patients with anti-NMDAR encephalitis, *Neurology* **77**, 589–593 (2011).

36. J. Kreye, N. K. Wenke, M. Chayka, J. Leubner, R. Murugan, N. Maier, B. Jurek, L.-T. Ly, D. Brandl, B. R. Rost, A. Stumpf, P. Schulz, H. Radbruch, A. E. Hauser, F. Pache, A. Meisel, L. Harms, F. Paul, U. Dirnagl, C. Garner, D. Schmitz, H. Wardemann, H. Prüss, Human cerebrospinal fluid monoclonal *N* -methyl-D-aspartate receptor autoantibodies are sufficient for encephalitis pathogenesis, *Brain* **139**, 2641–2652 (2016).

37. E. G. Hughes, X. Peng, A. J. Gleichman, M. Lai, L. Zhou, R. Tsou, T. D. Parsons, D. R. Lynch, J. Dalmau, R. J. Balice-Gordon, Cellular and synaptic mechanisms of anti-NMDA receptor encephalitis, *J. Neurosci.* **30**, 5866–5875 (2010).

38. Goebels N, *Organotypic CNS Slice Cultures as an In Vitro Model for Immune Mediated Tissue Damage and Repair in Multiple Sclerosis.* (2007).

39. B. Sobottka, M. D. Harrer, U. Ziegler, K. Fischer, H. Wiendl, T. Hünig, B. Becher, N. Goebels, Collateral bystander damage by myelin-directed CD8+ T cells causes axonal loss, *Am. J. Pathol.* **175**, 1160–1166 (2009).

40. A. Lossius, J. N. Johansen, F. Vartdal, H. Robins, B. Jūratė Šaltytė, T. Holmøy, J. Olweus, High-throughput sequencing of TCR repertoires in multiple sclerosis reveals intrathecal enrichment of EBV-reactive CD8 $^{+}$ T cells, *Eur. J. Immunol.* **44**, 3439–3452 (2014).

41. M. Salou, A. Garcia, L. Michel, A. Gainche-Salmon, D. Loussouarn, B. Nicol, F. Guillot, P. Hulin, S. Nedellec, D. Baron, G. Ramstein, J.-P. Soulillou, S. Brouard, A. B. Nicot, N. Degauque, D. A. Laplaud, Expanded CD8 T-cell sharing between periphery and CNS in multiple sclerosis., *Ann. Clin. Transl. Neurol.* **2**, 609–22 (2015).

42. C. Skulina, S. Schmidt, K. Dornmair, H. Babbe, A. Roers, K. Rajewsky, H. Wekerle, R. Hohlfeld, N. Goebels, Multiple sclerosis: Brain-infiltrating CD8+ T cells persist as clonal expansions in the cerebrospinal fluid and blood, *Proc. Natl. Acad. Sci. U. S. A.* **101**, 2428–2433 (2004).

43. H.-C. Von Büdingen, T. C. Kuo, M. Sirota, C. J. Van Belle, L. Apeltsin, J. Glanville, B. A. Cree, P.-A. Gourraud, A. Schwartzburg, G. Huerta, D. Telman, P. D. Sundar, T. Casey, D. R. Cox, S. L. Hauser, B cell exchange across the blood-brain barrier in multiple sclerosis, *J. Clin. Invest.* (2012), doi:10.1172/JCI63842.

44. Jacquelyn L. Bainbridge; Augusto Miravalle; Pei Shieen Wong, Multiple Sclerosis | Pharmacotherapy: A Pathophysiologic Approach, 10e | AccessPharmacy | McGraw-Hill Medical (available at https://accesspharmacy.mhmedical.com/content.aspx?bookid=1861&sectionid=146062622).

45. P. Gallo, D. Centonze, M. G. Marrosu, Alemtuzumab for multiple sclerosis: the new concept of immunomodulation, , doi:10.1186/s40893-017-0024-4.

46. L. Klotz, S. G. Meuth, H. Wiendl, Immune mechanisms of new therapeutic strategies in multiple sclerosis—A focus on alemtuzumab, *Clin. Immunol.* **142**, 25–30 (2012).

47. A. J. Coles, E. Fox, A. Vladic, S. K. Gazda, V. Brinar, K. W. Selmaj, A. Skoromets, I. Stolyarov, A. Bass, H. Sullivan, D. H. Margolin, S. L. Lake, S. Moran, J. Palmer, M. S. Smith, D. A. S. Compston, Alemtuzumab more effective than interferon β-1a at 5-year follow-up of CAMMS223 Clinical Trial, *Neurology* **78**, 1069–1078 (2012).

48. G. A. Hill-Cawthorne, T. Button, O. Tuohy, J. L. Jones, K. May, J. Somerfield, A. Green, G. Giovannoni, D. A. S. Compston, M. T. Fahey, A. J. Coles, Long term lymphocyte reconstitution after alemtuzumab treatment of multiple sclerosis, *J. Neurol. Neurosurg. Psychiatry* **83**, 298–304 (2012).

49. M. D. Cossburn, K. Harding, G. Ingram, T. El-Shanawany, A. Heaps, T. P. Pickersgill, S. Jolles, N. P. Robertson, Clinical relevance of differential lymphocyte recovery after alemtuzumab therapy for multiple sclerosis, *Neurology* **80**, 55–61 (2013).

50. P. A. Muraro, H. Robins, S. Malhotra, M. Howell, D. Phippard, C. Desmarais, A. de P. A. Sousa, L. M. Griffith, N. Lim, R. A. Nash, L. A. Turka, T cell repertoire following autologous stem cell transplantation for multiple sclerosis, *J. Clin. Invest.* **124**, 1168 (2014).

51. J. L. Jones, S. A. J. Thompson, P. Loh, J. L. Davies, O. C. Tuohy, A. J. Curry, L. Azzopardi, G. Hill-Cawthorne, M. T. Fahey, A. Compston, A. J. Coles, Human autoimmunity after lymphocyte depletion is caused by homeostatic T-cell proliferation., *Proc. Natl. Acad. Sci. U. S. A.* **110**, 20200–5 (2013).

Manuscript I

"Reprogramming the immune system" with alemtuzumab in multiple sclerosis (MS) patients: Cell type specific longitudinal immune repertoire dynamics and emergence of secondary autoimmunity

"Reprogramming the immune system" with alemtuzumab in multiple sclerosis (MS) patients: Cell type specific longitudinal immune repertoire dynamics and emergence of secondary autoimmunity

Sumanta Barman[1], Tobias Ruck[1], Armin Scheffler[2], Steffen Pfeuffer[3], Christoph Lehrich[3], Vera Balz[4], Heinz Wiendl[3], Nico Melzer[1], Sven Meuth[1], Norbert Goebels[1]

[1]Department of Neurology, Medical Faculty, Heinrich Heine University Düsseldorf, Düsseldorf, Germany
[2]Department of Neurology, University Hospital Essen, Essen, Germany
[3]Department of Neurology with Institute of Translational Neurology, University Hospital Münster, Münster, Germany
[4]Institute of Transplantation Diagnostics and Cell Therapeutics, Heinrich Heine University Düsseldorf, Düsseldorf, Germany

Title character count: 185 (with spaces)
Number of figures and tables: 32 figures and 1 table
Word count abstract: 421
Word count manuscript: 14,411 words
Supplemental information: 14 figures and 4 tables

Corresponding author:
Professor Dr. med. Norbert Goebels, Department of Neurology, Heinrich Heine University Düsseldorf, Moorenstrasse 5, 40225 Düsseldorf, Germany; Tel: +49-211-8104594; Fax: +49-211-8104597; E-mail: norbert.goebels@uni-duesseldorf.de

Abstract

Alemtuzumab (ALEM) is a recombinant, humanized IgG1 monoclonal antibody targeting the surface molecule CD52 expressed on T- and B-lymphocytes. This study aims to characterize longitudinal evolutions in the clonal compositions of multiple sclerosis (MS) patients' peripheral lymphocyte repertoires pre- and post-ALEM treatment, to better understand the beneficial properties and potential side effects of this drug. The T cell receptor (TCR) repertoire of CD4+ and CD8+ T cells, and expressed immunoglobulin genes (Ig) of naïve and memory B cells, FACS-purified from peripheral blood of 12 patients with MS before and at three time points within 40 months after the onset of treatment with ALEM, and five untreated controls were analyzed by high-throughput immune repertoire sequencing (RepSeq). Our longitudinal FACS analysis data confirmed a decrease of the relative proportions of CD8+ and CD4+ T, and memory B lymphocytes after each ALEM cycle, contrasting the increase of the naïve B cell population. Our immune repertoire analysis data showed that ALEM has distinctive effects on T cell and B cell repertoires. Reconstituted post-ALEM CD4+ TCR repertoires were largely composed of newly generated low-abundant clones. In contrast, the dominant CD8+ T cell clones were not effectively removed by alemtuzumab, so the post-ALEM CD8+ T cell repertoires were restored from clones already existing and highly abundant in pre-treatment repertoires. Memory B cell repertoires, particularly in the IgG+ populations, consist of dominant clones, of which hardly any persist over time, even in untreated controls. This repertoire behavior seems hardly affected by ALEM treatment. However, in the subgroup of 4 patients with secondary autoimmunity few memory B cell clones expanded and persisted. Treating one of them with rituximab to cope secondary autoimmunity aborted most of these persisting clones. Naïve B cell repertoires are composed by non-persisting low abundant clones. Except for the mentioned increase in proportion, ALEM treatment did not induce notable repertoire changes in naïve B cell repertoires. Post-alemtuzumab T and B cell repertoires are more diverse than pre-treatment repertoires predominantly in non-secondary autoimmunity patients, in contrast, secondary autoimmunity patients had reduced T cell repertoire diversity, particularly in post-secondary autoimmunity repertoires. Importantly, secondary autoimmunity patients showed significantly increased persistence and expansion of T cell clones already after the first alemtuzumab infusion and a delayed expansion of memory B cell clones after the second infusion, which provides a novel mechanistic explanation for development of secondary autoimmunity combining current B or T cell-related hypotheses. Further immune repertoire study with a larger cohort of SA patients

might give deeper insight about the consequences of alemtuzumab treatment and development of secondary autoimmunity.

Keywords: Multiple sclerosis, Alemtuzumab, Immune repertoire, T cell receptor, B cell receptor, Secondary autoimmunity.

Graphical abstract

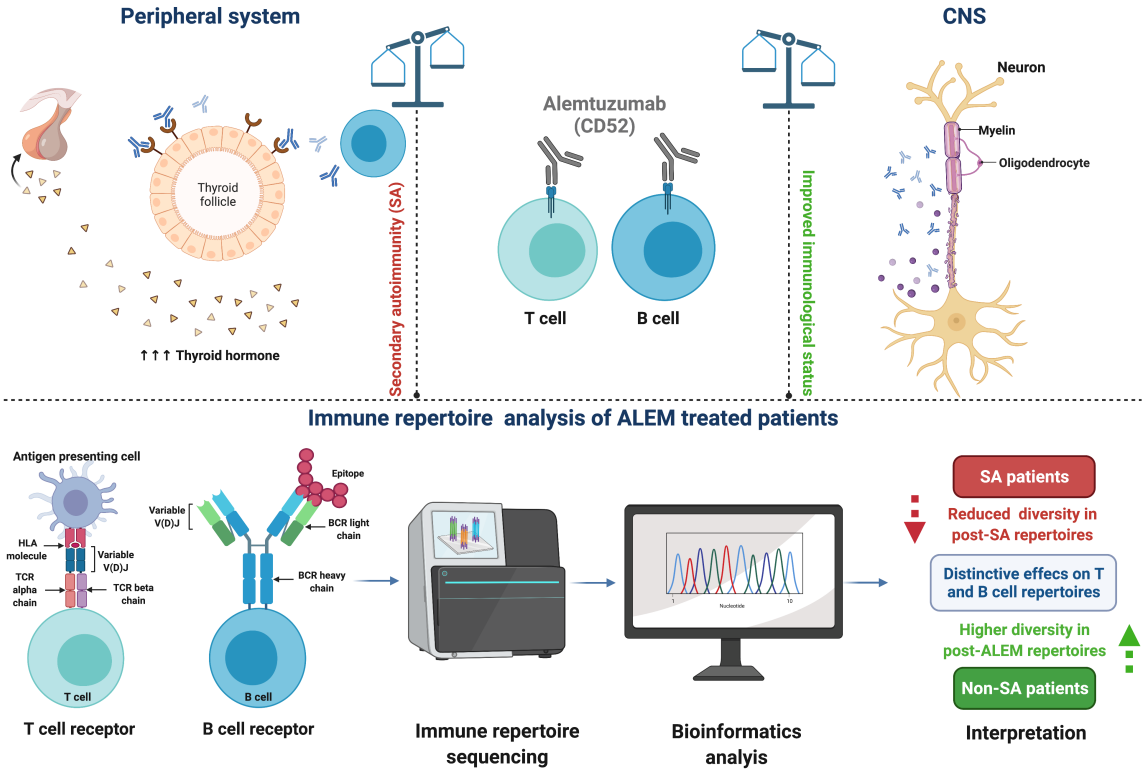

Alemtuzumab (ALEM) has distinctive effects on T cell and B cell repertoires. SA-secondary autoimmunity (Graphic is created with BioRender.com).

Introduction

Multiple sclerosis (MS) is the most common chronic inflammatory disease of the central nervous system (CNS) and characterized by inflammatory infiltrates, demyelination and axonal damage *(1)*. MS commonly affects young adults, with an onset between 20 and 40 years of age, and has a higher prevalence in women *(2)*. In most patients (80-90%), the first clinical manifestation (clinically isolated syndrome, CIS) and early disease course of MS is experienced as reversible episodes of neurological deficits known as relapse, usually lasting for days or weeks, followed by partial or complete remission (relapsing remitting MS, RRMS) *(1)*. In later disease stages, a significant proportion of RRMS patients continuously accumulate neurological disability, with or without superimposed relapses (secondary progressive MS, SPMS) *(3)*. A distinct population (10-15% of MS patients), often above 40 years of age and without a clear gender bias in prevalence, develop gradual worsening of neurological function from onset (primary progressive MS, PPMS) *(3)*. Current treatment strategies for MS focus on the management of symptoms and the use of disease modifying drugs, the latter aiming to reduce the frequency of relapses and to slow the progression of disability. Several disease modifying agents have been developed and approved for the treatment of MS patients within the last decades *(4)*. In recent years, a number of monoclonal antibodies targeting and depleting defined lymphocyte populations have been approved for the treatment of multiple sclerosis and others are under development. Among these therapeutic monoclonal antibodies, alemtuzumab (LEMTRADA®) is a recombinant, humanized, monoclonal IgG1 kappa antibody targeting the cell-surface glycoprotein CD52. Alemtuzumab (ALEM) induces both antibody-dependent cellular cytotoxicity (ADCC) and complement-dependent cytotoxicity (CDC), and activates pro-apoptotic pathways in CD52-expressing cells *(5)*. Clinical and radiologic data from clinical trials and long-term observational studies, indicate that ALEM induces a marked immunomodulation related to the depletion of circulating T and B lymphocytes *(5)*. Following alemtuzumab treatment, the re-population of the peripheral blood compartment with T and B lymphocytes is thought to lead to a re-balancing of the immune system *(6)*. The dynamics of recovery of lymphocyte sub-populations vary: B cells recover faster than T cells, with CD4+ and CD8+ T cells taking up to 35 and 20 months, respectively *(7)*. One study suggested that the peripheral CD4+ T cell recovery can be used to predict the return of the disease activity after ALEM treatment in MS patients *(8)*. During the period of the re-population of immune cells, a significant percentage of patients experience new, secondary autoimmunity *(9)*. The peculiar reconstitution of the B

cell compartment has been suggested to be the one of the main reasons behind the development of secondary autoimmunity. B cell depletion followed by hyper population of B cells, in a phase with lowered T cell regulation, as well as the hyper population of naïve B cells in association with long-lasting depletion of memory B cells, could be the key factors in the development of autoimmunity in an individual with genetic susceptibility for autoimmunity *(10)*. Moreover, the recovery of T cells after ALEM treatment stems from proliferation of mature lymphocytes that escape depletion, and a peripheral expansion that could promote immune cell populations that respond to self-antigen *(11, 12)*.

We hypothesize that alemtuzumab treatment leads to a "reprogramming" of the auto-aggressive immune system in MS. This study aims to characterize longitudinal changes in the clonal compositions of patients' peripheral lymphocyte repertoires before and during ALEM treatment, to better understand the beneficial properties and potential side effects of this drug.

Material and methods

Study design

Details of the study design are described in figure 1.

Patients and biomaterials

Peripheral mononuclear blood cells (PBMCs) from multiple sclerosis patients and untreated controls were isolated and cryopreserved at the Department of Neurology, Westfälische Wilhelms University of Münster, Germany. Longitudinal PBMC samples from twelve patients with MS, acquired prior to and up to 40 months after alemtuzumab (Lemtrada®, Genzyme) treatment, three untreated MS controls (up to 14 months interval) and two healthy controls (up to 15 months interval) were included in this study. Among the 12 alemtuzumab treated patients, four patients (Patient 9_6666, Patient 10_0063, Patient 11_4434 and Patient 12_2789) developed secondary autoimmunity (SA) after the 2nd or 3rd ALEM cycle; one patient (Patient 3_4292) developed paradox disease reactivation (PDR) at month 24 (after 2nd cycle). Male to female patient ratio was 5:7, aged between 26 and 50. Some alemtuzumab treated patients had previously received other treatments including beta interferons (IFNs), fingolimod, natalizumab, mitoxantrone, teriflunomide, and copaxone. The detailed clinical data of the patients is shown in table 1. Peripheral blood mononuclear cells (PBMCs) were isolated using Ficoll-paque density centrifugation and cryopreserved in liquid nitrogen using standard protocols.

Standard protocol approvals, registration, and patient consents

This study was approved by the local ethics committee. All donors gave written informed consent.

Flow cytometry

Using a MoFlo XDP High-Speed Cell Sorter (Beckman Coulter) of the Heinrich Heine University Düsseldorf (core facility “Biomedical Research Center, BMFZ”), the following sub-populations were isolated from each PBMC sample after thawing, appropriate multicolor antibody staining and live gating: CD4+ T cells (CD3+CD4+), CD8+ T cells (CD3+CD8+), naïve B cells (CD19+CD27-IgD+), and memory B cells (CD19+CD27+IgD+/-). Sorted cells were collected in tubes containing 0.75 ml of Trizol reagent (Invitrogen) for immediate RNA conservation.

TCR beta-chain and IG-heavy chain library preparation

Total RNA was isolated from documented numbers of sorted cells (maximum 200,000/sub-population) using a standard Trizol protocol. The first-strand cDNA synthesis was performed using the anchored switch 5' rapid amplification of cDNA ends (5'RACE) PCR based commercial SMARTer® RACE 5'/3' Kit (Takara Bio). Based on recommendations in the SMARTer Human TCR a/b and BCR IgG IgM H/K/L profiling kit (Takara Bio) user manual, two rounds of PCR were performed in succession to amplify cDNA sequences corresponding to the variable regions of TCR-β/IGH transcripts. The first PCR (amplifying TCR-β transcripts from CD4+ or CD8+ T cells; IGH transcripts of IgD, IgM or IgG isotypes from memory B cells; and IGH transcripts of IgD or IgM isotypes from naïve B cells) uses the first-strand cDNA as a template and includes a forward primer (10 μM) with complementarity to the SMART sequence (5' RACE region), and a reverse primer that is complementary to the constant region of the corresponding TCR-β/IG-H. By priming from the 5' RACE region and the constant region, the "touch down" first PCR round (2 cycles at 94°C for 30 sec and 72°C for 2 mins; touch down 2 cycles at 94°C for 30 sec, 70°C and 72°C for 1 min each; touch down 2-10 cycles at 94°C for 30 sec, 68°C and 72°C for 1 min each) specifically amplifies the entire variable region and a considerable portion of the constant region of TCR-β/IG-H cDNA. After the first PCR, amplicons were purified using Ampure magnetic beads (Beckman Coulter). Using the purified first round amplicons as templates, the second PCR round (30 cycles at 94°C for 30 sec, 68°C for 1 min and 72°C for 1 min) was performed to amplify the first round amplicon (semi-nested PCR) and add adapter and index sequences compatible with the Illumina sequencing platform, which allows for multiplexing of up to 96 samples in a single flow-cell lane. Amplicons resulting from the 2nd round PCR were recovered from 2% agarose gels using the QIAquick gel extraction kit (Qiagen). The concentration of amplicons eluted from excised gel fragments, containing the amplified TCR-β-chain or IG-H-chain libraries, was measured on a Qubit Fluorometric Quantification System (Invitrogen). Samples were diluted to a concentration of up to 12nM. Considering the initial cell count of every single library, the amplicons of second round PCR were pooled proportionally without changing the molarity. The pooled library was cleaned using Ampure magnetic beads (Beckman Coulter) and quantified using the KAPA Library Quantification kit according to the manufacturer's instructions (Kapa Biosystems). Each library was sequenced from both sides using the Miseq Reagent Kit v3 (600-cycle, Illumina). Before sequencing, 12.5% PhiX (1.25 pM PhiX) were spiked into each final library pool to increase sequence diversity/cluster

differentiation, and eventually, data quality. Libraries were denatured and a final pooled library (10 pM) was further processed for high throughput sequencing (Illumina MiSeq).

Sequencing of TCR-β and IG-H repertoires and bioinformatics analysis

As outlined above, libraries containing TCR-β-chain and Ig-H-chain repertoires were paired-end sequenced on the MiSeq Illumina sequencing platform in a 2 x 300 bp modality at the Institute of Transplantation Diagnostics and Cell Therapeutics, or at the Department of Gynecology of the Medical Faculty of the Heinrich Heine University Düsseldorf, Germany. Approx. 25 million sequence reads were generated per Illumina Miseq run. Raw sequence reads were processed using the MiXCR software pipeline (https://milaboratory.com/software/mixcr/) *(13)*. MiXCR pre-processed data were post-analyzed by using VDJtools to evaluate clonal expansions, TCR-β/IG-H repertoire diversity estimation, clonotype overlap, clonotype tracking or variable-joining (V-J) segment pairing (https://milaboratory.com/software/vdjtools/) *(14)*. VDJdb CDR3 database was used to identify known CD8+ T cell receptor antigen specificities *(15)*.

Statistics

All graphics were generated using R (version 3.6, https://www.r-project.org/), R studio (https://www.rstudio.com/), Prism (version 8.0) and Microsoft Excel. Statistical data were analyzed by IBM SPSS software (https://www.ibm.com/analytics/spss-statistics-software). Statistical significance was set at 5% ($P \leq 0.05$). Measurements expressed as mean (M) ± standard error of the mean (SEM). To evaluate the diversity of TCR/BCR V-beta/H-chain CDR3 sequences in patients and untreated controls 1) the number of clonotypes (ChaoE-diversity); 2) d50 index (recently developed immune diversity estimate); 3) "clonal richness" as reflected by a) the number of specific V-J pairings and b) the Chao1 index (diversity estimator); 4) "clonal evenness" as reflected by the similarity of the frequencies of V-J pairings to each other; 5) the Shannon Wiener index mean, which has been used widely in antigen receptor diversity analysis, 6) unique clonotypes (%), and 6) the frequency of the most abundant "Top10" clones were determined. The non-parametric Wilcoxon signed-rank test was used to compare the number of clonotypes, d50 index, Chao1 index mean, Shannon Wiener index mean, unique clonotypes (%), frequency of top 10 clones pre- and post-treatment among patients. The non-parametric Mann-Whitney U test was used to compare the expansion of top 100 clones in alemtuzumab treated non SA and SA patients.

Results

Change of lymphocyte populations before and following alemtuzumab treatment

Alemtuzumab is a humanized monoclonal antibody specific for CD52, a surface molecule that is expressed at high levels on T and B lymphocytes *(16)*. CD8+ T lymphocytes (CD3+CD8+), CD4+ T lymphocytes (CD3+CD4+), naïve B lymphocytes (CD19+CD27-IgD+), and memory B lymphocytes (CD19+CD27+IgD+/-) were sorted from PBMC of 12 patients (up to four different time points each) and five untreated controls (two time points each) ***(Figure 1)***. Representative flow cytometry data and sorting strategy of CD8+ and CD4+ T cells, and naïve and memory B cells of one patient's PBMC (before ALEM treatment) is shown in ***figure 2 (a)*** and changes of lymphocyte populations before and during ALEM treatment of a representative patient are depicted in ***figure 2 (b)***. Longitudinal FACS analysis data confirmed a strong reduction of the relative proportions of CD8+ and CD4+ T lymphocytes, and memory B lymphocytes after each ALEM cycle. In contrast, a relative increase of the naïve B cell population was noticed following the treatment. In untreated controls the relative proportions of FACS sorted lymphocyte subpopulations remained comparatively stable over time (data not shown). After the initial depletion, we observed a consistent sequence of lymphocyte recovery. The recovery of CD19+ lymphocytes was followed by CD8+ and CD4+ lymphocytes after alemtuzumab treatment.

Longitudinal evolution of immune repertoires of T and B lymphocytes after alemtuzumab treatment

Clonotype tracking is a common approach to monitor the evolution of clonotypes of interest. A specific clonotype can be tracked across different time points in pre- and post-treatment repertoires. A frequently used and feasible way for tracking lymphocyte clones in peripheral blood is to focus on the most abundant clonotypes (e.g., 25%), thus avoiding "background noise" from less frequent clones *(17–19)*. Clonotype tracking data from alemtuzumab treated patients and untreated controls suggest that CD8+ and CD4+ T lymphocytes, as well as memory and naïve B lymphocytes show differential, yet for each sub-population remarkably characteristic patterns of clonal abundance and clonal persistence over time. To determine how the abundance of individual clones evolved as a result of ALEM treatment, each clone was assigned to one of 5 classes: ablated (removed), depleted (reduction), persistent, expanded, or newly appearing/non-persistent clones.

a) Strongly expanded and persisting clones dominate CD8+ T cell repertoires

To monitor the evolution of immune repertoires we first generated clonotype abundance stack area plots to visualize the relative abundance of up to 100 top clonotypes on stack ***(Figure 3)***. In this type of visualization, persisting clones are color coded according to their relative abundance: Common persister clones are represented by stacks with individual colors and the thickness of each stack correlates with its relative abundance at the time point indicated. Less frequent persisters are summarized in light grey. The fractions of the CD8+ T cell repertoire composed of non-persisting clones are shown in dark-grey/black. As shown in ***figure 3***, the CD8+ T cell compartments of most ALEM treated patients as well as untreated controls are dominated by strongly expanded, persisting T cell clones, thus many of the top clones, which were present at baseline not only persisted but also expanded over ALEM treatment. In untreated controls, the relative abundance of persisters remains remarkably stable over time (as documented by the longitudinal analysis of PBMC samples taken up to 15 months apart). In alemtuzumab treated patients, both further increase/expansion (particularly between first and second ALEM treatment cycle), as well as the reduction of persisting clones can be observed. However, most expansion is observed after first ALEM treatment cycle. More than 50% of the most abundant clones persisted over time, and dominated the CD8+ T lymphocyte compartment. Abundant CD8+ T cell clones, which were present before ALEM treatment expanded and occupied a major part of homeostatic space in the post-ALEM treated TCR repertoire. In patients who did not develop secondary autoimmunity (non-SA patients), the CD8+ TCR repertoire was dominated by persisting huge clones in 1 out of 8 patients (Patient 3_4292) and fluctuating abundance of residual persisting, non/less-dominant clones were also observed. Remarkably, Patient 3_4292 developed paradox disease reactivation (PDR) at month 24. In contrast, persisting “big clones” dominated the CD8+ TCR repertoire in 3/4 patients who developed secondary autoimmunity (SA patients). The expansion of these persisting abundant clones was comparatively higher *in these* three SA patients and 1 non-SA patient than other seven non-SA patients ***(Figure 3)***.

b) Newly generated low-abundant clones form CD4+ T cell repertoires

Contrasting CD8+ TCR repertoires, high numbers of low abundant, non-persisting clones predominate CD4+ TCR repertoires of all untreated controls and most ALEM treated patients. In ALEM treated patients both expansion and reduction of persisting clones were noticed. Of note, more clonal expansion was observed after the first treatment cycles than after the second. Strikingly, and similar but less pronounced compared to the corresponding CD8+

populations, after the first ALEM cycle temporary expansion of persisting clones was observed in the CD4+ T lymphocyte compartment of the same 3/4 SA patients and 1/8 non-SA patient (Patient 3_4292, who developed PDR) as we described in Figure 3 for CD8+ T lymphocyte compartments ***(Figure 4)***.

c) More clones persist in CD8+ than CD4+ TCR repertoires

As indicated above, the expansion pattern of persisting abundant clones (up to top 100 clones) was significantly more pronounced in the CD8+ than in the CD4+ T cell compartments. Accordingly, persisting CD8+ T cell clones of high abundance occupied a large volume of the CD8+ TCR repertoires, whereas top abundant CD4+ clones (up to top 100 persisting clones) constituted less than 10% of the CD4+ TCR repertoire volumes in both ALEM treated patients and untreated controls ***(Figure 5)***.

Next, we created joint clonotype abundance Venn diagrams, which visualize a union of all clonotype variants in all samples that match under the specific criteria used (e.g. identical CDR3nt and V segment), their samples of origin and corresponding abundances *(14)*. Joint clonotype abundance data give an overview of the number of clones shared between different time points vs. the dynamic change of the repertoire ***(detailed explanation about the graph in supplementary figure 1)***. The total number of clones in the CD4+ TCR repertoire was higher than the CD8+ TCR repertoire in both, untreated controls and ALEM treated patients. Conversely, the proportion of persisting vs. the total number of clonotypes (shared clonotypes at different time points) was significantly higher ($P < 0.05$) in CD8+ TCR repertoire than CD4+ TCR repertoire ***(Figure 6-7)***.

To visualize clonal evolution over time we generated clonotypes tracking heatmaps. Clonotype tracking heatmap data of untreated controls showed a remarkable stability of persisting CD8+ T cell clones over time, with some changes in abundance mostly among less frequent (*green/blue*) persisting clones (***Figure 8 and supplementary figure 2)***. In contrast, ALEM treatment was followed by severe repertoire perturbations, with pre-existing clones disappearing or changing in abundance and new clones appearing/re-appearing over time. Persisting highly abundant clones were also detectable. Alemtuzumab treatment induced expansion of many CD8+ T lymphocyte clones and “reshuffled“ CD8+ TCR repertoires, including some apparent clonal “losses“ (*white areas*), with partial recovery and clonal reappearance over time.

Similar to CD8+ populations, clonotype tracking heatmap data of CD4+ T cells from untreated controls showed a remarkable stability of persisting clones over time, yet with less

abundant top clones and stronger fluctuations in abundance (***Figure 9)***. ALEM treatment also "reshuffled" the CD4+ TCR repertoire, including some apparent clonal "losses", with partial recovery and clonal reappearance over time. Likewise, some CD4+ T cell clonal expansions were observed. We observed a high temporal variation in abundance and persistence of CD4+ T lymphocyte clones ***(Figure 9 and supplementary figure 2)***. Heatmaps and top ten clones tables data clearly showed that especially highly abundant clones (***Figure 8, heatmaps: red arrows, supplementary table 1***: Top ten CD8+ T cell clones, persisting clones colored, occupied up to 85 % of the CD8 repertoire) persist within the CD8+ T cell populations, whereas CD4+ T cell clones showed a high temporal variation in abundance (***Figure 9, heatmaps: red arrows, supplementary table 2***: Top ten CD4+ T cell clones make up less than 5% of the CD4 repertoire, with exceptions in SA and PDR patients; no/few „colored" clones). Therefore, highly abundant clone distribution and their persistence were significantly higher in CD8+ than CD4+ T lymphocyte clones.

d) Newly generated, expanded, but mostly non-persisting clones characterize memory B cell repertoires

In contrast to previously mentioned T cell populations, clonotype abundance stack area plot of IgG+ memory B cell compartment showed expanded clones, few of which persisted over time however, both in untreated controls as well as the ALEM treated patients ***(Figure 10, 11)***. Most of the abundant clones are new or exchanged after each treatment. In the IgM+ memory B lymphocyte compartment, expanded clones were also observed in the repertoire, but few of these dominant clones persisted following alemtuzumab treatment (Data not shown); even fewer dominant clones persisted in the IgD+ memory BCR repertoires, both in treated patients and untreated controls (Data not shown). Nonetheless, the topmost clonal composition in the IgG+, IgM+ and IgD+ memory B cells repertoires was relatively stable in untreated clones, though there was no persisting IgG+ memory B cell clones in two untreated controls.

Joint clonotype abundance data of IgG+, IgM+, and IgD+ memory B lymphocyte population showed that few clones (below 1%) overlapped between two-time points and even fewer clones among three-time points. In IgG+ memory BCR repertoire more than half of the non-SA patients (5/8) showed no persisting clones among three-time points, however, all four SA patients showed very few persisting clones (< 0.1%) among three-time points (Data not shown).

Clonotype tracking heatmap data showed that ALEM treatment induces clonal expansion of a few IgG+ and IgM+ memory B cell clones, and even fewer IgD+ memory B cell clones.

Alemtuzumab treatment also "reshuffled" the IgG+, IgM+ and IgD+ memory B cell repertoires, including some apparent clonal "losses", with partial recovery over time ***(IgG+ memory BCR repertoires data in Figure 11)***. Very few clones persisted following ALEM treatment. In untreated controls, overlapping clones were relatively stable in frequency over time. Remarkably, however, one healthy control and one untreated MS control did not show any persisting IgG+ memory B lymphocyte clones over time.

We assume that autoantibody clones which could be responsible for developing SA might appear after ALEM infusion. To uncover the autoantibody clones, we tracked IgG+ memory B cell clonotypes before and after development of secondary autoimmunity. We discovered that the frequency of the most abundant persisting clone was greater after the development of secondary autoimmunity in all four SA patients and each most abundant persisting clone was completely absent before the treatment ***(Figure 12)***. Of note, post-ALEM repertoires are mostly composed of newly generated and non-persisting, but comparatively high abundant memory B cell clones.

e) Naïve BCR repertoires are composed of newly generated low-abundant, mostly non-persisting clones

Clonotype abundance stack area plot of IgM+ and IgD+ naïve B lymphocytes showed the naïve BCR repertoires are composed of a large number of very low-abundant clones in both untreated controls and ALEM treated patients. Very few persisting clones (less than 0.1 %) were observed in treated patients and untreated controls. The naïve B cell repertoires are dominated by new clones after each alemtuzumab cycle. Moreover, in untreated controls the repertoires are also dominated by new clones. In contrast to the memory B cell compartment, ALEM treatment was not followed by clonal expansions within the naïve B cell receptor repertoires ***(IgM+ naïve B cell repertoires data in supplementary figure 3)***. From joint clonotype abundance data of IgM+ and IgD+ naïve B cell population, it is shown that only one third of patients (4/12) showed overlapping clones among all three-time points, but the number of overlapping clones was very few (only 1-2 clones). Though there are many clones (Up to 82000 clones) present at each time point, only a few clones (< 30 clones - less than 0.1%) persisted at two-time points in treated patients. Untreated controls also showed similar patterns of results (data not shown). Clonotype tracking heatmap data also confirmed that very few clones persisted over time and ALEM treatment "reshuffled" the naïve BCR repertoire, including some apparent clonal "losses", with partial recovery and clonal apparency over time. Nevertheless, a few clones persisted and the frequency of the persister clones was

relatively steady in untreated controls ***(IgM+ naïve B cell repertoires data in supplementary figure 4)***.

Impact of alemtuzumab treatment on the clonal composition of highly abundant T cell clones

Next, we explored the effects of ALEM treatment on the clonal composition of T and B cell receptor repertoires by three-layer donut chart ***(detailed explanation of the chart in supplementary figure 5)***. In the CD8+ TCR repertoire, highly abundant clones (top ten clones) either expanded or contracted following treatment, while the top ten clonal distribution was unchanged in untreated controls. However, the top ten CD8+ T cell clones occupied a large volume of the repertoires in both treated patients and untreated controls ***(Figure 13)***. In the CD4+ TCR repertoires, some expansion of the top ten clones was observed predominantly in SA patients, though they occupied relatively small volumes of the CD4+ T cell repertoires ***(Figure 14)***. After each ALEM cycle, most of the highly abundant clones (top 10 clones) persisted in the CD8+ T cell receptor repertoires, while very few top clones persisted in the CD4+ TCR repertoires ***(Supplementary table 1 and 2)***. Interestingly, compared to non-SA patients, more CD8+ and CD4+ TCR top clones persisted - especially post-ALEM treatment - in SA patients repertoires, and one non-SA patient who developed side effects. Moreover, in the CD8+ TCR repertoire of ALEM treated patients, the tendency of the persistence of the top ten clones was higher after ALEM treatment ***(Supplementary table 1)***. In untreated controls, most of the top 10 in the CD8+ TCR repertoires also persisted over time in, while there were no overlapping top 10 clones detected CD4+ TCR repertoires ***(Supplementary table 1 and 2)***.

In both CD8+ and CD4+ TCR repertoires, we observed a statistically significant ($P < 0.05$) expansion of the top 10 clonal volume after ALEM cycle 1. On the contrary, there was no significant expansion of the top 10 clonal distributions in untreated controls ***(Figure 15)***. Furthermore, the top ten CD8+ T lymphocyte clones occupied significantly higher ($P < 0.05$) repertoire volumes than the top ten CD4+ T lymphocyte clones within their corresponding populations in both ALEM treated patients and untreated controls ***(Figure 16)***.

Moreover, in both CD4+ and CD8+ TCR repertoires, a higher tendency of expansion following alemtuzumab treatment was observed in 3 of 4 SA patients as compared to non-SA patients ***(Figure 13 and supplementary table 1; Figure 14 and supplementary table 2)***, and in the one non-SA patient who developed PDR. “Top ten“ clones occupied only a very small percentage (less than 5% of the CD4+ TCR repertoire) of CD4+ T cell receptor repertoires in

7/8 non-SA and hardly persisted within the "Top ten" group over ALEM treatment (exception is Patient 3_4292 who developed PDR). In contrast, "Top ten" clones occupied a larger volume of the repertoire (5-30% of the CD4+ TCR repertoire) in 3/4 of SA patients and one non-SA patients who developed PDR, and relatively more clones persisted within the "Top ten group" over ALEM treatment ***(Figure 14 and supplementary table 2)***. Similar trends were observed in the CD8+ TCR repertoires ***(Figure 15 and supplementary table 1)***. It is also noticeable that the top 20% clones accounted for up to 90% of the entire repertoire of treated patients and untreated controls in the CD8+ T cell population, whereas, in the CD4+ T cell population, the top 20% clones occupied less than 60% of the repertoire ***(Figure 13 and 14)***.

In general, persisting clones (green) make up larger proportions of CD8+ T cell repertoires than of CD4+ T cell repertoires ***(Figure 17a, b)***. Already after the 1st alemtuzumab cycle, in SA patients, these persisting clones occupied significantly larger proportions of both, the CD8+ ***(Figure 17a, upper panel)*** and CD4+ TCR ***(Figure 17b, middle panel)*** repertoires as compared to non-SA patients. On the other hand, new clones (blue) occupied the majority of the repertoire volumes in non-SA patients. Investigating the dynamics of the cumulative volumes of the "Top 100" persisting T cell clones over time, we detected further expansion, as well as the reduction of individual persisting clones, in both $CD8^+$ and $CD4^+$ TCR repertoires of ALEM-treated patients ***(Figure 18)***. In general, the strongest expansions were observed after the first ALEM infusion course. However, strong, significant expansions of persisting "Top 100" $CD8^+$ (***Figure 18b,e***) and $CD4^+$ T cell clones (***Figure 18d,f***) could only be observed in SA patients.

Alemtuzumab treatment effect on the clonal composition of highly abundant B cell clones

In IgG+, IgM+, and IgD+ memory B cell receptor repertoires, the most prominent clones (top 10 clones) both expanded and contracted over ALEM treatment, whereas the top ten clonal distributions were quite steady in untreated controls ***(Figure 19)***. Surprisingly, only very few expanded clones persisted over time in both treated patients and untreated controls, in line with the appearance of mostly new clones at each time point ***(Supplementary table 3)***. The top ten IgG+ memory B cell clones occupied up to 60 % of the IgG+ memory BCR repertoire, whereas the top ten IgM+ and IgD+ memory B cell clones constituted less than 40% of the repertoire volume in both treated patients and untreated controls (Data not shown). It was also noticeable that the top 20% of IgG+ memory B clones constituted higher volumes of the

corresponding repertoires than that of IgM+ and IgD+ memory B cell clones. There were very steady, but non-persistent top 10 clonal distributions of IgG+, IgM+, and IgD+ memory B lymphocytes in untreated controls.

Within IgM+ and IgD+ naïve B cell receptor repertoires, we did not observe clonal expansions or persistence, irrespective of ALEM treatment. The top ten clones occupied tiny volumes of the repertoire (less than 5%) in both patients and controls ***(Supplementary figure 6)***. Moreover, the top 20% of the naïve B cell clones constituted around 50% of the entire repertoire, which is much lower than the top 20% memory B lymphocyte clones constituted ***(Supplementary figure 6)***. Interestingly, a small but considerably higher number of singleton and doubleton clonotypes were present in IgM+ and IgD+ naïve BCR repertoires than in other BCR and TCR repertoires.

Furthermore, only a few IgG^+ memory B cell clones persisted after the 1st ALEM cycle (data not shown), which occupy small fractions of the post-ALEM repertoires in both SA and non-SA patients ***(Figure 17c, lower panel)***. Therefore, almost the entire post-treatment IgG+ memory B cell repertoires consisted of new clones (blue).

We did not observe any significant expansions of the very few IgG^+ memory B cell clones persisting over 1st and 2nd ALEM infusion cycle (***Figure 20a-d***). However, as SA peaks around years two to three *(20)* , we analyzed further time points. To correct for the different timing of SA occurrence, PBMCs were sampled approx. 1-3 months after SA diagnosis and 9-12 months before SA (preSA). Comparing repertoire volumes occupied by the "Top 100" memory B cell clones irrespective of their persistence over time, we discovered remarkable expansions only in SA patients (***Figure 20e-f***).

Effect of alemtuzumab on the diversity of the T and B cell receptor repertoires

An appropriate diversity of the immune repertoire is necessary to mount an efficient adaptive immune response *(21)*. VDJ tools derived data was visualized by excel software as three-dimensional V-J usage maps. The X-Y axis of the map reflects the presence of a particular V-J recombination event, the Z-axis reflects its relative frequency/abundance. Two separate metrics - richness and evenness - were used to characterize the diversity of the TCR/BCR repertoires. Richness correlates with the number of specific V-J rearrangements present and the number of clones with unique TCRs/BCRs. A higher richness may indicate high diversity. Evenness reflects how similar the frequencies of V-J rearrangements are to each other. A high evenness corresponds to V-J rearrangements evenly presented in terms of frequency. Low evenness corresponds to a TCR/BCR repertoire dominated by specific V-J rearrangements

that may indicate reduced diversity. So, low evenness relates to a TCR/BCR repertoire dominated by certain specific CDR3 sequences. To further quantify TCR and IG repertoire diversities, we in addition calculated singleton or unique clonotype frequencies, the Shannon Wiener index mean, the d50 index mean, the number of clonotypes, and the Chao1 index mean as measures. The unique clonotype frequency is an important factor in estimating the total repertoire diversity *(22)*. The Chao1 diversity estimator is used to calculating the frequency of unique clonotypes. The increasing frequency of unique clonotypes corresponds to higher richness. The Shannon Wiener index (Shannon index), which is a function of both the relative number of clonotypes present and the relative abundance or distribution of each clonotype, is used to calculate repertoire diversity *(23)*. It has been used widely in antigen receptor diversity analysis *(24)*. It accounts for both richness and relative abundance (evenness) of the TCR V-beta/IGH CDR3 sequences present in each sample. The larger the Shannon diversity index is, the more diverse the distribution of the TCR V-beta/IGH CDR3 sequences *(17)*. Furthermore, to facilitate the comparison of diversities easier and to analyze diversity statistically, we used the d50 index mean. The d50 index is a recently developed immune diversity estimate. In TCR and BCR repertoires, it is the percentage of distinct V-beta/V_H segments or CDR3 sequences making up half of the V-beta/V_H or CDR3 sequences in a population. It is the calculated percentage of dominant unique clones, accumulative reads, which make up for 50% of the total CDR3 sequences (ranging, in theory, from 0 to 50). D50 has been used to compare the degree of clonal expansion or clonal dominance. The d50 value of a specific repertoire is positively related to ist diversity *(24, 25)*.

a) Limited numbers of expanded V-J combinations dominate CD8+ TCR repertoires

To visualize repertoire diversities, we employed 3D histograms of V-J usages. 3D histograms of V-J usages (i.e., the combination of any one of 54 V genes with any one of 13 J genes) indicate major changes of V-J preference in the CD8+ TCR repertoire due to ALEM treatment. V-J usages of CD8+ TCR repertoires visualized the increasing relative dominance of a limited number of V-J combinations under ALEM treatment, contrasting the relative homogeneous V-J usage distribution in untreated controls ***(representative data in figure 21)***.

In secondary autoimmunity patients the frequency of the dominant V-J combinations was higher than that of non-SA patients in the CD8+ T cell compartment. Strikingly, in all SA patients certain V-J combinations gained dominance after the 1st ALEM cycle and persisted as one of the top V-J combinations after the following infusion cycle ***(Figure 22)***. However, in most of the non-SA patients (7/8 patients) we did not observe such dominant V-J usages

after the 1st ALEM cycle. Nevertheless, similar to SA patients one non-SA patients who developed PRD showed that certain V-J usage gained dominance after cycle 1 and persisted as one of the top V-J usages in the following cycles ***(Figure 22).*** Few of the top 10 V-Beta segments persisted following treatment, but the frequency was not stable in all treated patients, while in untreated controls, persistency and frequency of top 10 V-beta segments were relatively stable over time (Data not shown). In addition, the V-beta segments can be tracked in spectratype V plots, which display information about CDR3 length distribution of clonotypes from top variable (V) segment families. From CDR3 length distribution for variable (V) segment families, we observed that highly abundant V-beta segments were scattered among the clonotypes with different CDR3 lengths, but often certain big clone comprises a specific V-beta family, which drives to become the most abundant V-beta gene. The CDR3 length distribution for V segment families was similar to a Gaussian distribution.

b) CD4+ TCR repertoires are composed of homogeneous and evenly distributed V-J combinations

3D histograms of V-J usages (i.e., the combination of any one of 54 V genes with any one of 13 J genes) showed a relatively homogeneous and balanced distribution of V-J combinations before/under ALEM treatment (predominantly in non-SA patients) in CD4+ T lymphocyte populations ***(representative data in figure 23)***. In post-ALEM repertoires, evenly distributed V-J usage was observed in most of the non-SA patients, however certain dominant V-J pairs were seen in 3/4 of secondary autoimmune patients ***(Figure 24)***. In untreated controls we observed a homogeneous and very stable usage of top V-J combinations, thus representing high richness and evenness ***(representative data in figure 23)***. Furthermore, in ALEM treated patients and untreated controls most of the top 10 V-beta signatures persisted over time and their frequency was relatively stable. Remarkably, TRBV5-1 is the most overrepresented V-beta segment in almost all patients and controls. Interestingly, TRBV5-1 is evenly combined with various J segments, without a predominant TRBV5-1-BJ but many non-abundant TRBV5-1-BJ combinations ***(representative data in supplementary figure 7)***. From CDR3 length distribution of the V segment families, it was also observed that top V-beta usage was scattered among the clones with different CDR3 lengths. The CDR3 length distribution for V segment families was similar to a Gaussian distribution. ***(representative data in supplementary figure 8)***.

c) Consequences of alemtuzumab treatment on V-J recombination of B cell populations

Next, we investigated V-J usages of the memory and naïve B cell receptor repertoires. 3D histograms of VH-JH usages (i.e., the combination of any one of 44 VH genes with any one of 6 JH genes) visualization in IgG+, IgM+, and IgD+ memory B lymphocyte population showed expansion or contraction of the frequency of V-J pairs in post-ALEM treatment but mostly new V-J pairs appeared after each ALEM cycle ***(representative data in figure 25)***. In untreated controls, the frequency of overall VH-JH usage was stable, though many new VH-JH pairs appeared over time ***(representative data in figure 25)***. Notably, certain dominant VH-JH pairs were spotted at baseline, while the frequency of these VH-JH combinations decreased dramatically after the first ALEM cycle in all four patients who developed secondary autoimmunity ***(Figure 26).*** However, this occurrence was only observed in the IgG+ memory B cell compartment. Top V-beta usages were scattered among clones with different CDR3 lengths, and the pattern follows statistical sampling / 'Gaussian' distribution. We noticed VH4-39 as one of the most abundant IGH-V genes in MS patients and this V gene also persisted as one of the dominant V genes in post-ALEM treatment.

In IgM+ and IgD+ naïve B cell receptor repertoires, 3D histograms of V-J usages showed a relatively homogeneous and balanced distribution of V-J combinations in treated patients and untreated controls. Top ten V-J usage distributions were stable over time in treated patients and untreated controls, and the relative frequencies of these V-J usages remained remarkably stable. In addition, the abundant IGH-V segments distribution was also very steady, and the frequency also remained stable in both treated patients and untreated controls ***(representative data in supplementary figure 9)***.

d) Higher diversity in post-alemtuzumab TCR and BCR repertoires in non-SA patients

Before statistical analysis, diversity metrics per sample were normalized according to cell count. In CD8+ T cell populations, the d50 index increased significantly after the first ALEM cycle ($P < 0.05$), while in untreated controls the d50 index remained stable over time ***(Figure 27 a-b)***. Moreover, higher Chao1 index, number of clonotypes, and unique clonotypes (%) were observed in post-ALEM repertoires than pre-ALEM repertoires in treated patients, but a steady pattern was observed in untreated controls ***(Supplementary figure 10 a-b, e-f, i-j)***. In CD4+ T cell population, unique clonotypes (%) increased significantly ($P < 0.05$) in treated patients, but it was relatively steady in untreated controls ***(Figure 28 a-b)***. Furthermore, after ALEM treatment we also detected higher Chao1 index, number of clonotypes, and d50 index than in pre-ALEM repertoires in treated patients, however, relatively steady diversity metrics

were observed in untreated controls ***(Supplementary figure 11a-b, e-f, i-j)***. From V-J recombination data, we also observed homogeneous and diverse distribution of V-J pairing combination after ALEM infusions in CD4+ T cell repertoires, which resembles relative homogeneous richness and evenness of the CD4+ TCR repertoires over the treatment.

In IgG+ memory B cell populations, we observed significantly higher ($P < 0.05$) numbers of clonotypes, Chao1 index, Shannon Wiener index, and unique clonotypes (%) after ALEM treatment, whereas in untreated controls pattern were relatively stable ***(Figure 29)***. In IgM+ and IgD+ memory B cell populations, we also noticed higher number of clonotypes, Chao1 index, Shannon Wiener index, and unique clonotypes (%) in post-treatment compared to pre-treatment repertoires, while in untreated controls we observed relatively stable diversity metrics over time ***(Supplementary figure 13 and 14)***. However, we did not notice substantial diversity changes between non-SA and SA patient groups. After ALEM treatment, we observed no significant changes of the diversity metrics in naïve BCR repertoires ***(Figure 30)***. In TCR repertoires, higher diversity and consistent richness and evenness over the ALEM treatment were observed predominantly in non-SA patients. Whereas in memory BCR repertoires a significantly higher ($P < 0.05$) diversity and appearance of mostly new V-J pairs were noticed.

e) Lower diversity in post-secondary autoimmunity TCR repertoires and development of autoimmunity

For both SA and non-SA patients, higher diversities were noticed in CD8+ and CD4+ TCR repertoires after the first ALEM cycle. After the 2nd ALEM cycle, non-SA patients maintained high diversities ***(Figure 27c, 28c, and supplementary figure 10c, g, k and 11c, g, k)***, whereas TCR diversity of SA patients decreased compared to the diversity after the cycle 1 ***(Supplementary figure 12)***. Four patients developed SA after either the 2nd or 3rd ALEM cycles ***(detailed clinical data in Table 1: First manifestation of SA)***. In all four SA patients, we also tracked the diversity metrics including d50 index, number of clonotypes, Chao1 index, and unique clonotypes (%) before and after the development of secondary autoimmunity, and remarkably we discovered that the diversity was less after the patients developed SA compared to pre-SA repertoires in both CD8+ and CD4+ T cell populations ***(Figure 27d, 28d, and supplementary figure 11d, h, l and 12d, h, l)***. However, we did not find a specific trend (decrease or increase) of diversity change after the patients developed secondary autoimmunity in memory BCR repertoires.

Discussion

In this study, we analyzed the longitudinal T cell (TCR) and B cell repertoires (BCR) of 12 MS patients at pre-alemtuzumab and various post-alemtuzumab treatment time points, and 5 untreated controls at two time points. As expected, ALEM rapidly eliminated most circulating CD8+ and CD4+ T cells as well as the memory B cell population. In contrast, the naïve B cell population increased after treatment. Heidt *et al.* also found that alemtuzumab induction therapy results in a long-term shift toward naïve B cells in kidney transplant recipients (KTRs) *(26)*. The lack of effect of ALEM on CD52-negative cells, including bone marrow precursors, may explain the relatively fast increase of naïve B lymphocytes. Cossburn *et al.*, Li *et al.* and Baker *et al.* demonstrated that CD19+ cells were first to recover after alemtuzumab infusion, followed by CD8+ and finally CD4+ T cells *(8, 10, 27)*. Moreover, memory B cell counts remained low throughout 12–48 months post-treatment *(10)*. We observed similar patterns of lymphocyte recovery from all alemtuzumab treated patients.

After immunomodulatory therapy, de novo infections with or reactivation of opportunistic pathogens are common complications *(28)*. These infections are associated with the expansion of pathogen-reactive T cells. CD8+ T cells depletion can therefore be associated with an increased risk of viral infections. Accordingly, Herpes simplex virus (HSV) and varicella–zoster virus (VZV) infections have been frequently observed *(29)*. An increased risk of human papillomavirus (HPV) cervicitis and cytomegalovirus (CMV) infection has also been reported *(30–34)*. Similarly, reactivation of persisting viral infections including cytomegalovirus (CMV) can be observed after hematopoietic stem cell transplantation (HSCT) *(35–37)*. Using the VDJdb CDR3 motif database, we found that most known public CD8+ TCR amino acid sequences recognize cytomegalovirus (CMV), Epstein-Barr virus (EBV) or influenza-A-virus derived epitopes ***(representative CDR3 epitopes motif in supplementary Table 1)***. So, we hypothesized that CMV or EBV specific clones could substantially contribute to the enormous expansions of top CD8+ T cell clones observed after ALEM infusion.

The lymphocyte-depleting humanized monoclonal antibody ‘alemtuzumab’ is assumed to “reconstitute” the immune repertoire of MS patients. From our study, clonal renewal of CD4+ T and memory B cell repertoires including a diversification of the T and B cell repertoires, strongly support a reconstitution of the immune system. Autologous hematopoietic stem cell transplantation (AHSCT) is correlated with enhancement of thymopoiesis (“thymic rebound”),

naïve B and T cell repopulation, TCR and BCR repertoire diversification, and also T and B cell clonal renewal, which provides evidence for reconstitution of the immune system *(20, 38–40)*. These observations also support our assumption that alemtuzumab reconstitutes the immune repertoire of MS patients. In order to specify the effects of ALEM treatment, we analyzed the longitudinal evolution of peripheral blood T and B lymphocyte repertoires. Our observations show that alemtuzumab has distinctive effects on the immune repertoires of lymphocyte subpopulations. Data visualization by clonotype abundance stack area plot, clonotype tracking heatmap, joint clonotype abundance Venn diagram, and top ten clonal composition suggest that CD4+ T cell repertoires were mainly composed of newly generated low-abundant clones, while CD8+ T cell repertoires were majorly restored from highly abundant clones already existing before ALEM treatment. These findings are in keeping with Jones *et al.,* who suggested that T cell recovery after ALEM treatment was driven by homeostatic proliferation (HP) *(11)*. They also observed (predominantly in CD8+ repertoires) that the most common T cell clones before treatment were the ones that expanded afterwards, matching our findings. However, Jones and colleagues mainly relied on CDR3 spectratyping data and TCRβ sequencing (Immunoseq by Adaptive Biotechnologies) with very few alemtuzumab treated subjects. Moreover, we found that the proportion of persisting vs. the total number of clonotypes was significantly ($P < 0.05$) higher in CD8+ than CD4+ TCR repertoires. Post-ALEM repertoires were dominated by persisting (highly abundant) T cell clones in the CD8+ population, yet by non-persisting (low abundant) T cell clones in CD4+ population. Consecutively, the CD8+ top 100 and top ten most abundant clones accounted for substantial volumes of the CD8+ TCR repertoires, while the CD4+ top 100 and top ten most abundant clones made up only negligible portions of the CD4+ TCR repertoires. These findings may reflect that after alemtuzumab treatment CD8+ T cells are more likely to response by homeostatic proliferation than CD4+ T cells. Fortner *et al.* and Workman *et al.* suggested that up-regulation of the inhibitory receptors PD-1 and LAG-3 and prolonged CD95 (Fas) expression may limit CD4+ T cells expansion *(41, 42)*. Muraro *et al.* also demonstrated that even AHSCT did not remove dominant CD8+ clones effectively, and that the CD8+ TCR repertoires were reconstituted by clonal expansion of cells present at pre-treatment *(39)*. Harris and colleagues' 48 months follow-up data of the Muraro *et al.* study showed that the elimination of pre-existing peripheral blood T cell receptor repertoires by AHSCT were robust, however, the ablation of pre-existing CD8+ TCR repertoires was significantly less extensive compared to the CD4+ TCR repertoires *(43)*. In new repertoires reconstituted after AHSCT, Muraro *et al.* did not detect CD4+ clones which were dominant before treatment

(39). In contrast, we found many dominant CD4+ TCR clones also persisted after ALEM treatment, yet only occupied small fractions of the CD4+ T cell repertoire volumes. This might be because of less pronounced CD4+ TCR reconstitution by alemtuzumab than the reconstitution of CD4+ TCR repertoire by AHSCT. As complement-mediated T-cell subset killing is proportional to the surface expression of CD52 *(44)*, this suggests that a certain minimum level of CD52 expression is required for this killing to occur. CD4+ T cells express approximately twice the amount of surface CD52 compared to CD8+ T cells, as a result complement-mediated killing predominates in CD4+ T cells *(44)*. Therefore, we could interpret that ALEM treatment eliminates CD4+ T cells more efficiently than CD8+ T cells in peripheral blood. Our findings suggest that a lower level of CD52 expression in CD8+ T cells may trigger incomplete depletion of dominant CD8+ clones after ALEM infusions, which allows for homeostatic proliferation. On the contrary, higher CD52 expression in CD4+ T cells apparently results in a comparatively higher degree of depletion of CD4+ T cells by ALEM, which may support the generation of new, low-abundant CD4+ T cell clones in post-ALEM treatment.

A more diverse TCR repertoire may reflect better immunological health. van Heijst *et al.* demonstrated that a diverse TCR repertoire is associated with a decreased risk of infection after allogeneic stem cell transplantation for leukemia *(45)*. Muraro *et al.* showed that patients who failed to respond to AHSCT had less diverse TCR repertoires during the beginning of reconstitution process *(39)*. In TCR repertoires, Postow and colleagues found significant differences in richness (observed V-J rearrangements) and evenness (similarity between the frequencies of specific V-J rearrangements) between patients with and without clinical benefit from ipilimumab treatment in metastatic melanoma *(46)*. As mentioned before, two separate metrics, - richness and evenness - were used to characterize the diversity of the TCR/BCR repertoire. 3D histograms of V-J usage in CD8+ T cell repertoires showed a relative dominance of certain V-J combinations under the ALEM treatment, and this observation was less pronounced in non-SA patients. Dominance of certain V-J usages was higher in secondary autoimmunity patients than in non-SA patients. Although ALEM treatment triggered to develop a few dominant V-J pairs in CD8+ TCR repertoires, at the same time it also maintained the persistence of low abundant V-J pairs, particularly in non-SA patients, which are important for providing better immunological status in post-ALEM treatment period. In CD4+ T cell repertoires, mostly homogeneous and diverse distributions of V-J pairing were noticed after ALEM infusions in non-SA patients, resembling relative

homogeneous and consistent richness and evenness of CD4+ TCR repertoires. Furthermore, we observed more TCR diversity in both CD8+ and CD4+ TCR repertoires after ALEM treatment in all patients, whereas there was no notable diversity change in untreated controls. In contrast to non-SA patients, diversity decreased paralleling the development of secondary autoimmunity. Therefore, these observations may correspond to higher diversity in post-treatment TCR repertoires compared to pre-treatment TCR repertoires, predominantly in non-autoimmunity patients.

Jones *et al.* demonstrated in a patient who did not develop secondary autoimmunity that TCR diversity had recovered by month 6, and, at month 12, was higher than before ALEM treatment *(11)*. Our data from all ALEM treated patients indicate that TCR diversities (both CD8 and CD4) increased to levels higher than before ALEM treatment already after the 1st ALEM cycle (by month 4-6), yet continued to increase/raise after the 2nd ALEM cycle (by month 18-24) only in non-SA patients, suggesting that increased TCR repertoire diversity reflects better post-ALEM immunological health.

In memory B cell compartments, top clones of IgG, IgM and/or IgD+ isotypes occupied relatively large volumes of the corresponding memory BCR repertoires. However, we found that most of the dominant IgG+, IgM+, and IgD+ memory B cell clones were not persisting predominantly in ALEM treated patients but also untreated controls, which may resemble that the memory BCR repertoires were hardly affected by ALEM treatment and new clones appeared in post-ALEM repertoires. Sofar, fewer publications analyzed B cell repertoires as compared to T cell repertoires, particularly in MS patients. Pollastro *et al.* demonstrated that the persistence of baseline repertoires 4 weeks after rituximab treatment was associated with subsequent non-response in rheumatoid arthritis patients *(47)*. Hu *et al.* found that the increase of IGH repertoire diversity significantly correlates with better prognosis in avian influenza A (H7N9) virus-infected patients, while IGH repertoires of non-survivors converged to several particular IGH V-J gene pairs *(25)*. In the memory B cell repertoires of non-SA patients, the appearance of new V-J gene pairs after each ALEM cycle and relatively homogeneous V-J pairing distribution mirrored consistent homogeneous richness and evenness of the IGH chain repertoire. In memory B cell repertoires, we also observed higher repertoire diversity after each ALEM cycle than pre-treatment diversity in all ALEM treated patients. Homogeneous richness and evenness of the IGH chain repertoires, relatively new B cell clones, and higher diversity of IGH memory B cell repertoires following ALEM treatment may correlate to a beneficial treatment outcome, particularly in the non-SA patients. Higher BCR repertoire

diversity prior to treatment is very essential for persisting better post-alemtuzumab immunological health. Overall, our TCR and BCR immune repertoire data suggest that predominantly in non-SA patients ALEM treatment helps to improve post-treatment immunological health .

From the naïve B cell population, we found that IgM+ and IgD+ naïve B cell compartments are composed of a large number of very low-abundant clones, and most of the clones were not present after the treatment. Most abundant clones occupied a relatively very small volume of the naïve IGH chain repertoire, and; comparatively higher frequency of singleton and doubleton clonotypes were present than other B and T cell populations. Therefore, our data suggest that ALEM treatment did not induce clonal expansions and persistence of IgM+ and IgD+ naïve B cell clones. Relatively homogeneous and consistent richness and evenness were observed in IgM+ and IgD+ naïve B cell populations in ALEM treated patients and untreated controls. Our finding may refer to the assumption that alemtuzumab treatment did not induce substantial repertoire change in naïve B cell population. B cells development begins in the bone marrow, gradually become mature naïve B cells and migrate via the bloodstream to secondary lymphoid organs *(48)*. Since the anti-CD52 antibody does not express in bone marrow precursor cells, it could be an explanation that ALEM does not have notable effect on naïve B cell immune repertoires.

Alemtuzumab is associated with a high incidence of secondary autoimmunity that restrict constraint its usage *(49)*. Baker and colleagues proposed that hyper population of B cells after the B-cell depletion in the absence of effector T cell regulation, in addition to the hyper population of naïve B cells in association with long-lasting depletion of memory B cells could be the major factors in autoimmunity development in an individual with genetic susceptibility for autoimmunity *(10)*. Moreover, the recovery of T lymphocytes results out of a peripheral expansion and could promote that the immune cell population responds to itself *(12)*. The development of autoantibodies occurs months to years after ALEM administration because it requires CD4+ T cell involvement. CD4+ T lymphocytes regenerate only six months to three years after depletion, with a subsequent delay between B lymphocyte hyperreactivity and development of autoimmunity *(10)*. From our study, three patients developed secondary autoimmunity after 2nd ALEM cycle, and one patient developed SA after 3rd ALEM cycle. In addition, one patient developed paradox disease reactivation (PDR) at month 24 (after cycle 2). Along with the development of secondary autoimmunity, PDR and other rare complications represent potentially life-threatening adverse events associated with

alemtuzumab treatment in multiple sclerosis patients. Recently, Branningen *et al.* and Haghikia *et al.* reported severe paradoxical disease activation following ALEM treatment for multiple sclerosis *(50, 51)*. Branningen *et al.* also proposed that paradoxical disease activation after ALEM is more likely to result from the complex interplay of multiple reconstituting immune cell subsets *(50)*. Moreover, a couple of case reports were published, in which the authors reported disease activation after alemtuzumab those patients switched therapies directly from fingolimod *(52, 53)*, however, in our study the patient who developed PDR had not been treated with fingolimod.

Our TCR and BCR sequencing data provide deeper insights into the longitudinal immune repertories and now support the synthesis of those hypotheses. Consistent with enhanced homeostatic proliferation as a driver for SA, we observed a significantly increased persistence and expansion of $CD8^+$ and $CD4^+$ T cell clones already after the first ALEM course in SA patients. However, occurring not before the second ALEM course, we also detected a remarkable expansion of memory B cell clones only in SA patients. Thus, we hypothesize that alterations in the T cell repertoire provide the basis for delayed B cell-mediated autoimmunity in genetically susceptible individuals.

We also observed that expanded V-J usage is higher in secondary autoimmunity patients than non-SA patients in the CD8+ T cell compartment. In CD4+ T cell repertoires, we also noticed expanded V-J pairs in 3/4 of secondary autoimmune patients. Moreover, following ALEM infusions, all SA patients and one non-SA patient showed higher expansion in their top ten clone distribution in both CD8+ and CD4+ TCR repertoires. From this observation, we speculate that ALEM treatment might be responsible for emerging the expansion of these persisting CD8+ and CD4+ T cell clones in homeostatic space, which might trigger to develop SA or other side effects in these patients. Jones *et al*. also found that T cell homeostatic proliferation leads to the autoimmunity after alemtuzumab treatment *(11)*. Surprisingly, in CD8+ TCR repertoire of all SA patients and one non-SA PDR patient, we observed that certain V-J usage gained dominance in each patient after 1st ALEM cycle and that dominant V-J usage persisted following ALEM infusions. In addition, in IgG+ memory BCR repertoires a highly expanded V-J pair was spotted in the baseline, while the frequency of that V-J pair decreased intensely after 1st alemtuzumab cycle in all four patients who developed secondary autoimmunity. These findings may give an early indication about the possibility who might develop SA or side effects following ALEM treatment. Further investigation with more SA

patients may give deeper insight about the consequences of alemtuzumab treatment and development of secondary autoimmunity.

In addition, we observed higher CD8+ and CD4+ TCR repertoire diversity after each alemtuzumab cycle compared to the diversity of pre-ALEM repertoires in non-SA patients. However, in SA patients the TCR diversity was less in post-autoimmunity repertoires compared to the diversity of pre-autoimmunity repertoires. As mentioned before we also discovered the dominance of certain V-J pairs in CD8+ and CD4+ TCR repertoires of SA and PDR patients, which refer to lower evenness (reduced TCR repertoire diversity). Ruck *et al.* demonstrated that patients who developed secondary autoimmunity (vitiligo) after ALEM treatment have highly increased clonality and reduced CD8+ TCR repertoire diversity compared to healthy controls and treatment-naïve patients *(54)*. However, they analyzed only CD8+ TCR repertoire, while we analyzed both CD8+ and CD4+ TCR repertoires and found reduced diversity after developing autoimmunity. Jones *et al.* found that patients who developed autoimmunity after ALEM showed greater clonal restriction compared to the non-autoimmune cohort *(11)*. Taken together, our findings may reflect that the patients who developed SA have reduced CD8+ and CD4+ TCR repertoire diversity (particularly in post-autoimmunity repertoires) comparison with non-SA cohort.

Thyroid is the most involved organ in alemtuzumab induced autoimmunity, with most analyses reporting an occurrence in 17% to 34% of patients who receive alemtuzumab for MS *(55)*. Graves' disease, which is occurring in 60% to 70% of cases, is the major cause of thyroid dysfunction *(56, 57)*. Other autoimmune conditions are immune thrombocytopenic purpura (ITP) in 3% of cases and anti-Glomerular Basement Membrane disease (GBM) at a much lower frequency *(58)*. In our study, all four patients developed autoimmune thyroid dysfunction, among them three patients developed Graves' disease. We tracked the IgG+ memory B cell clones in pre- and post- autoimmunity repertoires in all four SA patients and found that the frequency of the most abundant persisting clone was higher in post-autoimmunity repertoires and those abundant clones were completely absent at baseline ***(Figure 12)***. We suspect that the frequency of the autoantibody clones, which might responsible for developing autoimmunity expanded after the manifestation of secondary autoimmunity. These findings predict the possible candidates of autoantibody clones for Graves' disease/thyroid autoimmunity in SA patients. Further investigation with more SA patients may give greater insight about generating autoantibody clones and developing autoimmunity in ALEM treated MS patients.

Depletion of switched and non-switched memory B cells could play an important role in the efficacy of ALEM therapy. From flow cyclometric data we found that ALEM strongly depleted memory B cell populations. In the BCR repertoire study, we found that only a few memory B cell clones persisted over ALEM treatment. In addition, we also discovered that very few IgM+ and IgD+ memory B cell clones have undergone class-switch recombination to IgG+ memory B cell clones. The divergent maturation of IgM+ and IgD+ naïve B cell clones into functionally diverse IgM and IgG expressing memory B cell clones were not observed between pre-and post-treatment compartments. However, we only observed the divergent maturation of IgM+ naïve B cell clones into IgG expressing memory B cell clones at the same time point either pre-treatment or post-treatment compartment.

Remarkably, in CD4+ TCR repertoires we detected that TRBV5-1 was the most overrepresented V-beta gene in most of the patients before and following ALEM treatment and untreated controls. Interestingly, this V-beta usage was scattered in diverse clones with distinctive CDR3 lengths and V-J pairs. Davey *et al.* demonstrated that TRBV5-1 and TRBV6-7a genes were consistently overrepresented in the CD4 population *(59)*. Moreover, Shugay and colleagues reported that TRBV5-6 and TRBV5-1 were the variable segments that were significantly overrepresented in MS samples comparing to healthy controls *(14)*, however, we spotted TRBV5-1 as the most abundant variable segment in two healthy controls as well. Owen *et al.* and Baranzini *et al.* reported that VH4–39 was the most frequently expressed VH4 gene in an MS brain sample *(60, 61)*. Surprisingly from peripheral blood samples, we also found VH4-39 as one of the most abundant IGH-V genes in most of the MS patients and following ALEM treatment VH4-39 persisted as one of the dominant IGH-V genes.

In our study, one patient (Pat12_2789) who developed secondary autoimmunity was treated with rituximab and the treatment started after 3rd ALEM cycle. We demonstrated that almost all IgG+ memory B cell clones that were present before rituximab treatment were depleted by the treatment; only two clones persisted following rituximab treatment. Moreover, after rituximab treatment we also noticed reduced richness and evenness of the V-J usage, and top ten clonal expansion of the IgG memory BCR ***(Figure 31)***. Maurer *et al.* also demonstrated that B-cell reconstitution following rituximab therapy is associated with clonal expansion of the IgG memory B-cell compartment *(62)*. Moreover, we performed longitudinal repertoire

analysis in fingolimod and ocrelizumab treated patients. Treatment with oral fingolimod prevents the egress of naïve (CCR7+CD45RA+) and central memory (CCR7+CD45RA-) T lymphocytes but not effector memory (CCR7-CD45RA-) T lymphocytes *(63)*. This result appears to be a consequence of the fact that naïve T cells and central memory cells, but not effector memory cells, express the chemokine receptor CCR7, which induces homing of lymph nodes. As a consequence, these cells recirculate to lymph nodes and sequestered there *(64)*. In fingolimod treated patients, we observed that CD8+ and CD4+ T cell clones expanded over the treatment. Persistence of CD8+ T cell clones is much higher than CD4+ T cell clones. In addition, we noticed in CCR7+CD8+ and CCR7+CD4+ compartment that few clones persisted and expanded over the treatment, whereas comparatively more clones persisted and expanded in CCR7-CD8+ and CCR7-CD4+ compartment (Unpublished data). In both groups (alemtuzumab treated and fingolimod treated patients), CD8+ T cell clones expanded and persisted over the treatment, however mostly alemtuzumab treated patients develop SA. Fingolimod treatment sequesters the autoreactive naïve and central memory T cells in lymph nodes, and may enhance the functionality and frequency of potent circulating regulatory T cells *(64)*. This could be one of the reasons that patients treated with fingolimod do not develop SA unlike alemtuzumab treated patients do. Moreover, we noticed from one ocrelizumab treated patient that CD8+ and CD4+ TCR repertoires were slightly altered by the treatment, however, naïve and memory B cell compartment were immensely altered by the treatment. A few CD8+ and CD4+ T cell clones expanded following ocrelizumab treatment, while rest of the clones remain relatively unchanged. In contrast, most of the clones were depleted by the treatment in memory and naïve B cell repertoires, moreover a few clones survived from ocrelizumab depletion and these clones occupied a large volume of the corresponding repertoires in post-ocrelizumab treatment (Unpublished data). Furthermore, from one alemtuzumab treated SA patient who also treated with rituximab, we found that CD8+ and CD4+ TCR repertoires were relatively stable over rituximab therapy ***(Figure 32 and supplementary table 4)***. Unaffected TCR repertoire might maintain the T cell repertoire balance, thus limits the development of secondary autoimmunity in patients treated with CD20 + B cell-depleting therapies. It is relatively common strategy to treat alemtuzumab induced SA patients with rituximab, and after the treatment patients often cured from secondary autoimmune disease. From our data we demonstrated that stable TCR repertoire and vastly depleted BCR repertoire by rituximab therapy might trigger to overcome the alemtuzumab induced secondary autoimmunity in MS patients. Further research with more

subjects treated with B-cell depleting drugs might give better understanding about the role of combinational B cell-depleting therapies in ALEM treated SA patients.

In addition, methodological limitations must be mentioned. It is important to bear in mind that it is not possible to interrogate the whole immune repertoire in a living person. One limitation of current RNA-seq approaches is reverse transcriptase template switching and false alternative transcripts during cDNA synthesis *(65)*. Another limitation is RNA copy number, which depend on the activation status, and may therefore not be proportional to the number of cells *(66, 67)*. An approach to address this problem is the integration of so-called unique molecular identifiers (UMI), which can be incorporated during cDNA synthesis and provide a way to conclude the original molecule amount from the sequencing data and has been used for TCR and BCR repertoires recently *(68–72)*. However, errors in the UMI itself can again cause an analysis bias after sequencing *(73)*. Nevertheless, we also applied UMI-based cDNA synthesis in a few samples, but the available tools have limitations to analyze the UMI- tagged raw sequences. In addition, PCR artifacts and different levels of amplification can also be a source of bias. However, to overcome the bias as much as possible we considered the initial cell count of every single library, and the amplicons of second round PCR were pooled proportionally without changing the molarity.

In summary, we confirmed a strong decrease of the relative proportions of particularly CD4+, but also CD8+ T lymphocytes and memory B lymphocytes after each alemtuzumab cycle, on the contrary, naïve B cells increase in proportion. We discovered that reconstituted post-ALEM CD4+ TCR repertoires were mostly composed of newly generated low-abundant clones. In contrast, the dominant CD8+ T cell clones were not effectively removed by the treatment, thus the post-ALEM CD8+ T cell repertoires were restored from clones already existing and highly abundant before ALEM treatment. Memory B cell repertoires, particularly in the IgG+ populations, consist of dominant clones, of which hardly any persist over time, even in untreated controls. This repertoire behavior seems hardly affected by ALEM treatment. ALEM treatment did not induce notable repertoire changes in naïve B cell repertoires. Treating one of the four SA patients with rituximab to cope secondary autoimmunity aborted most of the persisting clones. Post-alemtuzumab T and B cell repertoires are more diverse than pre-treatment repertoires predominantly in non-secondary autoimmunity patients, in contrast, secondary autoimmunity patients had reduced T cell repertoire diversity, particularly in post-secondary autoimmunity repertoires. Importantly, SA

patients show persistence and expansion of T cell clones already after the first ALEM course and a delayed expansion of memory B cell clones after the second cycle, which provides a mechanistic explanation for SA development combining current hypotheses. Further immune repertoire study with a larger cohort of SA patients might give deeper insight about the consequences of alemtuzumab treatment and development of secondary autoimmunity.

Acknowledgements

We thank all the patients and healthy controls for participating in this study and permitting us to use their specimens for this research. The authors thank Anna Coordt, Pia Sporkmann, Nora Hinssen, Katharina Raba and Lena Schünemann for excellent technical assistance.

Funding information

This work was largely supported by the Forschungskommission of the Medical Faculty of the Heinrich-Heine-University Düsseldorf (HHU), Germany, Novartis and Sanofi-Genzyme. The funding by Sanofi-Genzyme had no impact on conducted experiments or drafting the content of this manuscript.

Author contributions

SB contributed to designed the research, carried out all experimental procedures, acquired and analyzed all data including bioinformatics and statistical analysis, and wrote the manuscript. TR, SP, CL and NM provided the patients and controls biomaterials and clinical information, and critically revised the manuscript. AR, VB, HW, SV critically revised the manuscript. NG designed the research, wrote the manuscript and supervised the project.

Conflicts of interest

All authors declare no relevant conflicts of interest.

References

1. M. Filippi, A. Bar-Or, F. Piehl, P. Preziosa, A. Solari, S. Vukusic, M. A. Rocca, Multiple sclerosis, *Nat. Rev. Dis. Prim.* **4**, 43 (2018).
2. J. M. Greer, P. A. McCombe, Role of gender in multiple sclerosis: Clinical effects and potential molecular mechanisms, *J. Neuroimmunol.* **234**, 7–18 (2011).
3. S. Klineova, F. D. Lublin, Clinical Course of Multiple Sclerosis, *Cold Spring Harb. Perspect. Med.* **8**, a028928 (2018).
4. D. S. Reich, C. F. Lucchinetti, P. A. Calabresi, D. L. Longo, Ed. Multiple Sclerosis, *N. Engl. J. Med.* **378**, 169–180 (2018).
5. P. Gallo, D. Centonze, M. G. Marrosu, Alemtuzumab for multiple sclerosis: the new concept of immunomodulation, , doi:10.1186/s40893-017-0024-4.
6. L. Klotz, S. G. Meuth, H. Wiendl, Immune mechanisms of new therapeutic strategies in multiple sclerosis—A focus on alemtuzumab, *Clin. Immunol.* **142**, 25–30 (2012).
7. G. A. Hill-Cawthorne, T. Button, O. Tuohy, J. L. Jones, K. May, J. Somerfield, A. Green, G. Giovannoni, D. A. S. Compston, M. T. Fahey, A. J. Coles, Long term lymphocyte reconstitution after alemtuzumab treatment of multiple sclerosis, *J. Neurol. Neurosurg. Psychiatry* **83**, 298–304 (2012).
8. M. D. Cossburn, K. Harding, G. Ingram, T. El-Shanawany, A. Heaps, T. P. Pickersgill, S. Jolles, N. P. Robertson, Clinical relevance of differential lymphocyte recovery after alemtuzumab therapy for multiple sclerosis, *Neurology* **80**, 55–61 (2013).
9. A. J. Coles, E. Fox, A. Vladic, S. K. Gazda, V. Brinar, K. W. Selmaj, A. Skoromets, I. Stolyarov, A. Bass, H. Sullivan, D. H. Margolin, S. L. Lake, S. Moran, J. Palmer, M. S. Smith, D. A. S. Compston, Alemtuzumab more effective than interferon β-1a at 5-year follow-up of CAMMS223 Clinical Trial, *Neurology* **78**, 1069–1078 (2012).
10. D. Baker, S. S. Herrod, C. Alvarez-Gonzalez, G. Giovannoni, K. Schmierer, Interpreting lymphocyte reconstitution data from the pivotal phase 3 trials of alemtuzumab, *JAMA Neurol.* **74**, 961–969 (2017).
11. J. L. Jones, S. A. J. Thompson, P. Loh, J. L. Davies, O. C. Tuohy, A. J. Curry, L. Azzopardi, G. Hill-Cawthorne, M. T. Fahey, A. Compston, A. J. Coles, Human autoimmunity after lymphocyte depletion is caused by homeostatic T-cell proliferation, *Proc. Natl. Acad. Sci. U. S. A.* **110**, 20200–20205 (2013).
12. J. Sellner, P. S. Rommer, Immunological consequences of “immune reconstitution

therapy" in multiple sclerosis: A systematic review*Autoimmun. Rev.* **19**, 102492 (2020).
13. D. A. Bolotin, S. Poslavsky, I. Mitrophanov, M. Shugay, I. Z. Mamedov, E. V Putintseva, D. M. Chudakov, MiXCR: software for comprehensive adaptive immunity profiling, *Nat. Methods* **12**, 380–381 (2015).
14. M. Shugay, D. V Bagaev, M. A. Turchaninova, D. A. Bolotin, O. V Britanova, E. V Putintseva, M. V Pogorelyy, V. I. Nazarov, I. V Zvyagin, V. I. Kirgizova, K. I. Kirgizov, E. V Skorobogatova, D. M. Chudakov, VDJtools: Unifying Post-analysis of T Cell Receptor Repertoires, *Reper. PLoS Comput Biol* **11**, 1004503 (2015).
15. M. Shugay, D. V Bagaev, I. V Zvyagin, R. M. Vroomans, J. C. Crawford, G. Dolton, E. A. Komech, A. L. Sycheva, A. E. Koneva, E. S. Egorov, A. V Eliseev, E. Van Dyk, P. Dash, M. Attaf, C. Rius, K. Ladell, J. E. McLaren, K. K. Matthews, E. B. Clemens, D. C. Douek, F. Luciani, D. van Baarle, K. Kedzierska, C. Kesmir, P. G. Thomas, D. A. Price, A. K. Sewell, D. M. Chudakov, VDJdb: a curated database of T-cell receptor sequences with known antigen specificity, *Nucleic Acids Res.* **46**, D419–D427 (2018).
16. Y. Hu, M. J. Turner, J. Shields, M. S. Gale, E. Hutto, B. L. Roberts, W. M. Siders, J. M. Kaplan, Investigation of the mechanism of action of alemtuzumab in a human CD52 transgenic mouse model., *Immunology* **128**, 260–70 (2009).
17. L. Robert, J. Tsoi, X. Wang, R. Emerson, B. Homet, T. Chodon, S. Mok, R. R. Huang, A. J. Cochran, B. Comin-Anduix, R. C. Koya, T. G. Graeber, H. Robins, A. Ribas, CTLA4 blockade broadens the peripheral T cell receptor repertoire, *Clin Cancer Res* **20**, 2424–2432 (2014).
18. M. A. Neller, J. M. Burrows, M. J. Rist, J. J. Miles, S. R. Burrows, High Frequency of Herpesvirus-Specific Clonotypes in the Human T Cell Repertoire Can Remain Stable over Decades with Minimal Turnover Downloaded from, *J. Virol.* **87**, 697–700 (2013).
19. I. Aversa, D. Malanga, G. Fiume, C. Palmieri, Molecular T-cell repertoire analysis as source of prognostic and predictive biomarkers for checkpoint blockade immunotherapy*Int. J. Mol. Sci.* **21** (2020), doi:10.3390/ijms21072378.
20. J. D. Lünemann, T. Ruck, P. A. Muraro, A. Bar'Or, H. Wiendl, Immune reconstitution therapies: concepts for durable remission in multiple sclerosis, *Nat. Rev. Neurol.* **16**, 56–62 (2020).
21. P. J. Gearhart, The roots of antibody diversity*Nature* **419**, 29–31 (2002).
22. M. Shugay, D. V Bagaev, M. A. Turchaninova, D. A. Bolotin, O. V Britanova, E. V Putintseva, M. V Pogorelyy, V. I. Nazarov, I. V Zvyagin, V. I. Kirgizova, K. I. Kirgizov, E. V Skorobogatova, D. M. Chudakov, VDJtools: Unifying Post-analysis of T Cell Receptor

Repertoires, , doi:10.1371/journal.pcbi.1004503.

23. E. Ruggiero, J. P. Nicolay, R. Fronza, A. Arens, A. Paruzynski, A. Nowrouzi, G. Ürenden, C. Lulay, S. Schneider, S. Goerdt, H. Glimm, P. H. Krammer, M. Schmidt, C. Von Kalle, High-resolution analysis of the human T-cell receptor repertoire, *Nat. Commun.* **6**, 1–7 (2015).

24. N. Chaudhary, D. R. Wesemann, Analyzing Immunoglobulin Repertoires, *Front. Immunol.* **9**, 462 (2018).

25. D. Hou, T. Ying, L. Wang, C. Chen, S. Lu, Q. Wang, E. Seeley, J. Xu, X. Xi, T. Li, J. Liu, X. Tang, Z. Zhang, J. Zhou, C. Bai, C. Wang, M. Byrne-Steele, J. Qu, J. Han, Y. Song, Immune Repertoire Diversity Correlated with Mortality in Avian Influenza A (H7N9) Virus Infected Patients OPEN, (2016), doi:10.1038/srep33843.

26. S. Heidt, J. Hester, S. Shankar, P. J. Friend, K. J. Wood, B Cell Repopulation After Alemtuzumab Induction-Transient Increase in Transitional B Cells and Long-Term Dominance of Na¨ıveNa¨ıve B Cells, *Am. J. Transplant.* **12**, 1784–1792 (2012).

27. Z. Li, S. Richards, H. K. Surks, A. Jacobs, M. A. Panzara, Clinical pharmacology of alemtuzumab, an anti-CD52 immunomodulator, in multiple sclerosis, *Clin. Exp. Immunol.* **194**, 295–314 (2018).

28. J. A. Fishman, Infection in Solid-Organ Transplant Recipients, *N. Engl. J. Med.* **357**, 2601–2614 (2007).

29. A. Winkelmann, M. Loebermann, E. C. Reisinger, H. P. Hartung, U. K. Zettl, Disease-modifying therapies and infectious risks in multiple sclerosis*Nat. Rev. Neurol.* **12**, 217–233 (2016).

30. A. R. Buonomo, E. Zappulo, G. Viceconte, R. Scotto, G. Borgia, I. Gentile, Risk of opportunistic infections in patients treated with alemtuzumab for multiple sclerosis*Expert Opin. Drug Saf.* **17**, 709–717 (2018).

31. K. Yann, J. Fran, S. Nazar, M. Tatiana, T. Paul, R. David, P. Adrian, Acute respiratory distress syndrome following alemtuzumab therapy for relapsing multiple sclerosis, *Mult. Scler. Relat. Disord.* **14**, 1–3 (2017).

32. M. Clerico, S. De Mercanti, C. A. Artusi, L. Durelli, R. T. Naismith, Active CMV infection in two patients with multiple sclerosis treated with alemtuzumab, *Mult. Scler.* **23**, 874–876 (2017).

33. W. J. Brownlee, J. Chataway, Opportunistic infections after alemtuzumab: New cases of norcardial infection and cytomegalovirus syndrome*Mult. Scler.* **23**, 876–877 (2017).

34. S. Barone, S. Scannapieco, C. Torti, E. Filippelli, V. Pisani, A. Granata, D. Console, G. Demonte, T. Tallarico, S. Polidoro, A. Quattrone, P. Valentino, Hepatic microabscesses

during CMV reactivation in a multiple sclerosis patient after alemtuzumab treatment, *Mult. Scler. Relat. Disord.* **20**, 6–8 (2018).

35. P. Ljungman, M. Hakki, M. Boeckh, Cytomegalovirus in Hematopoietic Stem Cell Transplant Recipients*Hematol. Oncol. Clin. North Am.* **25**, 151–169 (2011).

36. J. Inagaki, M. Noguchi, K. Kurauchi, S. Tanioka, R. Fukano, J. Okamura, Effect of Cytomegalovirus Reactivation on Relapse after Allogeneic Hematopoietic Stem Cell Transplantation in Pediatric Acute Leukemia, *Biol. Blood Marrow Transplant.* **22**, 300–306 (2016).

37. G. Lugthart, M. M. van Ostaijen-ten Dam, C. M. Jol - van der Zijde, T. C. van Holten, M. G. D. Kester, M. H. M. Heemskerk, R. G. M. Bredius, M. J. D. van Tol, A. C. Lankester, Early Cytomegalovirus Reactivation Leaves a Specific and Dynamic Imprint on the Reconstituting T Cell Compartment Long-Term after Hematopoietic Stem Cell Transplantation, *Biol. Blood Marrow Transplant.* **20**, 655–661 (2014).

38. P. A. Muraro, R. Martin, G. L. Mancardi, R. Nicholas, M. P. Sormani, R. Saccardi, Autologous haematopoietic stem cell transplantation for treatment of multiple sclerosis, *Nat. Rev. Neurol.* **13**, 391–405 (2017).

39. P. A. Muraro, H. Robins, S. Malhotra, M. Howell, D. Phippard, C. Desmarais, A. de P. A. Sousa, L. M. Griffith, N. Lim, R. A. Nash, L. A. Turka, T cell repertoire following autologous stem cell transplantation for multiple sclerosis, *J. Clin. Invest.* **124**, 1168 (2014).

40. P. A. Muraro, D. C. Douek, A. Packer, K. Chung, F. J. Guenaga, R. Cassiani-Ingoni, C. Campbell, S. Memon, J. W. Nagle, F. T. Hakim, R. E. Gress, H. F. McFarland, R. K. Burt, R. Martin, Thymic output generates a new and diverse TCR repertoire after autologous stem cell transplantation in multiple sclerosis patients, *J. Exp. Med.* **201**, 805–816 (2005).

41. K. A. Fortner, R. C. Budd, The Death Receptor Fas (CD95/APO-1) Mediates the Deletion of T Lymphocytes Undergoing Homeostatic Proliferation, *J. Immunol.* **175**, 4374–4382 (2005).

42. C. J. Workman, D. A. A. Vignali, Negative Regulation of T Cell Homeostasis by Lymphocyte Activation Gene-3 (CD223), *J. Immunol.* **174**, 688–695 (2005).

43. K. M. Harris, N. Lim, P. Lindau, H. Robins, L. M. Griffith, R. A. Nash, L. A. Turka, P. A. Muraro, Extensive intrathecal T cell renewal following hematopoietic transplantation for multiple sclerosis, *JCI Insight* **5** (2020), doi:10.1172/jci.insight.127655.

44. H. Lowenstein, A. Shah, A. Chant, A. Khan, Different mechanisms of Campath-1H-mediated depletion for $CD4^+$ and $CD8^+$ T cells in peripheral blood, *Transpl. Int.* **19**, 927–936 (2006).

45. J. W. J. van Heijst, I. Ceberio, L. B. Lipuma, D. W. Samilo, G. D. Wasilewski, A. M. R. Gonzales, J. L. Nieves, M. R. M. van den Brink, M. A. Perales, E. G. Pamer, Quantitative assessment of T cell repertoire recovery after hematopoietic stem cell transplantation, *Nat. Med.* **19**, 372–377 (2013).

46. M. A. Postow, M. Manuel, P. Wong, J. Yuan, Z. Dong, C. Liu, S. Perez, I. Tanneau, M. Noel, A. Courtier, N. Pasqual, J. D. Wolchok, Peripheral T cell receptor diversity is associated with clinical outcomes following ipilimumab treatment in metastatic melanoma, (2016), doi:10.1186/s40425-015-0070-4.

47. S. Pollastro, P. L. Klarenbeek, M. E. Doorenspleet, B. D. C. Van Schaik, R. E. E. Esveldt, R. M. Thurlings, M. J. H. Boumans, D. M. Gerlag, P. P. Tak, K. Vos, F. Baas, A. H. C. Van Kampen, N. De Vries, Non-response to rituximab therapy in rheumatoid arthritis is associated with incomplete disruption of the B cell receptor repertoire, *Ann. Rheum. Dis.* **78**, 1339–1345 (2019).

48. M. Krumbholz, T. Derfuss, R. Hohlfeld, E. Meinl, B cells and antibodies in multiple sclerosis pathogenesis and therapy*Nat. Rev. Neurol.* **8**, 613–623 (2012).

49. S. Rolla, A. Maglione, S. F. De Mercanti, M. Clerico, cells The Meaning of Immune Reconstitution after Alemtuzumab Therapy in Multiple Sclerosis, , doi:10.3390/cells9061396.

50. J. Brannigan, J. L. Jones, S. R. L. Stacpoole, Severe paradoxical disease activation following alemtuzumab treatment for multiple sclerosis, *Neurol. Neuroimmunol. neuroinflammation* **7**, 799 (2020).

51. A. Haghikia, C. A. Dendrou, R. Schneider, T. GrÃ, T. Postert, M. Matzke, H. Stephanik, L. Fugger, R. Gold, *Severe B-cell-mediated CNS disease secondary to alemtuzumab therapy* (2017; www.thelancet.com/neurology).

52. M. Willis, O. Pearson, Z. Illes, T. Sejbaek, C. Nielsen, M. Duddy, K. Petheram, C. Van Munster, J. Killestein, C. Malmeström, E. Tallantyre, N. Robertson, An observational study of alemtuzumab following fingolimod for multiple sclerosis, *Neurol. Neuroimmunol. NeuroInflammation* **4** (2017), doi:10.1212/NXI.0000000000000320.

53. T. Wehrum, L. A. Beume, O. Stich, I. Mader, M. Mäurer, A. Czaplinski, C. Weiller, S. Rauer, Activation of disease during therapy with alemtuzumab in 3 patients with multiple sclerosis, *Neurology* **90**, e601–e605 (2018).

54. T. Ruck, S. Pfeuffer, A. Schulte-Mecklenbeck, C. C. Gross, M. Lindner, D. Metze, J. Ehrchen, W. Sondermann, R. Pul, C. Kleinschnitz, H. Wiendl, S. G. Meuth, L. Klotz, Vitiligo after alemtuzumab treatment: Secondary autoimmunity is not all about B cells, *Neurology* **91**, E2233–E2237 (2018).

55. N. Pariani, M. Willis, I. Muller, S. Healy, T. Nasser, A. Mcgowan, G. Lyons, J. Jones, K. Chatterjee, C. Dayan, N. Robertson, A. Coles, C. Moran, Alemtuzumab-Induced Thyroid Dysfunction Exhibits Distinctive Clinical and Immunological Features, *J Clin Endocrinol Metab* **103**, 3010–3018 (2018).

56. T. C. T. Investigators, Alemtuzumab vs. Interferon Beta-1a in Early Multiple Sclerosis, *N. Engl. J. Med.* **359**, 1786–1801 (2008).

57. O. Tuohy, L. Costelloe, G. Hill-Cawthorne, I. Bjornson, K. Harding, N. Robertson, K. May, T. Button, L. Azzopardi, O. Kousin-Ezewu, M. T. Fahey, J. Jones, D. A. S. Compston, A. Coles, Alemtuzumab treatment of multiple sclerosis: Long-term safety and efficacy, *J. Neurol. Neurosurg. Psychiatry* **86**, 208–215 (2015).

58. A. J. Coles, M. Wing, S. Smith, F. Coraddu, S. Greer, C. Taylor, A. Weetman, G. Hale, V. K. Chatterjee, H. Waldmann, A. Compston, Pulsed monoclonal antibody treatment and autoimmune thyroid disease in multiple sclerosis, *Lancet* **354**, 1691–1695 (1999).

59. M. P. Davey, M. M. Meyer, D. D. Munkirs, D. Babcock, M. P. Braun, J. B. Hayden, A. C. Bakke, T-cell receptor variable β genes show differential expression in CD4 and CD8 T cells, *Hum. Immunol.* **32**, 194–202 (1991).

60. G. P. Owens, H. Kannus, M. P. Burgoon, T. Smith-Jensen, M. E. Devlin, D. H. Gilden, Restricted use of VH4 Germline segments in an acute multiple sclerosis brain, *Ann. Neurol.* **43**, 236–243 (1998).

61. S. E. Baranzini, M. C. Jeong, C. Butunoi, R. S. Murray, C. C. Bernard, J. R. Oksenberg, B cell repertoire diversity and clonal expansion in multiple sclerosis brain lesions., *J. Immunol.* **163**, 5133–44 (1999).

62. M. A. Maurer, F. Tuller, V. Gredler, T. Berger, A. Lutterotti, J. D. Lünemann, M. Reindl, Rituximab induces clonal expansion of IgG memory B-cells in patients with inflammatory central nervous system demyelination, *J. Neuroimmunol.* **290**, 49–53 (2016).

63. J. Chun, H.-P. Hartung, Mechanism of action of oral fingolimod (FTY720) in multiple sclerosis., *Clin. Neuropharmacol.* **33**, 91–101 (2010).

64. D. Pelletier, D. A. Hafler, Fingolimod for Multiple Sclerosis, *N. Engl. J. Med.* **366**, 339–347 (2012).

65. J. Cocquet, A. Chong, G. Zhang, R. A. Veitia, Reverse transcriptase template switching and false alternative transcripts, *Genomics* **88**, 127–131 (2006).

66. J. Benichou, R. Ben-Hamo, Y. Louzoun, S. Efroni, Rep-Seq: Uncovering the immunological repertoire through next-generation sequencing*Immunology* **135**, 183–191 (2012).

67. A. Lossius, J. N. Johansen, F. Vartdal, T. Holmøy, C. A. Lossius, High-throughput sequencing of immune repertoires in multiple sclerosis, *Ann. Clin. Transl. Neurol.* **3**, 295–306 (2016).

68. T. Kivioja, A. Vähärautio, K. Karlsson, M. Bonke, M. Enge, S. Linnarsson, J. Taipale, Counting absolute numbers of molecules using unique molecular identifiers, *Nat. Methods* **9**, 72–74 (2012).

69. M. A. Turchaninova, A. Davydov, O. V. Britanova, M. Shugay, V. Bikos, E. S. Egorov, V. I. Kirgizova, E. M. Merzlyak, D. B. Staroverov, D. A. Bolotin, I. Z. Mamedov, M. Izraelson, M. D. Logacheva, O. Kladova, K. Plevova, S. Pospisilova, D. M. Chudakov, High-quality full-length immunoglobulin profiling with unique molecular barcoding, *Nat. Protoc.* **11**, 1599–1616 (2016).

70. I. Z. Mamedov, O. V. Britanova, I. V. Zvyagin, M. A. Turchaninova, D. A. Bolotin, E. V. Putintseva, Y. B. Lebedev, D. M. Chudakov, Preparing Unbiased T-Cell Receptor and Antibody cDNA Libraries for the Deep Next Generation Sequencing Profiling, *Front. Immunol.* **4**, 456 (2013).

71. O. V. Britanova, E. V. Putintseva, M. Shugay, E. M. Merzlyak, M. A. Turchaninova, D. B. Staroverov, D. A. Bolotin, S. Lukyanov, E. A. Bogdanova, I. Z. Mamedov, Y. B. Lebedev, D. M. Chudakov, Age-Related Decrease in TCR Repertoire Diversity Measured with Deep and Normalized Sequence Profiling, *J. Immunol.* **192** (2014) (available at http://www.jimmunol.org/content/192/6/2689.long).

72. E. S. Egorov, E. M. Merzlyak, A. A. Shelenkov, O. V. Britanova, G. V. Sharonov, D. B. Staroverov, D. A. Bolotin, A. N. Davydov, E. Barsova, Y. B. Lebedev, M. Shugay, D. M. Chudakov, Quantitative Profiling of Immune Repertoires for Minor Lymphocyte Counts Using Unique Molecular Identifiers, *J. Immunol.* **194**, 6155–6163 (2015).

73. J. Brodin, C. Hedskog, A. Heddini, E. Benard, R. A. Neher, M. Mild, J. Albert, Challenges with using Primer IDs to improve accuracy of next generation sequencing, *PLoS One* **10** (2015), doi:10.1371/journal.pone.0119123.

Patients:

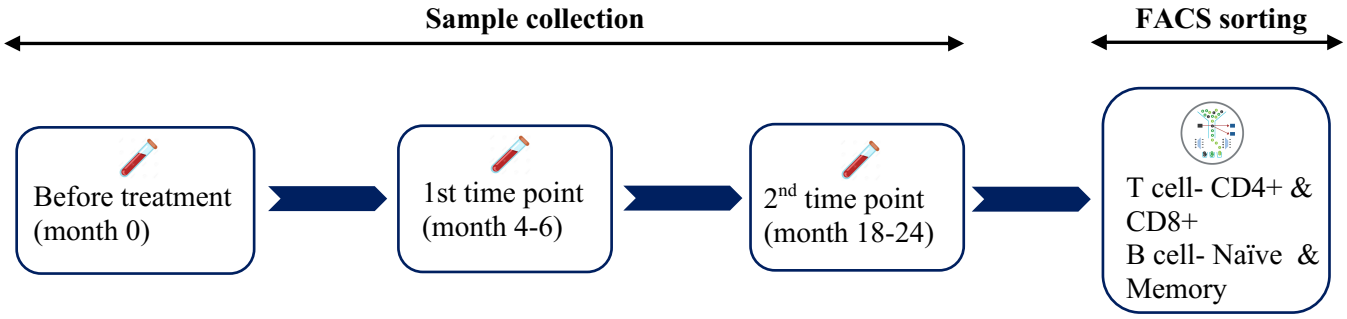

Patients with secondary autoimmunity:

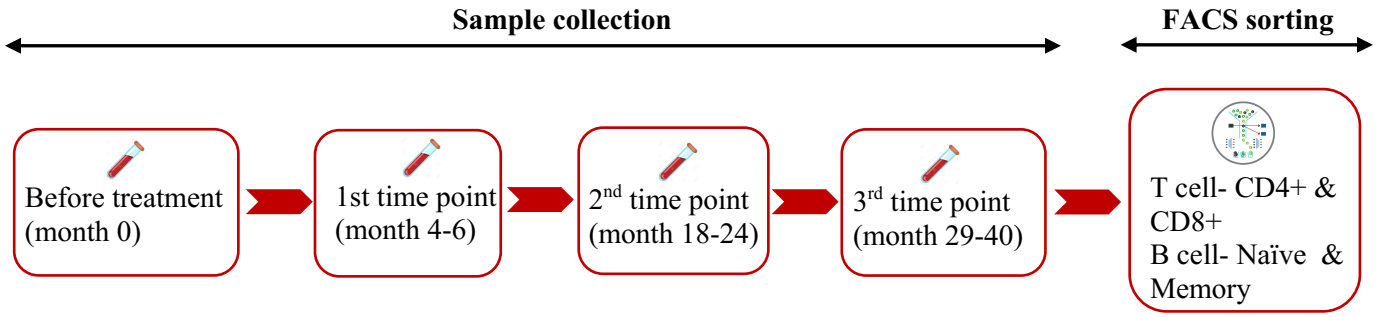

Untreated controls:

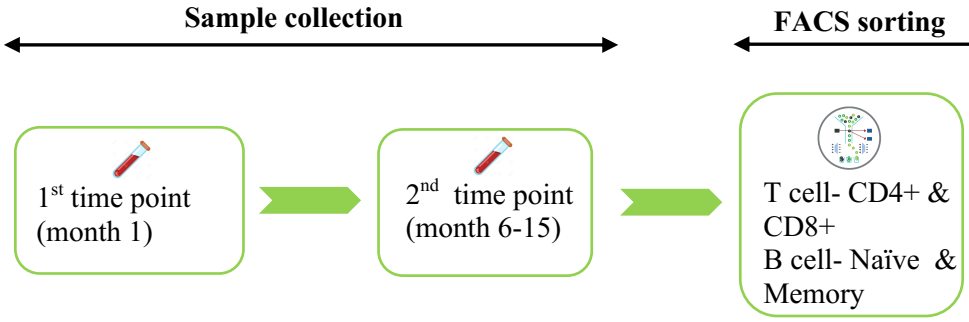

Figure 1. Study design. *Peripheral blood mononuclear cells (PBMCs) from twelve patients with MS, prior to and up to 40 months after initiation of alemtuzumab treatment, two healthy controls (up to 15 months interval), and three untreated MS control patients (up to 14 months interval) were collected and FACS sorted.*

***In all following figures and tables**, "**before C1**" corresponds to samples taken before the first alemtuzumab treatment cycle; "**C1 + x**"; "**C2 + y**" indicate samples acquired "x" or "y" months after treatment cycle 1 or 2, correspondingly. Samples taken from untreated controls are indicated as "m1" for the first time point and "mx" for a second time point taken x months later.*

*For statistical evaluations, "**Before C1**" refers to time point before alemtuzumab treatment, "**C1+T1**" refers to first time point after first treatment cycle, and **C2+T1** corresponds to first time point after second treatment cycle. In samples from untreated controls, " **T1**" and "**T2**" represent first and second time point, respectively.*

(a)

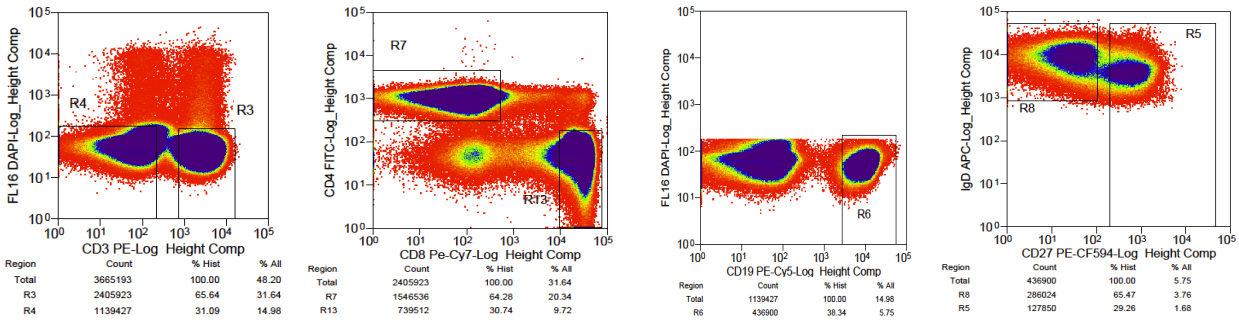

(b)

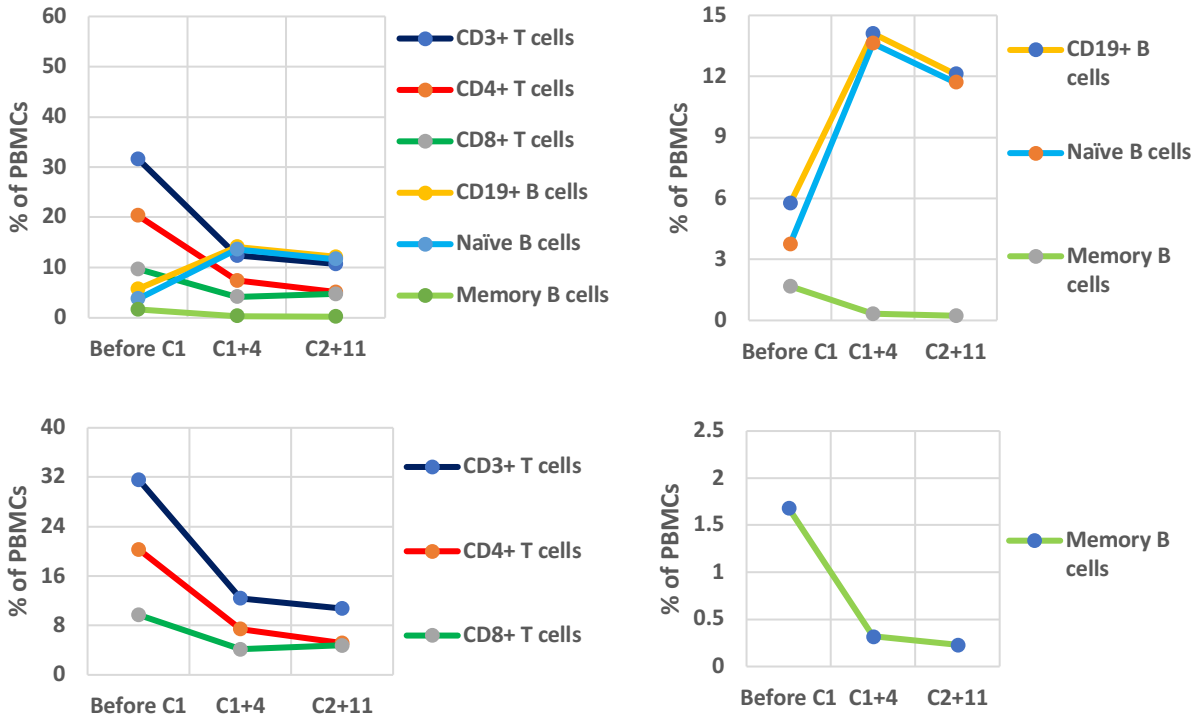

Figure 2. Longitudinal FACS data of PBMC from a representative patient treated with alemtuzumab. ***(a)*** *Gating strategy for FACS-sorting of CD8+ and CD4+ T cells, as well as naïve and memory B cells from PBMC.* ***(b)*** *Relative abundance of lymphocyte populations at different time points before and during alemtuzumab treatment: After each alemtuzumab infusion the relative proportions of CD8+ and CD4+ T cells, as well as memory B cells decrease, whereas naïve B cells increase in proportion (Patient 3_4292).*

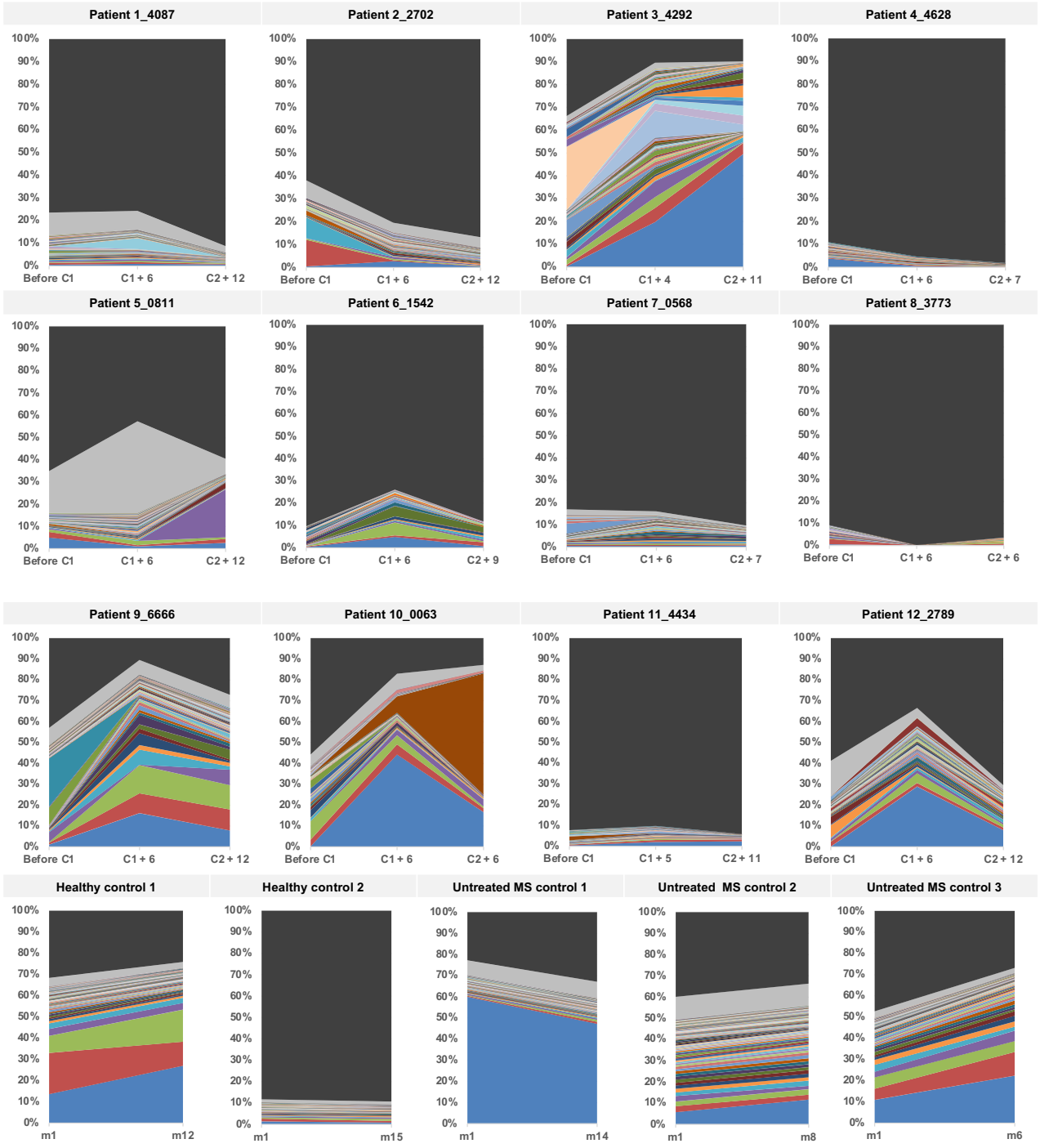

Figure 3. Clonotype tracking stack area plots of CD8+ T cells from alemtuzumab treated patients and untreated controls. *Strongly expanded and mostly persisting clones dominate the CD8+ T cell repertoires.* ***Colored areas indicate*** *evolution/persistence/relative abundance of individual clones, persisting among up to the top hundred most abundant clones at least two consecutive time points; light grey areas represent the sum of persisting, not individually shown clones; dark grey areas represent residual, non-persisting clones.*

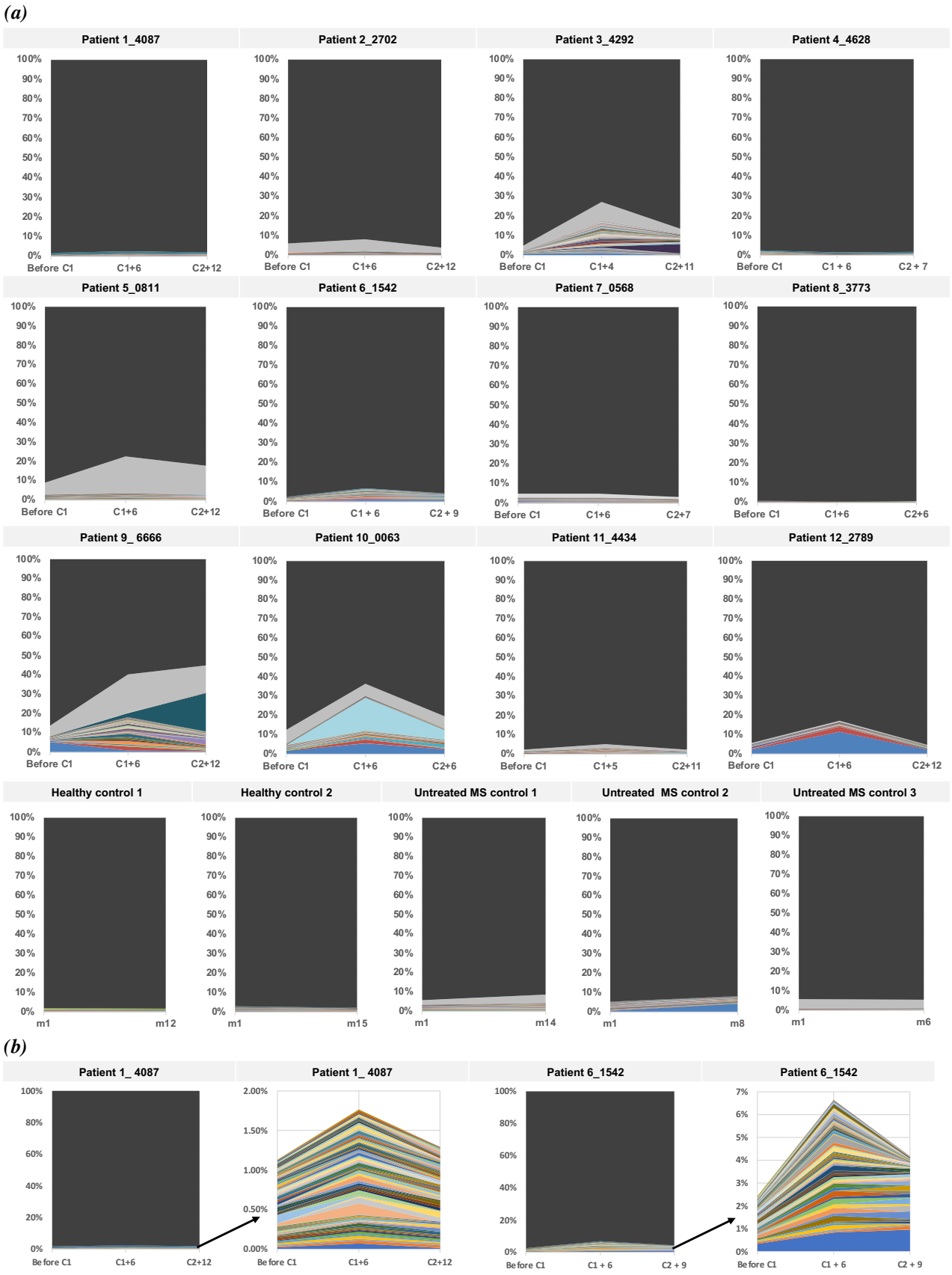

Figure 4. Clonotype tracking stack area plots of CD4+ T cells *from* ***(a)*** *Alemtuzumab treated patients and untreated controls, and* ***(b)*** *magnified presentation of the stack area plots of up to top 100 clonotypes of patient 1_4087 and patient 6_1542. A striking predominance of non-persisting and high number of low-abundant clones was observe in most of the treated patients and all untreated controls. For explanation of the clonotype tracking stack area plot see figure 3.*

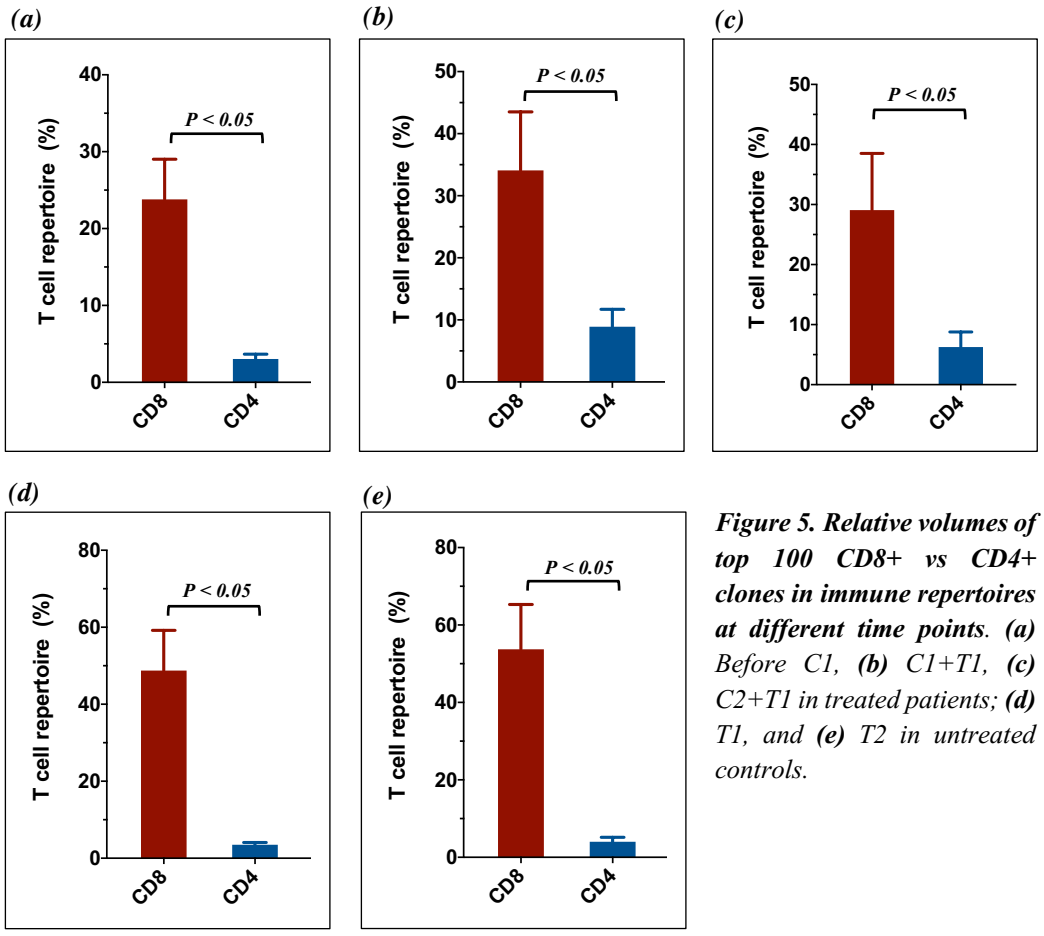

Figure 5. Relative volumes of top 100 CD8+ vs CD4+ clones in immune repertoires at different time points. ***(a)*** *Before C1,* ***(b)*** *C1+T1,* ***(c)*** *C2+T1 in treated patients;* ***(d)*** *T1, and* ***(e)*** *T2 in untreated controls.*

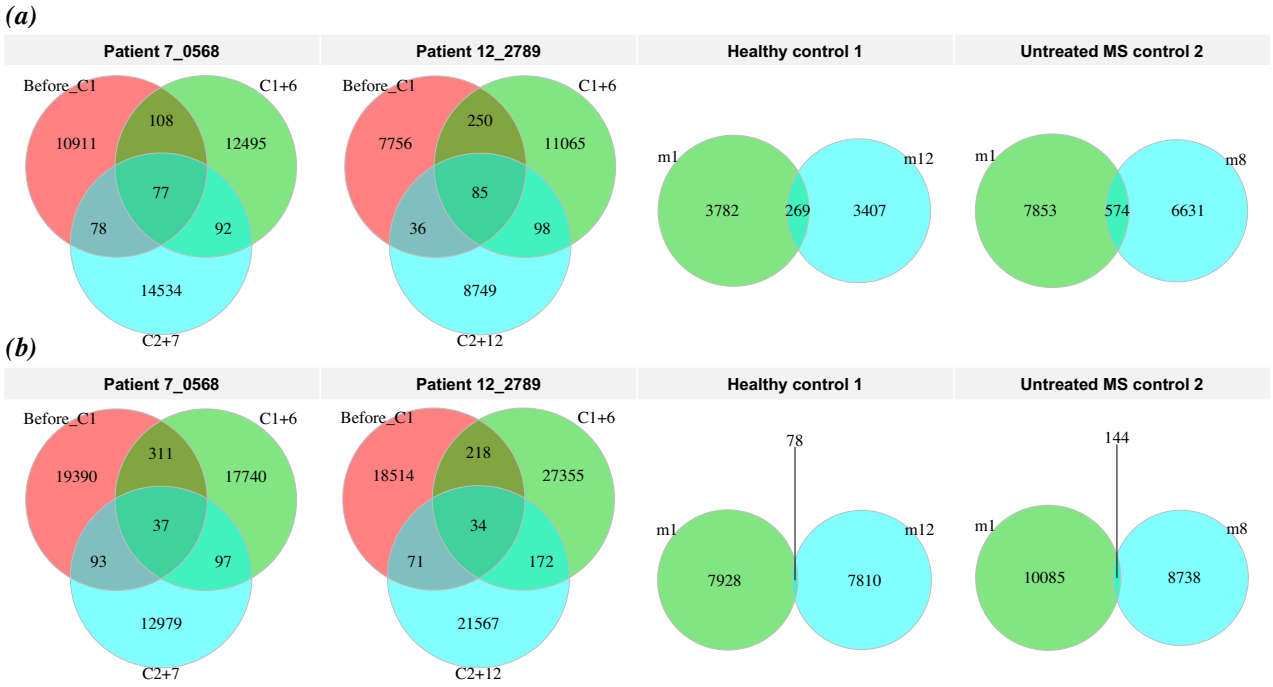

Figure 6. Joint clonotype abundance graph ("VENN diagramme") of ***(a)*** *CD8+ T cells, and* ***(b)*** *CD4+ T cells from representative alemtuzumab treated non-SA patient (Patient 7_0568), SA patient (Patient 12_2789), and representative untreated controls (Healthy control 1 and Untreated MS control 2). This figure gives information on all clonotypes (defined by their CDR3 amino acid sequences) identified at the time points indicated. Overlapping sections contain the numbers of clones detected at both or all three time points indicated. Areas are not proportional to numbers or volumes of clones. For explanation of the joint clonotype abundance graph see supplementary figure 1.*

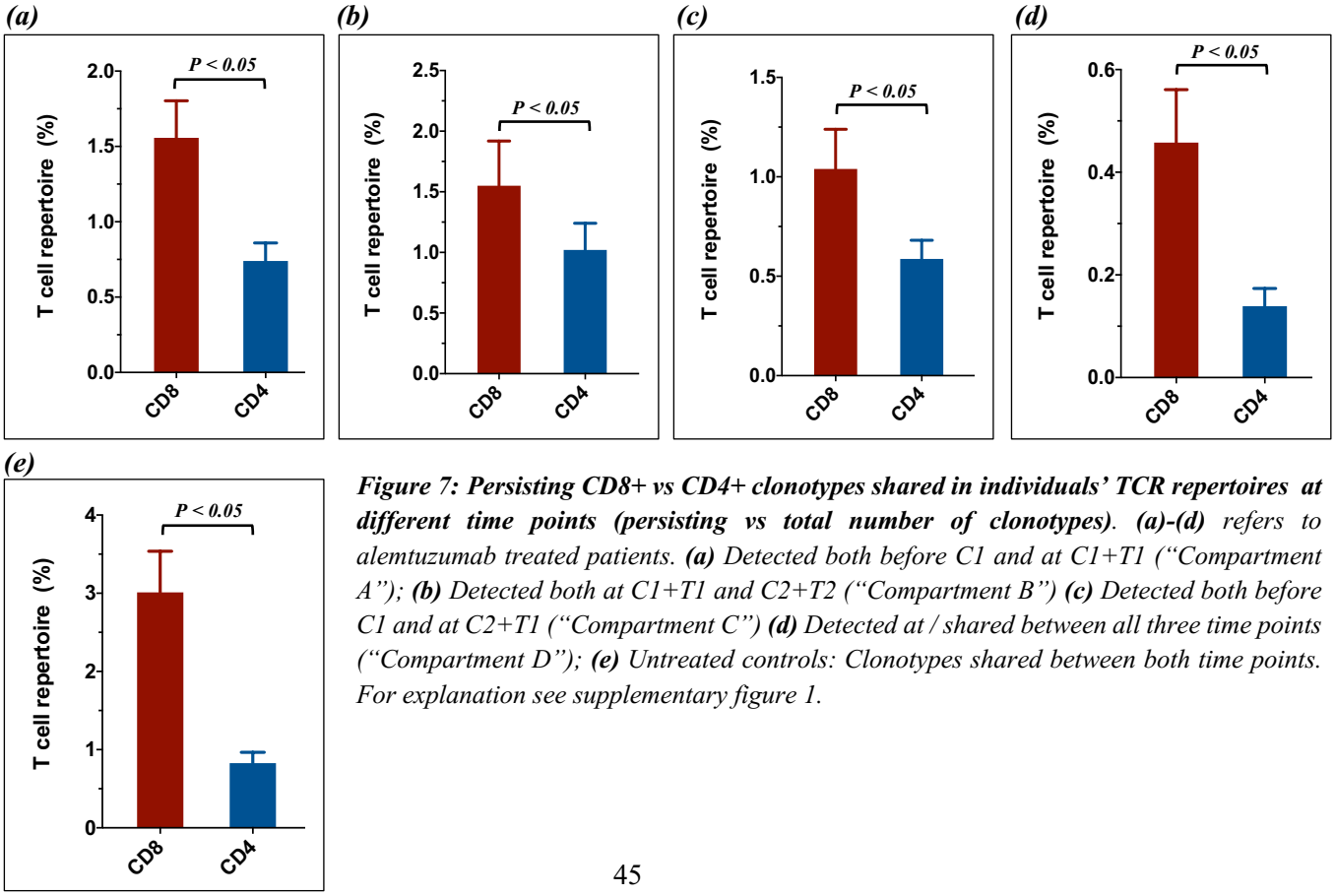

Figure 7: Persisting CD8+ vs CD4+ clonotypes shared in individuals' TCR repertoires at different time points (persisting vs total number of clonotypes). ***(a)-(d)*** *refers to alemtuzumab treated patients.* ***(a)*** *Detected both before C1 and at C1+T1 ("Compartment A");* ***(b)*** *Detected both at C1+T1 and C2+T2 ("Compartment B")* ***(c)*** *Detected both before C1 and at C2+T1 ("Compartment C")* ***(d)*** *Detected at / shared between all three time points ("Compartment D");* ***(e)*** *Untreated controls: Clonotypes shared between both time points. For explanation see supplementary figure 1.*

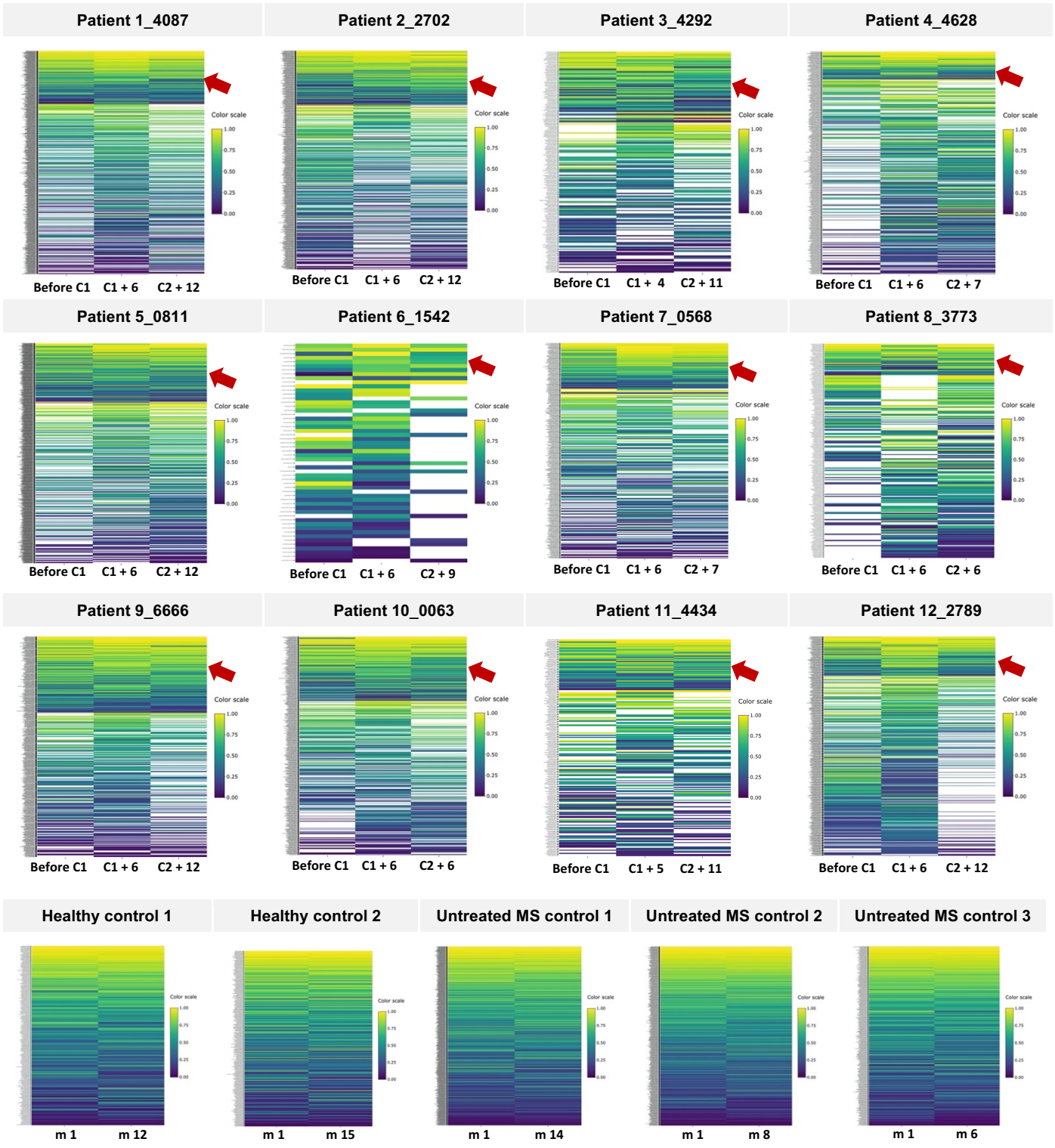

Figure 8. Clonotype tracking heatmaps of CD8+ T cell immune repertoires from alemtuzumab treated patients and untreated controls. *Here, the relative abundance and persistence (at least two consecutive time points) of the entire immune repertoires are visualized: Colored lines represent evolution/persistence of abundance of individual clones over time. Yellow lines imply higher abundance than green > blue lines. Persisting clones of lowest abundance are shown in dark blue/violet. Non-persisting clones are shown in white.*

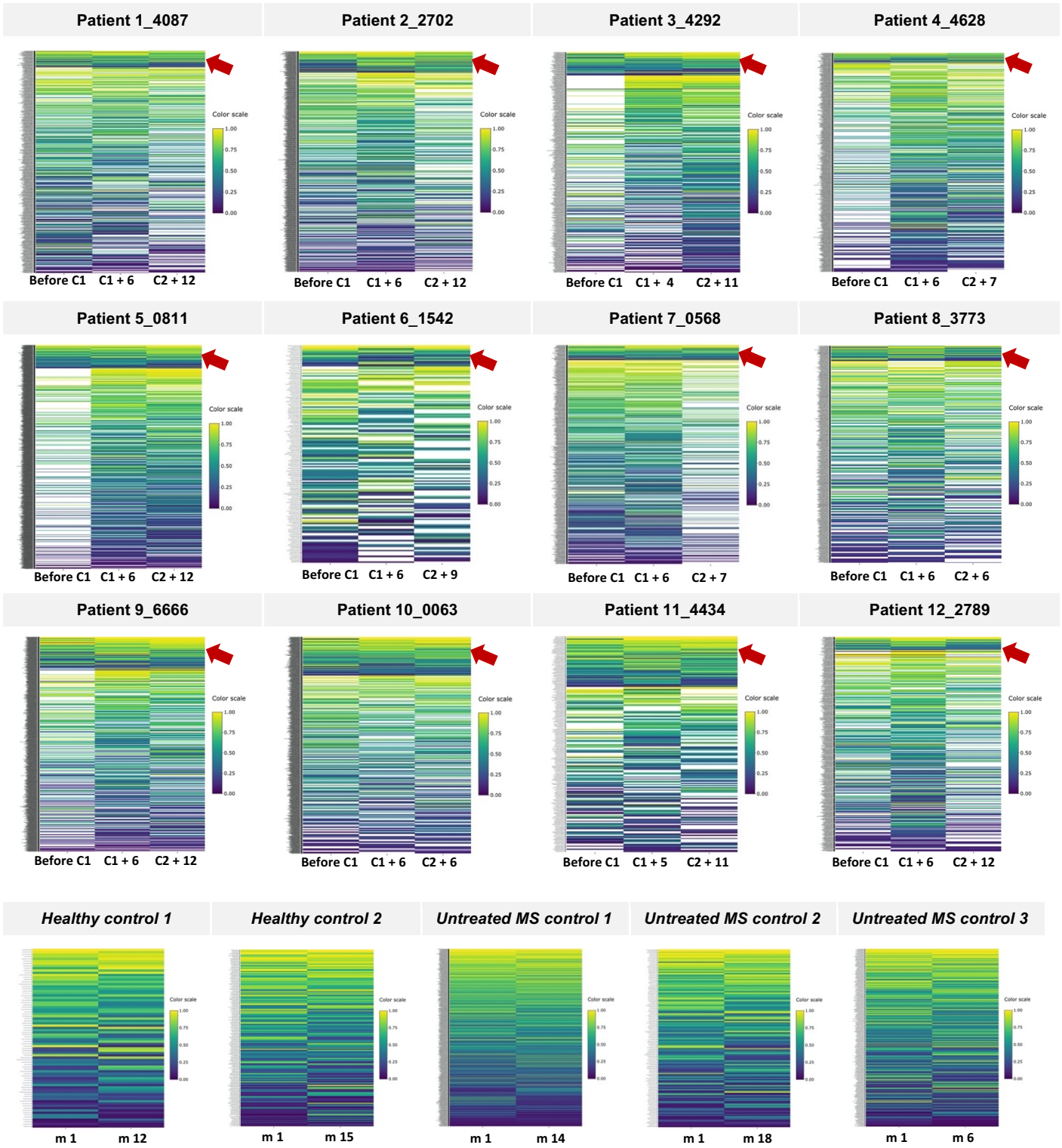

Figure 9. Clonotype tracking heatmaps of CD4+ T cell immune repertoires from alemtuzumab treated patients and untreated controls. *Here, the relative abundance and persistence (at least two consecutive time points) of the entire immune repertoires are visualized. For explanation of the clonotype tracking heatmap see figure 8.*

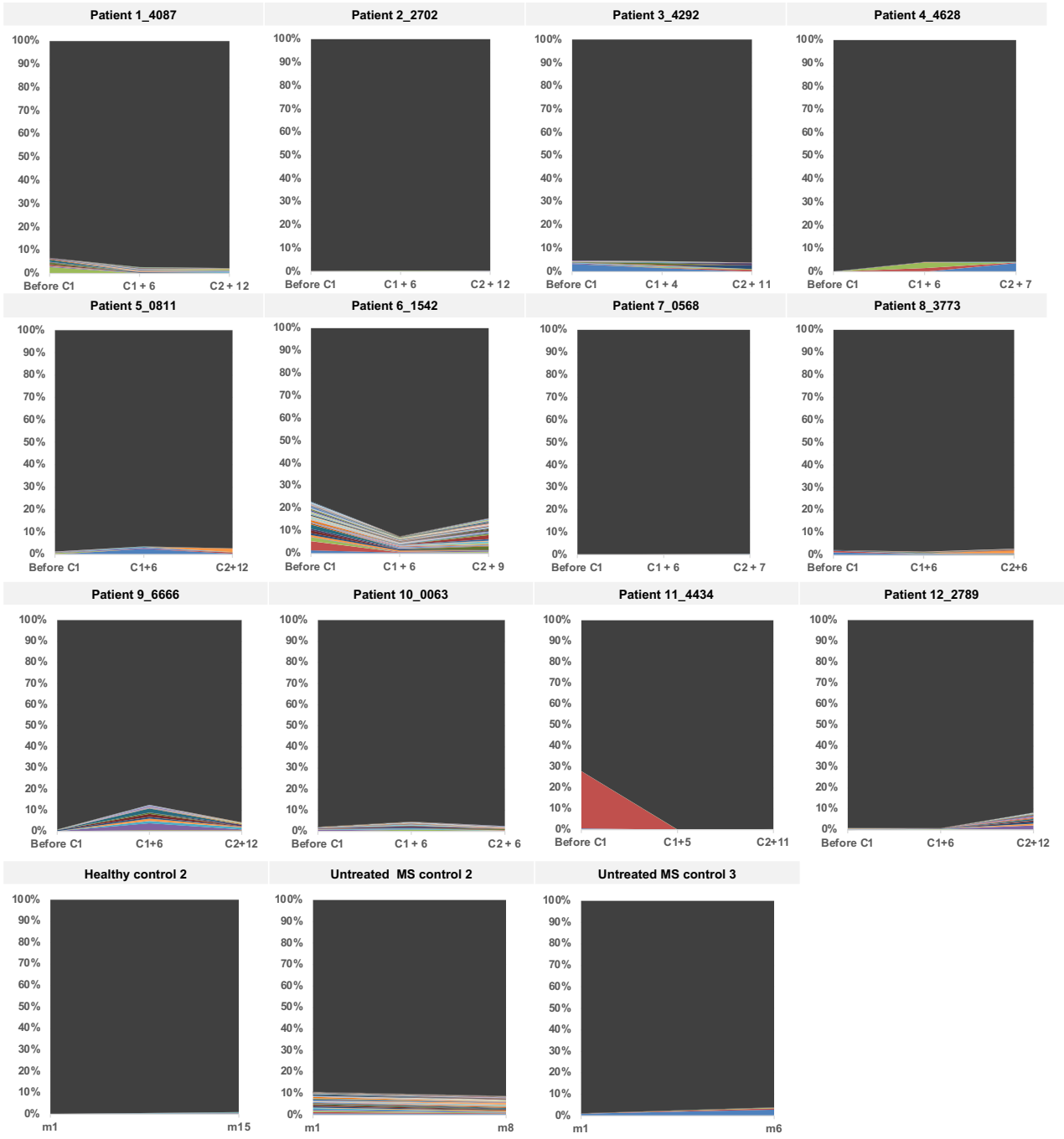

Figure 10. Clonotype tracking stack area plots of IgG+ memory B cells from alemtuzumab treated patients and untreated controls. *There was no persisting clone in healthy control 1 and untreated MS control 1. For explanation of the clonotype tracking stack area plot see figure 3.*

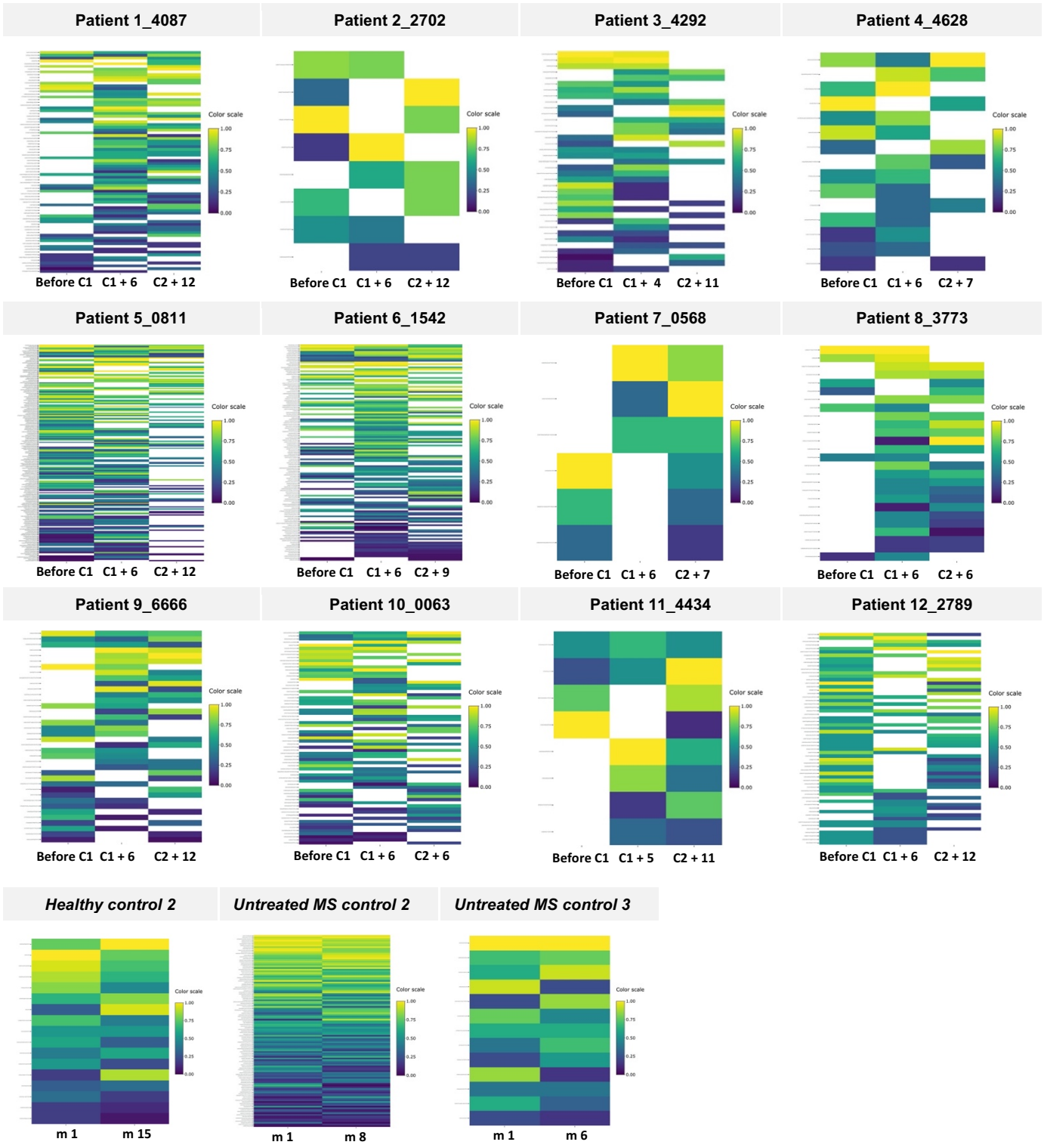

Figure 11. Clonotype tracking heatmaps of IgG+ memory B cell immune repertoires from alemtuzumab treated patients and untreated controls. *Here, the relative abundance and persistence (at least two consecutive time points) of the entire immune repertoires are visualized. There was no persisting clone in healthy control 1 and untreated MS control 1. For explanation of the clonotype tracking heatmap see figure 8.*

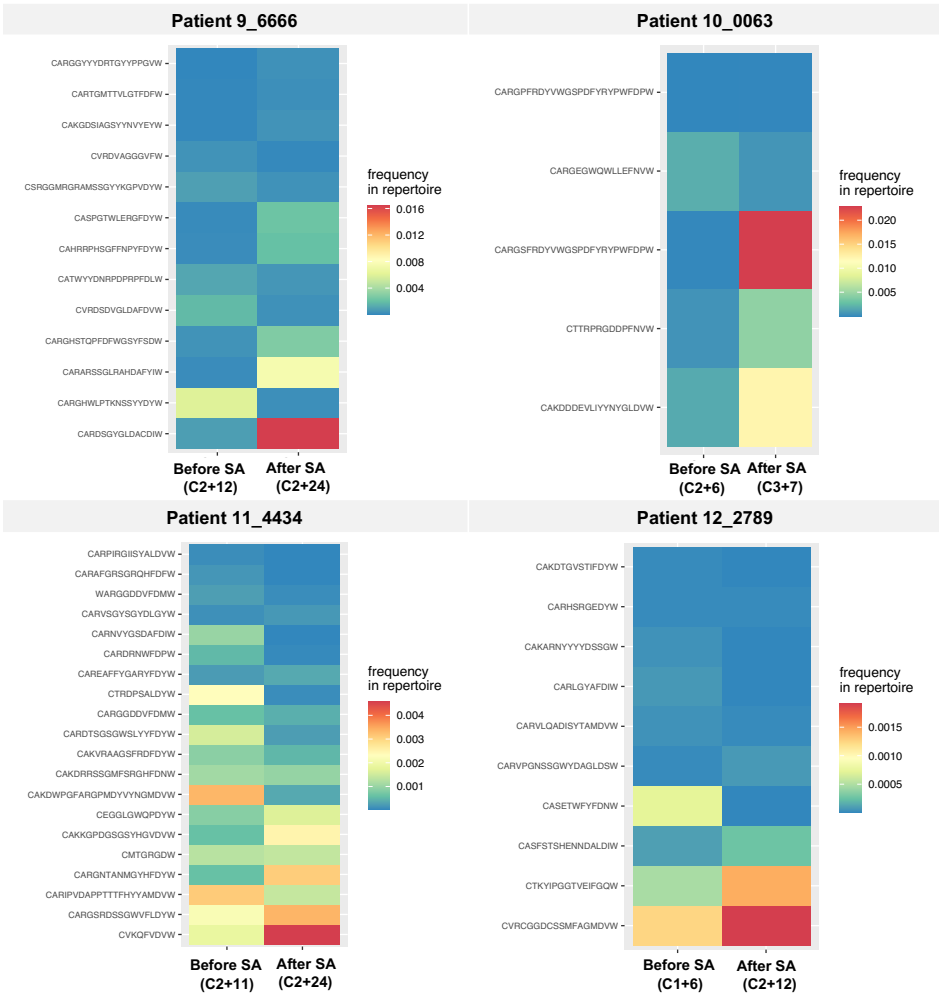

Figure 12: Tracking of IgG+ memory B cell clonotypes before and after development of secondary autoimmunity. *The frequency of the most abundant persisting clone was greater after the development of secondary autoimmunity in all SA patients and each most abundant persisting clone was absent before the treatment.*

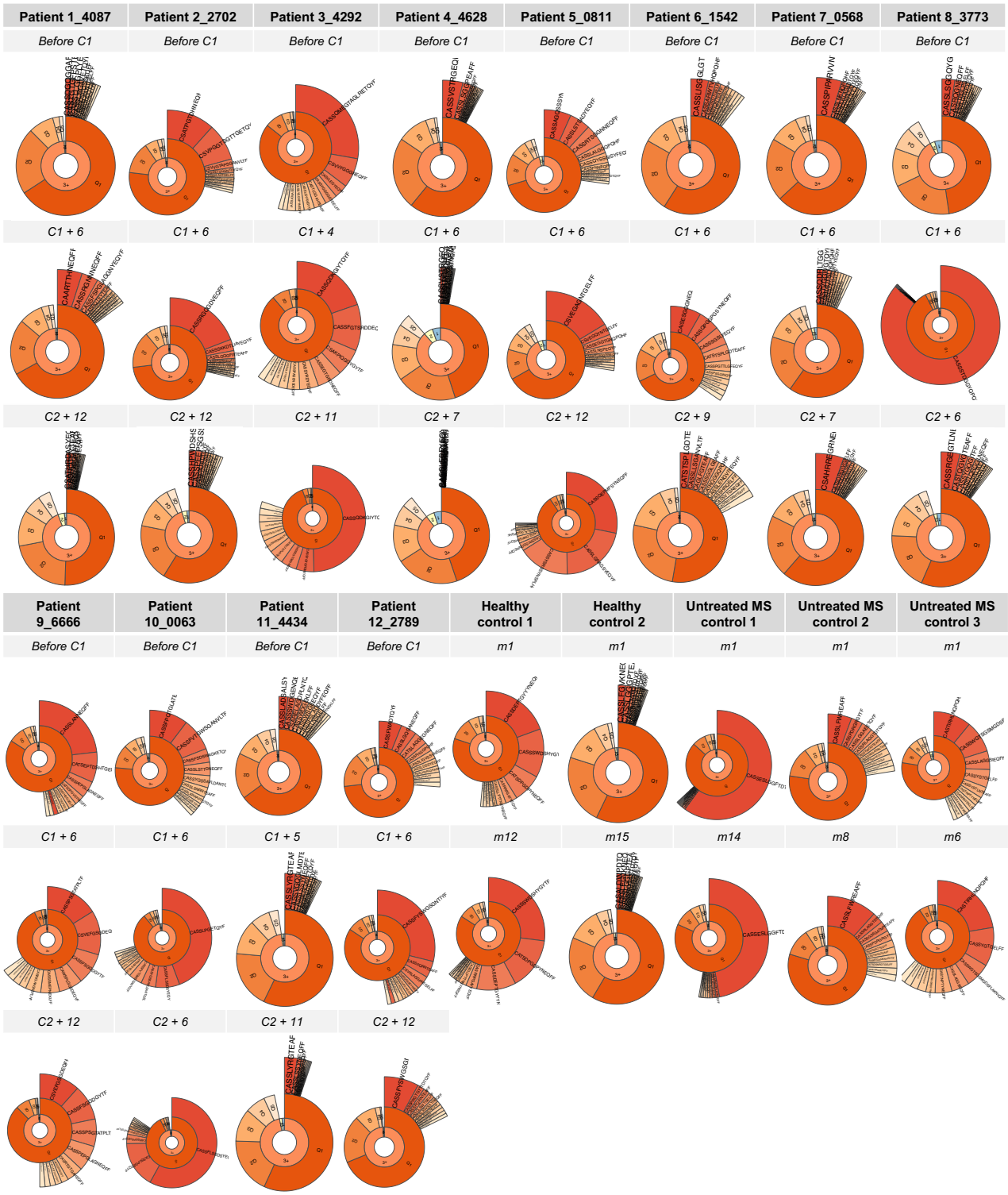

Figure 13: Three layer donut charts of CD8+ T cell immune repertoires from alemtuzumab treated patients and untreated controls: *For explanation of the three layer donut chart see supplementary figure 5.*

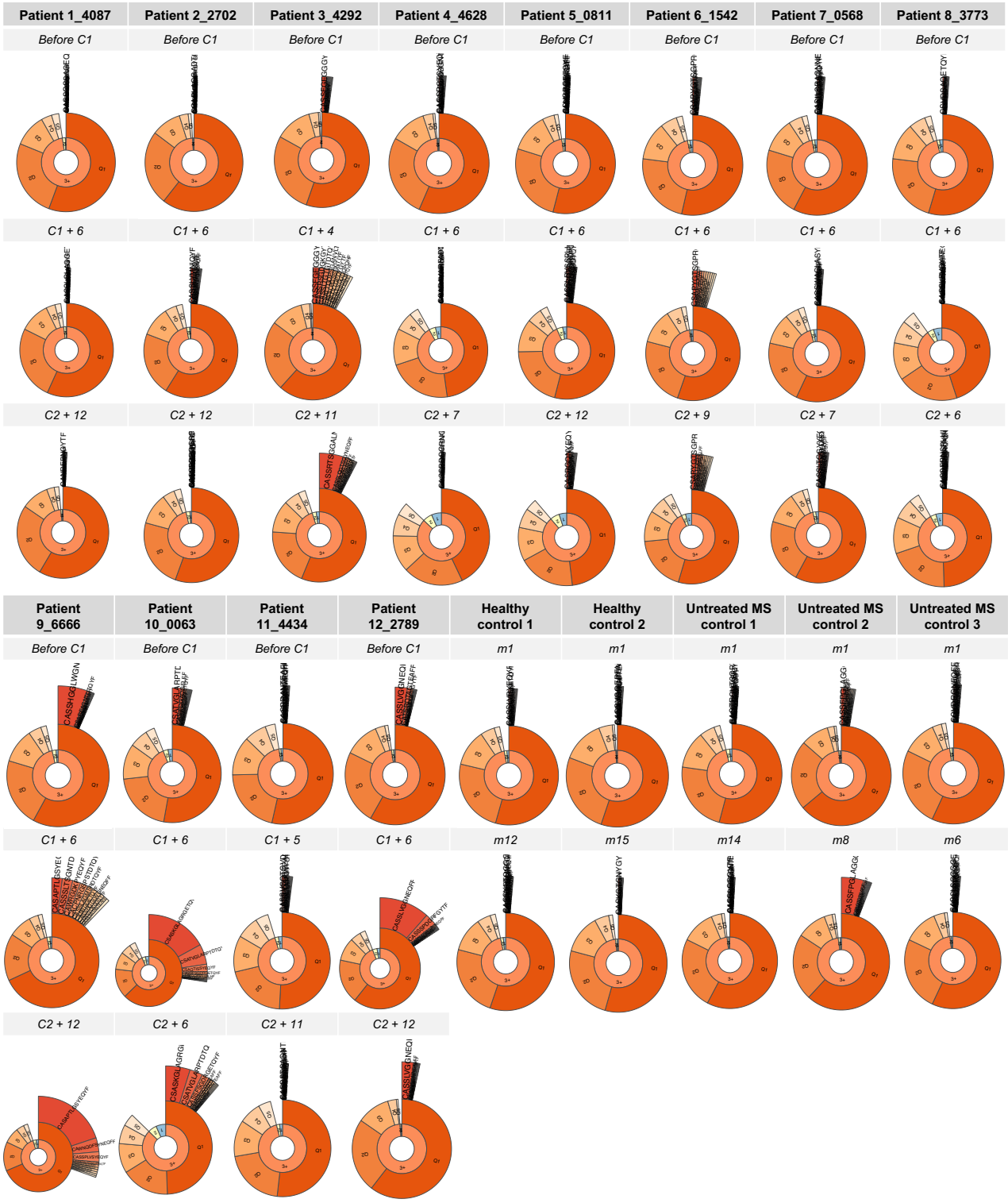

Figure 14. Three layer donut charts of CD4+ T cell immune repertoires from alemtuzumab treated patients and untreated controls. *For explanation of the three layer donut chart see supplementary figure 5.*

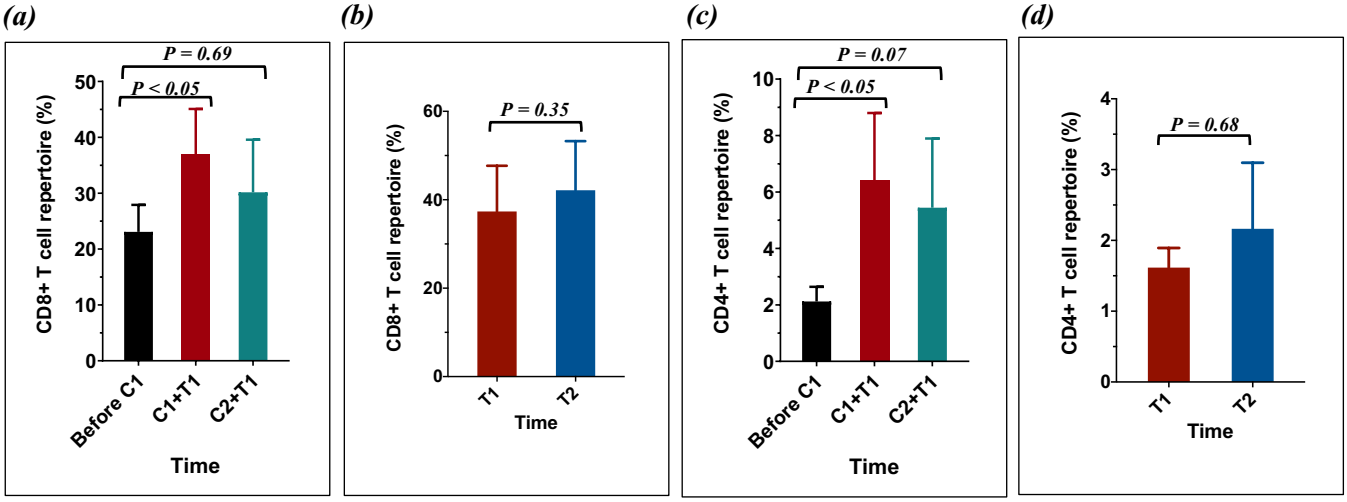

Figure 15: Abundance of the Top 10 CD8+ T cell clonotypes *(relative to the total CD8+ T cell repertoire) in* ***(a)*** *12 alemtuzumab treated MS patients, and* ***(b)*** *untreated controls;* ***Abundance of the Top 10 CD4+ T cell clonotypes*** *(relative to the total CD4+ T cell repertoire) of* ***(c)*** *12 alemtuzumab treated MS patients, and* ***(d)*** *untreated controls. Before C1: before the first treatment cycle; C1+T1: Time point 1 after 1st treatment cycle; C2+T1: Time point 1 after 2nd treatment cycle; T1: Time point 1; T2: Time point 2.*

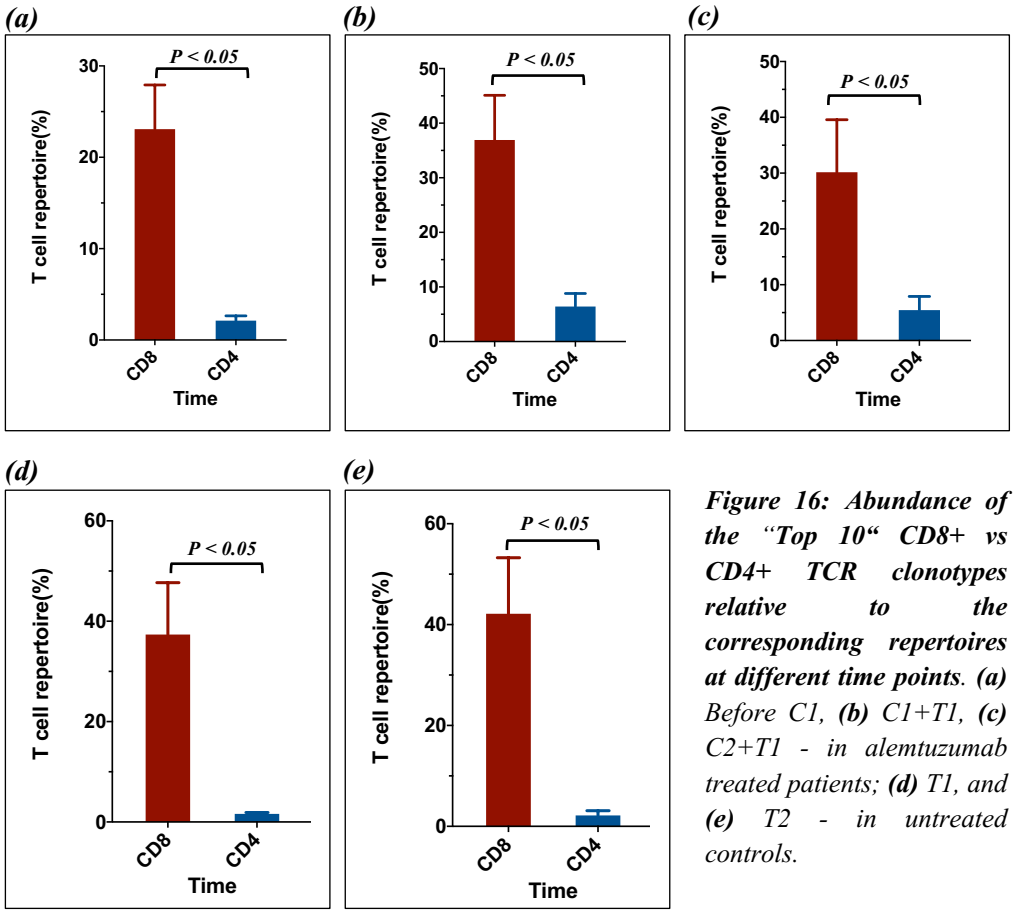

Figure 16: Abundance of the "Top 10" CD8+ vs CD4+ TCR clonotypes relative to the corresponding repertoires at different time points. ***(a)*** *Before C1,* ***(b)*** *C1+T1,* ***(c)*** *C2+T1 - in alemtuzumab treated patients;* ***(d)*** *T1, and* ***(e)*** *T2 - in untreated controls.*

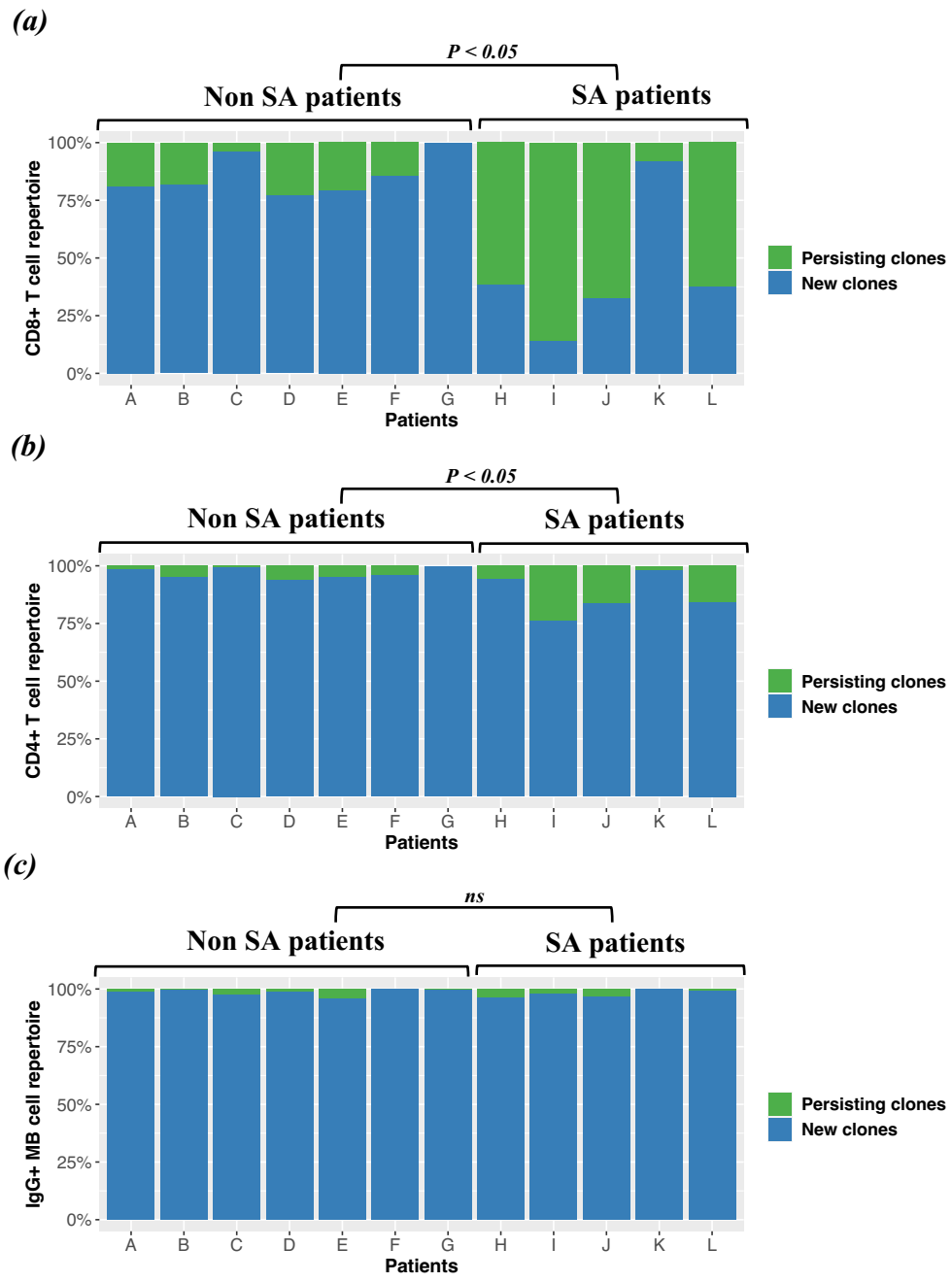

Figure 17. *Longitudinal evolution of the immune repertoire volumes occupied by persisting vs new clones in* ***(a)*** *CD8+ T cells,* ***(b)*** *CD4+ T cells, and* ***(c)*** *IgG+ memory B cells from non SA and SA patients after the first alemtuzumab treatment cycles. (P<0.05 in Mann-Whitney U test, ns = not significant). After alemtuzumab infusion, patient 3 who developed paradox disease reactivation (PDR) showed the very similar immune repertoire changes alike other secondary autoimmunity patients. Therefore, we grouped this patient as secondary autoimmunity (SA). The result is included in a manuscript which is under revision in journal 'Brain'. (Patients are denoted as follows: Patient 1=A, Patient 2 = B, Patient 4 = C, Patient 5 = D, Patient 6 = E, Patient 7 = F, Patient 8 = G, Patient 3 = H, Patient 9 = I, Patient 10 = J, Patient 11 = K, Patient 12 = L).*

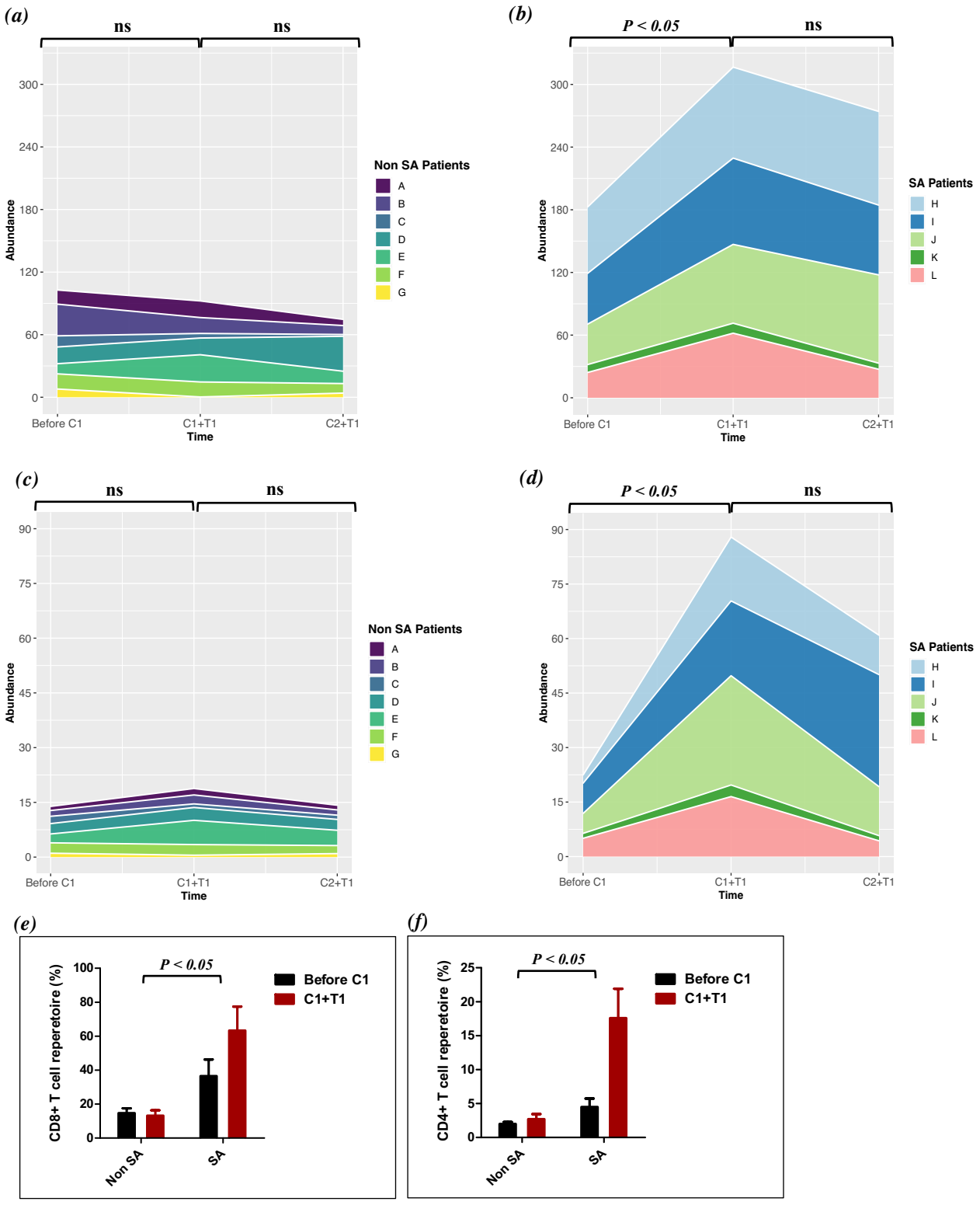

Figure 18. *Tracking stack area plots of CD8* ***(a, b, e)*** *and CD4 T cells* ***(c, d, f)*** *from alemtuzumab treated non SA patients* ***(a, c)*** *and SA patients* ***(b, d):*** *Note the significantly stronger expansions of the top 100 persisting clones both in the CD8+ and CD4+ T cell repertoires after the first alemtuzumab treatment cycles in SA patients and respective quantifications between non-SA and SA patients (e, f). For detail information see figure 17. (a-d: P<0.05 in Wilcoxon signed-rank test, ns = not significant; e, f: P<0.05 in Mann-Whitney U test).*

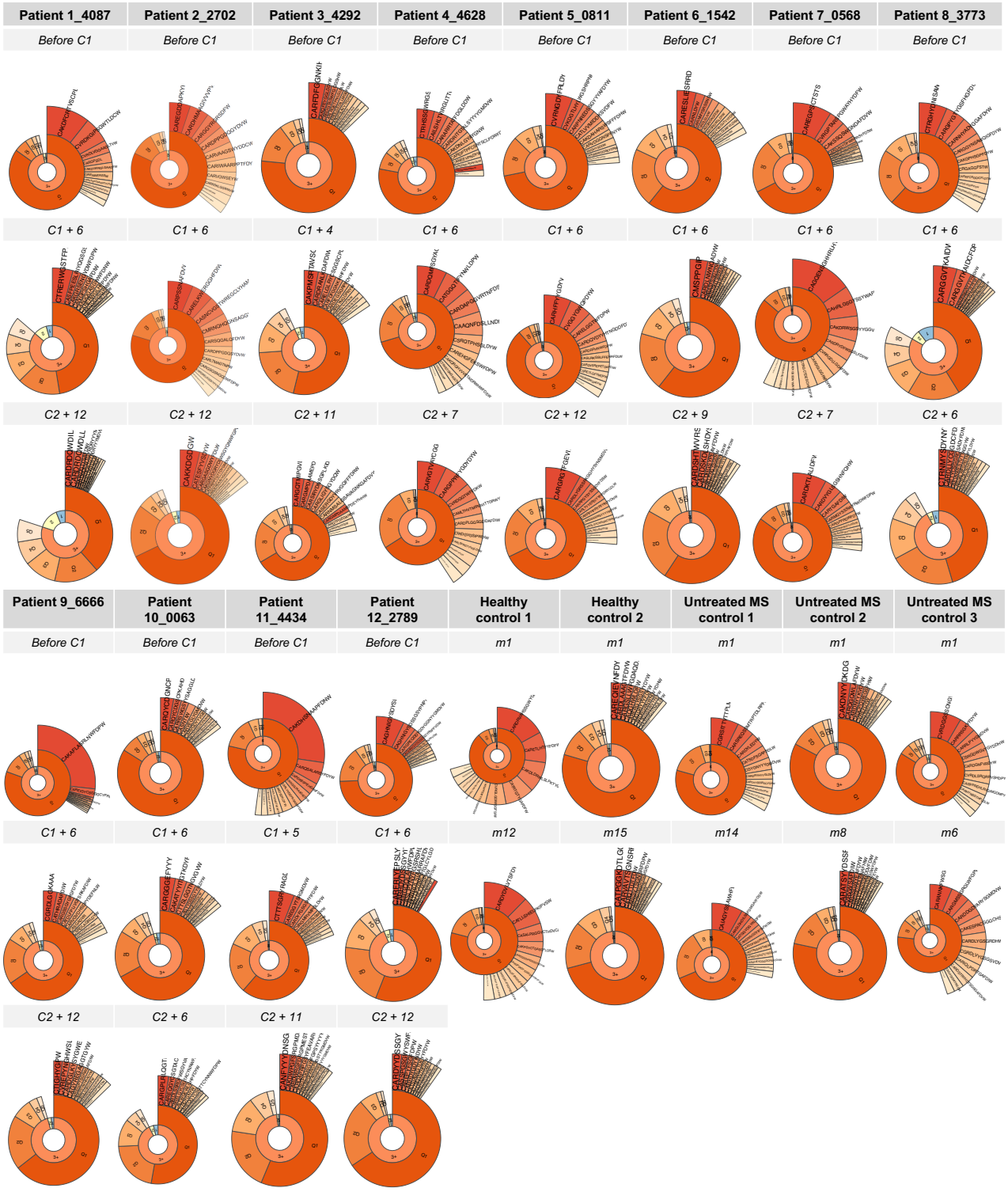

Figure 19: Three layer donut charts of immune repertoires of IgG+ memory B cells from alemtuzumab treated patients and untreated controls. *For explanation of the three layer donut chart see supplementary figure 5.*

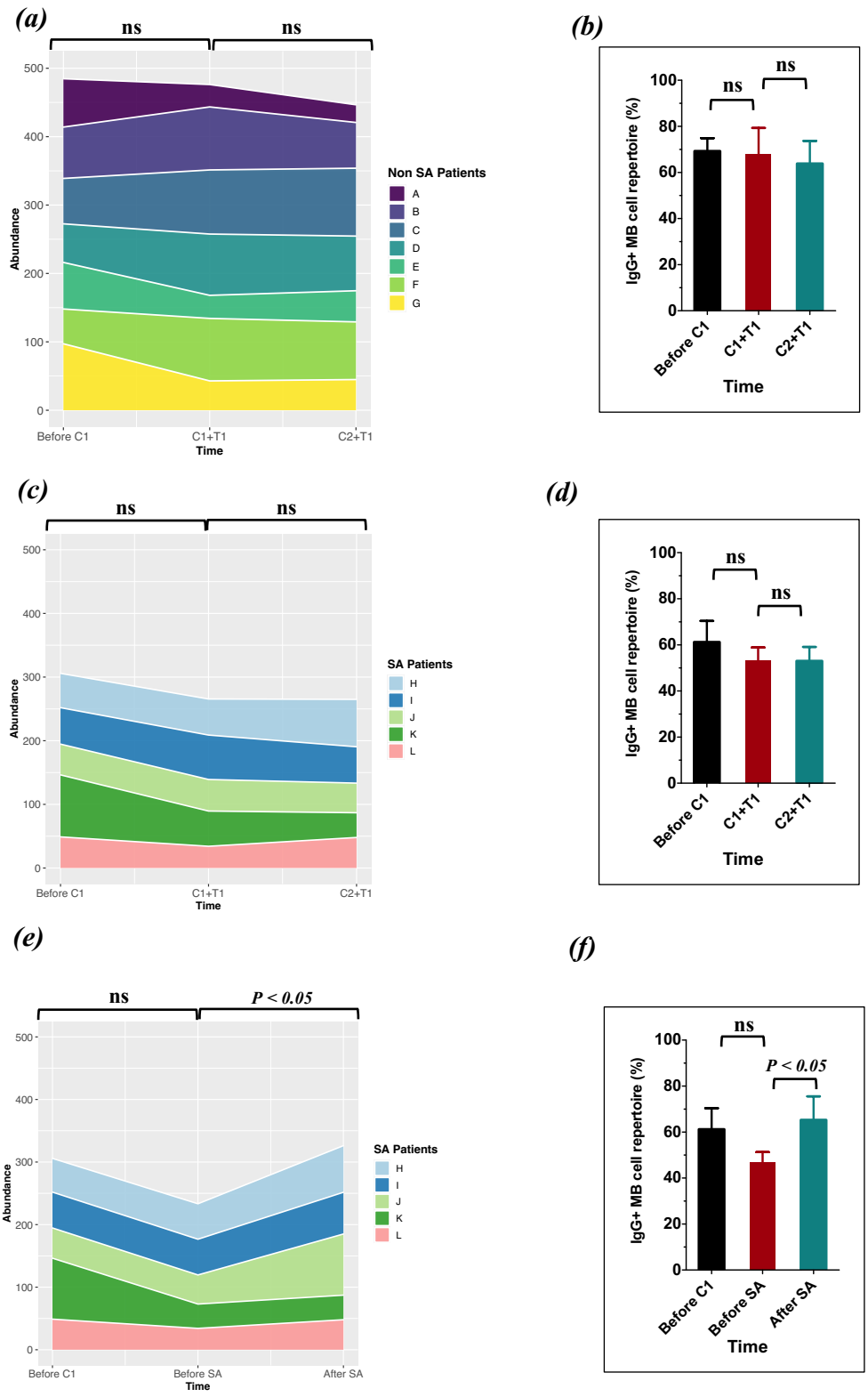

Figure 20. *Tracking stack area plots of IgG+ memory B cells from alemtuzumab treated non SA patients* ***(a)****, SA patients at Before C1, C1+T1, C2+T1* ***(b)****, SA patients at Before C1, Before SA, After SA* ***(c)*** *and quantifications thereof* ***(b, d, f)****. Depicted are the top100 clones (irrespective of persistence). Note the significantly stronger expansions of the top 100 memory B cell clones in SA patients occurring earliest after the second alemtuzumab cycles, which we did not observe in non-SA patients. For detail information see figure 17. (P<0.05 in Wilcoxon signed-rank test, ns = not significant).*

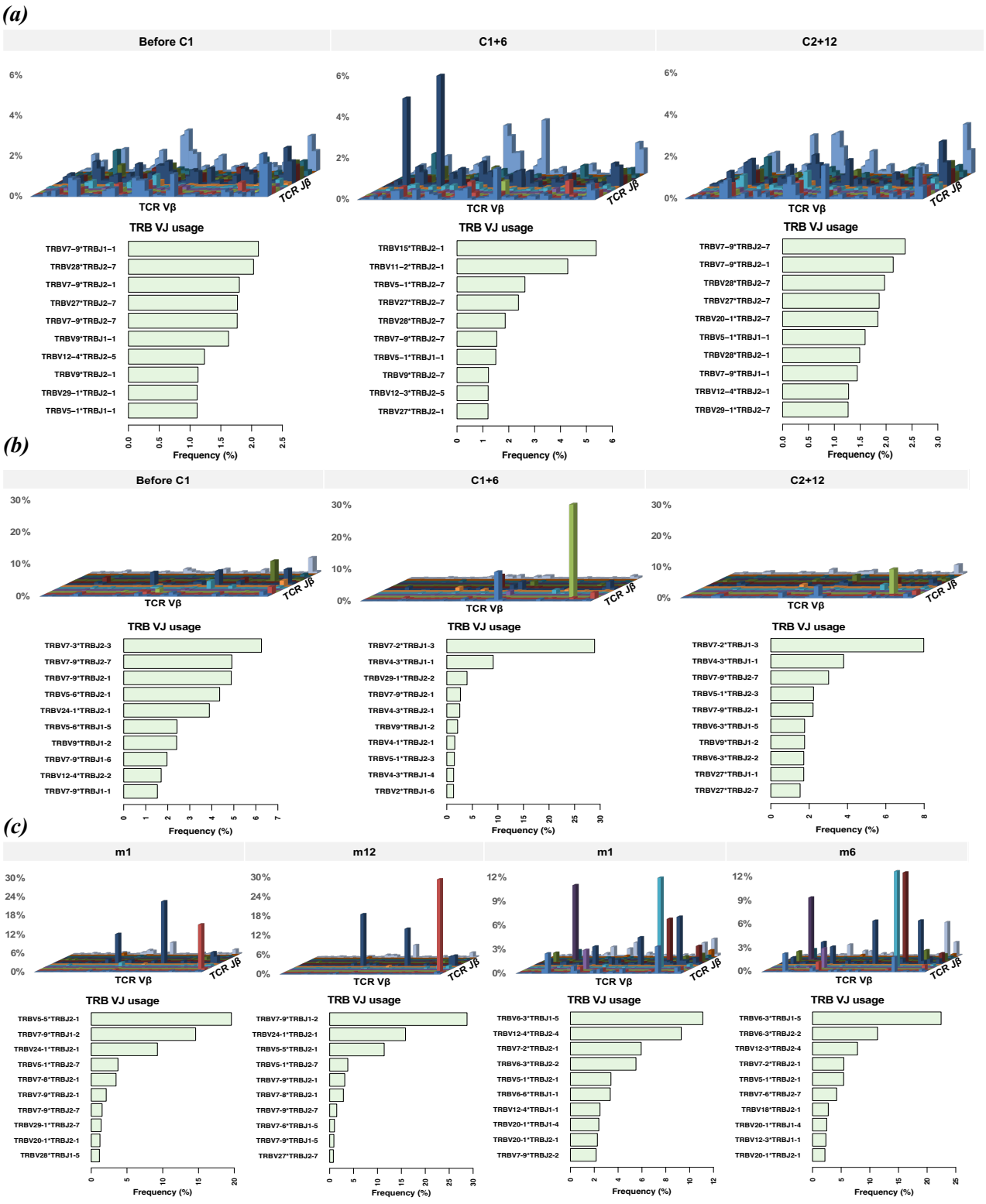

Figure 21: Upper Rows: 3D histograms of relative V-J usage *within the immune repertoires of CD8+ T cells from representative* ***(a)*** *alemtuzumab treated non-SA patient (Patient 1_4087),* ***(b)*** *alemtuzumab treated SA patient (Patient 12_2789), and* ***(c)*** *untreated controls (Healthy control 1 and Untreated MS control 3). Shown is the relative abundance within the immune repertoires (time points as specified). The X-Y axis reflects the presence of a particular V-J recombination event/ frequency of various V-J junctions. The number of different V-J rearrangements correlates with the "Richness" of the immune repertoire. The Z-axis indicates the relative frequency of a particular V-J combination, which is used to calculate the "evenness" of the repertoire.* ***Lower Rows:*** *Bar graphs of „Top 10" relative V-J usage within the shown repertoires of the corresponding patients and untreated controls.*

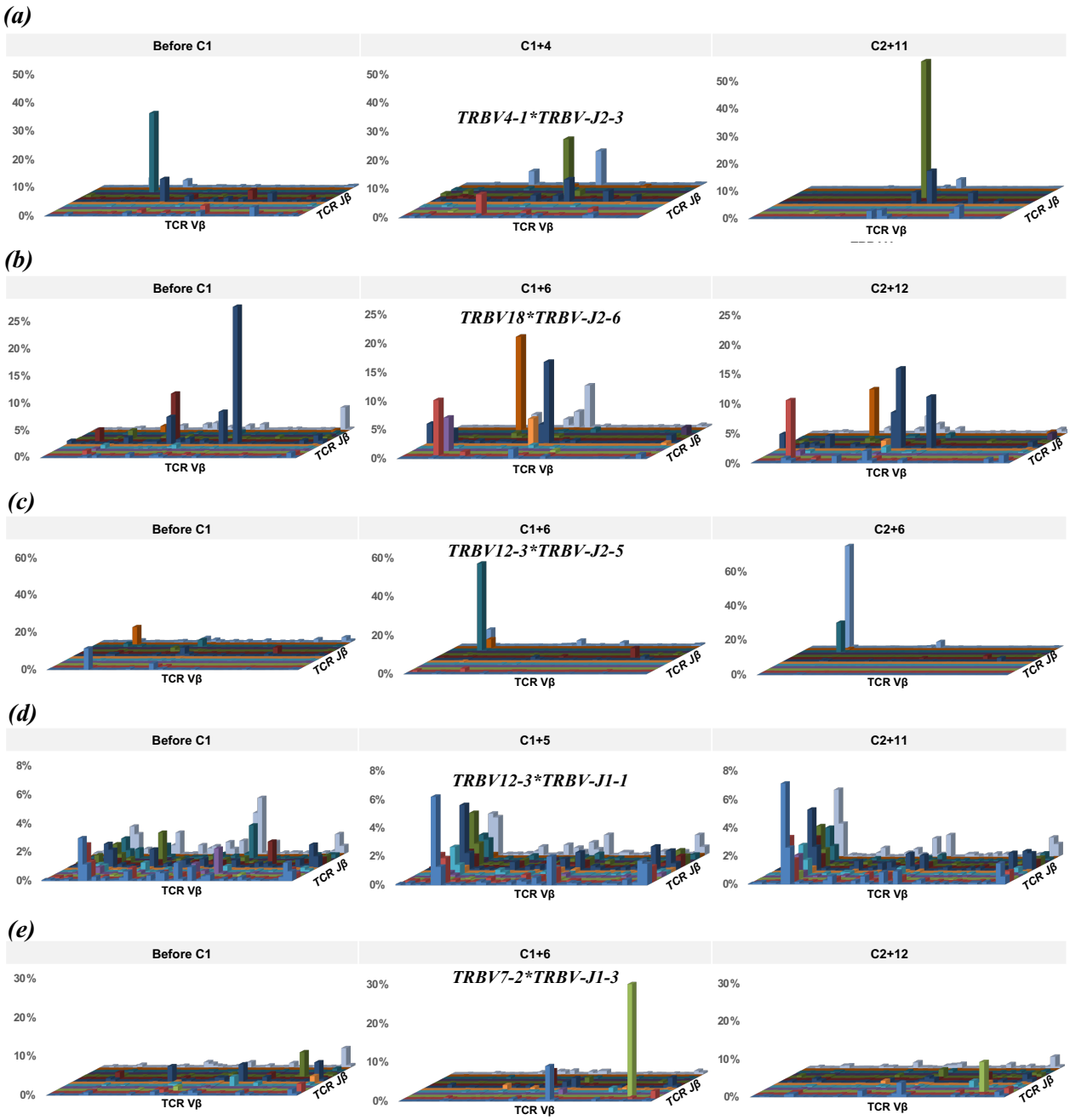

Figure 22: 3D histograms of relative V-J usage *within the immune repertoires of CD8+ T cell from* ***(a)*** *alemtuzumab treated patients who developed PDR (Patient 3_4292),* ***TRBV4-1*TRBV-J2-3*** *is the most prominat V-J pair and persisted after the second infusion as the top clone;* ***(b-e)*** *alemtuzumab treated patients who developed SA* ***(b)****Patient 9_6666,* ***TRBV18*TRBV-J2-6*** *is the most prominat V-J pair and persisted after the second infusion as one of the top clones;* ***(c)*** *Patient 10_0063,* ***TRBV12-3*TRBV-J2-5*** *is the most prominat V-J pair and persisted after the second infusion as one of the top clones;* ***(d)*** *Patient 11_4434,* ***TRBV12-3*TRBV-J1-1*** *is the most prominat V-J pair and persisted after the second infusion as the top clone;* ***(e)*** *Patient 12_2789,* ***TRBV7-2*TRBV-J1-3*** *is the most prominat V-J pair and persisted after the second infusion as the top clone. Shown is the relative abundance within the immune repertoires, (time points as specified). For explanation of the 3D V-J usage see figure 18.*

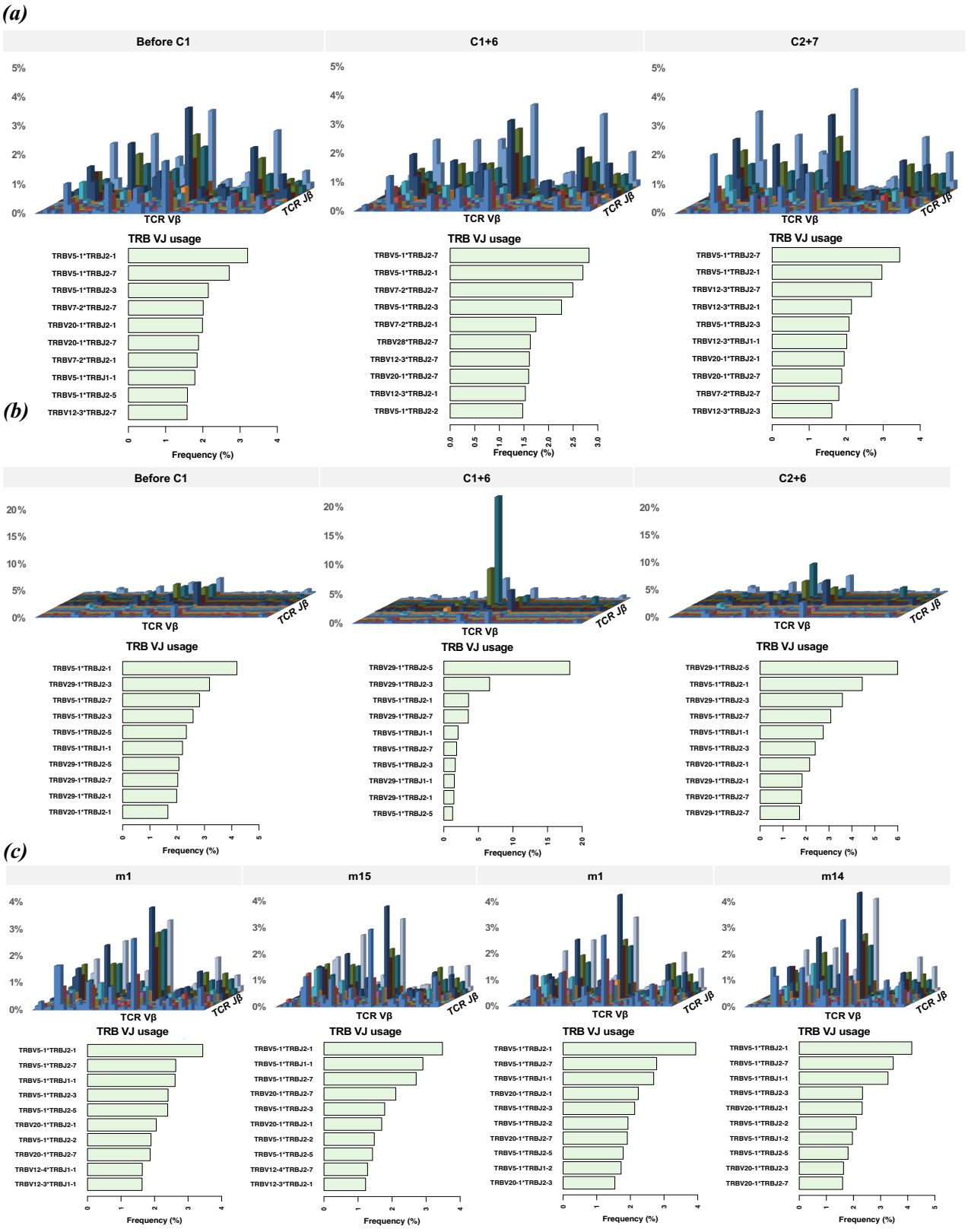

Figure 23: Upper Rows: 3D histograms of relative V-J usage *within the immune repertoires of CD4+ T cells from representative* ***(a)*** *alemtuzumab treated non-SA patient (Patient 4_4628),* ***(b)*** *alemtuzumab treated SA patient (Patient 10_0063), and* ***(c)*** *untreated controls (Healthy control 2 and Untreated MS control 1). Shown is the relative abundance within the immune repertoires.* ***Lower Rows:*** *Bar graphs of „Top 10" relative V-J within the shown repertoires of the corresponding patients and untreated controls (time points as specified). For explanation of the 3D V-J usage see figure 18.*

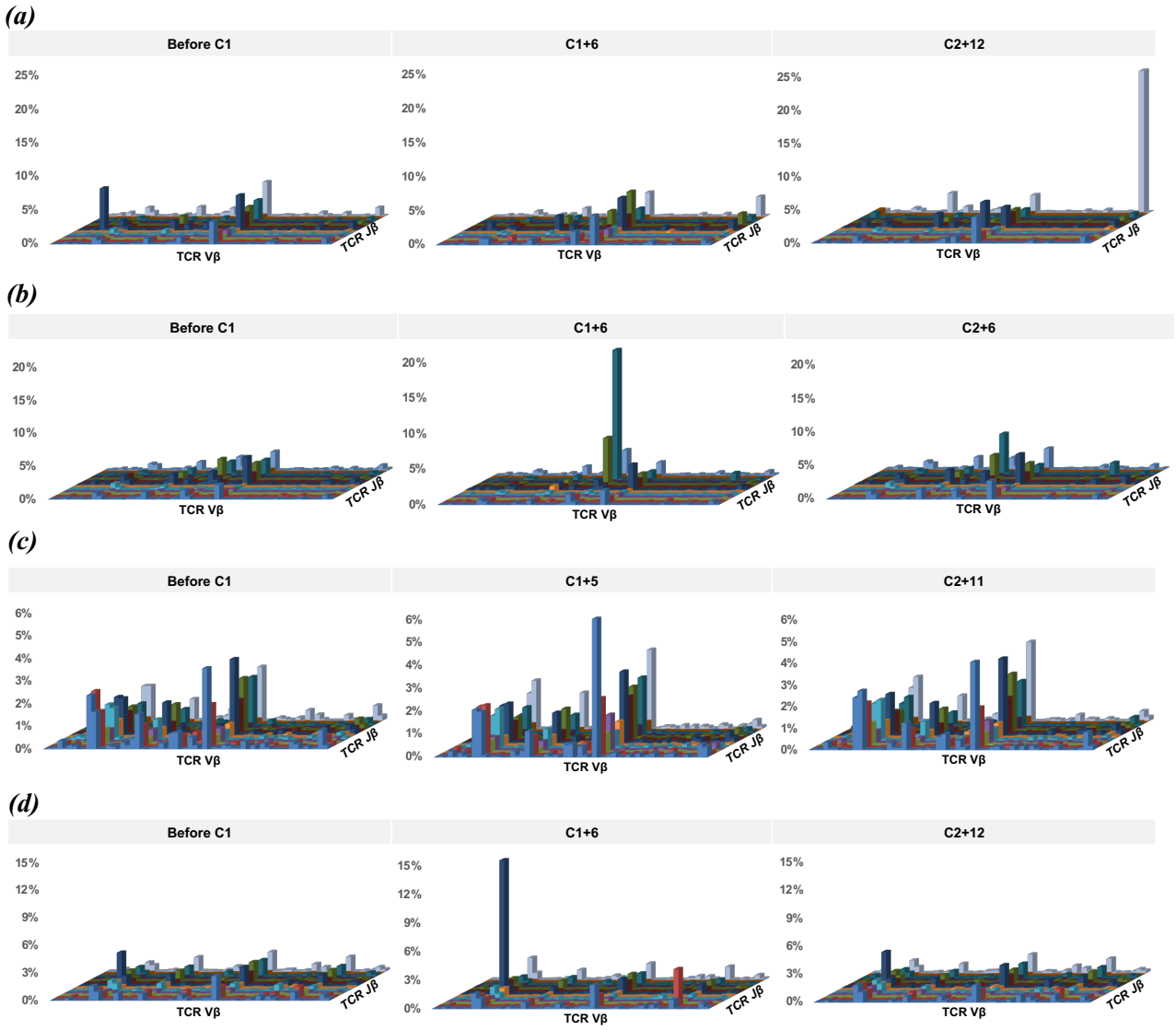

Figure 24: 3D histograms of relative V-J usage *within the immune repertoires of CD4+ T cell from alemtuzumab treated patients who developed secondary autoimmunity* ***(a)*** *Patient 9_6666,* ***(b)*** *Patient 10_0063,* ***(c)*** *Patient 11_4434, and* ***(d)*** *Patient 12_2789. Shown is the relative abundance within the immune repertoires (time points as specified). Certain V-J usage dominate the repertoire after alemtuzumab infusion. For explanation of the 3D V-J usage see figure 18.*

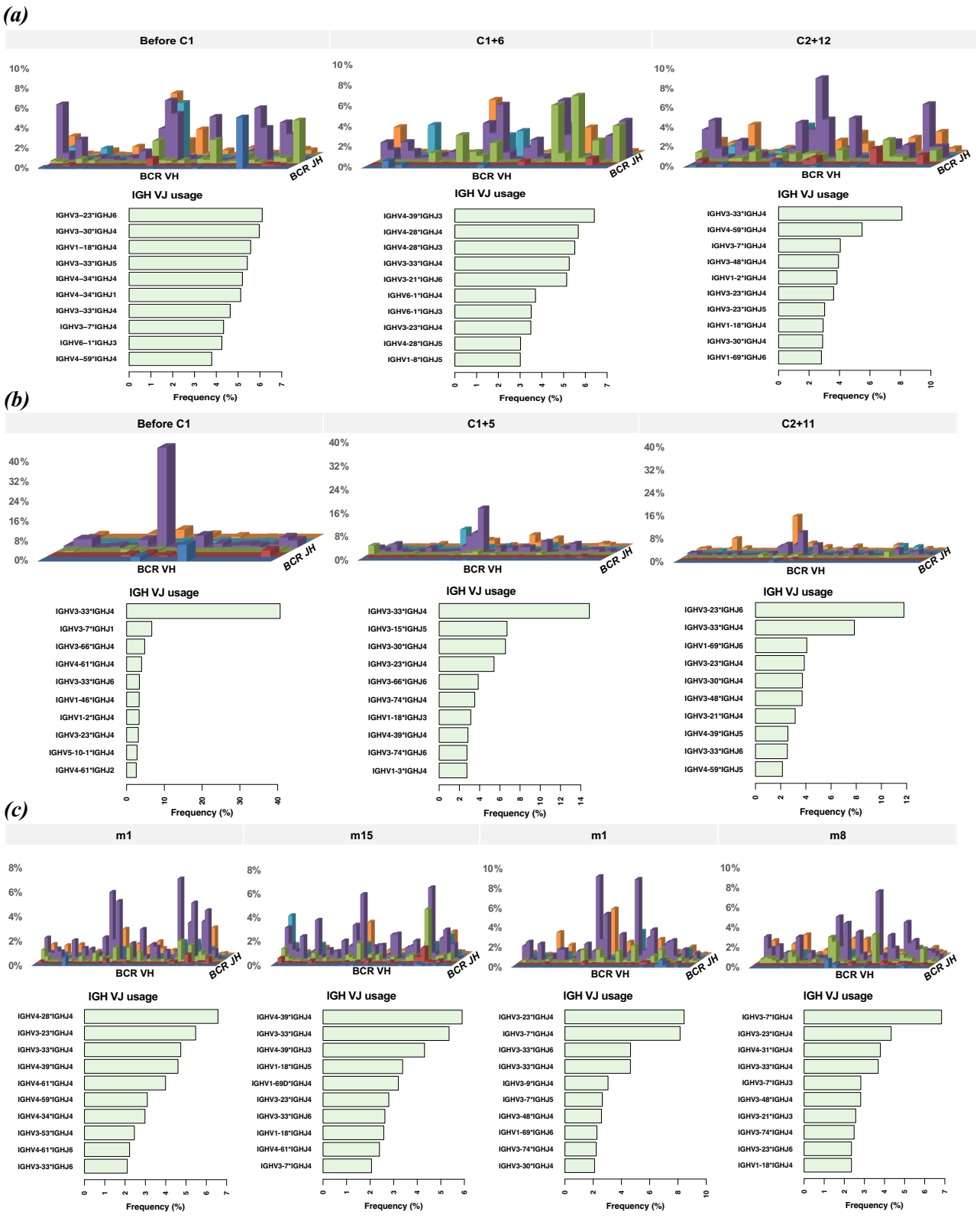

Figure 25: Upper Rows: 3D histograms of relative V-J usage *within the immune repertoires of IgG+ MB cells from representative* ***(a)*** *alemtuzumab treated non-SA patient (Patient 2_2702),* ***(b)*** *alemtuzumab treated SA patient (Patient 11_4433), and* ***(c)*** *untreated controls (Healthy control 2 and Untreated MS control 2). Shown is the relative abundance within the immune repertoires. Lower Rows: Bar graphs of „Top 10" relative V-J within the shown repertoires of the corresponding patients and untreated controls (time points as specified). For explanation of the 3D V-J usage see figure 18*

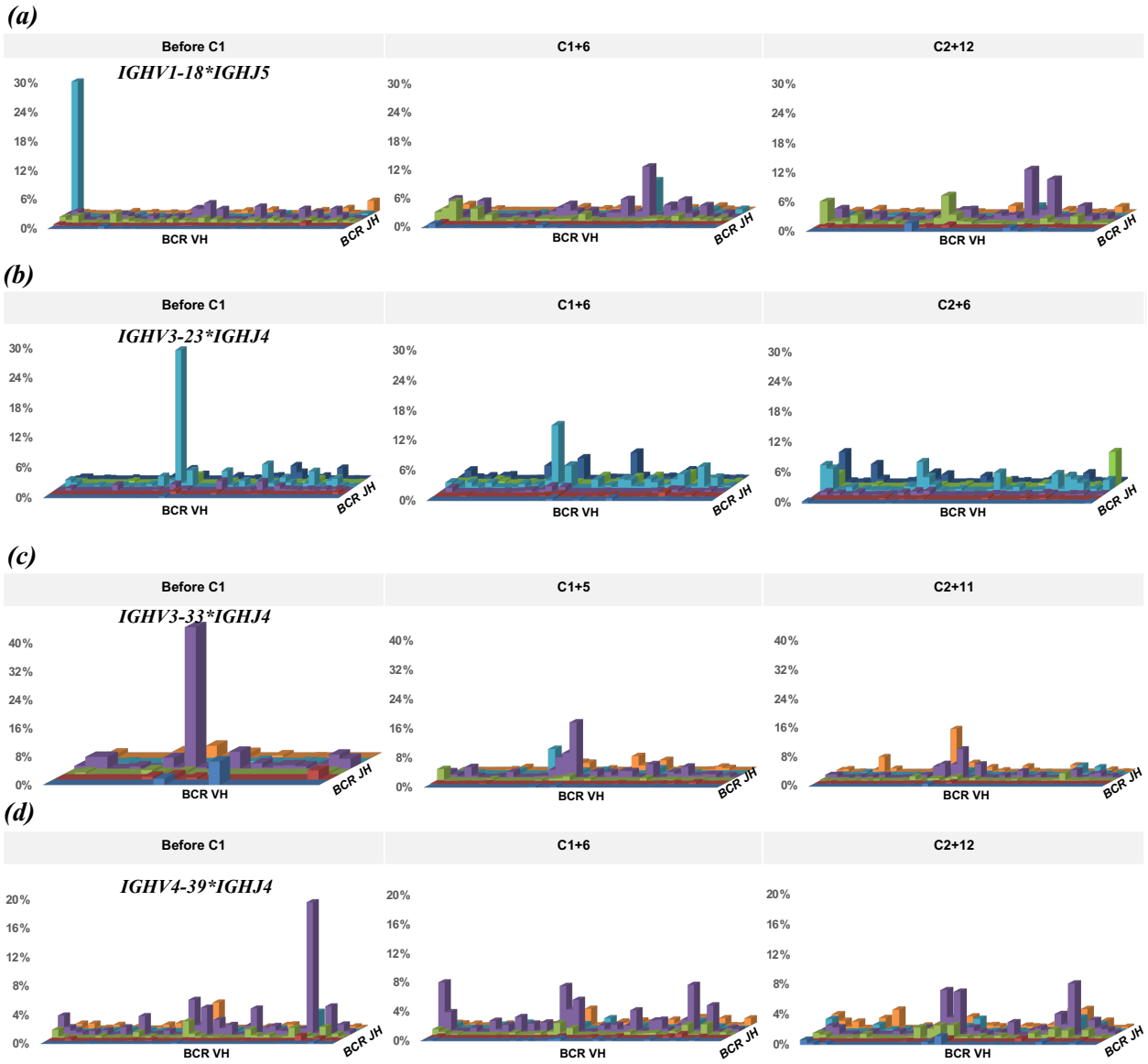

Figure 26: 3D histograms of relative V-J usage *within the immune repertoires of IgG+ MB cells from alemtuzumab treated patients who developed secondary autoimmunity* ***(a)*** *Patient 9_6666,* ***(b)*** *Patient 10_0063,* ***(c)*** *Patient 11_4434, (d) Patient 12_2789. Shown is the relative abundance within the immune repertoires (time points as specified).* ***IGHV1-18*IGHJ5, IGHV3-23*IGHJ4, IGHV3-33*IGHJ4, and IGHV4-39*IGHJ4*** *expanded heavily before treatment in Patient9_6666, Patient 10_0063, Patient 11_4434, and Patient 12_2789 respectively. For explanation of the 3D V-J usage see figure 18.*

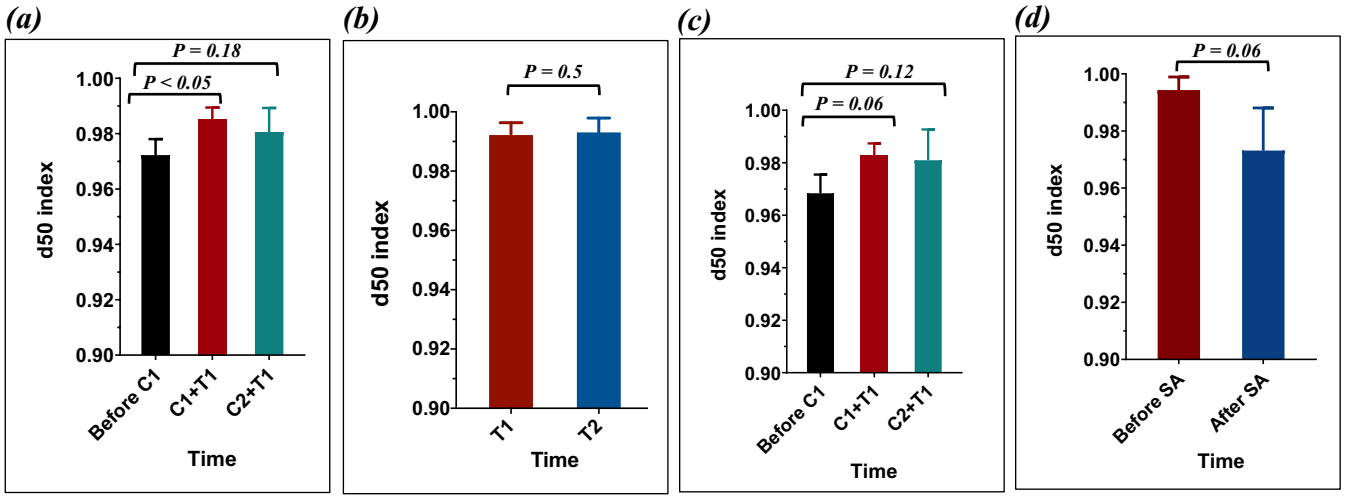

Figure 27. D50 Indices *of* ***(a)*** *all 12 patients,* ***(b)*** *untreated controls,* ***(c)*** *non- SA patients, and* ***(d)*** *SA patients (before and after development of secondary autoimmunity); in* ***CD8+ TCR repertoire.***

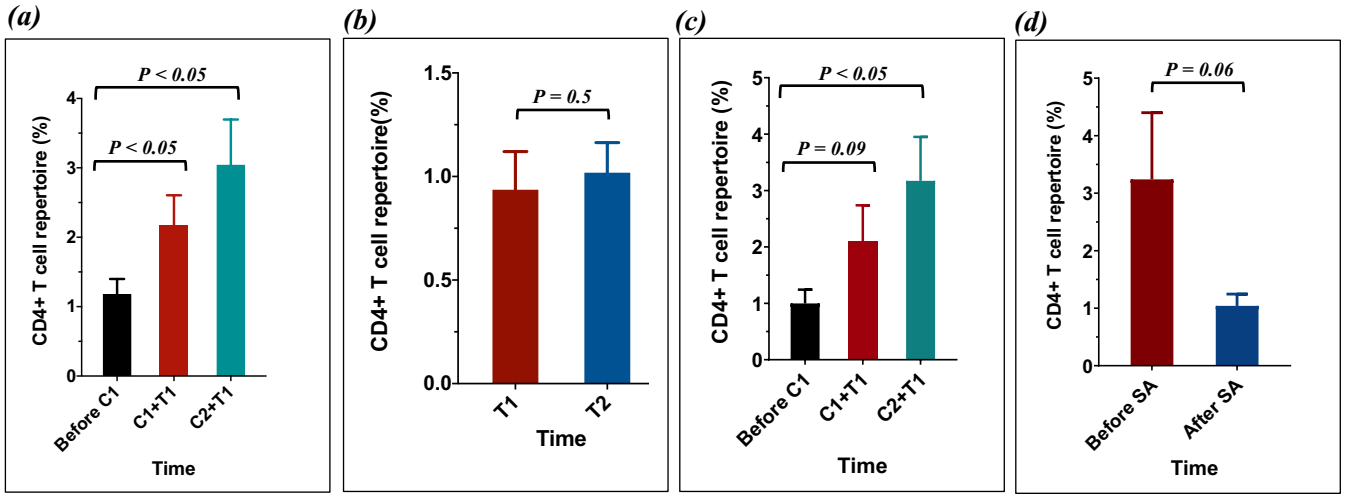

Figure 28: Unique clonotypes (%) *of* ***(a)*** *all 12 alemtuzumab treated MS patients,* ***(b)*** *untreated controls,* ***(c)*** *non-SA patients, and* ***(d)*** *SA patients (before and after development of secondary autoimmunity); in* ***CD4+ T cell repertoire.***

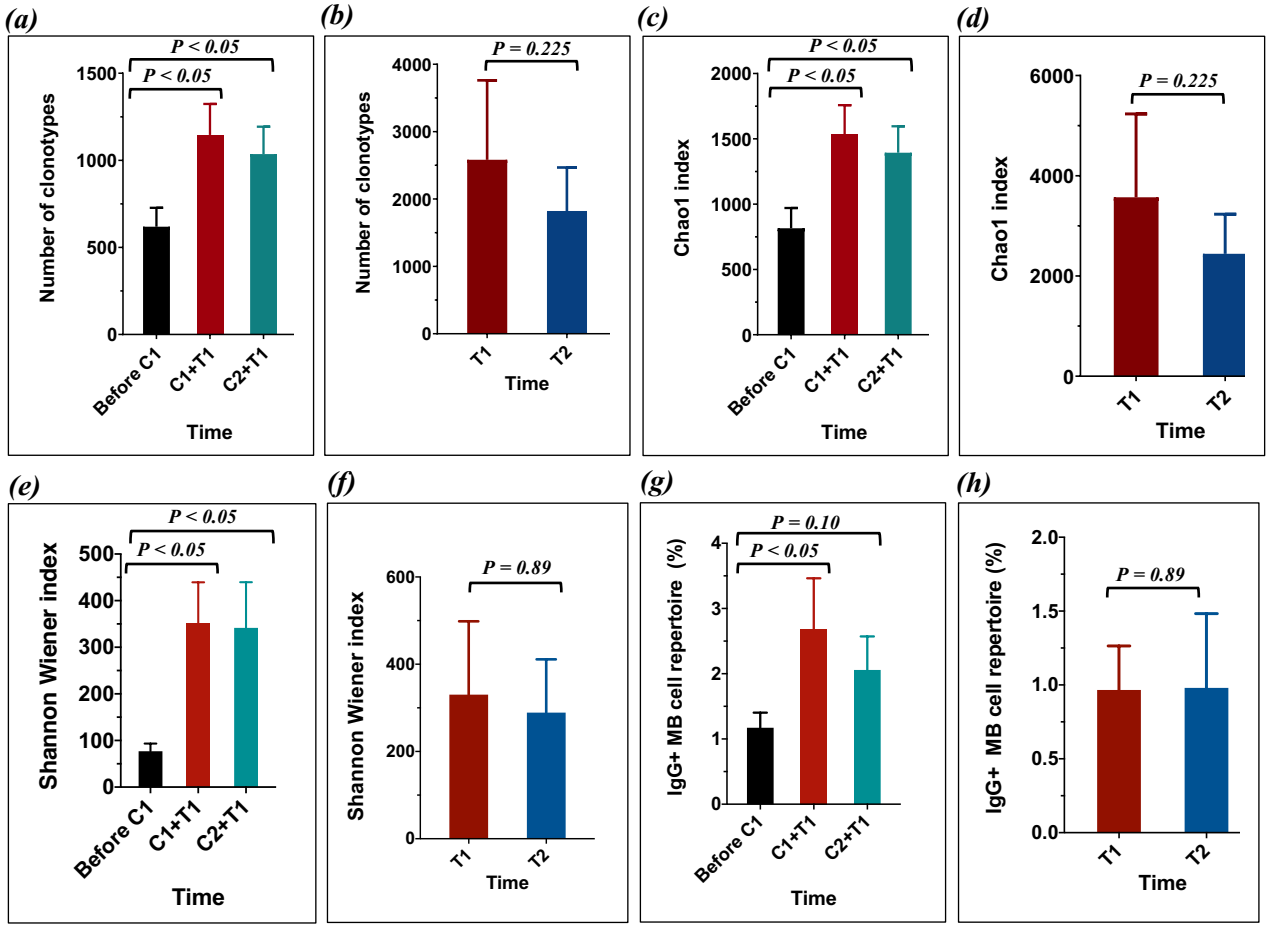

Figure 29. Total number of clonotypes within the IgG+ memory B cell repertoires *of* ***(a)*** *all 12 alemtuzumab treated patients,* ***(b)*** *untreated controls,* ***(c) - (d)*** *corresponding* ***Chao1 indices*** *of clonotypes;* ***(e) - (f)*** *corresponding* ***Shannon Wiener indices****;* ***(g) – (h)*** *corresponding* ***unique clonotypes (%).***

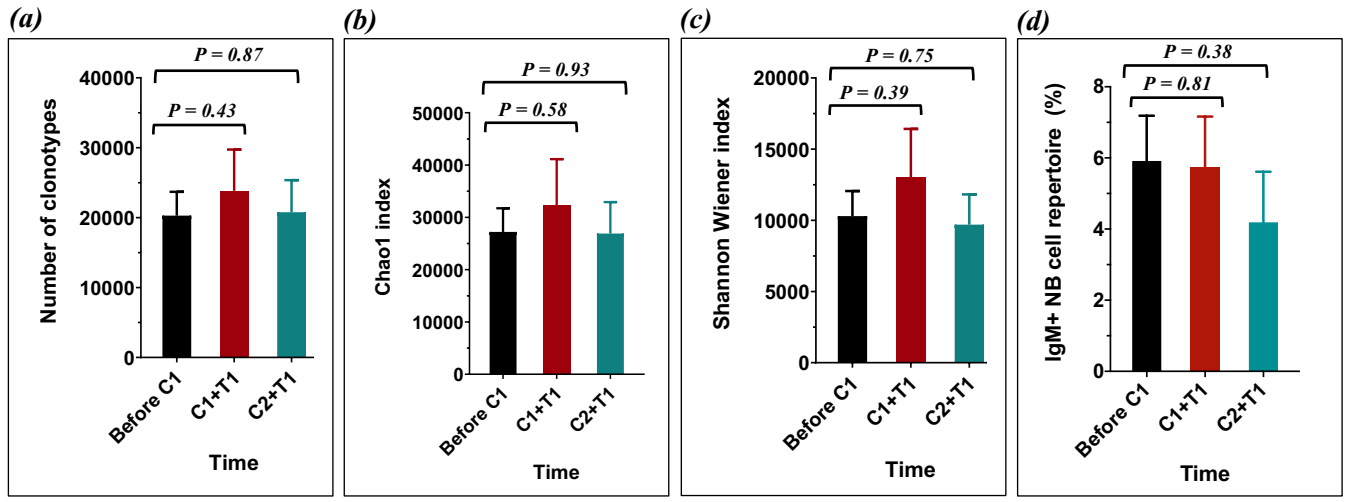

Figure 30: Diversity metrices of IgM+ naive B cell receptor repertoires *of all 12 alemtuzumab treated patients* ***(a) Number of clonotypes, (b) Chao1 indices, (c) Shannon Wiener indices, (d) unique clonotypes (%).*** *No significant change in diversity metrices over the treatment (P > 0.05).*

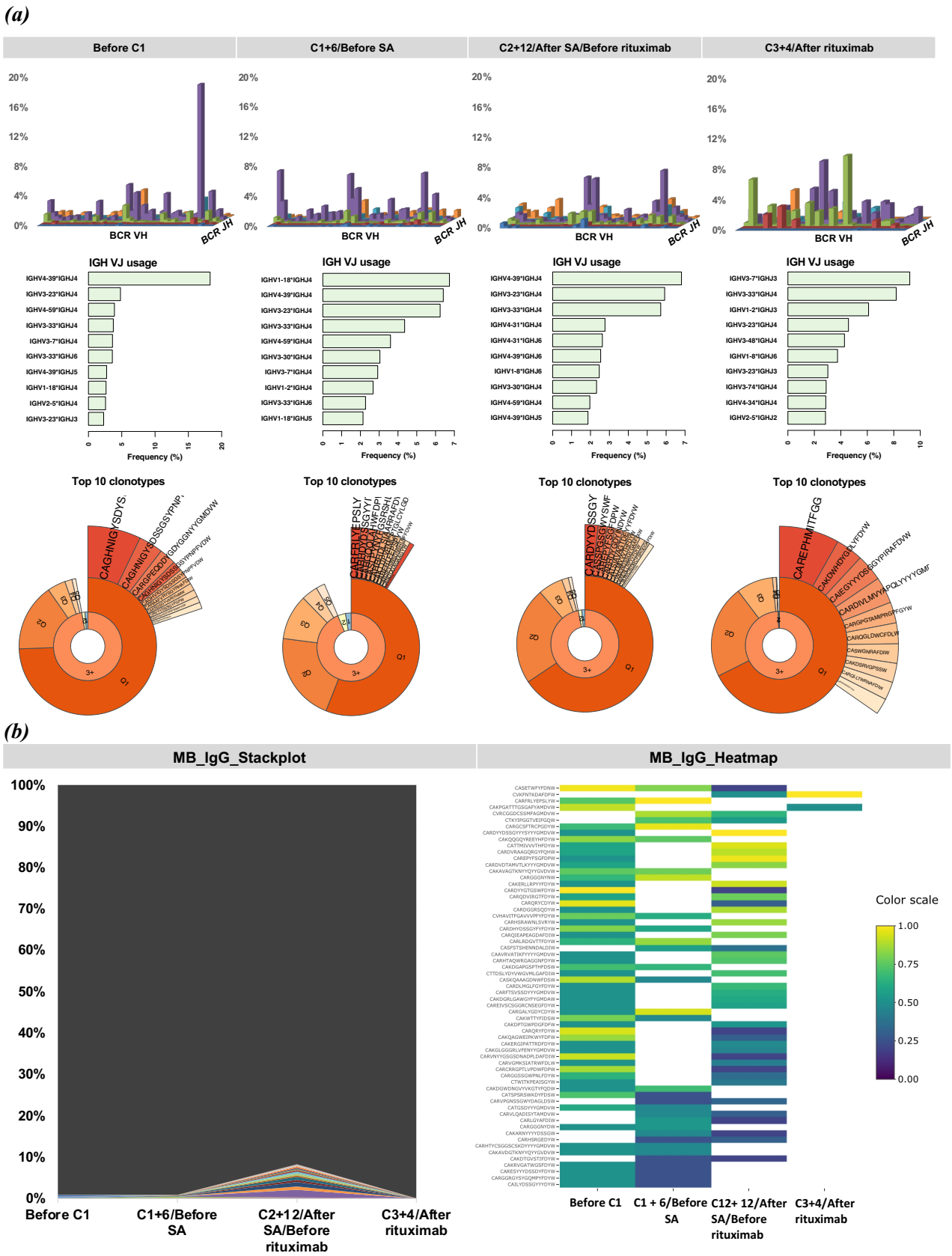

Figure 31. Effect of rituximab on IgG+ memory BCR repertoire in Patient 12_2789. (a) Upper row: *3D histograms of relative V-J usage;* ***middle row:*** *Bar graphs of „Top 10" relative V-J usage within the shown repertoires;* ***lower row:*** *Top ten clonal expansion visualize in three layer donut charts, and* ***(b)*** *Clonal depletion by rituximab treatment. Only two clones persisted after the rituximab treatment (time points as specified).*

(a)

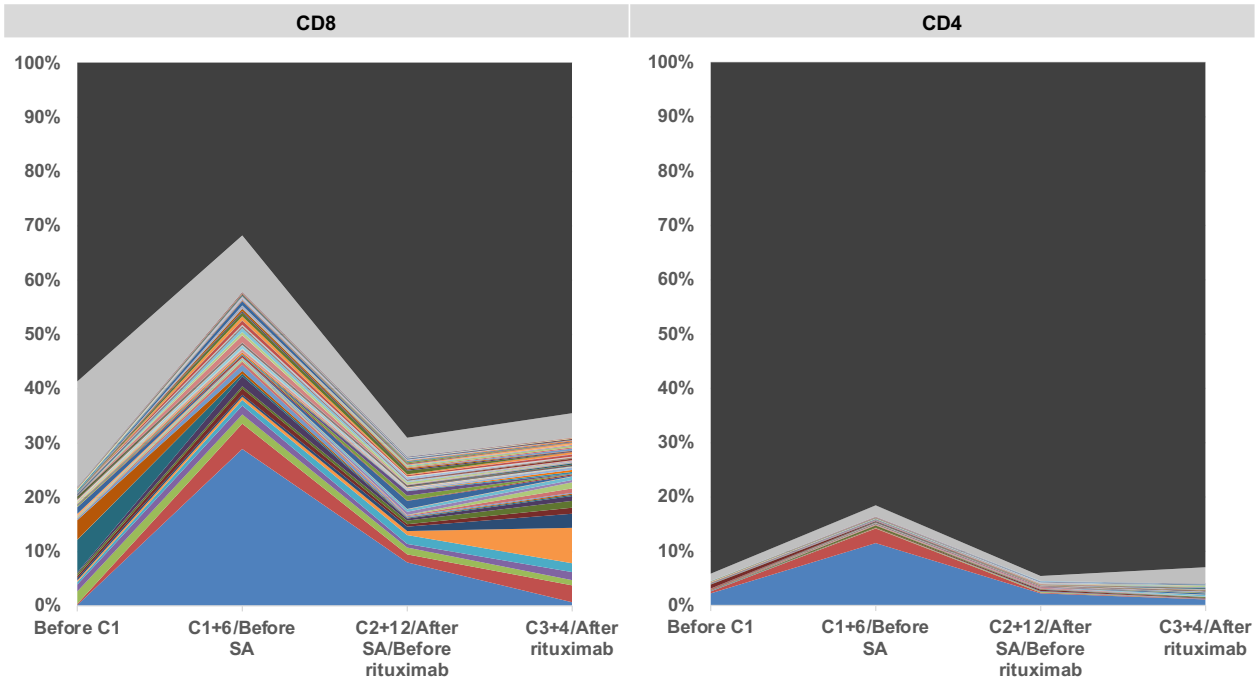

(b)

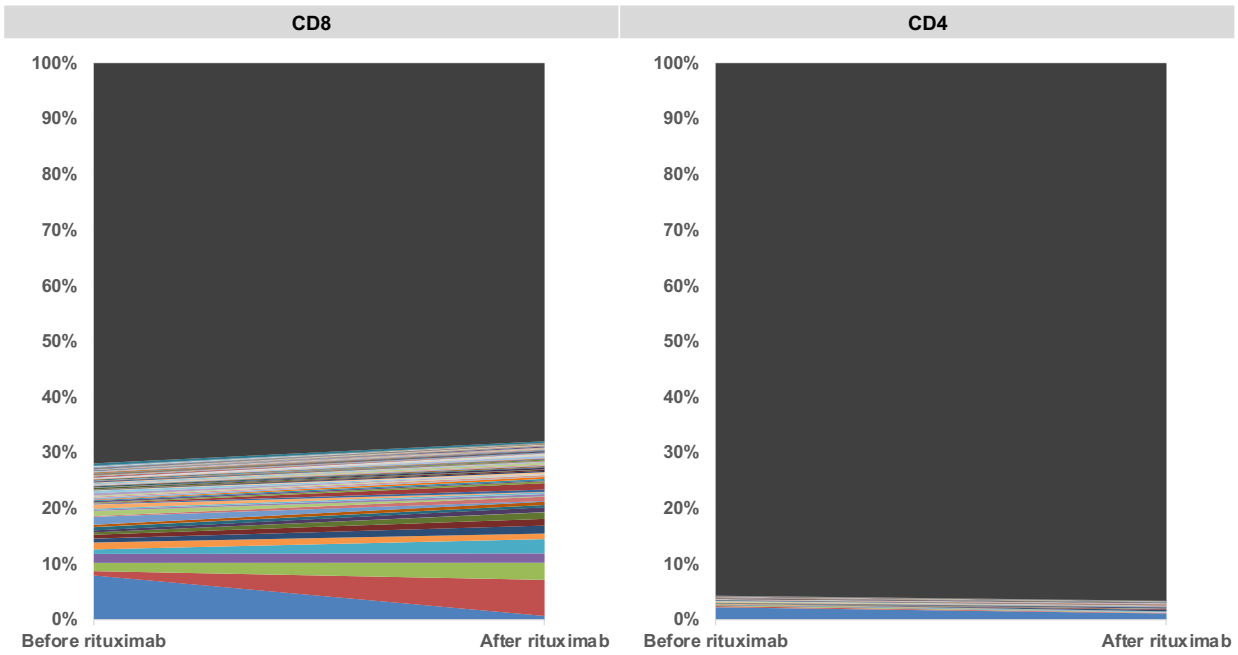

Figure 32. Clonotype tracking stack area plots of CD8+ and CD4+ TCR repertoire (a) *following alemtuzumab and rituximab treatment,* ***(b)*** *before and after rituximab treatment. For explanation of the clonotype tracking stack area plot see figure 3.*

Table 1: Overview of patients clinical Data

Patient	***Pat 1 -4087***	***Pat 2 -2702***	***Pat 3 -4292***	***Pat 4 -4628***	***Pat 5 -0811***	***Pat 6 -1542***	***Pat 7 -0568***	***Pat 8 -3773***	***Pat 9 -6666***	***Pat 10 -0063***	***Pat 11 - 4434***	***Pat 12 - 2789***
Birth year	*1976*	*1976*	*1966*	*1989*	*1982*	*1969*	*1963*	*1985*	*1974*	*1988*	*1983*	*1987*
Sex	*F*	*F*	*M*	*M*	*M*	*F*	*F*	*M*	*F*	*F*	*M*	*F*
Disease onset	*2012*	*2005*	*2013*	*2006*	*2011*	*1995*	*1989*	*2006*	*2012*	*2010*	*2005*	*2012*
Diagnosis	*2014*	*2005*	*2014*	*2007*	*2015*	*2010*	*2008*	*2006*	*2012*	*2010*	*2006*	*2012*
Treatment before alemtuzumab	*X*	*Gilene-ya*	*X*	*Aubagio*	*Copax-one*	*Mitoxa-ntron*	*Tysabri*	*Rebif*	*Tecfidera*	*File-neya*	*Copax-one*	*Copax-one*
JC antibody status	*+ve*	*n.d*	*n.d*	*-ve*	*n.d*	*n.d*	*-ve*	*+ve*	*n.d*	*-ve*	*+ve*	*n.d*
Time points	*Before Cycle 1*	*Before Cycle 1*	*Before Cycle 1*	*Before Cycle 1*	*Before Cycle 1*	*Before Cycle1*	*Before Cycle1*	*Before Cycle 1*	*Before Cycle 1*	*Before Cycle 1*	*Before Cycle 1*	*Before Cycle 1*
	C1+6	*C1+6*	*C1+4*	*C1+6*	*C1+6*	*C1+6*	*C1+6*	*C1+6*	*C1+6*	*C1+6*	*C1+5*	*C1+6*
	C2+12	*C2+12*	*C2+11*	*C2+7*	*C2+12*	*C2+9*	*C2+7*	*C2+6*	*C2+12*	*C2+6*	*C2+11*	*C2+12*
	-	*-*	*-*	*-*	*-*	*-*	*-*	*-*	*C2+24*	*C3+7*	*C2+24*	*C3+4*
EDSS (Baseline)	*2.5*	*4.0*	*3.0*	*2.5*	*3.0*	*3.5*	*3.0*	*2.0*	*4.5*	*4.0*	*1.0*	*1.0*
Relapse (C1-C3)	*No*	*No*	*Yes*	*No*	*Yes*	*Yes*	*No*	*No*	*No*	*Yes*	*No*	*Yes*
Secondary autoimmunity	*X*	*X*	*X*	*X*	*X*	*X*	*X*	*X*	*Thyroid autoimmunity*	*Graves*	*Graves*	*Graves*
First manifestation of SA	*-*	*-*	*-*	*-*	*-*	*-*	*-*	*-*	*C2+22*	*C3+6*	*C2+13*	*C2+11*
Other post-alemtuzumab disease/complication	*X*	*X*	*Paradox disease reactivation (PDR)*	*X*	*X*	*X*	*X*	*X*	*X*	*X*	*X*	*X*
First manifestation of PDR			*C1+12*									

Compartment A = Shared clones between (Before cycle 1 and Cycle1 + Time point1),
Compartment B = Shared clones between (Cycle 1 + Time point 1 and Cycle 2 + Time point 1)
Compartment C = Shared clones between (Before cycle 1 and Cycle 2 + Time point1)
Compartment D = Shared clones between all three time points

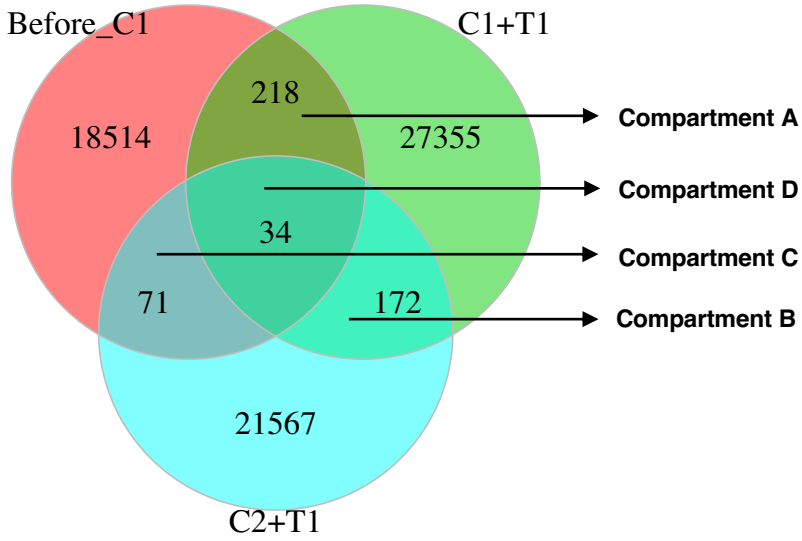

Suppeimentary figure 1. Overview of joint clonotype abundance graph ("VENN diagramme").

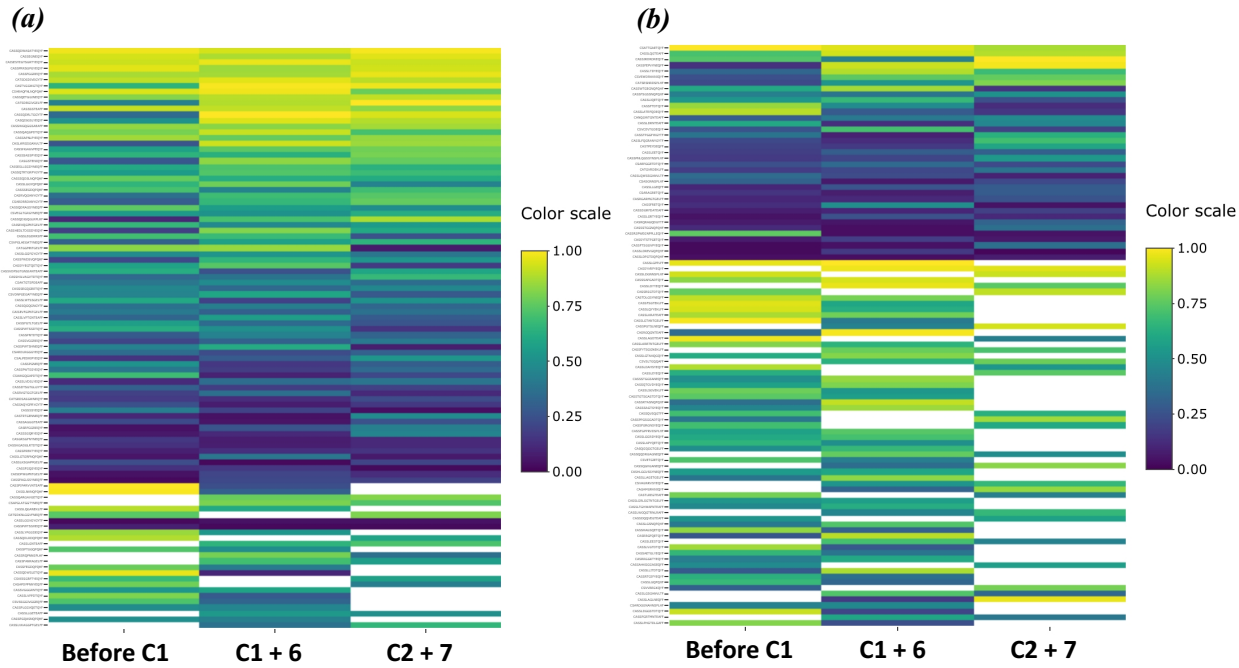

Supplementary figure 2. Clonotype tracking heatmaps of top 100 clones *of* ***(a)*** *CD8+ T cell, and* ***(b)*** *CD4+ T cell immune repertoires from a representative alemtuzumab treated patient 7_3773. Here, the relative abundance and persistence (at least two consecutive time points) of the top 100 clones are visualized. Clonal persistence is dominant in CD8+ TCR than CD4+ TCR. For explanation of the clonotype tracking heatmap see figure 8.*

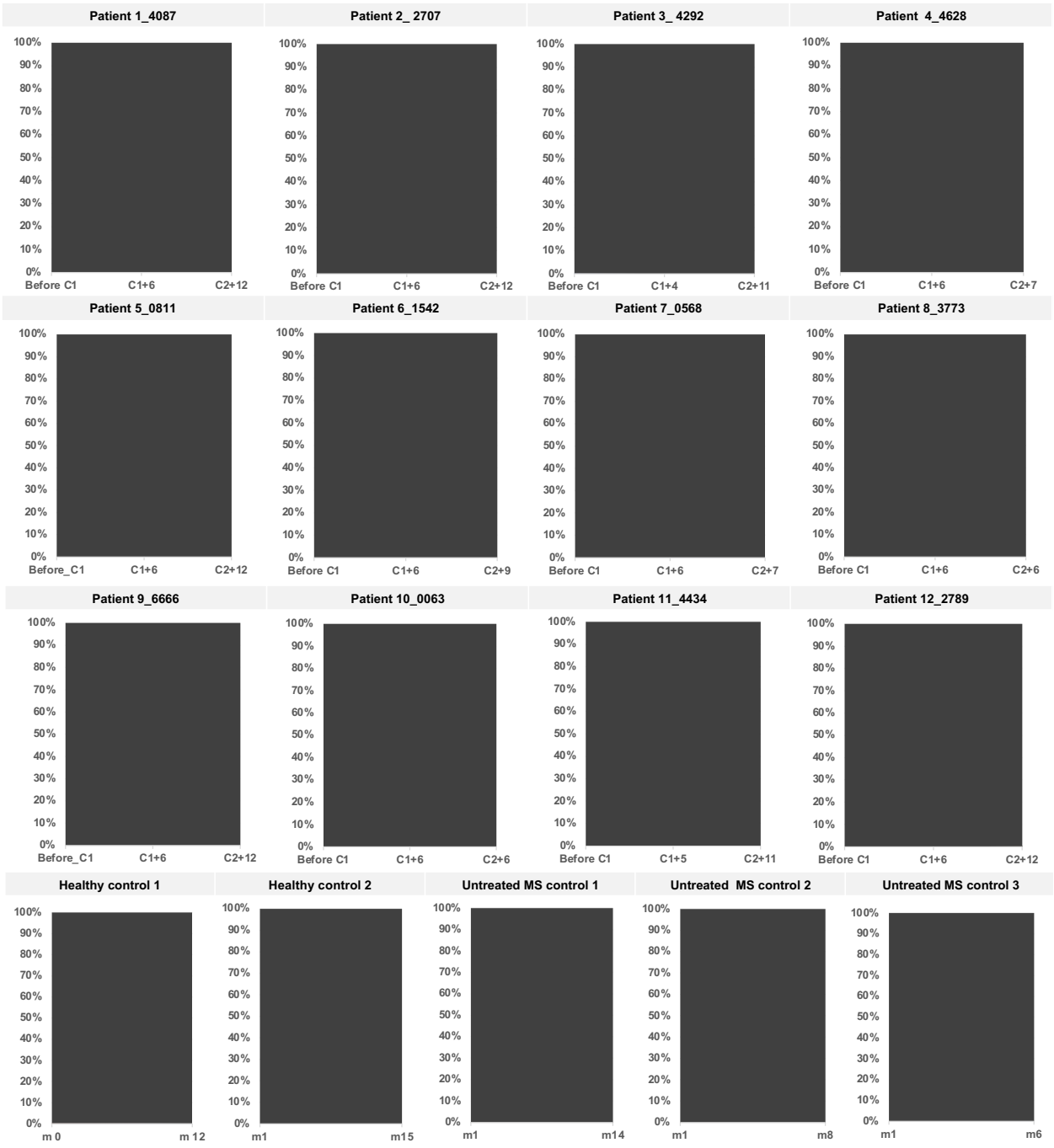

Supplementary figure 3. Clonotype tracking stackplots of IgM+ naïve B cells from alemtuzumab treated patients and untreated controls. *Very few low-abundant persisting clones are observed in treated patients and untreated controls. For explanation of the clonotype tracking stack area plot see figure 3.*

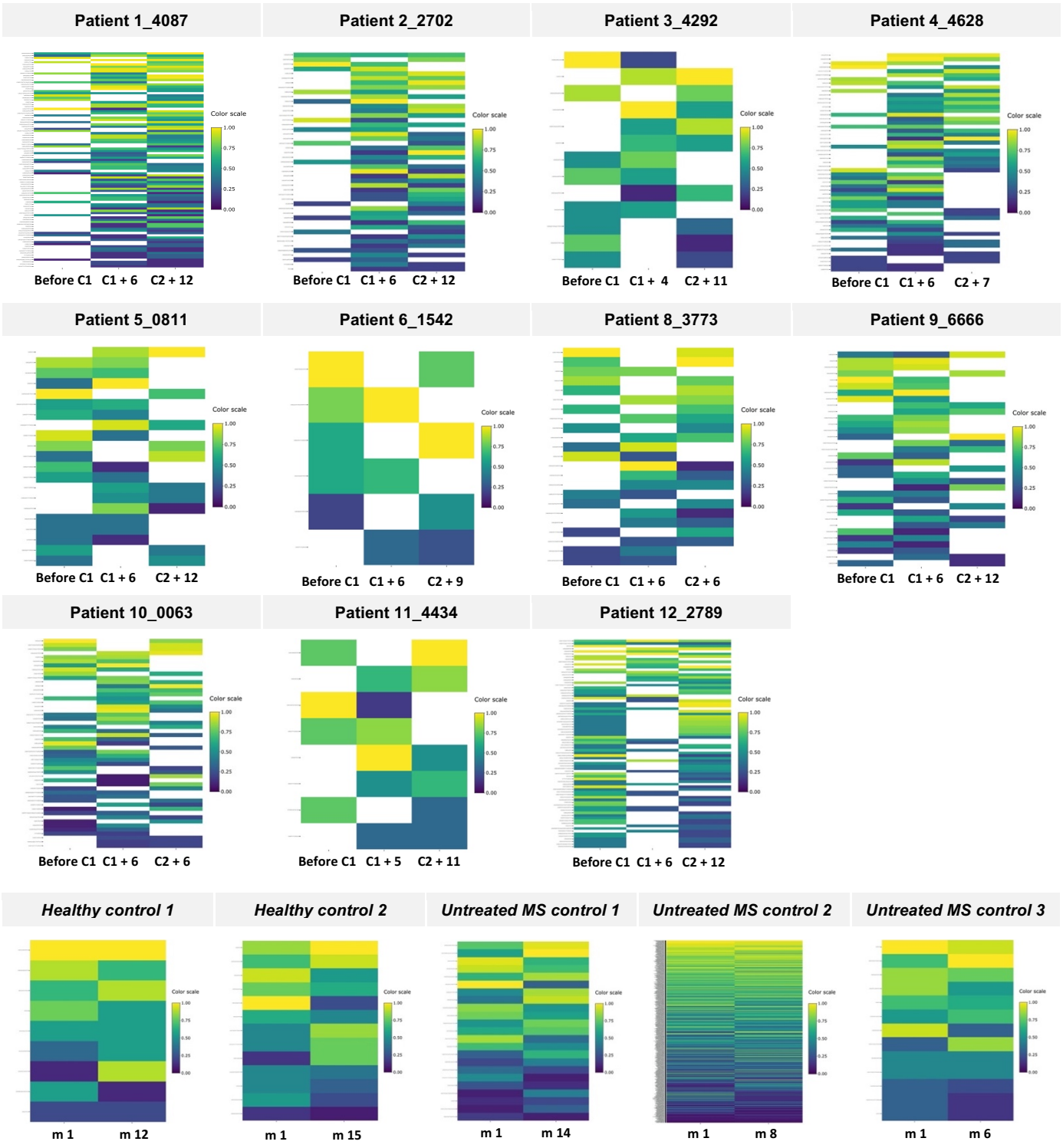

Supplementary figure 4: Clonotype tracking heatmaps of IgM+ naïve B cell immune repertoires from alemtuzumab treated patients and untreated controls. *There is no persisting clone in patient 7_0568. Here, the relative abundance and persistence (at least two consecutive timepoints) of the entire immune repertoires is visualized. For explanation of the clonotype tracking heatmap see figure 8.*

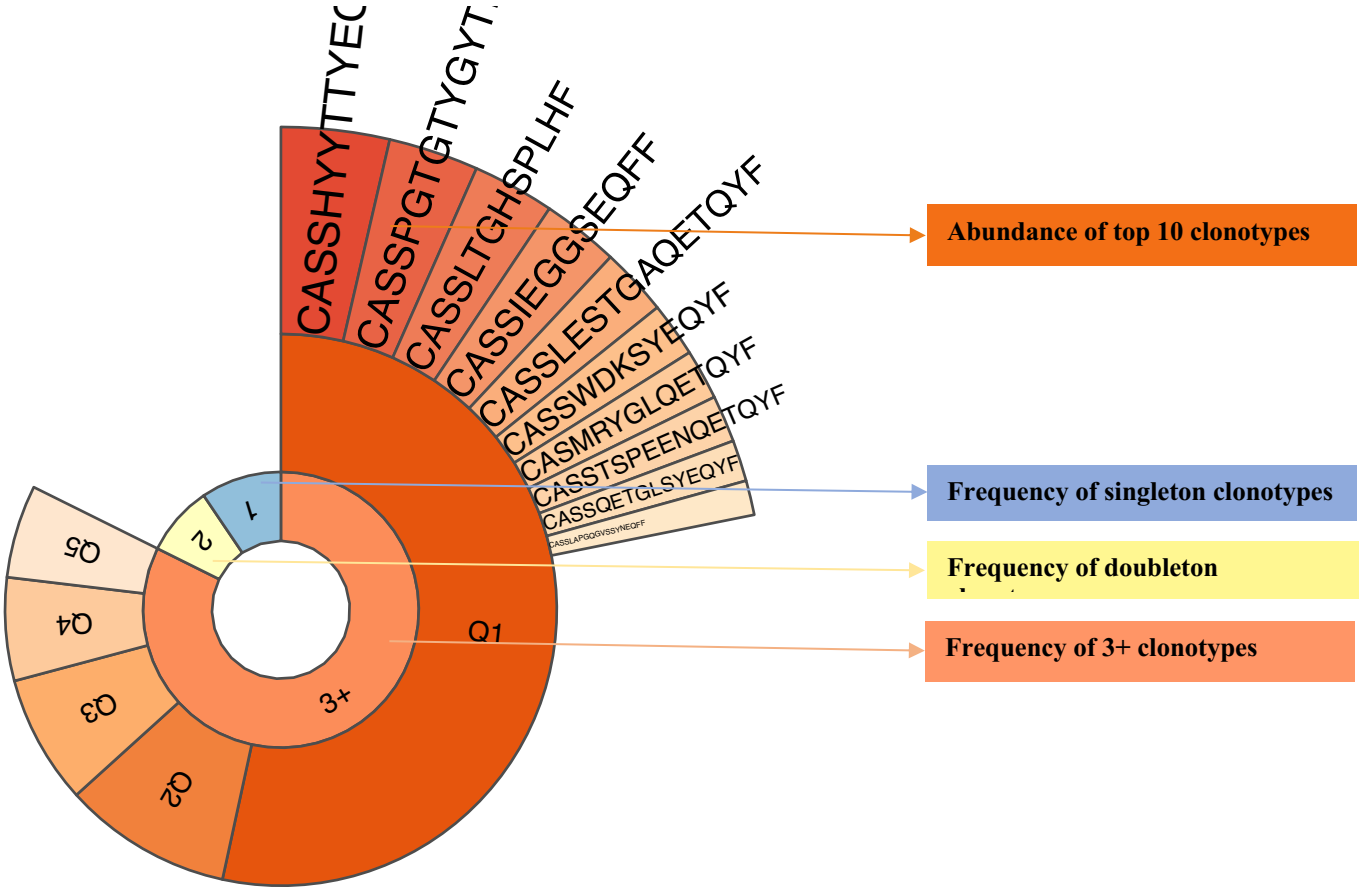

Plots a three-layer donut chart to visualize the repertoire clonality.
The first (inner) layer ("set") includes the frequency of singleton ("1", met once), doubleton ("2", met twice) and high order ("3+", met three or more times) clonotypes.
The second (middle) layer ("quantile"), displays the abundance of top 20% ("Q1"), next 20% ("Q2"), . . (up to "Q5") clonotypes for clonotypes of the "3+" set.
The last (outer) layer ("top") displays the individual abundances of top N (10) clonotypes.

Supplementary figure 5. Overview of three layer donut chart.

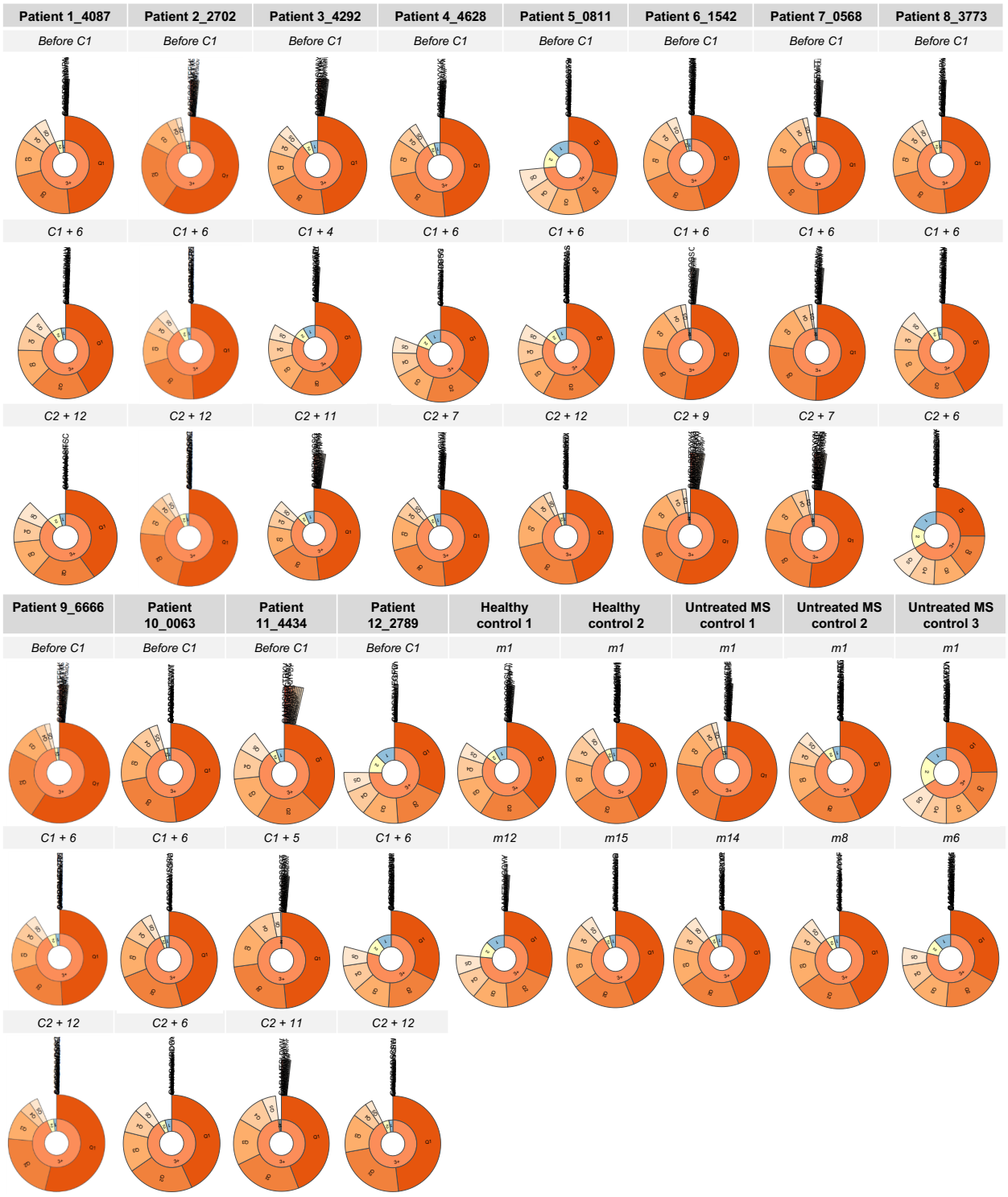

Supplementary figure 6: Three layer donut charts of immune repertoires of IgM+ naïve B cells from alemtuzumab treated patients and untreated controls. *For explanation about the three layer donut chart see supplementary figure 5.*

(a)

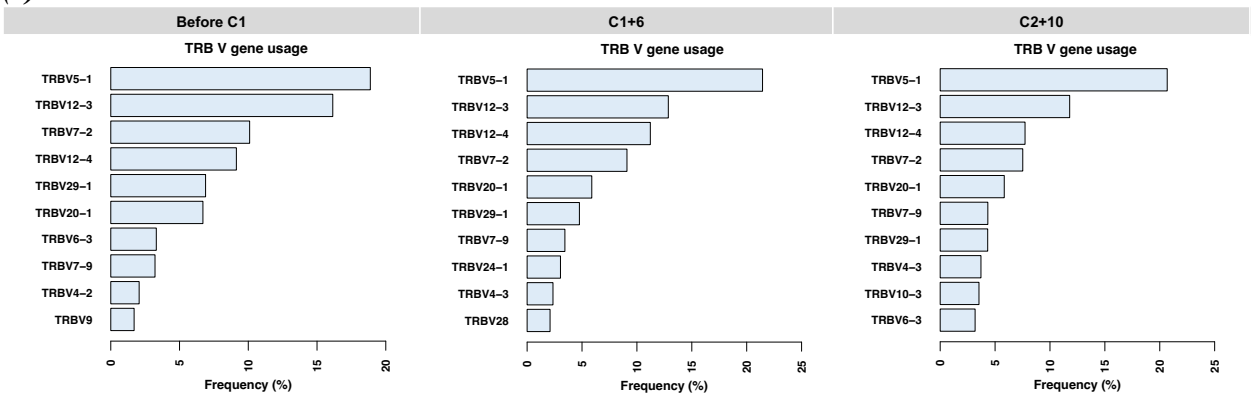

(b)

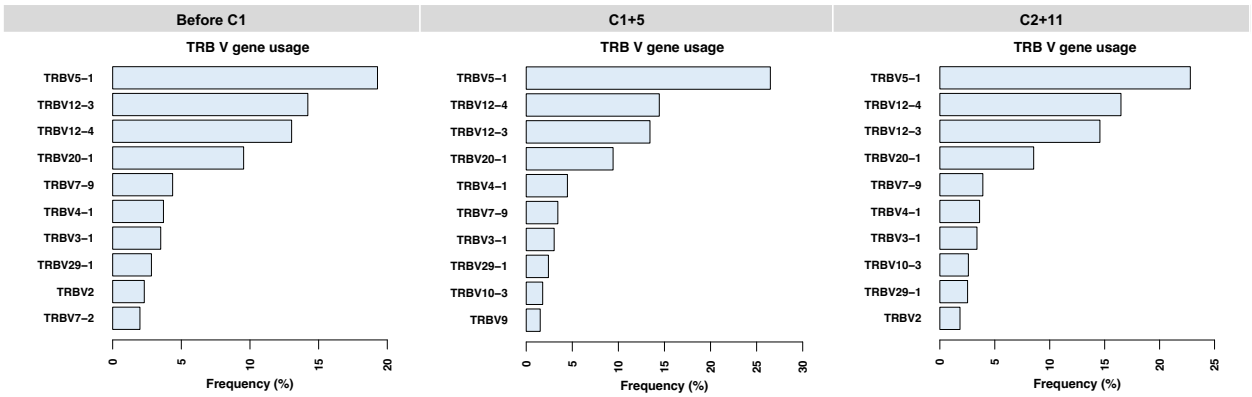

(c)

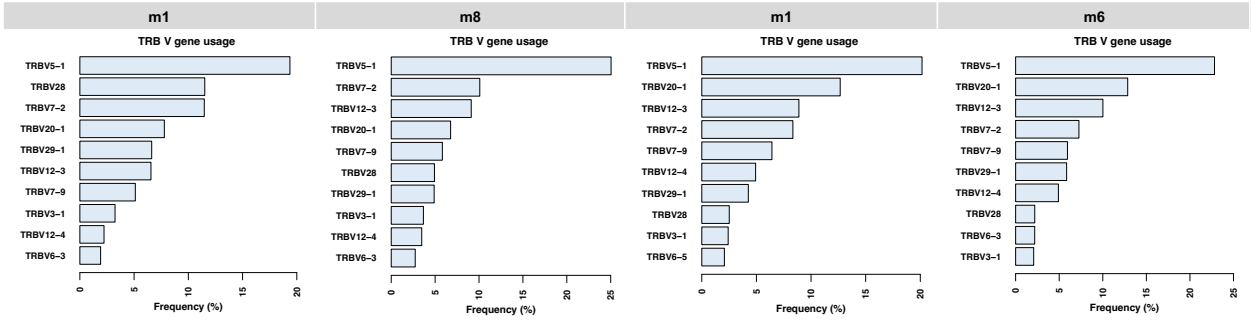

Supplementary figure 7: Bar graphs of „Top 10" relative V usage within the immune repertoires of CD4+ T cells from representative (a) *altemtuzumab treated non-SA patient (Patient 7_0568),* ***(b)*** *altemtuzumab treated SA patient (Patient 11_4434), and* ***(c)*** *untreated controls (Healthy control 1 and Untreated MS control 1) within the shown repertoires. Time points as indicated. TRBV5-1 is the over-represented V-beta usage in most of the patients before and following ALEM treatment, and untreated controls.*

(a)

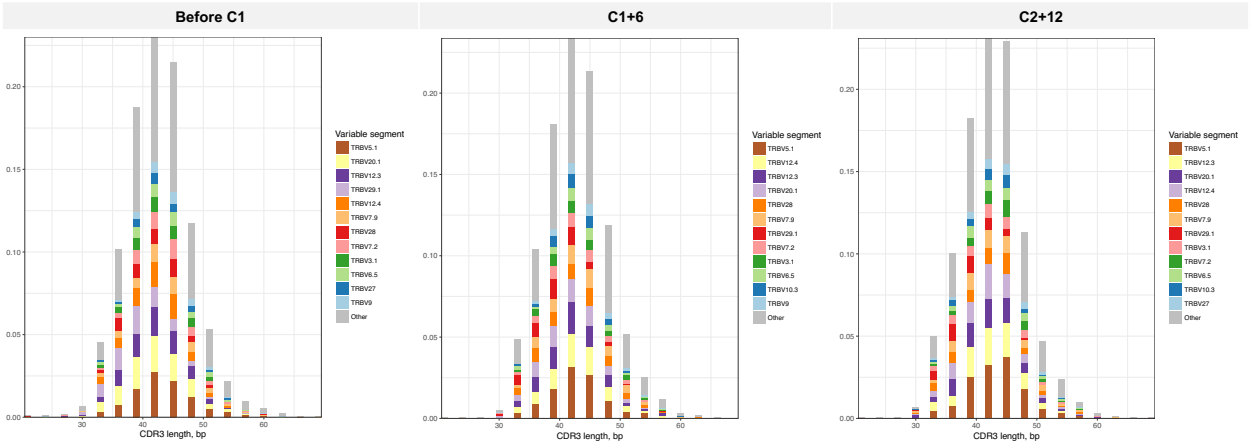

(b)

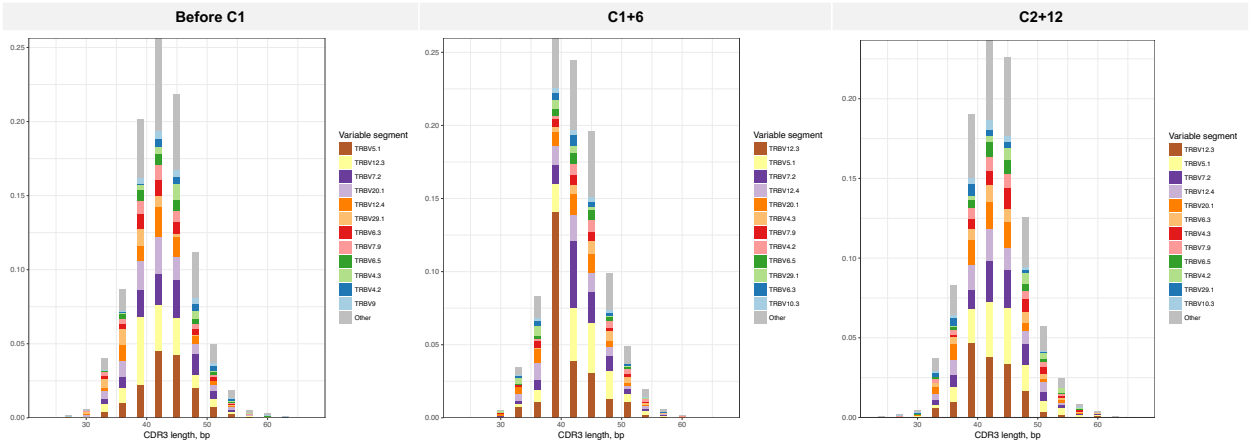

(c)

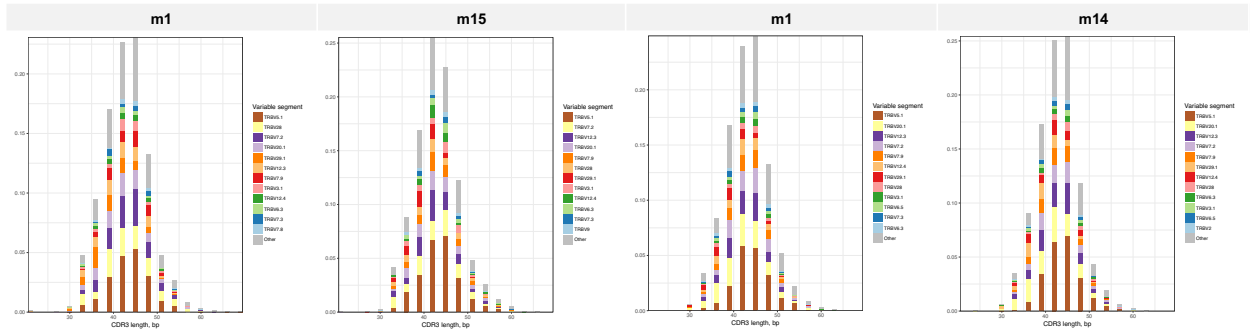

Supplementary figure 8: CDR3 length distribution of V segment families within immune repertoires of CD4+ T cells from representative (a) *alemtuzumab treated non-SA patient (Patient 1_4087),* ***(b)*** *alemtuzumab treated SA patient (Patient 12_2789), and* ***(c)*** *untreated controls (Healthy control 2 and Untreated MS control 1). CDR3 length distribution is similar to a Gaussian distribution.*

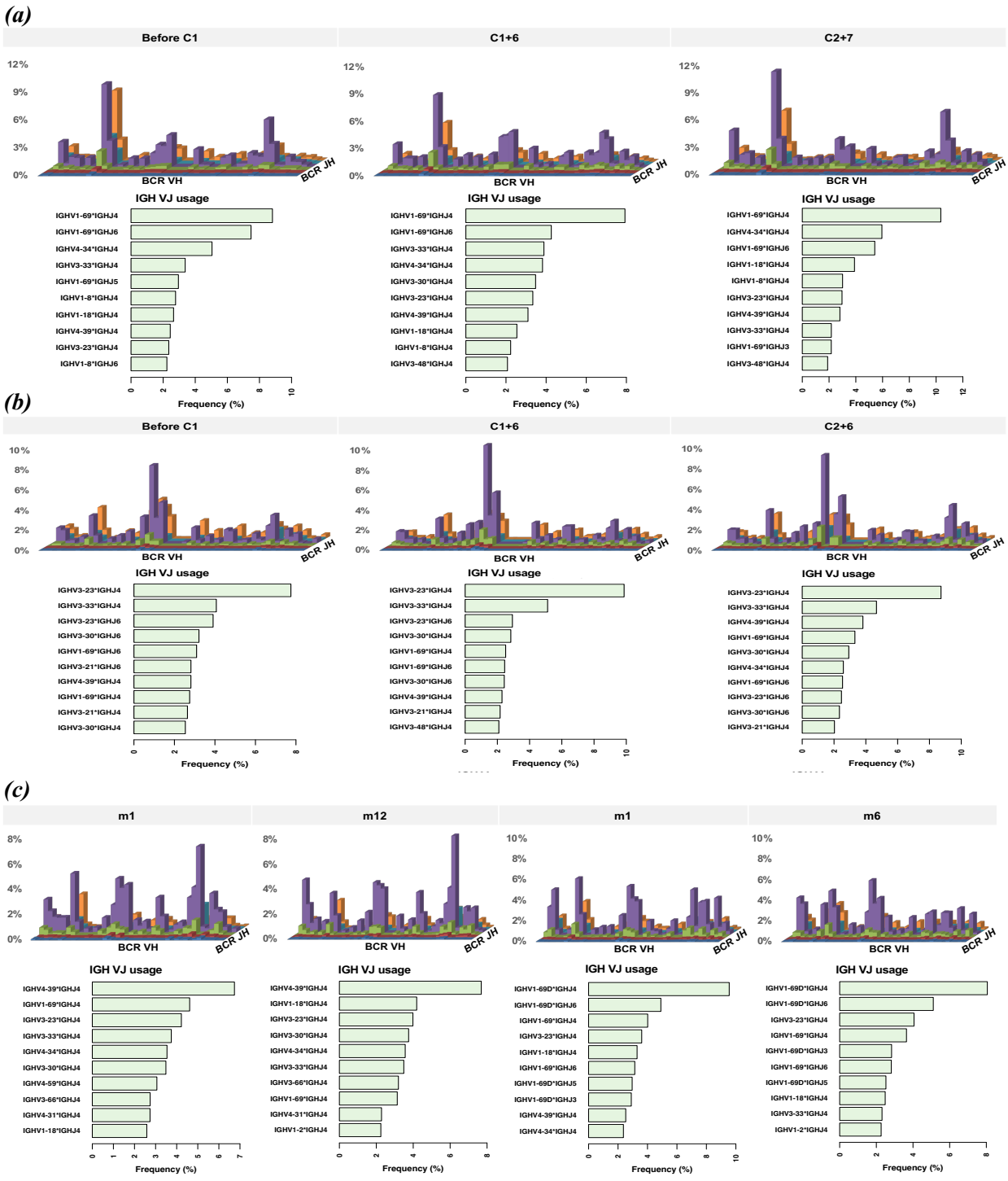

Supplementary figure 9: Upper Rows: 3D histograms of relative V-J usage within the immune repertoires of IgM+ NB cells from representative (a) *alemtuzumab treated non-SA patient (Patient 4_4628),* ***(b)*** *alemtuzumab treated SA patient (Patient 10_0063), and* ***(c)*** *from untreated controls (Healthy control 1 and Untreated MS control 3). Shown is the relative abundance within the immune repertoires (time points as specified).* ***Lower Rows:*** *Bar graphs of „Top 10" relative V-J within the shown repertoires of the corresponding patients and untreated controls.*

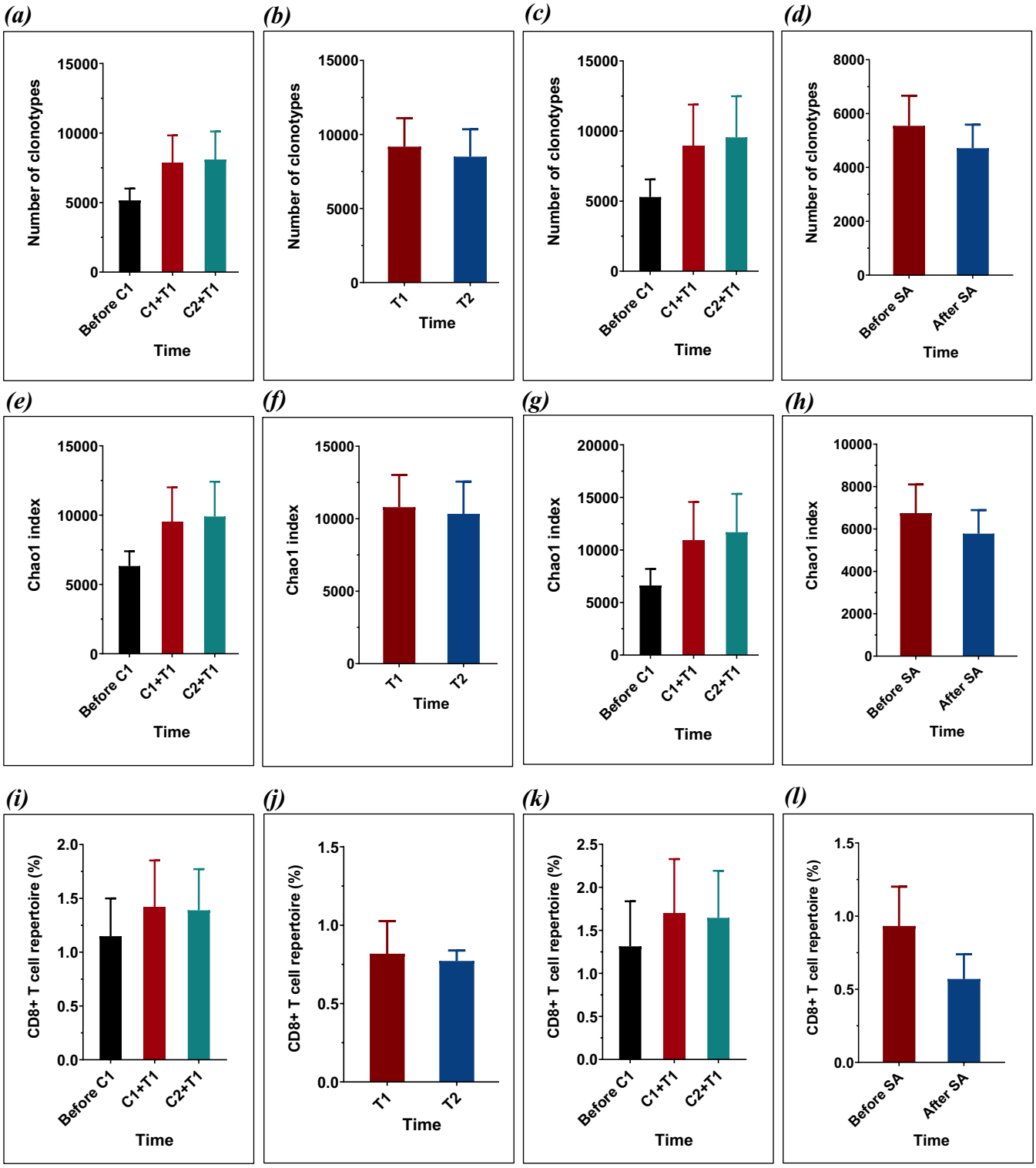

Supplementary figure 10. Total number of clonotypes of (a) *12 patients,* ***(b)*** *untreated controls,* ***(c)*** *non-SA patients, and* ***(d)*** *SA patients (before and after development of secondary autoimmunity);* ***Chao1 indices of (e)*** *12 patients,* ***(f)*** *untreated controls,* ***(g)*** *non-SA patients, and* ***(h)*** *SA patients (before and after development of secondary autoimmunity);* ***unique clonotypes (%) of (i)*** *12 patients,* ***(j)*** *untreated controls,* ***(k)*** *non-SA patients, and* ***(l)*** *SA patients (before and after development of secondary autoimmunity - in* ***CD8+ TCR repertoire****. Increasing trend of the CD8+ TCR repertoire diversity following ALEM treatment, while the decreasing trend in SA patients after developing secondary autoimmunity. P > 0.05 in Wilcoxon signed-rank test.*

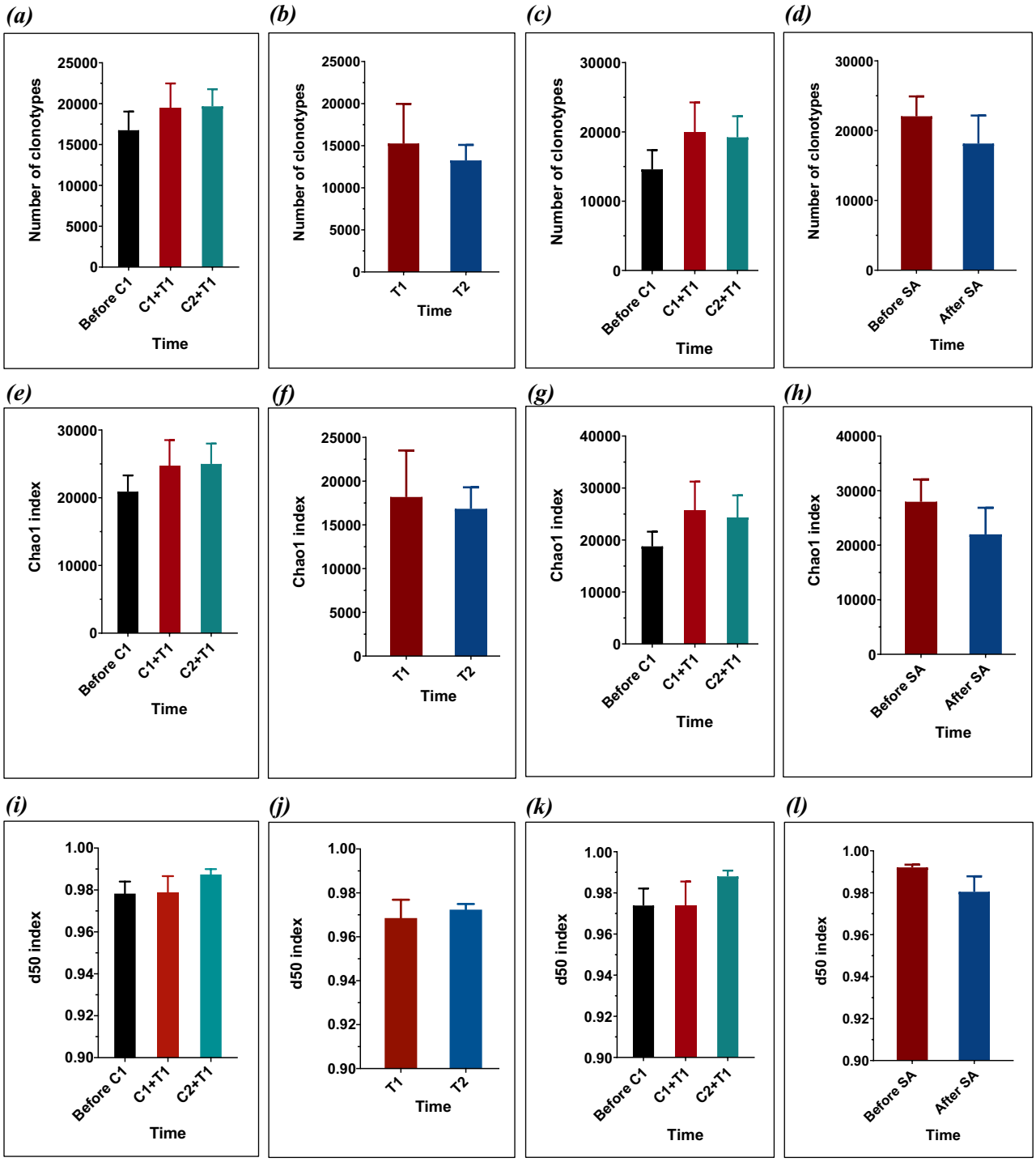

Supplementary figure 11: Total number of clonotypes of (a) *all 12 alemtuzumab treated MS patients,* ***(b)*** *untreated controls,****(c)*** *non-SA patients, and* ***(d)*** *SA patients (before and after development of secondary autoimmunity);* ***Chao1 indices of (e)*** *all 12 alemtuzumab treated MS patients,* ***(f)*** *untreated controls****, (g)*** *non-SA patients, and* ***(h)*** *SA patients (before and after development of secondary autoimmunity);* ***d50 index of (i)*** *all 12 alemtuzumab treated MS patients,* ***(j)*** *untreated controls****, (k)*** *non-SA patients, and* ***(l)*** *SA patients (before and after development of secondary autoimmunity)in* ***CD4+ TCR repertoire****. Increasing trend of the CD4+ TCR repertoire diversity following ALEM treatment, while the decreasing trend in SA patients after developing secondary autoimmunity. P > 0.05 in Wilcoxon signed-rank test.*

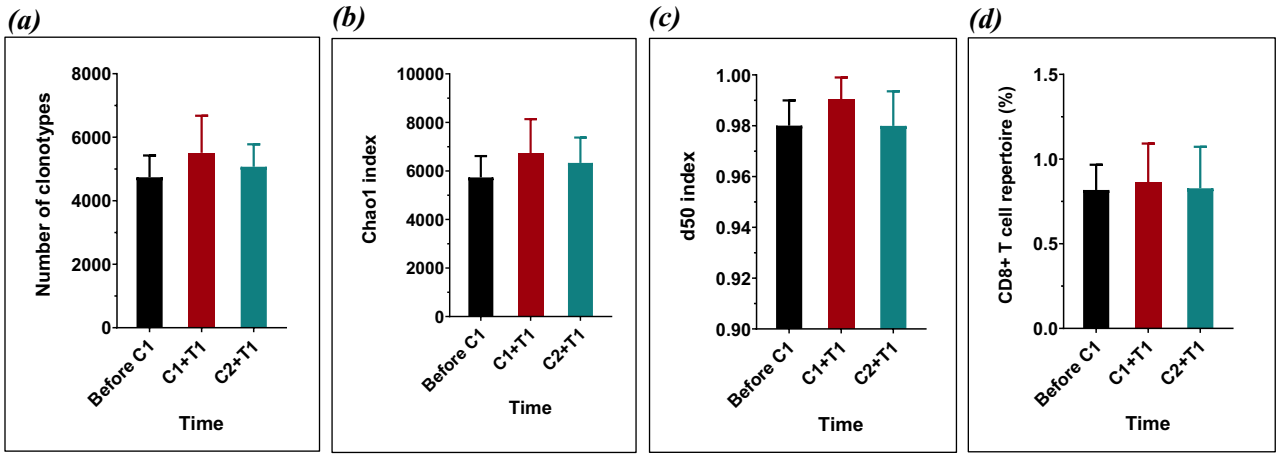

Supplementary figure 12. Total number of clonotypes (a), Chao1 indices (b), d50 indices (c), and unique clonotypes (%) (d) *of 4 patients who developped secondary autoimmunity in* ***CD8+ TCR repertoire****. After the second alemtuzumab cycle diversity was less than after cycle 1. P > 0.05 in Wilcoxon signed-rank test.*

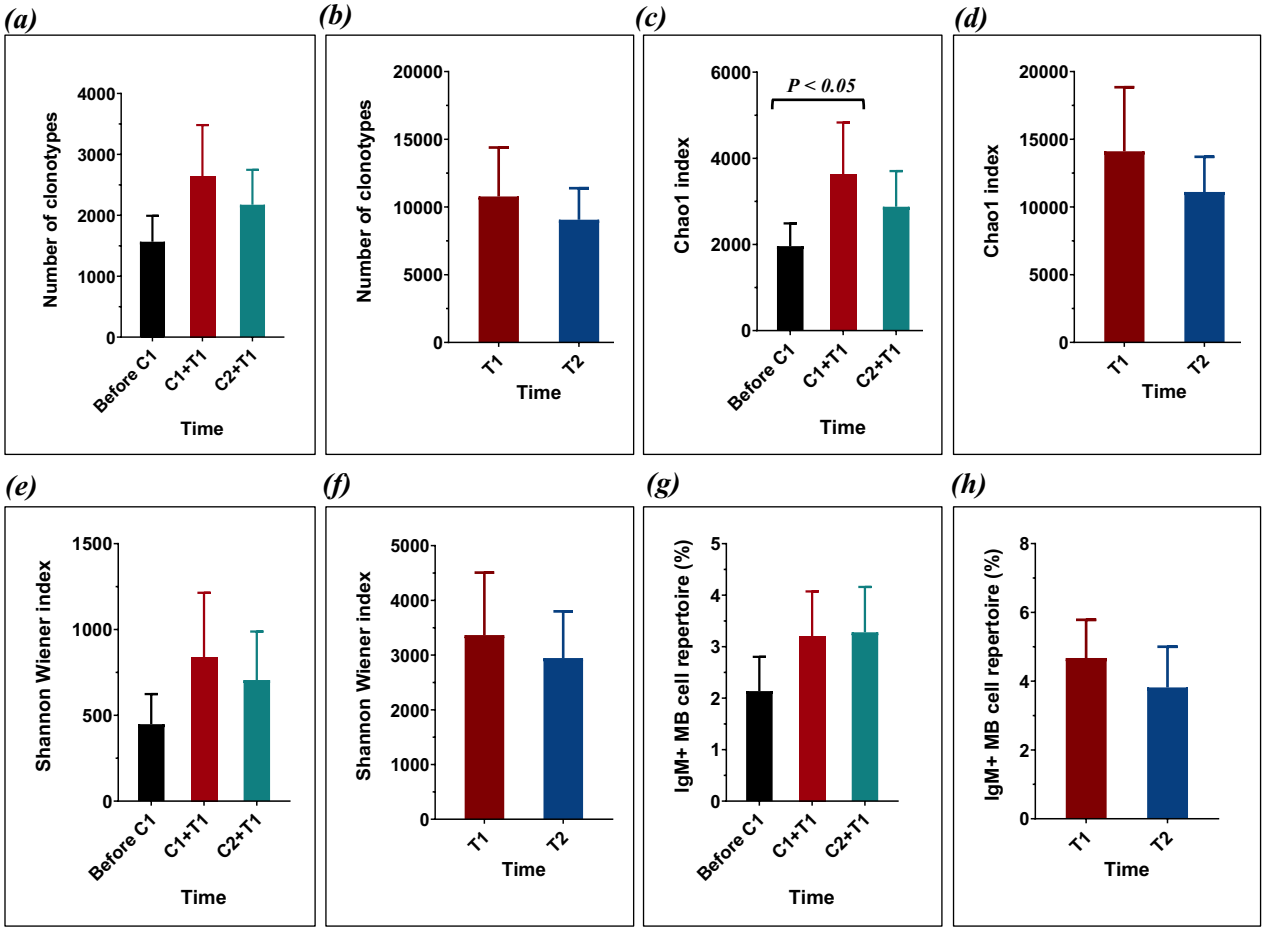

Supplementary figure 13. Total number of clonotypes within the IgM+ memory B cell repertoires *of* ***(a)*** *all 12 alemtuzumab treated patients,* ***(b)*** *untreated controls,* ***(c) - (d)*** *corresponding* ***Chao1 indices*** *of clonotypes;* ***(e) - (f)*** *corresponding* ***Shannon Wiener indices*** *of clonotypes;* ***(g) - (h*** *corresponding* ***unique clonotypes (%).*** *Not shown P value is > 0.05 in Wilcoxon signed-rank test.*

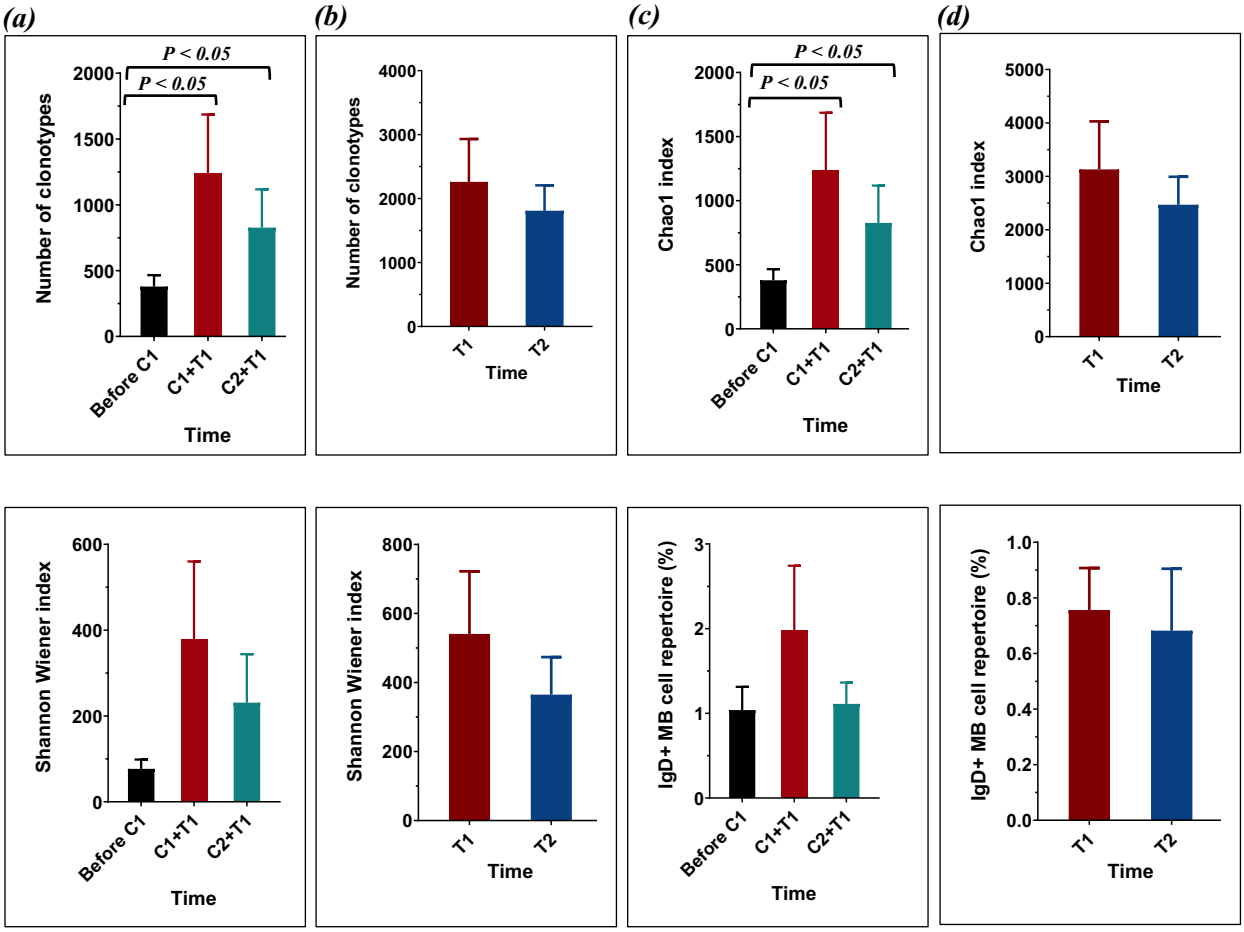

Supplementary figure 14. Total number of clonotypes within the IgD+ memory B cell repertoires *of* ***(a)*** *all 12 alemtuzumab treated patients,* ***(b)*** *untreated controls,* ***(c) - (d)*** *corresponding* ***Chao1 indices*** *of clonotypes;* ***(e) - (f)*** *corresponding* ***Shannon Wiener indices*** *of clonotypes;* ***(g) - (h*** *corresponding* ***unique clonotypes (%).*** *Not shown P value is > 0.05 in Wilcoxon signed-rank test.*

Supplementary table 1. *Persistence of highly abundant („Top Ten") CD8+ T cell clones in alemtuzumab treated patients,and untreated controls: Coloured CDR3 sequences indicate T cell clones found among the "Top Ten" most frequent clones before and during alemtuzumab treatment, and untreated controls (up to 15 months interval). Epitope species motif identified as *CMV, **EBV ***Influenza-A, #others in representative patiens and untreated controls.*

	Before C1		C1 + 6		C2 + 12	
	Top 10 expanded clone's CDR3 sequences	% of the repertoire	Top 10 expanded clone's CDR3 sequences	% of the repertoire	Top 10 expanded clone's CDR3 sequences	% of the repertoire
Patient 1_4087	CASSDGQGGAFF #	0.87	CAARTTHNEQFF *	4.90	CSATHRDASYEQYF #	0.66
	CASTGTGFPSTEAFF *	0.87	CASSRGNNNEQFF *	3.29	CASRQTEYTEAFF 3 ***	0.63
	CASSLLGGPLYEQYF 1 *	0.85	CASSFSPGLAGGNYEQYF	1.90	CASTGQGAAYEQYF #	0.47
	CASSLRGAVETQYF 2 *	0.76	CASRQTEYTEAFF 3 ***	1.00	CASSLRGAVETQYF 2 *	0.41
	CASSDSPQSSKQFF #	0.62	CASSLGPAQGYTF 5 *	0.67	CASSLLGGPLYEQYF 1 *	0.32
	CASSELAANTGELFF #	0.59	CASSLLGGPLYEQYF 1 *	0.66	CASSLRDRRQETQYF 4 *	0.25
	CASRQTEYTEAFF 3 ***	0.55	CASSSDGGSGNTIYF #	0.65	CASSSVLEAFF *	0.22
	CATSGVVSGELFF ***	0.54	CASTGQGAAYEQYF *	0.65	CASSYSYEQYF **	0.22
	CASSLRDRRQETQYF 4 *	0.46	CASSLRGAVETQYF 2 *	0.65	CASSLGPAQGYTF 5 *	0.21
	CASSQQIAGGPDTQYF #	0.45	CASSHQRTSGSGLREQYF	0.48	CASSPRGPGSNQPQHF #	0.21
		6.56		14.85		3.60
	Before C1		C1 + 6		C2 + 12	
	Top 10 expanded clone's CDR3 sequences	% of the repertoire	Top 10 expanded clone's CDR3 sequences	% of the repertoire	Top 10 expanded clone's CDR3 sequences	% of the repertoire
Patient 2_2702	CSATPGTDHNEQFF 1	11.65	CASSRGQGDVEQFF	19.16	CASSHPWDSHSGANVLTF	1.28
	CSVPGGTSGTTGETQYF	9.03	CASSSKKDTLIAYEQYF 2	2.82	CASSPEEPSGSSGELFF	1.19
	CSVVGTAPSGANVLTF	2.06	CASSLGQGFRTEAFF	1.92	CASSPAPADTQYF	0.66
	CASSETSGSNTDTQYF	1.27	CASSPSRNEQFF	0.96	CASSPTTSSYNEQFF	0.57
	CASKPLAATGELFF	1.1	CASSYRPNTGELFF	0.81	CASSWGSGSNYGYTF	0.53
	CSARDNDRESQPQHF	0.97	CASSSIPGTYYNEQFF	0.8	CASSSKKDTLIAYEQYF 2	0.52
	CASSFAAGEVNEQFF	0.87	CSVAGTGLNTLTGELFF 3	0.64	CASTLGRGTGELFF	0.49
	CASSPAGGGDTQYF	0.66	CASSVGTNNEQFF	0.61	CASSPGTGWNTEAFF	0.49
	CSVEGAPGLAGSDTQYF	0.66	CASSQGVRTGADGTEAFF	0.59	CASSWRGGYEQYV	0.44
	CASSLSLNTEAFF	0.63	CSATPGTDHNEQFF 1	0.39	CASSYGGGRLYEQYV	0.42
		28.9		28.7		6.59
	Before C1		C1 + 4		C2 + 11	
	Top 10 expanded clone's CDR3 sequences	% of the repertoire	Top 10 expanded clone's CDR3 sequences	% of the repertoire	Top 10 expanded clone's CDR3 sequences	% of the repertoire
Patient 3_4292	CASSQMEGTAGLRETQYF	27.80	CASSQDKGIYTQYF 4	19.69	CASSQDKGIYTQYF 4	49.57
	CSVVFGGGREQFF	7.5	CASSFGTSRDDEQYF 5	11.72	CASSFGTGRDNEQFF	5.44
	CASVLEGYEQYF	3.48	CSAKPIQGGYGYTF 3	6.84	CASSEGTGRDNEQFF 6	4.84
	CASSFGQGGGTGELFF	3.16	CASSEGTGRDNEQFF 6	6.30	CASSLTGTVNTEAFF	4.43
	CASTLGGAHTEAFF 1	3.13	CASSYRDYEQYF 2	4.76	CASSPAGENSDEQFF 7	3.82
	CASSLGYRVGYTF	2.67	CASSPAGENSDEQFF7	3.17	CASSFGTSRDDEQYF 5	3.07
	CASSYSGVPYNEQFF	2.19	CASSLGLAYYEQFF	2.19	CSVDGQGETEAFF	2.82
	CASSYRDYEQYF 2	2.16	CASSYGGDGYTF	2.11	CASSQDWTNAYNEQFF	2.12
	CSAKPIQGGYGYTF 3	1.15	CATGRGGGHNEQFF	1.85	CAWSGNTEAFF	2.05
	CASRDTSGGAYNEQFF	1.11	CASSGGQDRTDTQYF	1.68	CASTLGGAHTEAFF 1	2.01
		54.39		60.31		80.17
	Before C1		C1 + 6		C2 + 7	
	Top 10 expanded clone's CDR3 sequences	% of the repertoire	Top 10 expanded clone's CDR3 sequences	% of the repertoire	Top 10 expanded clone's CDR3 sequences	% of the repertoire
Patient 4_4628	CASSVSTRGEQFF 1 *	3.78	CASSVSTRGEQFF 1 *	0.49	CASSLEPFYEQYF *	0.23
	CASSLSGGPEAFF *	1.56	CASSLGDEKLFF 3 *	0.36	CASSLDGAQPQHF 5 *	0.19
	CASSVYAGEGGHNEQFF *	0.38	CASSLDGAQPQHF 5 *	0.36	CASSLGDEKLFF 3 *	0.16
	CASSQDWGDGGNEQFF *	0.34	CASSGRLSGGTDTQYF 6 #	0.33	CASSVSTRGEQFF 1 *	0.13
	CASSQEREIRGGYGYTF *	0.33	CASSQGESSYNEQFF *	0.31	CASSYSGQGGDNEQFF *	0.12
	CASSLSRPDTQYF 2 *	0.32	CASGDRGQGGNQPQHF 4 #	0.27	CASSDSQGPDNYGYTF *	0.11
	CASSLSGGHQPQHF *	0.32	CSVDLGNANTGELFF #	0.20	CASSLSRPDTQYF 2 *	0.10
	CASSLGDEKLFF 3 *	0.30	CASSSPRDRGQGEQFF *	0.18	CASSVGTGGQFF 7 ***	0.07
	CATSSPTSGRATDTQYF *	0.25	CASSLLAGRSYEQYF ***	0.16	CASSLGSYEQYF #	0.07
	CASGDRGQGGNQPQHF 4 #	0.22	CASSVGTGGQFF 7 ***	0.16	CASSGRLSGGTDTQYF 6 #	0.06
		7.8		2.82		1.24

	Before C1		C1 + 6		C2 + 12	
	Top 10 expanded clone's CDR3 sequences	% of the repertoire	Top 10 expanded clone's CDR3 sequences	% of the repertoire	Top 10 expanded clone's CDR3 sequences	% of the repertoire
Patient 5_0811	CASSAGQSSSYNEQFF *	6.72	CSVEGAGNTGELFF *	16.35	CASSQEPMFSYNEQFF *	28.21
	CASSLSTSADYEQYF *	5.16	CSVEGQTNTGELFF ***	2.66	CASSLGRAGSYEQYF *	21.5
	CASSRTSGGNNEQFF 1***	5.02	CASSEGGTGNQPQHF #	2.25	CASSYSRSSYNSPLHF #	16.31
	CASSLALGGQPQHF 2 *	2.52	CASSLNSPEQYF 3*	1.91	CASSRTSGGNNEQFF 1 ***	2.56
	CASSQYSSGISYFEQYF *	2.47	CASSRTSGGNNEQFF 1 ***	1.02	CASSLDWPSPHEQYF *	2.23
	CASSFNNEQFF #	1.63	CASSSPMDGGPNTEAFF *	0.78	CASSLALGGQPQHF 2 *	1.84
	CASSLNSPEQYF 3 *	1.07	CASTTRGGAPDTQYF #	0.74	CASSLSSESYNEQFF *	0.98
	CASSVGYGGDRDGDTQYF	1.04	CASSQEVPPLHF **	0.69	CASSLNSPEQYF 3 *	0.76
	CASSLGANPYEQYF #	0.94	CASSLSENESKNIQYF *	0.6	CATSTGDSNQPQHF **	0.33
	CASSQEWRGRGNQPQHF*	0.65	CASSLALGGQPQHF 2 *	0.57	CASSLGGGTQPQHF *	0.31
		27.22		27.57		75.03
	Before C1		C1 + 6		C2 + 9	
	Top 10 expanded clone's CDR3 sequences	% of the repertoire	Top 10 expanded clone's CDR3 sequences	% of the repertoire	Top 10 expanded clone's CDR3 sequences	% of the repertoire
Patient 6_1542	CASSLISGGLGTQYF	3.32	CAISESGGGNEQFF	8.27	CATSTSPLGDTEAFF 1	2.36
	CASSARWTVHQPQHF	1.4	CASSQPGGPGSYNEQFF	5.7	CASSLLSGANVLTF	1.87
	CASSDRDTGELFF	0.96	CASSSGSLYEQYF	4.94	CAGLFGTEAFF	1.82
	CAWRQNTEAFF	0.9	CATSTSPLGDTEAFF 1	4.52	CASSSGGLGEAFF	1.73
	CASSLARGPGGNQPQHF	0.74	CASSPGTTLGFEQYF	3	CATRQGGQPQHF	1.71
	CASSGGGEVDTQYF	0.71	CASSPSGGWIQYF	2.15	CASSLENGVIYEQYF	1.7
	CASSVGAGFYNEQFF	0.69	CASLTGYNSPLHF	1.62	CASSHRQELFF	1.62
	CASSLRLNTEAFF	0.68	CASSTTGLGDSPLHF	1.54	CASSVTGNEQFF	1.56
	CASSPLDRIYGYTF	0.67	CASSTDRDRDYEQYF	1.47	CASRRTGKNTEAFF	1.47
	CASYRPGEQFF	0.61	CASSFGPINQPQHF	1.38	CASSLGQGTQYF	1.38
		10.68		34.59		17.22
	Before C1		C1 + 6		C2 + 7	
	Top 10 expanded clone's CDR3 sequences	% of the repertoire	Top 10 expanded clone's CDR3 sequences	% of the repertoire	Top 10 expanded clone's CDR3 sequences	% of the repertoire
Patient 7_0568	CASSPIPARVVNTEAFF *	4.7	CASSQDRLTGGYTF 6 **	1.19	CSAHRREGRNEQFF #	5.42
	CASSLNKNQPQHF ***	0.99	CASTVGGWGTQYF 7 *	0.92	CATSDRGIVGELFF *	0.95
	CATSDLRLAGADTQYF *	0.73	CSARAQFNLNQPQHF 3 *	0.79	CASSQDWASATYEQYF 1 *	0.72
	CASSQDWASATYEQYF 1 *	0.66	CAISESYEGTSGRTYEQYF 5	0.7	CASTVGGWGTQYF 7 *	0.69
	CASSQDWSLETQYF *	0.65	CATSDSDIVEGYTF **	0.66	CASSFGGREQYF *	0.56
	CASSPRRSGPGYEQYF 2 #	0.47	CASSLTAGEETFF *	0.58	CASSEGNEQYF 4 **	0.53
	CSARAQFNLNQPQHF 3 *	0.38	CASQISGSLYEQYF *	0.57	CASSQDRLTGGYTF *	0.48
	CASSEGNEQYF 4 **	0.37	CASSQDWASATYEQYF 1 *	0.55	CASIHGNFYNEQFF 6 **	0.39
	CAISESYEGTSGRTYEQYF 5	0.29	CASLWRSSGANVLTF *	0.55	CASSPRRSGPGYEQYF 2 #	0.35
	CASSSSTEAFF *	0.28	CASSQAQGPDTQYF ***	0.54	CAISESYEGTSGRTYEQYF 5	0.34
		9.52		7.05		10.43
	Before C1		C1 + 6		C2 + 6	
	Top 10 expanded clone's CDR3 sequences	% of the repertoire	Top 10 expanded clone's CDR3 sequences	% of the repertoire	Top 10 expanded clone's CDR3 sequences	% of the repertoire
Patient 8_3773	CASSLSGGQYGYTF 1	2.44	CASSSTDGGYQPQHF	86.22	CASSRGEGTLNEQFF	3.57
	CASRQGNEQFF	1.42	CASSQGPGYEQYF	0.12	CASTQGVGTEAFF	1.59
	CASGITPGLPGELFF	0.71	CASSQTGVGQPQHF	0.11	CASSYGQGITFF	1.43
	CASSLGRVPYEQYF	0.67	CASSSDGRPQHF	0.1	CASSLQRGGLNEQFF	0.95
	CASTLGTGLTDTQYF 2	0.54	CASSLGQPQHF	0.09	CASSLSPGTAEAFF 3	0.7
	CASSIDGPYEQYF	0.47	CASSPPGTLNTGELFF	0.09	CASSLSGGQYGYTF 1	0.6
	CASSFFWGLNTEAFF	0.36	CASARDNQPQHF	0.08	CASDKTGGGAFF	0.52
	CASSLSPGTAEAFF 3	0.36	CASSLVQSNQPQHF	0.08	CASSGRNTEAFF	0.34
	CATSSSSLALSYNEQFF	0.35	CASSAINQPQHF	0.07	CASSQEIVSYNEQFF	0.3
	CASSFGGGNQPQHF	0.31	CASSLEGGLRDQHF	0.07	CASTLGTGLTDTQYF 2	0.3
		7.63		87.03		10.3

	Before C1		C1 + 6		C2 + 12	
	Top 10 expanded clone's CDR3 sequences	% of the repertoire	Top 10 expanded clone's CDR3 sequences	% of the repertoire	Top 10 expanded clone's CDR3 sequences	% of the repertoire
Patient 9_6666	CASSLANNEQFF *	23.15	CASSPSGTATPLTF 2 **	16.11	CSVEFGSGDEQFF 3 *	11.63
	CATSEPTDSHTGELFF *	8.46	CSVEFGSGDEQFF 3 *	13.48	CASSFSGGDGYTF 4 *	10.12
	CASSPEPGLAGNEQFF 1 *	4.74	CASSFSGGDGYTF 4 *	9.55	CASSPSGTATPLTF 2 **	7.83
	CATSDPGVSYNEQFF ***	2.77	CAWSPLGGSDEQYF 5 *	7.23	CASSPEPGLAGNEQFF 1 *	7.39
	CASSTHEGGELFF ***	2.21	CASSSMEPNEKLFF **	5.73	CASRTGTGAHEQFF 8 #	4.66
	CASSDGTSGYEQYF #	1.74	CASRIGAAGNSPLHF 6 #	4.68	CASSLGSNEQFF #	2
	CASSSGTAGTDTQYF *	1.6	CASSLISGSSYNEQFF *	2.21	CSVEGAGTDLGYEQYF 7 *	1.84
	CASSLANNEQFF *	1.23	CASSEGATPPYEQYF *	2.2	CAWSPLGGSDEQYF 5 *	1.52
	CASSPSGTATPLTF 2 **	1.1	CSVEGAGTDLGYEQYF 7 *	2.13	CASSLDGYNEQFF *	1.51
	CATSIPVASGSDEQFF *	1.03	CASRTGTGAHEQFF 8 #	1.97	CASRIGAAGNSPLHF 6 #	1.5
		48.03		65.29		50
	Before C1		C1 + 6		C2 + 6	
	Top 10 expanded clone's CDR3 sequences	% of the repertoire	Top 10 expanded clone's CDR3 sequences	% of the repertoire	Top 10 expanded clone's CDR3 sequences	% of the repertoire
Patient 10_0063	CASSFPQTGLATEAFF *	10.31	CASSLPGETQYF 3 *	44.29	CASSFLSSDSYEQYF 4 #	58.01
	CASSFVTGWSGANVLTF 1 *	8.74	CASSFLSSDSYEQYF 4 #	7.86	CASSLPGETQYF 3 *	16.71
	CASSFSDSWAGKETQYF *	3.66	CASSYQSSAVLDANTGELFF 2	4.83	CAWSSPSYEQYF 3 *	3.39
	CASSLSTTDNEQFF *	3.6	CASSFVTGWSGANVLTF 1 *	4.36	CASSYQSSAVLDANTGELFF 2	1.89
	CASSYQSSAVLDANTGELFF 2	3.22	CAWSSPSYEQYF 3 *	2.66	CASSLVWPRNEQFF 5 *	1.14
	CASSLSNRNTEAFF *	2.66	CATSITSGYYYGYTF **	1.69	CASSLGRVGVIEQFF #	0.77
	CASSLKRRAPTDTQYF #	2	CASSLVWPRNEQFF 5 *	1.63	CASSFVTGWSGANVLTF 1 *	0.76
	CASSQSDAEETQYF *	1.51	CASSLGGNEQFF *	1.3	CASSFQESGVADTQYF #	0.69
	CASSLEDGHSYEQYF *	1.35	CASTYRGLTYEQYF *	0.96	CASSEGTGELFF #	0.55
	CASSDSWGTSYNEQFF *	1.01	CASSPGTGTYGYTF **	0.78	CASSRLASDSYEQYF ***	0.52
		38.06		70.36		84.43
	Before C1		C1 + 5		C2 + 11	
	Top 10 expanded clone's CDR3 sequences	% of the repertoire	Top 10 expanded clone's CDR3 sequences	% of the repertoire	Top 10 expanded clone's CDR3 sequences	% of the repertoire
Patient 11_4434	CASSLADSALSYEQYF *	1.94	CASSLYRGTEAFF 1 #	2.02	CASSLYRGTEAFF 1 #	2.45
	CASSSWDGENQETQYF #	1.67	CASSVGQGLMDTEAFF *	1.1	CASSLSSYNEQFF 2 *	0.82
	CSARELAGDPLNTQYF *	1.49	CASSLSSYNEQFF 2 *	0.98	CASSFRGAVETQYF 3 *	0.41
	CASSWDGEKLFF *	1.41	CASSFRGAVETQYF 3 *	0.74	CASSRSGGALDTQYF #	0.27
	CASSWSGEEQYF *	1.36	CASGTGGDTQYF *	0.59	CASSSGPNTEAFF 4 *	0.26
	CASSFSLAGDYFEQFF #	1.17	CATAPPRVGAIGGYTF #	0.44	CASSQEWGIGELFF ***	0.23
	CASSLNSGELFF **	1.03	CASSSGPNTEAFF 4 *	0.43	CASSLNSLNQPQHF *	0.21
	CASSQDGQGVGGPTNEKLFF	0.72	CASSLKGTYGYTF #	0.32	CASSLFRGEKLFF ***	0.21
	CASSADREDEQYF #	0.62	CASRDRGIDNQPQHF #	0.27	CASSPGTDFLYGYTF **	0.19
	CASSEAVEETYEQYF *	0.56	CASSQYSYEQYF #	0.27	CASSAFRGFTEAFF *	0.18
		11.97		7.16		2.45
	Before C1		C1 + 6		C2 + 12	
	Top 10 expanded clone's CDR3 sequences	% of the repertoire	Top 10 expanded clone's CDR3 sequences	% of the repertoire	Top 10 expanded clone's CDR3 sequences	% of the repertoire
Patient 12_2789	CASSFWADTQYF *	6.03	CASSFYSWGSGNTIYF 4 *	28.86	CASSFYSWGSGNTIYF 4 *	7.97
	CASSLGQGANEQFF *	4.21	CASSPQRNTEAFF 5 *	4.67	CASSPRGTGYTTDTQYF 6 *	1.6
	CATSLAGGEGNEQFF *	3.62	CSVRLAGGPNTGELFF #	3.83	CASSPQRNTEAFF 5 *	1.5
	CASSFHGGPQHF #	2.39	CASSQGSSSYNEQFF ***	1.85	CASCLSWTGELFF 3 *	1.43
	CASSLIGVSSYNEQFF 1 *	2.29	CASSLIGVSSYNEQFF 1 *	1.73	CASSLIGVSSYNEQFF 1 *	1.24
	CASSLDSSYEQYF **	2.05	CASSSPTRGNYGYTF 2 **	1.6	CASSLAGMVNEQYF *	0.94
	CASSLHDRLGKASPLHF ***	1.69	CASSENRANSPLHF *	1.29	CASSLSGGRAFF *	0.8
	CASSLDSGELFF **	1.41	CASSQGGILNEKLFF *	1.11	CASSLGWTGAYGYTF **	0.78
	CASSSPTRGNYGYTF 2 **	1.26	CASSPQRNTEAFF *	1.11	CASSLGVAPLHF *	0.77
	CASCLSWTGELFF 3 *	1.23	CASSPRGTGYTTDTQYF 6 *	1.04	CASSSPTRGNYGYTF 2 **	0.71
		26.18		47.09		17.74

	Month 1		*Month 12*	
	Top 10 expanded clone's CDR3 sequences	*% of the repertoire*	*Top 10 expanded clone's CDR3 sequences*	*% of the repertoire*
Healthy control 1	CASSDEPTGYYYNEQFF 1 *	19.42	CASSSWDSHYGYTF 2 **	27.03
	CASSSWDSHYGYTF 2 **	13.61	CATSDPGDPYNEQFF 3 *	15.04
	CATSDPGDPYNEQFF 3 *	8.04	CASSDEPTGYYYNEQFF 1 *	11.32
	CASRRPGAYYEQYF 4 *	3.27	CASRRPGAYYEQYF 4 *	3.20
	CASSLLPTTNSYNEQFF 5 *	2.58	CASSLLPTTNSYNEQFF 5 *	2.36
	CASSPGTDSNQPQHF 6 #	1.06	CASSPGTDSNQPQHF 6 #	0.98
	CASVGTGIDQPQHF #	0.97	CASSLPGQENYGYTF **	0.75
	CASSSTGTSATDTQYF 7 *	0.96	CASSPGLAEQFF ***	0.64
	CASSQGTESTYEQYF *	0.86	CASSSTGTSATDTQYF 7 *	0.57
	CSASDRGTSGANVLTF *	0.72	CASSPLAGVQNEQFF ***	0.43
		51.49		62.32
	Month 1		*Month 15*	
	Top 10 expanded clone's CDR3 sequences	*% of the repertoire*	*Top 10 expanded clone's CDR3 sequences*	*% of the repertoire*
Healthy control 2	CASSLFGVKNEQFF 1	1.37	CASALDWPDTQYF 3	0.92
	CASSLGGGPTEAFF 2	1.3	CASSLFGVKNEQFF 1	0.82
	CASALDWPDTQYF 3	0.56	CASSLGGGPTEAFF 2	0.79
	CASSRDGASTDTQYF 4	0.48	CASSRDGASTDTQYF 4	0.52
	CASSPTGYYNEQFF	0.47	CASRGDLSSYEQYF 6	0.46
	CASSFSVPGTNEKLFF 5	0.39	CASSLDGYTEAFF	0.38
	CASSRTRSDRGRGTEAFF	0.28	CASSQDKGTPDYNEQFF	0.32
	CASSGGLAGATGELFF	0.27	CASSLLGQTPPYEQYF	0.3
	CASSLALGELFF	0.23	CASSLSSGPGELFF	0.26
	CASRGDLSSYEQYF 6	0.2	CASSFSVPGTNEKLFF 5	0.25
		5.55		5.02
	Month 1		*Month 14*	
	Top 10 expanded clone's CDR3 sequences	*% of the repertoire*	*Top 10 expanded clone's CDR3 sequences*	*% of the repertoire*
Untreated MS control 1	CASSESLGGFTDTQYF 1	60	CASSESLGGFTDTQYF 1	47.18
	CSATGTSSYEQYF 2	0.58	CASSPAGGHLAYNEQFF 4	0.98
	CAIRLAGTYNEQFF 3	0.46	CAIRLAGTYNEQFF 3	0.94
	CASSPAGGHLAYNEQFF 4	0.36	CASSSSGTATYGYTF	0.74
	CASSLLLAGTDTQYF	0.35	CASSWVGDEQFF	0.64
	CASSLSGRVIGEQYF	0.3	CSATGTSSYEQYF 2	0.59
	CASSLGLLGQPQHF	0.27	CASSLGQIYEQYF 5	0.53
	CSARVNTEAFF	0.27	CSARDRGLGNTIYF	0.44
	CASSQDPGDSNEQFF	0.25	CATSGSQDTGELFF	0.38
	CASSLGQIYEQYF 5	0.22	CASSDMYGNNSPLHF	0.35
		63.06		52.77
	Month 1		*Month 8*	
	Top 10 expanded clone's CDR3 sequences	*% of the repertoire*	*Top 10 expanded clone's CDR3 sequences*	*% of the repertoire*
Untreated MS control 2	CASSLFWREAFF 1 #	5.7	CASSLFWREAFF 1 #	11.65
	CASSPDRGRGYTF 2 *	2.8	CASSRLAGGTDTQYF 4 *	2.57
	CASSLGGAEETQYF 3 *	2.62	CASSGSEGATMNTEAFF 6 *	2.44
	CASSRLAGGTDTQYF 4 *	2.25	CASSPDRGRGYTF 2 *	2.33
	CASSYWGDTEAFF 5 *	1.78	CASSFSSLTYEQYF 7 *	1.68
	CASSGSEGATMNTEAFF 6 *	1.61	CASSYWGDTEAFF 5 *	1.67
	CASSPSSWNEQYF **	1.52	CSARATGAQKNYGYTF ***	1.66
	CASSFSSLTYEQYF 7 *	1.49	CATSDSNRDTGELFF **	1.65
	CASSLDRAGGRTDTQYF ***	1.42	CASSLGGAEETQYF 3 *	1.6
	CASSPWGEQRTGELFF *	1.3	CASSQDAGNTEAFF *	1.42
		22.49		28.67

	Month 1		*Month 6*	
	Top 10 expanded clone's CDR3 sequences	*% of the repertoire*	*Top 10 expanded clone's CDR3 sequences*	*% of the repertoire*
Untreated MS control 3	CASTIRHLNQPQHF 1	10.95	CASTIRHLNQPQHF 1	22.36
	CASSWGTSGSMGDSFLAKNIQYF 2	9.21	CASSYGTGELFF 4	11.19
	CASSLAGGSIEQFF 3	5.36	CASSWGTSGSMGDSFLAKNIQYF 2	7.16
	CASSYGTGELFF 4	5.21	CASSLAGGSIEQFF 3	5.17
	CASSYSTLNTEAFF 5	3.26	CASTNPTYNEQFF 6	4.84
	CASTNPTYNEQFF 6	2.63	CASSPWALGRSGYNEQFF 9	2.69
	CSANRNYEKLFF 7	2.37	CSANRNYEKLFF 7	2.45
	CASSFWSGWDTEAFF 8	2.33	CASSMTANEQYF	2.16
	CASKNSLNTGELFF	1.65	CASSFWSGWDTEAFF 8	2.00
	CASSPWALGRSGYNEQFF 9	1.19	CASSYSTLNTEAFF 5	1.90
		44.16		61.92

Supplementary table 2. *Persistence of highly abundant (top ten) CD4+ T cell clones in representative alemtuzumab treated patients,and untreated controls: Coloured CDR3 sequences indicate T cell clones found among the "Top Ten" most frequent clones before and during alemtuzumab treatment, and untreated controls (up to 15 months interval.)*

	Before C1		C1 + 6		C2 + 12	
	Top 10 expanded clone's CDR3 sequences	% of the repertoire	Top 10 expanded clone's CDR3 sequences	% of the repertoire	Top 10 expanded clone's CDR3 sequences	% of the repertoire
Patient 2_2702	CSAPLAGGADTQYF	0.080	CASSLVMNIQYF	0.54	CASSPRPGGSGNTIYF	0.076
	CASKGYTF	0.066	CASTRDILYEQYF	0.31	CSANTGESPLHF	0.073
	CSVRPQETQYF	0.065	CASSQDWTAYEQYF	0.23	CASSFILGGTDTQYF	0.070
	CASSQGQASGRLDTGELFF	0.064	CASSPRTSPRGEQYF	0.19	CASSLGHPQHF	0.065
	CASSLGTSGRF	0.063	CASSSPTLTGNQPQHF	0.19	CASSLNGLGYTF	0.065
	CASSLGGHTEAFF	0.063	CASSSTSNQPQHF	0.17	CASSLASGSREQFF	0.064
	CASSSGASPLHF	0.058	CSATRSPDTQYF	0.13	CASSHGTVNEKLFF	0.063
	CASTYGTGYNEQFF	0.057	CSAPGPLYNEQFF	0.13	CASSLEPADEQYF	0.060
	CASSLTSGSGNSYEQYF	0.057	CASTPASGSKETQYF	0.13	CASSAGAAYNEQFF	0.059
	CSALNTEAFF	0.055	CASSSPDQPQHF	0.13	CASSLEGENTGELFF	0.057
		0.63		2.15		0.65
	Before C1		C1 + 4		C2 + 11	
	Top 10 expanded clone's CDR3 sequences	% of the repertoire	Top 10 expanded clone's CDR3 sequences	% of the repertoire	Top 10 expanded clone's CDR3 sequences	% of the repertoire
Patient 3_4292	CASSFGEGGGYTF 1	0.9	CASSFGEGGGYTF 1	1.22	CASSRTSGGALNTQYF 4	4.72
	CASMRSSTDTQYF	0.16	CASSRSGDGKGYTF	0.97	CASSLQGTSGYNEQFF	0.6
	CASLRDGPYEQYF	0.15	CASSLTGTGTDTQYF	0.96	CSPFRQNTEAFF 5	0.5
	CASSLLSDTEAFF	0.14	CSATTGDPSGANVLTF 2	0.8	CASSFSGTNEKLFF	0.41
	CSVELQAMNTEAFF	0.14	CASSLPGSSGNTIYF	0.79	CASTVTGPDYGYTF 3	0.31
	CASSLDKGMNTEAFF	0.13	CASTVTGPDYGYTF 3	0.75	CSATTGDPSGANVLTF 2	0.27
	CSVEDHDVSYGYTF	0.13	CASSLESGGGQPQHF	0.71	CASWGGPYNSPLHF	0.25
	CASQGQVNTEAFF	0.13	CASSRTSGGALNTQYF 4	0.59	CASSRSILAGGTYEQYF	0.21
	CASSYTGPITEAFF	0.12	CSPFRQNTEAFF 5	0.58	CAWSARGASNQPQHF	0.19
	CASSPGQGTYNEQFF	0.11	CASSQEILGAGTEAFF	0.47	CASSLTSWNTEAFF	0.16
		2.11		7.84		7.62
	Before C1		C1 + 6		C2 + 7	
	Top 10 expanded clone's CDR3 sequences	% of the repertoire	Top 10 expanded clone's CDR3 sequences	% of the repertoire	Top 10 expanded clone's CDR3 sequences	% of the repertoire
Patient 4_4628	CASSPGTSYEQYF	0.22	CSARAVARFADTQYF	0.06	CASSPDGGRNQPQHF 1	0.14
	CASSLDGGSGNTIYF	0.18	CASSWDGGRNQPQHF	0.05	CASSFRRGMNTEAFF	0.09
	CASSLNGETDTQYF	0.13	CASSLTNEQYF	0.05	CATLSFDEQFF	0.08
	CASSRDQETQYF	0.13	CASSQGGELFF	0.05	CASSHPETGTYEQYF	0.07
	CASTQRELSDEQYF	0.12	CASELSPLTYNEQFF	0.05	CASSLFRNNEQFF	0.07
	CASQYGTAKTEAFF	0.11	CASSQDPSSYNEQFF	0.05	CASSLDGNSGNTIYF	0.06
	CASSLAGYNEQFF	0.11	CASSPDGGRNQPQHF 1	0.05	CASGTVAASYEQYF	0.06
	CASSLEGTGNGYTF	0.11	CASSLGSGPNTEAFF	0.04	CASSPRASNTEAFF	0.06
	CASSSDPLEQFF	0.11	CASRRTGETEAFF	0.04	CASSLLAGAIEQFF	0.06
	CASSFGLSSYNEQFF	0.10	CASSLVGQPPTEAFF	0.04	CASSHTRLSLYEQYF	0.06
		1.32		0.48		0.75
	Before C1		C1 + 6		C2 + 6	
	Top 10 expanded clone's CDR3 sequences	% of the repertoire	Top 10 expanded clone's CDR3 sequences	% of the repertoire	Top 10 expanded clone's CDR3 sequences	% of the repertoire
Patient 8_3773	CSVDSAQETQYF	0.24	CASSLRVGYTF	0.08	CASSFRNSPLHF	0.18
	CASSRTTGLEAFF	0.11	CASSLGGGAHNEQFF	0.08	CASSMDIRNTIYF	0.16
	CASLDRAGEAFF	0.11	CASSVDYNEQFF	0.07	CASSLMEHLIPKPQHF	0.13
	CASSYRETNTEAFF	0.11	CASSFDQPQHF	0.07	CASSPQEGGNQPQHF	0.13
	CASSPRTGGNEQFF	0.11	CASSPYNSPLHF	0.07	CASSFGQGDNQPQHF	0.1
	CASRRGQVEAFF	0.1	CASRGQGYTEAFF	0.07	CASSLTGVTEAFF	0.1
	CASSLESQFF	0.1	CASSFLDSPLHF	0.06	CASGRQGNTEAFF	0.1
	CASSLEGNQPQHF	0.09	CASSLFMNTEAFF	0.06	CASSYGQGSGTEAFF	0.09
	CASSLNQPQHF	0.09	CASTQGSGNTIYF	0.06	CASSGLLAKNIQYF	0.09
	CASRLGDNEKLFF	0.09	CASSFGQYYEKLFF	0.06	CASSPSSGNTIYF	0.09
		1.15		0.68		1.18

	Before C1		*C1 + 6*		*C2 + 12*	
	Top 10 expanded clone's CDR3 sequences	*% of the repertoire*	*Top 10 expanded clone's CDR3 sequences*	*% of the repertoire*	*Top 10 expanded clone's CDR3 sequences*	*% of the repertoire*
Patient 9_6666	CASSHGGLWGNEQFF 1	5.31	CASAPTLGSYEQYF 3	2.06	CASAPTLGSYEQYF 3	19.87
	CSAREAGNTDTQYF	0.42	CASSSLTSGNTDTQYF 2	2.05	CAWNQDFSYNEQFF	3.71
	CASSLIVGGYEQYF	0.22	CAWRGDKPYEQYF	1.54	CASSPLVSYEQYF	2.73
	CASSYPNGGTEAFF	0.14	CACPNRGSPSTDTQYF	1.52	CAIRKDSLKSSGANVLTF	0.77
	CASSLVGSGSRNEQFF	0.1	CASSLAGMSRDTQYF	1.07	CASSSRTTNTEAFF	0.67
	CASRKADKLTYEQYF	0.1	CASRGGETQYF	0.95	CASSHGGLWGNEQFF 1	0.61
	CASSPGLGYEQFF	0.1	CASSHGGLWGNEQFF 1	0.92	CAISGRPLQETQYF	0.59
	CSAAPWGNEQFF	0.09	CAWSVDKGDGYTF	0.77	CASSSRTANTEAFF 4	0.57
	CASSLGSGEDTQYF	0.09	CASSSRTANTEAFF 4	0.71	CALSVKTEAFF	0.49
	CASSSLTSGNTDTQYF 2	0.08	CAWGGQKNTEAFF	0.56	CASSSLTSGNTDTQYF 2	0.42
		6.65		12.15		30.43
	Before C1		*C1 + 6*		*C2 + 6*	
	Top 10 expanded clone's CDR3 sequences	*% of the repertoire*	*Top 10 expanded clone's CDR3 sequences*	*% of the repertoire*	*Top 10 expanded clone's CDR3 sequences*	*% of the repertoire*
Patient 10_0063	CSATVGLARPTDTQYF 1	1.68	CSASKGLAGRGETQYF 3	16.99	CSASKGLAGRGETQYF 3	4.86
	CASIFQGAQGELFF 2	0.55	CSATVGLARPTDTQYF 1	5.58	CSATVGLARPTDTQYF 1	2.57
	CSVPRPPSNGETQYF	0.32	CSAQTISSYEQYF 4	2.01	CASSFSGDRGETQYF 5	1.49
	CSVDKYNEQFF	0.25	CASSFSGDRGETQYF 5	0.9	CSARDPGQGGSEAFF	0.48
	CASAGQGVGNYGYTF	0.17	CSAPGQPNNSPLHF	0.72	CSAQTISSYEQYF 4	0.47
	CSVEDPGGYSYEQYF	0.17	CASSLQLGAYNEQFF	0.48	CASSKGRQGGNTEAFF 6	0.43
	CSAIKAGISYNEQFF	0.16	CASIFQGAQGELFF 2	0.26	CANGQALERNEQFF	0.25
	CASSLETARKTQYF	0.15	CASSKGRQGGNTEAFF 6	0.17	CSAPLQPLNSPLHF	0.23
	CSVEDPMNTGELFF	0.14	CASSLPSRDGADTQYF	0.16	CASIFQGAQGELFF 2	0.23
	CSVETSAQYF	0.14	CASSQMTGNTEAFF	0.15	CASSLQLGAYNEQFF	0.2
		3.73		27.42		11.21
	Before C1		*C1 + 5*		*C2 + 11*	
	Top 10 expanded clone's CDR3 sequences	*% of the repertoire*	*Top 10 expanded clone's CDR3 sequences*	*% of the repertoire*	*Top 10 expanded clone's CDR3 sequences*	*% of the repertoire*
Patient 11_4434	CASRRANTEAFF	0.16	CASSVGQTGVDTEAFF	0.34	CASSSDSAGNTIYF 1	0.16
	CASSLQGNQPQHF	0.14	CASSVTGRTEAFF	0.32	CASSLPASPLHF	0.13
	CASSLGPTHQETQYF	0.13	CASSPTVDGNYGYTF	0.26	CASTPGGGVNEQFF	0.12
	CASSVQESNKYNEQFF	0.13	CASKTGTMNTEAFF	0.19	CASSPQGAGNSPLHF	0.11
	CASRTIDQNYGYTF	0.12	CASSPPDTEAFF	0.18	CASSRTGSNQPQHF	0.1
	CASSFAGIGEQYF	0.12	CASSVDSGANVLTF	0.15	CASSWGQKFGYTF	0.1
	CAISPFGGENTEAFF	0.12	CASSLYTEAFF	0.15	CASIRSRNTEAFF	0.1
	CASSLGTYEQYF	0.11	CASSSDSAGNTIYF 1	0.15	CASSLVGRGHNEQFF	0.1
	CASSPSRVRYGYTF	0.11	CASSLLGNTEAFF	0.15	CASSLAQNQPQHF	0.1
	CASSLDTRGNGYTF	0.11	CASTPGRTTEAFF	0.14	CASSLTYNEQFF	0.09
		1.25		2.03		1.11
	Before C1		*C1 + 6*		*C2 + 12*	
	Top 10 expanded clone's CDR3 sequences	*% of the repertoire*	*Top 10 expanded clone's CDR3 sequences*	*% of the repertoire*	*Top 10 expanded clone's CDR3 sequences*	*% of the repertoire*
Patient 12_2789	CASSLVGGNEQFF 1	2.25	CASSLVGGNEQFF 1	11.48	CASSLVGGNEQFF 1	2.23
	CATSRDTAGTEAFF	0.76	CASSSPDGRFGYTF 2	2.69	CSATQDSATNEKLFF	0.22
	CASSSPDGRFGYTF 2	0.35	CASKLFIGGGSYNEQFF	0.33	CASSSPDGRFGYTF 2	0.18
	CASSFQGSTEAFF	0.12	CASTTGVSPLHF	0.3	CRTMGQGDEGYGYTF	0.15
	CASSLSTPYQETQYF	0.11	CASSQERLAQNIQYF	0.19	CASSPLTEEKLFF	0.12
	CASSLMSQETQYF	0.1	CASSFAGRSSYNEQFF	0.18	CASTRNYGYTF	0.1
	CASSLEGQNQPQHF	0.09	CASSYDRSRNTEAFF	0.17	CASRNTGELFF	0.1
	CASKRTDHEQFF	0.09	CASSQVYRGANTDTQYF	0.13	CASSLGGGTSYF	0.09
	CASSTLWGLNTEAFF	0.08	CASSSDISTTGFEQYF	0.12	CASRDRVEQFF	0.09
	CASSWSGGGGDTQYF	0.08	CASSLYNEQFF	0.11	CASSPSGNSPLHF	0.09
		4.03		15.7		3.37

	Month 1		*Month 12*	
	Top 10 expanded clone's CDR3 sequences	*% of the repertoire*	*Top 10 expanded clone's CDR3 sequences*	*% of the repertoire*
Healthy control 1	CASSLVPYEQYF	0.24	CASSYRTGGGGELFF	0.16
	CASSIAGTEKETQYF	0.2	CASSDRGMNEQYF	0.16
	CASSRQGAADTQYF	0.16	CASSVRNEQFF	0.15
	CASRAELTGELFF	0.15	CASSPSGQSSYEQYF	0.15
	CASSPGATWGTEAFF	0.15	CASSPIPSNEQYF	0.15
	CSAGRGMDTQYF	0.15	CSVGTNGGNTIYF	0.14
	CASSLVGDSPLHF	0.14	CASSLGDRGDTQYF	0.14
	CASSSSGPYEQYF	0.14	CASSPRDGTYEQYF	0.14
	CASSLDASSYNSPLHF	0.14	CASRDNTGELFF	0.14
	CAISVQVMNTEAFF	0.14	CASSYTGGQQPQHF	0.13
		1.61		1.46
	Month 1		*Month 6*	
	Top 10 expanded clone's CDR3 sequences	*% of the repertoire*	*Top 10 expanded clone's CDR3 sequences*	*% of the repertoire*
Untreated MS control 3	CSVDRGNEQFF	0.22	CASSLSQGGGEQYF	0.22
	CASSFRLSGNTIYF	0.16	CASSLTGYNEQFF	0.18
	CASRRGLAGAPVKNIQYF	0.15	CASSLYANYGYTF	0.17
	CASSQQTGGSYNEQFF	0.15	CASSLEGTGGKEQFF	0.16
	CASSLSARRNSPLHF	0.14	CASSIGGLAGKLFF	0.15
	CASSWVTGPNQPQHF	0.14	CASSLEGNSYNEQFF	0.14
	CASSPRGQPSNEKLFF	0.13	CASSLNPSSPLHF	0.13
	CSVERGGELFF	0.13	CASSLGSGPNTEAFF	0.12
	CASSVSTGETQYF	0.11	CASSAEGEQYF	0.11
	CASSLVVNVYNEQFF	0.11	CASSPSVGYSEAFF	0.11
		1.44		1.49

Supplementary table 3. *Persistence of highly abundant (top ten) IgG+ memory B cell clones in representative alemtuzumab treated patients,and untreated controls: Coloured CDR3 sequences indicate T cell clones found among the "Top Ten" most frequent clones before and during alemtuzumab treatment, and untreated controls (up to 15 months interval.)*

	Before C1		C1 + 6		C2 + 12	
	Top 10 expanded clone's CDR3 sequences	% of the repertoire	Top 10 expanded clone's CDR3 sequences	% of the repertoire	Top 10 expanded clone's CDR3 sequences	% of the repertoire
Patient 2_2702	CAREGDDAPKYFQRW	5.12	CARPSSNAFDVW	6.37	CAKKDGDGW	3.69
	CARDHMAAGIVVVPVAVGPW	4.69	CARELKWERGGHFDIW	5.44	CATESFYVSDYW	1.81
	CARGGYRGRSDFW	4.23	CASNCVGSTWREGCLYHAMDVW	4.89	CARGASGDWYFDLW	1.53
	CARDPPGDQGYDVW	4.16	CMRNQHQGNSAGGYW	4.79	CAKGNVDGRYDLWSGYQNWFGPW	1.29
	CARVAAGSWYDDCW	3.79	CARSQGALQFDYW	3.71	CATPRPPTGTTDYGMDVW	1.14
	CARIWAARPPTFDYW	3.63	CARDPPGDQSYDVW	3.5	CARDEREAAVVGGVYFDYW	1.06
	CARVGWSEYW	3.26	CARLTMAGTNPW	2.98	CARLDFGVPNGAFDLW	1
	CARRSKLGGWNVW	2.63	CARGSGSNGQDWFDPW	2.92	CAKGPSNWYGFDFW	1
	CARGYHSFDAW	2.32	CARDRELKGDVYFYYGMDVW	2.47	CARDYDSTGYLPSFDYW	0.96
	CARFERGWLGNILTDYYGMDVW	2.26	CAGGPRKGYSGTSYHYYGMDVW	2.12	CARPRGAANSVGLDVW	0.96
		36.09		39.19		14.44
	Before C1		C1 + 4		C2 + 11	
	Top 10 expanded clone's CDR3 sequences	% of the repertoire	Top 10 expanded clone's CDR3 sequences	% of the repertoire	Top 10 expanded clone's CDR3 sequences	% of the repertoire
Patient 3_4292	CARFDFGGNKIHHFDYW 1	3.31	CAKPMSRTAVSGYDLW	2.91	CARGQTMIPGVLDIW	2.85
	CAKQFEYGGLDDYW	1.22	CARDRANLKDAFDIW 2	1.92	CARGMPDAAMEPDEYFHHW	2.49
	CARDGTASWFGQGSHW	1.22	CARELGLRYCSGGSCPDAFDIW	1.79	CARSIRYDNSGPLKIDSW	2.42
	CARLRQETPNLGLDLW	1.2	CARFDFGGNKIHHFDYW 1	1.56	CARGLIGYSGYDQW	2.41
	CARDLGEDILLMGEFDVW	1.13	CARDEGSGRPFDYW	1.54	CASERGDYVRVGQFFFDRW	2.35
	CARHPSLAVVTFDFW	1.06	CARGYNGDPRYW	1.38	CARNMSALGSAVAGNKGAFDVW	2.31
	CARDRANLKDAFDIW 2	0.95	CARHKGYYYFDYW	1.18	CARGMPDAAMEPDEYFHHW	1.96
	CARHQNYFDNSGYPVNW	0.94	CARVAWYYYGSGSYDFW	1.15	CARQTPGEGAHFW	1.85
	CVRDSTYFSQYYYDVLDSW	0.94	CARGRGGVSGHYFNYW	1.11	CATMGAKTFDIW	1.75
	CARGEFGELEDW	0.91	CARVFTYDFAW	1.08	CARQERQQLLGWFDSW	1.6
		12.88		15.62		21.99
	Before C1		C1 + 6		C2 + 7	
	Top 10 expanded clone's CDR3 sequences	% of the repertoire	Top 10 expanded clone's CDR3 sequences	% of the repertoire	Top 10 expanded clone's CDR3 sequences	% of the repertoire
Patient 4_4628	CTRHSSGWRGSDYW	4.25	CARDQMFSGYAQRGNYHYGMDVW	7.4	CARVGTVAYCGGDCNYFDYW	7.2
	CAILSHLTVIRGLITTGRWFAHW	3.41	CATGGQTIFYNWLDPW	6.57	CARGPPRFYGDYDYW	6.54
	CARARRTATFDGLDDW	3.26	CARDAPGGVRTNFDSW	6.11	CVRDGGTWFFDKW	3.96
	CARDRITGTALSYYYYGMDVW	2.76	CAAQNFDSLLNDFFDLW	5.93	CAMLTHVTMIRGVITTGRWYEHW	3.94
	CAKDNLGYAYGNW	2.71	CSRQTPHSGLDYW	4.63	CARDPLGGSGEIDAFDIW	3.86
	CARDPTPFCSNTSCLPDWFDPW	2.15	CAREHGFEKSWFDPW	4.39	CIRDGVGSIPWDIW	3.67
	CANEEVPNDYW	1.95	CAKQRGHVVVETAIDRWHWFDSW	3.06	CARLSFRGTYIVGLDSW	3.11
	CARDDWLRDAFDVW	1.66	CTRVSTGNGAGLTNDYW	2.45	CAKGGIIDFYFFDLW	2.86
	CTRHSSGWRGSDYW	1.47	CARGRMADNW	2.16	CARVLQRHRAYVDW	2.85
	CARGQYDVLTDSTRRPFDIW	1.41	CARDYTVVRGYFDYW	1.96	CTRQYCGADTCYQPFDYW	2.77
		25.03		44.66		40.76
	Before C1		C1 + 6		C2 + 7	
	Top 10 expanded clone's CDR3 sequences	% of the repertoire	Top 10 expanded clone's CDR3 sequences	% of the repertoire	Top 10 expanded clone's CDR3 sequences	% of the repertoire
Patient 7_0568	CAREGPSCTSTSCSRAFDIW	8.87	CAGQENSGHHRLHYW	15.32	CARDKTLALIDFW	7.93
	CVRGPTARSPGWAYHYDFW	3.66	CAHRLGSGYSSYWAFDYW	7.62	CARDVYGLSGSHNFQHW	4.13
	CAKSSQSWGNDAFDVW	3.65	CAKDRWSGSYYGGVFDYW	6.33	CARTGAFDIW	3.07
	CAKGAGYDFWRRRSYFDSW	1.37	CARDRYDFWSGSLFDPW	5.09	CARMGYSSSWYRWDWFDPW	2.3
	CAREGPSCTSTSCSRAFDMW	0.86	CVRRGDLLGDAFDIW	4.75	CARGPFRDWFDYW	2.11
	CAKDRSRLNYHYFDSW	0.84	CARDGLGGPAFDFW	4.7	CAKDYRIAVAGYYFDYW	1.6
	CVRSHYRWELKPFDQW	0.81	CTRGCTDESCHPFDFW	4.37	CAKAHGPGLYYYYGMDVW	1.58
	CTKDHRSFYSFDLW	0.78	CARDYGSSDWYNWFDPW	3.45	CARENWGSLDYW	1.49
	CARGGTISVQGVTYPPIFDSW	0.76	CTRGRSIAVAGYYWFEPW	3.06	CARGGLTYYSDSSGYDAFDIW	1.44
	CARGRVAASGTPTFVFDNW	0.69	CARDGRDYGDFVPYYRGLGVW	2.67	CARGTWELGAFDIW	1.35
		22.29		57.36		27

	Before C1		C1 + 6		C2 + 12	
	Top 10 expanded clone's CDR3 sequences	*% of the repertoire*	*Top 10 expanded clone's CDR3 sequences*	*% of the repertoire*	*Top 10 expanded clone's CDR3 sequences*	*% of the repertoire*
Patient 9_6666	CAKAFLASRLNWFDPW	26.69	CGRDLGGKAAAW	3.21	CTIGHYGPW	1.73
	CAREIGYCSGGGCYFRGEYYYYMDV	2.49	CATHRADAFDIW	2.23	CVREPYNGHWSLDYW	1.59
	CARVPYYSYYGMDVW	0.66	CARGSSGYGPGFDTW	1.86	CARDGLKYSYGWEVSFDVW	1.54
	CARDRFYDASGYYYYFYGMDVW	0.64	CATDLFPLIVGTSRKAFDIW	1.82	CAGYREGAGGTGYW	1.39
	CARDRSCSGGSCLDSW	0.62	CARVGVDHSDPYDEFNLW	1.82	CVREGPTSGRAGAFDIW	1.17
	CAAGHYHSSGYYYDSFDIW	0.61	CASGADVR	1.78	CAMDFSVWHRADYW	1.1
	CARHTRVHQYDVPVPAKDPFDAW	0.59	CSRDLAGRLDYW	1.69	CGRDLSGRDDFW	1.09
	CARVGVDDSDPYDEFDLW	0.53	CGRDQDYVLVAW	1.44	CAKASRGEHQLEVPAFDIW	1.07
	CATELCSGRFDCGFDIW	0.49	CATELIGGHGYSYSHFDSW	1.34	CARDAHDSSAPYAFEIW	1.06
	CARGDQSSGDYW	0.48	CTSAKNGVW	1.28	CVRDFIGPRDSW	1.02
		33.8		18.47		12.76
	Before C1		C1 + 6		C2 + 6	
	Top 10 expanded clone's CDR3 sequences	*% of the repertoire*	*Top 10 expanded clone's CDR3 sequences*	*% of the repertoire*	*Top 10 expanded clone's CDR3 sequences*	*% of the repertoire*
Patient 10_0063	CARQYCDGNCPKAHDSW	2.83	CARGGGEFYYYYGMDVW	3.18	CARGPLRLQGTLGVGMDVW	2.51
	CARQYCDGSCPKAHDCW	1.68	CAKATYYITGTKDYFDYW	2.4	CAREQGYCSGTACYNNWFDPW	1.8
	CARRSWGSYYSAGGLDVW	1.62	CTTSLGGTNGVGVW	2.01	CARDLSSRDFWSGYVAPDYW	1.34
	CASNTIW	1.61	CAGYYDSSGYYSLDYW	1.18	CARELGYCSGTACYNNWFDPW	1.32
	CARVEGLYGMDVW	1.47	CARAQQPDYFDYW	0.99	CALTWGEWLGHPFDYW	1.29
	CARVGDYYVGEW	1.33	CAREGTTDWFDPW	0.91	CVRDYGNYW	1.25
	CAKQYCDGSCPKAHDGW	1.09	CAKGYYENDYW	0.91	CAREQGYCSGTTCYNNWFDPW	1.2
	CARALGYCSGVSCYSIW	1.07	CARHVRTYYYDSSGLYYFDYW	0.9	CAKDGFGDSSGYHFDSW	0.84
	CAKQFCDGSCPKAHDCW	1.05	CARGGGGYPDAFDIW	0.87	CVRLGYCDATNCHGFDSW	0.79
	CARPPPYYSYAFDIW	0.97	CAKDTGLVGATTWW	0.83	CVREGSSGWYGGYW	0.76
		14.72		14.18		13.1
	Before C1		C1 + 5		C2 + 11	
	Top 10 expanded clone's CDR3 sequences	*% of the repertoire*	*Top 10 expanded clone's CDR3 sequences*	*% of the repertoire*	*Top 10 expanded clone's CDR3 sequences*	*% of the repertoire*
Patient 11_4434	CAKDHSNAAPFDNW	27.35	CTTTSGRYRAGDPW	5.88	CANFYYYDNSGHIYYSGVDVW	2.04
	CARQSALARSYPDYW	5.84	CAREGGYTSRGMDVW	2.23	CAKDWPGFSRGPMDDPYYGMDVW	1.28
	CARDRSSHEHGANFDFW	3.08	CARDYFGSGSHYIFDIW	2.11	CARDWRGFDRGPMESTYKGMDVW	1.14
	CARGGLTAAAGKLYYW	3	CVRGMRVMPGLDYW	2.06	CARQAPRPGSYFEAVARFDPW	1.11
	CARLYVDGYNGASHFDSW	2.78	CVRGSVGFRGMDVW	1.43	CARGPGGSGWFGPSYYYYYGMDVW	1.06
	CAKDSDYLDYW	2.76	CTRDQYLSYYFDHW	1.25	CARDWPGFARGPMDSTYKGMDVW	0.89
	CARDLPGDMSTVGWYFDLW	2.14	CARDYYGSGSNYYIDYW	1.2	CAKDWPGFARGPMDYVYYGMDVW	0.87
	CTRGGGDPLLHYYFDYW	1.84	CANLYTGSYYSLDYW	0.97	CARDTGNLYDIVGFLSTW	0.81
	CAKVLDQYSSGGNLDYW	1.66	CVRDSGNLELHLDNW	0.96	CAKVNPDYDIVTGYYPLDYW	0.81
	CAKDEIGGLITNW	1.63	CARESGVHYYDGSGYSTLRPDYW	0.93	CAKDWPGFARGPMDSGYRGMDVW	0.76
		52.08		19.02		10.77
	Before C1		C1 + 6		C2 + 12	
	Top 10 expanded clone's CDR3 sequences	*% of the repertoire*	*Top 10 expanded clone's CDR3 sequences*	*% of the repertoire*	*Top 10 expanded clone's CDR3 sequences*	*% of the repertoire*
Patient 12_2789	CAGHNIGYSDYSDSYPNPFVDW	7.16	CARFRLYEPSLYW 2	1.31	CARDYYDSSGYYYSYYYGMDVW	1.8
	CAGHNIGYSDSSGSYPNPFVDW 1	3.29	CARHDYDSSGYYITQFDYW	1.06	CASSPGSGWYSWFDPW	1.24
	CARGPEQDDYGDYGGNYYGMDV	2.25	CARGQQLAHWFDPW	1.02	CAREPYFSGFDPW	1.09
	CAGHNIGYSDSSGSYPNPFVDW 1	1.37	CASLPYNYFGSRSHLNYFHFW	0.96	CARHDYGDYINDYW	1.03
	CAGHVIGYSDSSGSYPNPFVDW	1.14	CAHRRDLSIAARRAFDYW	0.9	CATSIAVAGTDEYYFDYW	0.96
	CARAAFVRYSGYRHAFDIW	1.06	CAKTTIPVRMCPTGLCYLGDW	0.79	CATTMIVVVTHFDYW	0.79
	CAKEGSGYYARTFHMW	0.96	CARFRLFEPSPYW	0.77	CVKEWDSSGYGAAFDIW	0.76
	CIRYYYDSSGYFGFW	0.96	CARSPYSWSDNSHLNFFDVW	0.68	CAKERLLRPYYFDYW	0.73
	CAGHVIGYSDTSGSYPNPFVDW	0.86	CANDQGAGAAGYW	0.68	CTARYCISDRCFSRGDDAFDIW	0.72
	CAHRSQGYGFGIDYW	0.85	CARFRLYEPSLYW 2	0.62	CARREYSSGWYYYFYTMDVW	0.67
		19.9		8.79		9.79

	Month 1		*Month 15*	
	Top 10 expanded clone's CDR3 sequences	*% of the repertoire*	*Top 10 expanded clone's CDR3 sequences*	*% of the repertoire*
Healthy control 2	CAREQIEVNFDYW	1.82	CATPGGKDTLGGFDTW	1.69
	CARDLAAAGTFDYW	1.31	CARVAVTSGNSRFDPW	1.56
	CARGSLLWFGDAQDAFDIW	1.26	CARQTTDTFDIW	0.96
	CAQGHWLDFW	1.22	CARISVTSGNSRFDPW	0.94
	CARERGYSGSYYDYW	1.03	CARTMDRSGHYGLVGFDYW	0.76
	CAIGGRYYYFDYW	1.01	CVREVQPGDYFDYW	0.68
	CARDRGWNWNDVYDHW	0.96	CARRPSGLGGFDKW	0.66
	CATSGGSSWVYFEYW	0.94	CARTWCSEYSSSVCNGFEIW	0.66
	CAKSGVGDTNQLDYW	0.9	CARDRAAARIYYFDYW	0.65
	CARDQGRVRLFDYW	0.79	CAKDHLGTRYGMDVW	0.63
		11.24		9.19
	Month 1		*Month 8*	
	Top 10 expanded clone's CDR3 sequences	*% of the repertoire*	*Top 10 expanded clone's CDR3 sequences*	*% of the repertoire*
Untreated MS control 2	CAKDNYYDKDGMDVW	2.44	CARATSYYDSSFDYW	1.78
	CARQGQWLAFDYW	1.41	CVRVWSAFDIW	1.14
	CARDNYYKVDYW	1.24	CARSSGWYEAFDYW	0.93
	CAGCPQWEGSFHIW	1.07	CARGGDDDLWNAFHIW	0.83
	CVREFDYW	1.01	CARLEDSSSSRDDVFDIW	0.81
	CAKEVWWRFDQW	0.8	CARVATTIVRGVIVRGGWFDPW	0.71
	CARGRGFTYGYGPDYYYGMDVW	0.78	CGRLIPTRHYTNTRTEYW	0.7
	CARYLRIPYYFDYW	0.74	CARGYSSGLYYFDYW	0.68
	CAKIYYYDSNFDWW	0.74	CASYFWQSDGLDVW	0.68
	CAKGGFGFDSSGYHDYW	0.71	CARDGPVRAFDVW	0.57
		10.94		8.83

Supplementary table 4. *Persistence of highly abundant (top ten) CD8+ and CD4+ T cell clones before and after rituximab treatment in Patient 12_2789: Coloured CDR3 sequences indicate T cell clones found among the "Top Ten" most frequent clones before and after riyuximab treatment.*

	Before rituximab (C2+12)		*After rituximab (C2+24)*	
	Top 10 expanded clone's CDR3 sequences	*% of the repertoire*	*Top 10 expanded clone's CDR3 sequences*	*% of the repertoire*
CD8+ T cell	CASSFYSWGSGNTIYF	7.97	CASSLGVAPLHF 4	6.4
	CASSPRGTGYTTDTQYF 1	1.6	CASSPHEGAEAFF	4.5
	CASSPQRNTEAFF 2	1.5	CASSPPGGSGGFPYEQYF	3.8
	CASCLSWTGELFF	1.43	CASSPQRNTEAFF 2	3.07
	CASSLIGVSSYNEQFF	1.24	CASSLSGGRAFF 3	2.55
	CASSLAGMVNEQYF	0.94	CASSPRGTGYTTDTQYF 1	1.7
	CASSLSGGRAFF 3	0.8	CASSSPTRGNYGYTF 5	1.4
	CASSLGWTGAYGYTF	0.78	CASSVSNQPQHF	1.2
	CASSLGVAPLHF 4	0.77	CASSPQRNTEAFF 2	1.17
	CASSSPTRGNYGYTF 5	0.71	CASSYYGSYNEQFF	1.1
		17.74		26.89
	Before rituximab (C2+12)		*After rituximab (C2+24)*	
	Top 10 expanded clone's CDR3 sequences	*% of the repertoire*	*Top 10 expanded clone's CDR3 sequences*	*% of the repertoire*
CD4+ T cell	CASSLVGGNEQFF 1	2.23	CASSLVGGNEQFF 1	1.11
	CSATQDSATNEKLFF	0.22	CASSDNQFRETQYF	0.28
	CASSSPDGRFGYTF	0.17	CSARDYQHSGEAYNEQFF	0.26
	CRTMGQGDEGYGYTF	0.15	CASSYGKAWGEAFF	0.25
	CASSPLTEEKLFF	0.12	CASQGQYF	0.18
	CASTRNYGYTF	0.10	CASSFGNEQFF	0.17
	CASRNTGELFF	0.10	CSVGNFNEKLFF	0.16
	CASSLGGGTSYF	0.09	CASTTGVSPLHF	0.15
	CASRDRVEQFF	0.09	CASSFTNQPQHF	0.15
	CASSPSGNSPLHF	0.09	CASSYGPDEQYF	0.15
		3.37		2.87

Author "Sumanta Barman" contributed to designing the experiments. He carried out all experimental procedures including PBMC isolation, FACS sorting, TCR- β chain and IG-H chain library preparation for next generation sequencing (NGS), TCR-β and IG-H repertoire sequencing. SB also contributed to the acquisition and analysis of all data by using bioinformatics and statistical tools. He interpreted the data, prepared all figures and drafted the manuscript.

Published scientific article I

NMDAR encephalitis: passive transfer from man to mouse by a recombinant antibody

ANNALS of Clinical and Translational Neurology
Open Access
ANA American Neurological Association since 1875

RESEARCH ARTICLE

NMDAR encephalitis: passive transfer from man to mouse by a recombinant antibody

Manish Malviya[1,13,a,b], Sumanta Barman[1,a,b], Kristin S. Golombeck[2,a], Jesús Planagumà[3,a], Francesco Mannara[3,4,a], Nathalie Strutz-Seebohm[5], Claudia Wrzos[6], Fatih Demir[1,14], Christine Baksmeier[1,b], Julia Steckel[1,c], Kim Kristin Falk[7], Catharina C. Gross[2], Stjepana Kovac[2], Kathrin Bönte[2], Andreas Johnen[2], Klaus-Peter Wandinger[7], Elena Martín-García[4], Albert J. Becker[8], Christian E. Elger[9], Nikolaj Klöcker[10], Heinz Wiendl[2], Sven G. Meuth[2], Hans-Peter Hartung[1], Guiscard Seebohm[5], Frank Leypoldt[7], Rafael Maldonado[4], Christine Stadelmann[6], Josep Dalmau[3,11,12,a], Nico Melzer[2,a] & Norbert Goebels[1,a]

[1]Department of Neurology, Medical Faculty, Heinrich Heine University Düsseldorf, Düsseldorf, Germany
[2]Department of Neurology, University of Münster, Münster, Germany
[3]Institut d'Investigació Biomèdica August Pi i Sunyer, University of Barcelona, Barcelona, Spain
[4]Laboratori de Neurofarmacologia, Universitat Pompeu Fabra, Facultat de Ciències de la Salut i de la Vida, Barcelona, Spain
[5]Institute for Genetics of Heart Diseases (IfGH), University of Münster, Münster, Germany
[6]Institute of Neuropathology, University of Göttingen, Göttingen, Germany
[7]Institute of Clinical Chemistry and Department of Neurology, University Hospital of Schleswig-Holstein Lübeck/Kiel, Schleswig-Holstein, Germany
[8]Department of Neuropathology, University of Bonn, Bonn, Germany
[9]Department of Epileptology, University of Bonn, Bonn, Germany
[10]Institute of Neurophysiology, Medical Faculty, Heinrich Heine University Düsseldorf, Düsseldorf, Germany
[11]Catalan Institution for Research and Advanced Studies, Barcelona, Spain
[12]Department of Neurology, University of Pennsylvania, Philadelphia, Pennsylvania
[13]Current address: Centre Physiopathologie de Toulouse-Purpan, Université Toulouse III, Toulouse, France
[14]Current address: Forschungszentrum Jülich, Jülich, Germany

Correspondence
Norbert Goebels, Department of Neurology, University of Düsseldorf, Moorenstrasse 5, 40225 Düsseldorf, Germany. Tel: +49 211 81 04594; Fax: +49 211 81 04597; E-mail: norbert.goebels@uni-duesseldorf.de
Nico Melzer, Department of Neurology, University of Münster, Albert-Schweitzer-Campus 1, 48149 Münster, Germany. Tel: +49 251 83 48188; Fax: +49 251 83 48199; E-mail: nico.melzer@ukmuenster.de

Funding Information
This study was funded by the German Research Foundation (DFG, TR128, Project Z2 to HW, DFG, INST 2105/27-1 to SGM); NIH RO1NS077851 (to JD), Instituto Carlos III/FEDER, FIS PI14/00203 (to JD), CIBERER# CB15/00010 (to JD), and Fundacio Cellex (to JD); and the Walter und Ilse-Rose-Stiftung (to HPH), the Forschungskommission of the Heinrich Heine University Düsseldorf, Germany (to NG), and the Bundesministerium für Bildung und Forschung (BMBF 031A232 to NG).

Received: 23 June 2017; Accepted: 28 June 2017

Annals of Clinical and Translational Neurology **2017; 4(11): 768–783**

doi: 10.1002/acn3.444

Abstract

Objective: Autoimmune encephalitis is most frequently associated with anti-NMDAR autoantibodies. Their pathogenic relevance has been suggested by passive transfer of patients' cerebrospinal fluid (CSF) in mice in vivo. We aimed to analyze the intrathecal plasma cell repertoire, identify autoantibody-producing clones, and characterize their antibody signatures in recombinant form. **Methods**: Patients with recent onset typical anti-NMDAR encephalitis were subjected to flow cytometry analysis of the peripheral and intrathecal immune response before, during, and after immunotherapy. Recombinant human monoclonal antibodies (rhuMab) were cloned and expressed from matching immunoglobulin heavy- (IgH) and light-chain (IgL) amplicons of clonally expanded intrathecal plasma cells (cePc) and tested for their pathogenic relevance. **Results**: Intrathecal accumulation of B and plasma cells corresponded to the clinical course. The presence of cePc with hypermutated antigen receptors indicated an antigen-driven intrathecal immune response. Consistently, a single recombinant human GluN1-specific monoclonal antibody, rebuilt from intrathecal cePc, was sufficient to reproduce NMDAR epitope specificity in vitro. After intraventricular infusion in mice, it accumulated in the hippocampus, decreased synaptic NMDAR density, and caused severe reversible memory impairment, a key pathogenic feature of the human disease, in vivo. **Interpretation**: A CNS-specific humoral immune response is present in anti-NMDAR encephalitis specifically targeting the GluN1 subunit of the NMDAR. Using reverse genetics, we recovered the typical intrathecal antibody signature in recombinant form, and proved its pathogenic relevance by passive transfer of disease symptoms from man to mouse, providing the critical link between intrathecal

[a]These authors contributed equally.
[b]In partial fulfillment of the requirements for the degree "Doctor rerum naturalium (Dr. rer. nat.)" or
[c]diploma degree, respectively.

immune response and the pathogenesis of anti-NMDAR encephalitis as a humorally mediated autoimmune disease.

Introduction

Encephalitis associated with anti-*N*-methyl-D-asparate receptor (anti-NMDAR) antibodies ("antibodies") can be triggered by the presence of peripheral tumors[1,2] or preceding viral CNS infection or occur in the absence of such obvious events.[3,4] It typically presents with neurocognitive deficits variably accompanied by psychiatric symptoms, epileptic seizures, and disorders of movement and consciousness. Antibodies against NMDAR can be detected both in peripheral blood (PB) and cerebrospinal fluid (CSF), and patients typically exhibit intrathecal synthesis of anti-NMDAR antibodies.[1]

The pathogenic relevance of these antibodies is supported by the response of clinical symptoms to immunotherapy and the correlation between antibody titers and neurological outcome.[5] The intrathecal source of pathogenic antibodies in anti-NMDAR encephalitis has been suggested to originate from $CD138^+$ plasma cells identified in perivascular and interstitial spaces in biopsy and autopsy studies.[6,7]

In vitro, IgG antibodies contained in serum/CSF have been shown to bind to the N368/G369 region of the GluN1 subunit of NMDARs and reversibly decrease postsynaptic NMDAR surface density and synaptic localization in inhibitory as well as excitatory cultured rat hippocampal neurons by selective antibody-mediated cross-linking and internalization.[8,9] These effects are associated with a disruption of the normal interaction between the NMDAR and Ephrin-B2 (EphB2) receptor at the synapse.[10,11] Consistently, anti-NMDAR antibodies selectively decreased NMDAR-mediated miniature excitatory postsynaptic currents (mEPSC) without affecting α-amino-3-hydroxy-5-methyl-4-isoxazolepropionic acid receptor (AMPA-R)-mediated mEPSCs in cultured rat hippocampal neurons.[8,9] Once internalized, antibody-bound NMDARs traffic through both recycling endosomes and lysosomes, but do not induce compensatory changes in glutamate receptor gene expression.[8,12] Although anti-NMDAR antibodies are mainly of the complement-activating IgG1 and IgG3 subtypes, complement deposition was not detected in brain biopsy specimens from treatment-naïve patients with anti-NMDAR encephalitis, probably due to the low levels of complement present in CSF and relative preservation of the blood–brain barrier (BBB).[7,13] Consistently, anti-NMDAR IgG antibodies did not reduce the number of synapses, dendritic spines, dendritic complexity, or cell survival in cultured rat hippocampal neurons,[9] and neuronal damage was sparse in brain biopsy specimens.[13,14] Passive infusion of patients' CSF into the cerebroventricular system of mice via osmotic minipumps induced reversible memory impairment and behavioral changes consistent with symptoms found in patients with anti-NMDAR encephalitis in vivo.[15]

It has been postulated that NMDAR expressed in nervous tissue contained in peripheral tumors, or released by viral-induced neuronal destruction, is transported to the regional lymph nodes either in soluble form or loaded in antigen-presenting cells.[16] Naïve cognate antigen-specific B cells exposed to NMDAR in cooperation with antigen-specific $CD4^+$ T cells become activated and thus capable of entering the CNS crossing the BBB or the choroid plexus. In the brain, these NMDAR-specific B cells are thought to undergo further antigen stimulation with clonal expansion, affinity maturation of their antigen receptors, and differentiation into anti-NMDAR antibody-producing plasma cells.[16] Indeed, a recombinant human anti-NMDAR monoclonal antibody was recently cloned from intrathecal B cells and showed pathogenic effects in in vitro systems that were similar to those previously reported using CSF of patients.[9,17] However, whether the GluN1-reactive human monoclonal antibody indeed exerted any pathogenic effects in vivo was not investigated.

In this study, we focused on the analysis of clonally expanded intrathecal plasma cells (cePc), the cell population previously shown to be the main source of intrathecal immunoglobulin, often detectable as "oligoclonal bands."[18,19] We determined whether cePc are responsible for anti-NMDAR-specific autoantibody production in patients with acute treatment-naïve anti-NMDAR encephalitis and whether these autoantibodies functionally interact with NMDAR in vitro and are indeed capable of eliciting core clinical symptoms of the disease in mice in vivo.

Materials and Methods

Patients and rhuMab synthesis

Patients

Four patients with anti-NMDAR encephalitis and controls were recruited and analyzed using flow cytometry at the

Department of Neurology, Westfälische Wilhelms University of Münster, Germany. The study was approved by the local ethics committee of the Medical Faculty of the University of Münster, Germany (Az 2013-350-f-S). All participants (in retrospect after clinical recovery) and their nearest relatives (in prospect) gave written informed consent to the study including scientific evaluation and publication of all clinical, paraclinical, and scientific data obtained. Clinical and paraclinical assessments of patients (MRI, neuropsychological assessment, multiparameter flow cytometry of PB and CSF, antineuronal antibody testing, and histopathological studies) were essentially performed as described previously.[20]

Single cell RT-PCR analysis

Cryopreserved CSF cells were thawed in RPMI 1640 cell culture medium, washed, resuspended in FACS buffer (2% FBS in PBS), and incubated with PerCp-Cy5.5-labeled anti-human-CD19 antibody (BD Biosciences), APC-labeled anti-human-CD138 antibody (Miltenyi Biotec), and 300 nmol/L of DAPI for 30 min on ice. After washing, single-cell sorting was performed on a MoFlo XDP High Speed Cell Sorter (Beckman Coulter) at the flow cytometer facility of the Biomedical Research Center of the Heinrich Heine University Düsseldorf. Single $CD138^+$ plasma cells were sorted in individual microtiter wells and stored at −80°C until use. RT-PCR amplification of IgG heavy- and light-chain transcripts from single cells was performed as described previously[21] with minor modifications. PCR amplicons were purified from 1% agarose gel using QIAquick PCR purification kit and subsequently sequenced with the respective constant region primers at GATC Biotech (Germany). All Ig-VH, Ig-Vκ, and Ig-Vλ sequences were analyzed by IgBLAST in comparison with IMGT germline gene entry (http://www.ncbi.nlm.nih.gov/igblast/) to identify closest germline V(D)J gene segments with highest identity. Plasma cells from which sequences were amplified sharing more than 95% nucleotide identity, having highly similar or identical CDR3 regions, and belonging to the same V(D)J germline families were considered clonally expanded (cePc). Sequences that appeared to be clonally expanded were manually cross-checked to confirm the identity among them and accordingly processed for cloning and production of recombinant human monoclonal antibodies (rhuMab). The Ig-VH and Ig-VL complementarity-determining region 3 (CDR3) lengths were determined as indicated in IgBlast by counting the amino acid residues following framework region 3 (FR3) up to the conserved WG (tryptophan–glycine) motif in all JH segments or up to the conserved FG (phenylalanine–glycine) motif in JL segments.[22]

Ig–gene repertoire analysis

For Ig–gene repertoire analysis and phylogenetic tree construction, all sequences were trimmed before FR1 and after J regions, aligned in Ig-VH, Ig-Vκ, and Ig-Vλ groups, and analyzed using an online multiple alignment program for amino acid and nucleotide sequences called "MAFFT version 7" (http://mafft.cbrc.jp/alignment/server/). To construct phylogenetic trees of Ig-V sequences, "Newick file format" was generated by using default neighbor-joining (NJ) phylogeny method[23] on MAFFT (version 7) software. FigTree v1.4.2 software was used to construct unrooted phylogenetic trees. The bootstrap support values for each branch were calculated based on 100 resamplings of the original dataset. High values of the bootstrap (more than 70) represent a better statistical support for the topology in the tree.[24]

Ig expression vector cloning

Clonally expanded paired Ig heavy- and light-chain variable region amplicons identified and selected for rhuMab production were reamplified with primers containing restriction sites and cloned in frame into mammalian expression vectors containing the respective human Igγ1, Igκ, or Igλ2 constant gene regions. In brief, restriction digestion of PCR products and vectors were carried out with respective restriction enzymes, namely *Eco*RI, *Nhe*I, and *Avr*II (all from New England Biolabs), followed by 5′ dephosphorylation of the digested vectors using shrimp alkaline phosphatase (New England Biolabs). All digested products were purified from 1% agarose gel. The ligation reactions between restriction enzymes digested PCR products and corresponding vectors were performed using Liga-Fast™ Rapid DNA Ligation System (Promega), overnight at 4°C. Cloning of the second round PCR products was carried out into mammalian expression vectors containing a hEF1-HTLV promotor, an IL2 signal peptide sequence, and a multiple cloning site upstream of the human Ig constant regions (Invivogen). One Shot®TOP10 chemically competent *E. coli* cells were transformed with the ligated products at 42°C following the instruction protocol of the supplier (Invitrogen). The transformed Ig heavy-chain colonies were selected on Zeocin (Invitrogen) agar plates, whereas Ig light-chains colonies (Igκ or Igλ) were selected on Blasticidine (Invitrogen) agar plates. Mini-prep plasmid preparations (Qiagen miniprep kit), and subsequent sequencing, were carried out on the selected bacterial colonies to confirm the presence of original Ig variable regions. All cloned expression vectors were sequenced to confirm the presence of Ig-V region inserts with 100% identity to the respective original PCR products.

rhuMab production and purification

FreeStyle™ 293-F cells (Invitrogen) were cultured in TC-175 cm^2 flask (Greiner Bio-One) under standard conditions in Gibco® RPMI 1640 medium, supplemented with 10% heat-inactivated fetal calf serum (FCS), 100 μg/mL streptomycin, 100 U/mL penicillin (all from Invitrogen). Cotransfections of Ig heavy-chain and matching Ig light-chain expression vectors (20 μg each/flask) were performed using linear polyethylenimine (PEI) as a transfection reagent (Polysciences, Inc.)[25]. In brief, 1:3 concentration ratio of plasmids:PEI were mixed in 500 μL Opti-MEM-reduced serum media (Invitrogen), 30 min at RT, and subsequently incubated on 90% confluent cells in a total volume of 20 mL/flask for 24 h. The transfection medium was replaced with antibody-harvesting medium containing RPMI 1640 supplemented with 1× Nutridoma-SP (Roche), 100 μg/mL streptomycin, 100 U/mL penicillin, and cultured. The antibody harvesting medium was collected after 1 week of incubation, and transfected cells were either reincubated with fresh harvesting medium or stored in cell freezing medium (10% DMSO in FBS) at −80°C for future use.

RhuMab were purified from supernatants by using either HiTrap Protein G HP columns (GE Healthcare) on an FPLC system (ÄKTA Prime) or Magne™ Protein G Beads (Promega). In brief, harvested supernatants were centrifuged at 8000*g* for 10 min, filtered using 0.2-μm vacuum filters (Sarstedt), and adjusted to pH 7.4 using a 1 mol/L Tris-HCl buffer (pH 8.8). Supernatants were either pumped through protein G HP columns (columns pre-equilibrated with 20 mmol/L Tris-HCl, pH 7.4), or incubated with Magne™ protein G beads overnight at 4°C. Bound rhuMab were eluted with 0.1 mol/L glycine-HCl buffer (pH 2.7) and neutralized to pH 7.4 with 1 mol/L Tris-HCl buffer (pH 8.8). Buffer exchange was performed with PBS either by dialysis using 10 K MWCO Slide-A-Lyzer Dialysis Cassettes (Thermo Scientific) or using 30 K Amicon Ultra-15 centrifugal Filter Units (Merck Millipore). The protein concentrations of purified antibodies were determined by BC assay kit (Uptima).

Purity of the eluted rhuMab was determined by SDS-PAGE gel. Semidenatured samples were prepared by mixing 5 μg of eluted antibodies with 1X-NuPAGE sample reducing agent (Invitrogen), heated 10 min at 60°C, and loaded on 4–16% PreciseTM Protein gel (Thermo Scientific), along with Novex Sharp prestained protein standard (Invitrogen). The samples were run in NuPage-MOPS SDS running buffer (Invitrogen) for 30 min at 120 V and subsequently stained with Gel codeTM blue stain reagent (Thermo Scientific) to visualize the complete antibody bands along with separate Ig heavy- and light-chain bands. Purified rhuMab were aliquoted and stored at −80°C. Initial screening of rhuMab for antineuronal reactivity was performed by Euroimmun, Lübeck, Germany (http://www.euroimmun.de).

Characterization of rhuMab specificity

To demonstrate the specificity of rhuMab, we used techniques including immunoprecipitation, western blot, immunohistochemistry with rat brain, immunocompetition assays, and immunocytochemistry with transfected HEK cells essentially as previously reported.[26,27] As isotype control, a recombinant human antibody (12D7) with – in this context – irrelevant antigen specificity (cancer/testis antigen NY-ESO-1) was used as indicated.

Functional analysis of anti-NMDAR-specific rhuMab SSM5 in vitro and in vivo

To assess functional effects of rhuMab in vitro, we used two-electrode voltage-clamp analysis of GluN1-1a- and GluN2B-transfected *Xenopus laevis* oocytes together with rhuMab incubation in primary cultures of hippocampal neurons with quantification of the effects of rhuMab on total cell-surface and synaptic NMDAR clusters as described previously.[9,28]

To examine functional consequences of rhuMab in vivo, we used behavioral testing of mice receiving cerebroventricular infusion of patients' CSF or monoclonal antibodies together with subsequent determination of rhuMab binding to brain tissue and quantification of the effects of rhuMab on total cell-surface and synaptic NMDAR clusters as described previously.[11,15]

Statistical analysis

If not explicitly stated otherwise, all statistical analyses were performed using Sigma Plot 11 (Systat Software, Germany) or GraphPad Prism Version 6 (GraphPad Software, San Diego, CA). Data were tested for normality using the Shapiro–Wilk test. Depending on the result, unpaired Student's *t* test or Mann–Whitney test was used to compare means between two independent groups, whereas paired Student's *t* test or Wilcoxon matched pairs signed-rank test was used for different treatments within the same group. More than two datasets were compared using ANOVA with Bonferroni post hoc correction. All normally distributed data are given as mean together with the standard deviation (SD) or standard error of the mean (SEM). All not normally distributed data are given as median together with the interquartile range. If not explicitly stated otherwise, the prechosen significance level for all confirmatory tests was set to $P < 0.05$.

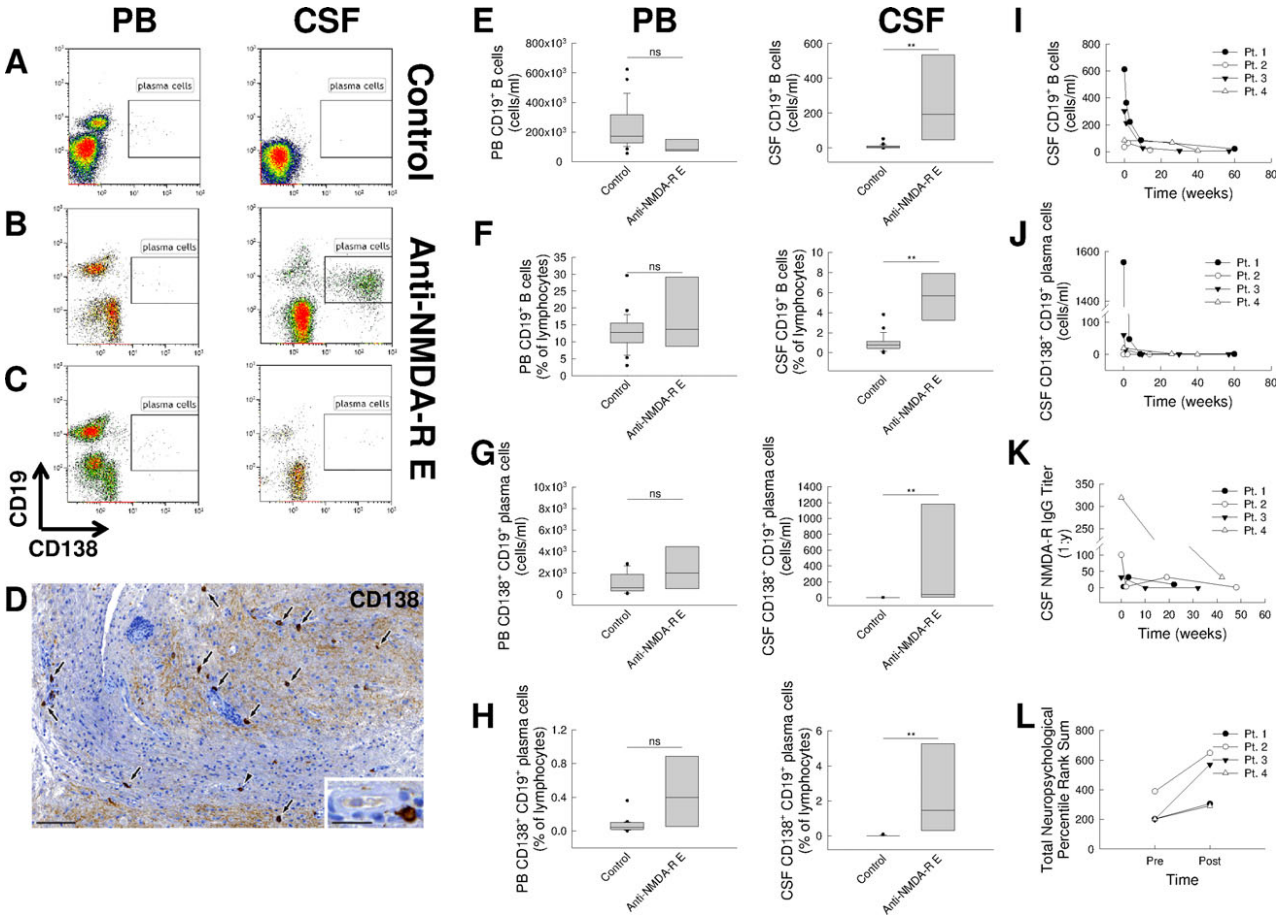

Figure 1. Intrathecal B-cell and plasma cell accumulation in patients with anti-NMDAR encephalitis corresponds to the clinical disease course. (A–C) Representative multiparameter flow cytometry analysis of $CD19^+$ B cells and $CD19^+$ $CD138^+$ plasma cells in peripheral blood (PB, left panels) and cerebrospinal fluid (CSF, right panels) in a healthy control (A) and a patient (Pt. 1) with anti-NMDAR encephalitis before (B) and after (C) immunotherapy. (D) Representative $CD138^+$ plasma cell staining of a biopsy specimen of a newly occurring cerebral MRI lesion in a patient with later on established anti-NMDAR encephalitis (scale bar represents 50 μm; insert scale bar represents 10 μm). (E–H) Multiparameter flow cytometry analysis of absolute numbers (E) and relative fractions (F) of $CD19^+$ B cells and absolute numbers (G) and relative fractions (H) of $CD138^+$ $CD19^+$ plasma cells within peripheral blood (PB, left panels) and cerebrospinal fluid (CSF, right panels) in four patients with anti-NMD-R encephalitis and 25 controls. Data are given as whisker plots. Statistical testing was performed using the Wilcoxon rank sum test with an α error of 0.05. Levels of significance are indicated by n.s. (not significant) for all $P > 0.05$, $^*P < 0.05$ and $^{**}P < 0.01$. (I–K) Time course of absolute numbers of $CD19^+$ B cells (I), $CD19^+$ $CD138^+$ plasma cells (J), and NMDAR IgG titers (K) in cerebrospinal fluid of anti-NMDAR encephalitis before, during, and after treatment. (L) Comprehensive results of detailed neuropsychological assessments (total rank sum of test of attention, memory and executive functions) of patients with anti-NMDAR encephalitis 1–16 weeks after admission (pre) and after 8–48 months (post).

Results

Intrathecal B-cell and plasma cell accumulation in patients with anti-NMDAR encephalitis corresponds to the clinical disease course

We identified four therapy-naive female Caucasian patients with recent onset typical anti-NMDAR encephalitis (for details, see Tables S1–S7). Cerebral MRI (1.5 Tesla, **Suppl. Fig. 1**) showed either frontal or temporal cortical lesions and was otherwise normal. All patients underwent multiparameter flow cytometry analysis of PB and CSF to characterize the systemic and intrathecal autoimmune response in detail before initiation of immunotherapy (Fig. 1, Table S6). Twenty-five patients that had PB and CSF analyses for suspected neurological disease but turned out to suffer from somatization disorders served as controls.

A representative flow cytometry of $CD19^+$ and $CD138^+$ cells in PB and CSF in anti-NMDAR encephalitis (Pt. 1) and controls is shown in Figure 1A

and B (PB left panels, CSF right panels). As compared to controls, the absolute numbers and relative fractions of $CD19^+$ B cells (Fig. 1E and F) and $CD138^+$ $CD19^+$ plasma cells (Fig. 1G and H) were significantly elevated in CSF of patients with anti-NMDAR encephalitis, but not in their PB (for details, see Table S6, PB left panels, CSF right panels). Notably, controls harbored some intrathecal $CD19^+$ B cells but no intrathecal $CD138^+$ $CD19^+$ plasma cells at all (Table S6). Likewise, all patients showed positive NMDAR-specific Ig indices (Table S2). These data demonstrate intrathecal B-cell and plasma cell accumulation as a likely intrathecal source of antibody production in patients with anti-NMDAR encephalitis. Consistently, prominent $CD138^+$ plasma cells could be detected in perivascular, and interstitial spaces of a biopsy specimen from another patient with anti-NMDAR encephalitis (Fig. 1D).[6,7]

All patients received immunotherapy consisting of repeated cycles of protein A immunoadsorption combined with pulses of intravenous methylprednisolone (Pt. 1–4) and immunosuppression using azathioprine or methotrexate (Pt. 1–3) or radiochemotherapy for small cell lung cancer (Pt. 4). Under these treatment regimens, clinical symptoms, EEG, and MRI findings as well as inflammatory CSF changes regressed almost completely (Tables S1 and S2). Moreover, absolute numbers and relative fractions of $CD19^+$ B cells (Fig. 1I, Table S7) and $CD138^+$ $CD19^+$ plasma cells (Fig. 1J, Table S7) as well as NMDAR IgG titers (Fig. 1K, Table S2) in CSF decreased rapidly. Neuropsychological performance (attention, memory, executive function) substantially improved in each patient upon follow-up assessment after 8–48 months (Fig. 1L, Tables S4 and S5).

Hence, intrathecal B-cell and plasma cell accumulation corresponded well to the clinical disease course of patients with anti-NMDAR encephalitis.

Presence of clonally expanded plasma cell with hypermutated antigen receptors indicates an intrathecal antigen-driven immune response in patients with anti-NMDAR encephalitis

Clonally expanded plasma cells/blasts (cePc) were identified among intrathecal $CD138^+$ cells by sequence analysis of Ig heavy-chain amplicons obtained by single-cell RT-PCR. In Figure 2, an example of one of the patients with anti-NMDAR encephalitis is shown: From this patient, a total of 120 single $CD138^+$ cells were collected by FACS (Fig. 2A) and subjected to single-cell PCR. Readable sequences were obtained from 81 Ig light-chain amplicons (51 kappa chains, 30 lambda chains) and 37 IgG heavy-chain amplicons. Unrooted phylogenetic trees constructed from IgG heavy (Fig. 2B), lambda (Fig. 2C), and kappa light-chain sequences (Fig. 2D) are shown: Clonally related sequences aggregate together as overlapping "leaves" on the same "branch" of the phylogenetic tree. Sequences, which are very different from another or even belong to different germ line gene families, are separated by distance. Recombinant human monoclonal antibodies (rhuMab) were reconstructed from matching IgH and IgL variable gene regions of seven cePc (Fig. 2, circled). All identified cePc sequences were hypermutated, containing silent as well as replacement mutations indicating an ongoing antigen-driven intrathecal immune response (Table 1).

A recombinant human monoclonal antibody (rhuMAb) produced from clonally expanded intrathecal plasma cells specifically recognizes the NMDAR

To elucidate whether cePc are the actual source of the intrathecal autoantibody response, we cloned paired immunoglobulin heavy- and light-chain variable gene regions from cePc essentially as previously described.[19,21] PEI mediated cotransfection of IgG-HC and matching Ig-LC expression vectors into FreeStyle 293-F cells were carried out to produce recombinant monoclonal antibodies in vitro. Secreted rhuMAb were purified from the supernatant of transfected cells by affinity chromatography. Successful antibody production was confirmed by SDS gel electrophoresis (data not shown).

From the seven rhuMab we cloned and expressed from CSF cePc of anti-NMDAR encephalitis patient SSM, rhuMab SSM5 was identified to react specifically with NMDAR, whereas the remaining showed no CNS tissue reaction at all (data not shown). To further characterize the antigen specificity of rhuMab, we performed additional assays.

The pattern of brain immunostaining and main epitope target of rhuMab SSM5 are similar to antibodies in serum and CSF from anti-NMDAR encephalitis patients

To characterize the tissue reactivity of rhuMab SSM5, immunohistochemistry on mildly fixed sagittal rat brain sections was performed, as previously described.[14] Patient-derived rhuMab SSM5 (Fig. 3A), but not the isotype control rhuMab 12D7 (Fig. 3B), produced an intense pattern of brain reactivity characteristic of NMDAR as previously reported using patients' sera or CSF,[14] with a strong emphasis of the hippocampal region. Tissue reactivity of rhuMab SSM5 was clearly reduced by preincubation of tissue sections with sera from patients with

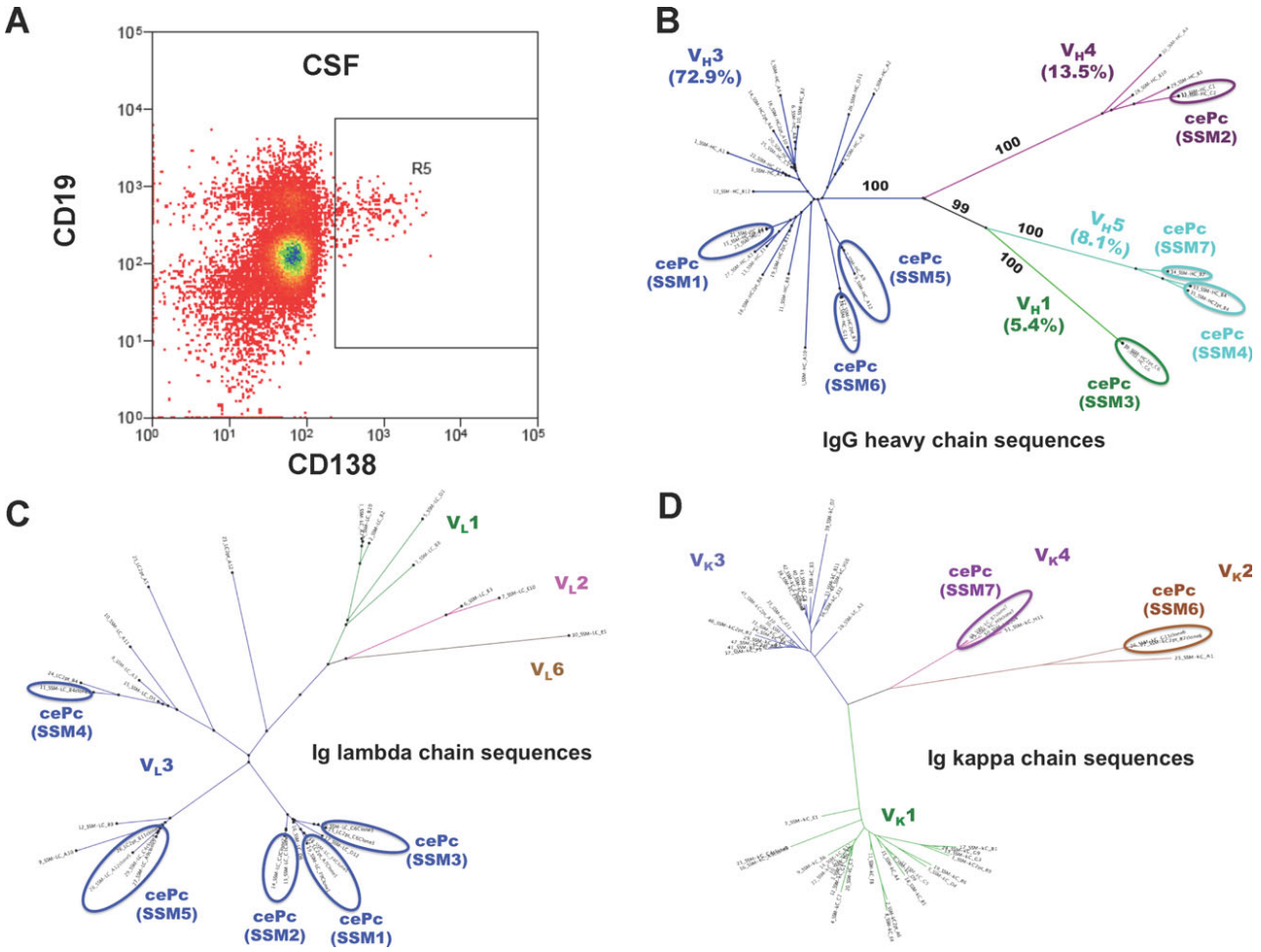

Figure 2. Presence of clonally expanded plasma cells with hypermutated antigen receptors indicates an intrathecal antigen-driven immune response in patients with anti-NMDAR encephalitis. Shown are unrooted phylogenetic trees of the IgG-VH (B), V lambda (C), and V kappa (D) gene family repertoires of sequences obtained from CSF plasma cells of a patient with anti-NMDAR encephalitis by single cell RT-PCR. Each colored branch of the tree represents a single V family. The external node of a branch represents a "leaf" or a "sequence." The branch length and distance between sequences correspond to sequence similarity/dissimilarity, shorter and closer branches relate to a greater sequence similarity. The bootstrap support values for each branch were calculated based on 100 resampling of the original dataset. Ovals indicate clonally expanded plasma cells (cePc) 1–7, from which recombinant monoclonal antibodies SSM 1–7 were derived. The gate (R5) in the FACS panel (A) shows the cell population used for single cell analysis.

anti-NMDAR encephalitis (Fig. 3D and E), but not by preincubation with serum of a healthy blood donor (Fig. 3C and E), suggesting that antibodies contained in patients' sera and rhuMab SSM5 compete for similar target epitopes of the NMDAR.

To further narrow down the epitope specificity of patient-derived rhuMab SSM5, reactivity with HEK293 cells transfected with wild-type GluN1/N2B or indicated GluN1 mutants was assessed by immunocytochemistry (Fig. 4A–C) as previously described.[29] Patient-derived rhuMab SSM5, but not isotype control rhuMab 12D7, specifically stained HEK293 cells cotransfected with wild-type GluN1/GluN2b in a similar pattern as CSF from a patient with anti-NMDAR encephalitis (green, Fig. 4A). Similar to patient's CSF, reactivity of rhuMab SSM5 with HEK293 transfectants was abrogated, when the main immunogenic hinge region of GluN1 was mutated replacing amino acid G369 by a nonpolar amino acid (mutant G369I) (Fig. 4B), while exchanging amino acid G369 for a polar residue (G369S) did not affect binding of rhuMab SSM5 or patient's CSF (Fig. 4C). Immunoprecipitation experiments with membrane fractions of brain tissue confirmed that rhuMab SSM5 specifically reacts with the 120 kDa GluN1subunit of the NMDAR (Fig. 4D).

We therefore conclude that rhuMab SSM5 targets the same restricted epitope on the extracellular amino terminal domain of the GluN1 subunit of the NMDA receptor as has been described for disease-relevant antibodies in

Table 1. Number of amino acid mutations in the sequences of reconstructed cePc-derived rhuMAb compared with nearest germline gene sequences.

		Amino acid mutations in the IgG-VH and matching VL genes of the cePc sequences from the corresponding germline genes						
rhuMab	Germline V(D)J gene	FR1	CDR1	FR2	CDR2	FR3	CDR3	Total mutations
SSM1.HC	IGHV3(D3)J6	1	1	1	1	4	–	8
SSM1.λC	IGLV3J2	–	–	–	1	–	–	1
SSM2.HC	IGHV4(D5)J2	–	1	1	1	4	–	7
SSM2.λC	IGLV3J2	–	–	–	1	–	–	1
SSM3.HC	IGHV1(D6)J6	–	–	–	4	4	–	8
SSM3.λC	IGLV3J2	–	–	–	1	–	–	1
SSM4.HC	IGHV5(D6)J5	3	3	1	2	4	–	13
SSM4.λC	IGLV3J1	1	1	1	1	–	1	5
SSM5.HC	IGHV3(D6)J2	1	–	–	–	–	–	1
SSM5.λC	IGLV3J2	–	–	–	–	–	1	1
SSM6.HC	IGHV3(D3)J4	1	1	2	1	9	1	15
SSM6.kC	IGKV2J4	1	3	1	1	1	1	8
SSM7.HC	IGHV5(D1)J4	–	3	2	1	–	–	6
SSM7.kC	IGKV4J2	1	4	–	–	1	1	7

(–) Either no mutation or silent mutation (not leading to an amino acid change).

serum and CSF of patients with anti-NMDAR encephalitis.[29]

RhuMab SSM5 decreases the density of cell surface and synaptic NMDAR in cultured neurons

Hippocampal neurons were cultured for 24 h with patient-derived rhuMab SSM5, isotype control rhuMab 12D7, or CSF of a patient with anti-NMDAR encephalitis. Patient-derived rhuMab (SSM5), but not the isotype control rhuMab (12D7), caused a significant decrease in cell surface NMDAR and synaptic NMDAR clusters, similar to that observed with CSF of a patient with anti-NMDAR encephalitis (Fig. 5A, green, quantified in Fig. 5B). In contrast, PSD95, an excitatory postsynaptic protein, was not reduced (Fig. 5 A, red, quantified in Fig. 5B). Together, these results show that patient-derived rhuMab SSM5 specifically reduces synaptic NMDAR clusters, as previously described for CSF of anti-NMDAR encephalitis patients.[9]

RhuMab SSM5 reduces NMDAR-mediated currents in transfected *Xenopus laevis* oocytes

We next assessed the effects of patient-derived rhuMab SSM5 on NMDAR function using two electrode voltage-clamp experiments in *X. laevis* oocytes in vitro. *Xenopus* oocytes coexpressing GluN1/GluN2B were preincubated with patient-derived rhuMab SSM5 in bath medium for 1 h prior to measurement ("antibody"), whereas GluN1/GluN2B expressing control oocytes were not preincubated ("control") (Fig. 6A). Nontransfected oocytes were treated the same way, either preincubated with patient rhuMab ("uninjected, antibody") or not preincubated ("uninjected"). Uninjected oocytes revealed no measurable currents. GluN1/GluN2B amplitudes in oocytes either without ("control") or with ("antibody") preincubation with autoantibody were measured and are shown normalized to control currents: RhuMab SSM5 significantly decreased NMDAR-mediated currents by about 20% (Fig. 6B), supporting a functional impact of this patient-derived rhuMab on NMDAR-mediated currents.

These results are in striking accordance with earlier results obtained by two electrode voltage-clamp experiments in *X. laevis* oocytes showing a time-dependent steady-state reduction of the NMDAR-mediated currents of about 30% within 16 min in oocytes exposed to dialyzed sera of patients with anti-NMDAR encephalitis.[33] The reason for the relatively small antibody-mediated functional effects obtained in the *X. laevis* oocyte expression system compared to the strong effects in mice on NMDA receptor expression on the neuronal cell surface in vitro and memory impairment in vivo may be due to the necessity to record NMDAR-mediated currents in Ca^{2+}-free media to block current inactivation in *Xenopus* oocytes.[34] These recording conditions may influence conformational changes of the NMDA receptor induced by binding of the antibody or modulate antibody binding itself and thus diminish subsequent receptor internalization.

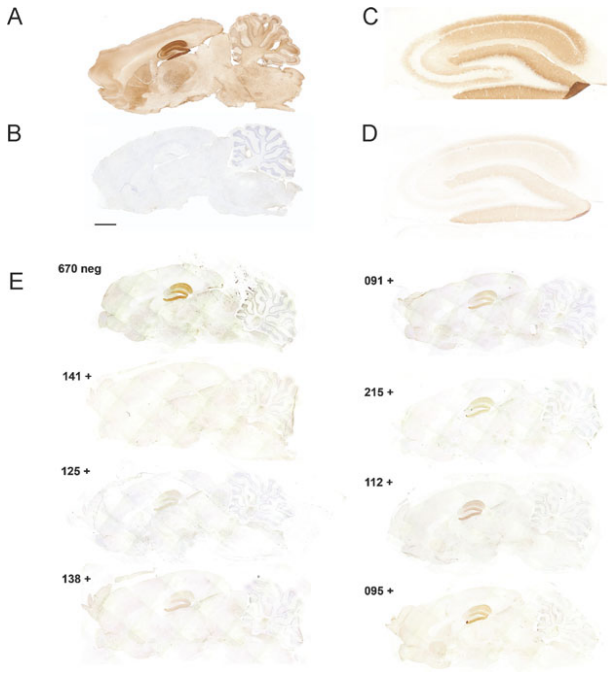

Figure 3. The pattern of brain tissue immunostaining of rhuMab SSM5 is characteristic of the NMDAR and blocked by serum antibodies from patients with anti-NMDAR encephalitis. (A, B) Patient-derived rhuMab reacts with brain tissue. Representative immunoreactivity of a patient-derived rhuMab (SSM5) (A) and control rhuMab (12D7) (B) with sagittal sections of rat brain. SSM5 antibody, but not the control antibody shows a robust immunostaining of brain in a pattern characteristic of the NMDAR. Scale bar 2 mm. (C, D, E) Patient-derived rhuMab competes for similar epitopes recognized by serum antibodies from patients with anti-NMDAR encephalitis. Reactivity of biotinylated rhuMab SSM5 (diluted 1:20) with rat hippocampus preincubated with serum from a healthy subject (C) and serum from a patient with anti-NMDAR encephalitis (diluted 1:2) (D). (E) Preincubation with sera of anti-NMDAR encephalitis patients substantially blocks the reactivity of SSM5. In this experiment, the tissue sections were preincubated with sera from seven different patients (091, 095, 112, 125, 138, 141, 215) and one control without antibodies (670). There is competition of reactivity by each of the patients' sera, while control serum (top left) does not reduce rhuMab SSM5 reactivity (as expected). Case to case variation of competition suggests that anti-NMDAR antibodies against epitopes recognized by rhuMab SSM5 are present in each of the patients but differ in concentration and/or affinity.

RhuMab SSM5 decreases the density of synaptic NMDAR and causes memory deficits in a mouse model of cerebroventricular antibody transfer

The in vitro results outlined above led us to determine the behavioral effects of patient-derived rhuMab SSM5 in vivo: To this end, rhuMab SSM5 or isotype control rhuMab 12D7 was infused for 14 days into both ventricles of mice using osmotic mini-pumps as previously described.[11,15] The most robust effect during the 14-day infusion of patients' CSF[15] was observed on the novel object recognition test, therefore we chose this test for assessing the effects of this patient-derived rhuMab (Fig. 6C). Compared with animals infused with isotype control rhuMab 12D7 (green circles), those infused with patient-derived rhuMab SSM5 (red circles) showed a progressive decrease of the object recognition index, indicative of a memory deficit.[15] A high index indicates better object recognition memory and vice versa. The memory deficit became apparent on Day 10 and was maximal on Day 18 (4 days after the infusion of rhuMab had stopped, representing the cumulative effects of antibodies still circulating in CSF). On Day 25, the object recognition index had normalized and was similar to that of animals treated with isotype control rhuMab (Fig. 6C). These findings are similar to those reported with the model of infusion of patients' CSF NMDAR antibodies and could not be explained by other systemic effects (e.g., overall motor activity, weight loss) as described previously.[15]

In mice infused with rhuMab SSM5, impairment of memory was paralleled by a gradual increase of brain-bound human IgG mainly in the hippocampus until Day 18, followed by a progressive decrease of immunostaining (Fig. 6D right panels, Fig. 6E dark gray columns), which was not observed in mice infused with control rhuMab 12D7 (Fig. 6D left panels, Fig. 6E pale gray columns).

Similar to studies in cultured hippocampal neurons mentioned above, the infusion of patient-derived rhuMAb SSM5 (Fig. 7A upper panels, Fig. 7B dark gray), but not isotype control rhuMAb 12D7 (Fig. 7A lower panels, Fig. 7B light gray), caused a significant decrease of hippocampal cell surface NMDAR (Fig. 7A, red) and synaptic NMDAR clusters (defined as NMDAR clusters colocalizing with PSD95) in vivo, without affecting PSD95 (Fig. 7A, green) and without causing neuronal death (data not shown).

These findings demonstrate that antibodies reconstructed from patient-derived clonally expanded intrathecal plasma cells recapitulate key features of anti-NMDAR encephalitis in vitro and in vivo.

Discussion

In this study, we show that a single recombinant human NMDAR-specific monoclonal antibody, rebuilt from patients' clonally expanded CSF plasma cells by reverse genetics, is sufficient to reproduce epitope specificity, and key pathogenic features typical of anti-NMDAR encephalitis in vitro and in vivo.

This disorder predominantly affects young women and children, with approximately 50% of women having an underlying ovarian teratoma that contains nervous tissue

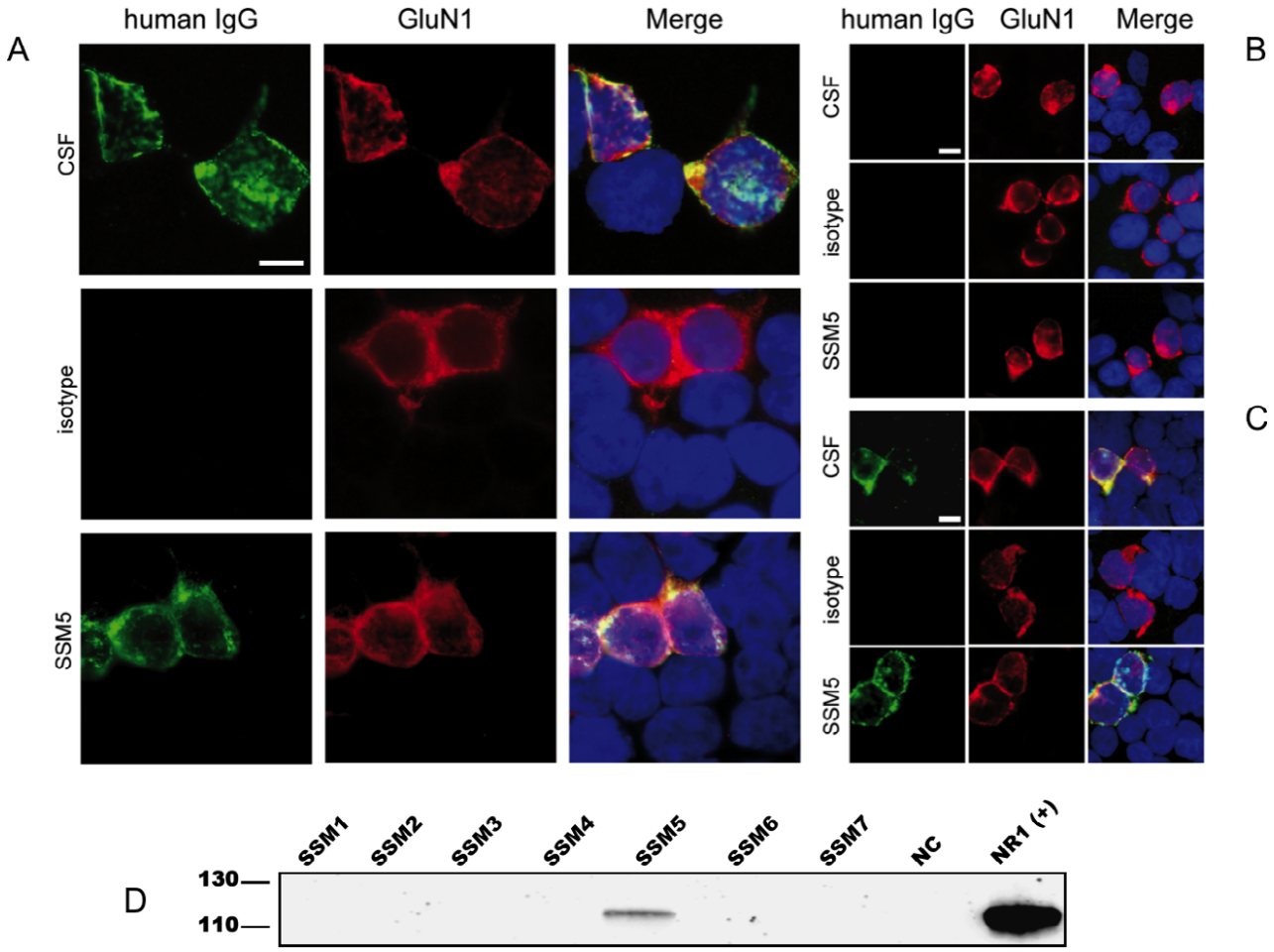

Figure 4. RhuMab SSM5 targets the same restricted epitope of the GluN1 subunit of the NMDAR as patient's CSF antibodies. (A–C) Patient-derived rhuMab shows the same staining pattern as CSF from a patient with anti-NMDAR encephalitis in immunohistochemistry with HEK cells expressing full-length or mutant GluN1/GluN2B. Immunofluorescence with HEK293 cells expressing full-length GluN1/GluN2B (A) or mutant GluN1 with full-length GluN2B (B, C) and stained for human IgG (green) and with a commercial GluN1-specific antibody (red); nuclear counterstaining with DAPI (blue). Cells were treated with human CSF (diluted 1:16), patient-derived rhuMab (SSM5, 4.3 μg/mL) or control rhuMab (isotype, rhuMab 12D7, 4.3 μg/mL). The epitope-disrupting G369I mutant (B) does not show staining by patients' CSF or rhuMab, while a mutant with less epitope disruption G369S (C) does not affect staining. Scale bar represents 10 μm. (D) Confirmation of antigen specificity of patient-derived rhuMab by immunoprecipitation (IP). Proteins precipitated from brain membrane lysates were separated by PAGE electrophoresis and blotted onto PVDF membranes. Western blot detection was performed with a commercial GluN1-specific antibody. A band of around 120 kDa corresponding to the GluN1 subunit of the NMDA receptor was identified using SSM5 rhuMab (5 μg, covalently coupled to Dynabeads) in the membrane fraction of brain tissue. Commercially available antibodies to the respective target antigen were used as positive control in IPs and in western blot detections. A rhuMab specific for an irrelevant target (12D7) was included as a negative control (NC) for IP experiments.

expressing NMDARs.[2] It is believed that the ectopic expression of NMDARs contributes to triggering the immune response. The trigger of the disease in the rest of female patients as well as in young children and male patients is largely unknown, although in some cases other tumors (such as small-cell lung cancer[2]) have been identified. In a small subset of patients the anti-NMDAR immune response is triggered by herpes simplex encephalitis.[4] Irrespective of the trigger of anti-NMDAR encephalitis, data from previous studies suggested an enhancement of the immune response within the CNS, with potential antigen-driven affinity maturation and clonal expansion of plasma cells.[16] This hypothesis was suggested by three findings, (1) a frequent intrathecal synthesis of NMDAR antibodies even early in the disease course,[1] (2) biopsy and autopsy material from patients showing brain inflammatory infiltrates containing plasma cells,[6,7] and (3) the better correlation of the course of the disease with CSF antibody titers than with serum antibody titers.[5] All four treatment-naive patients with recent

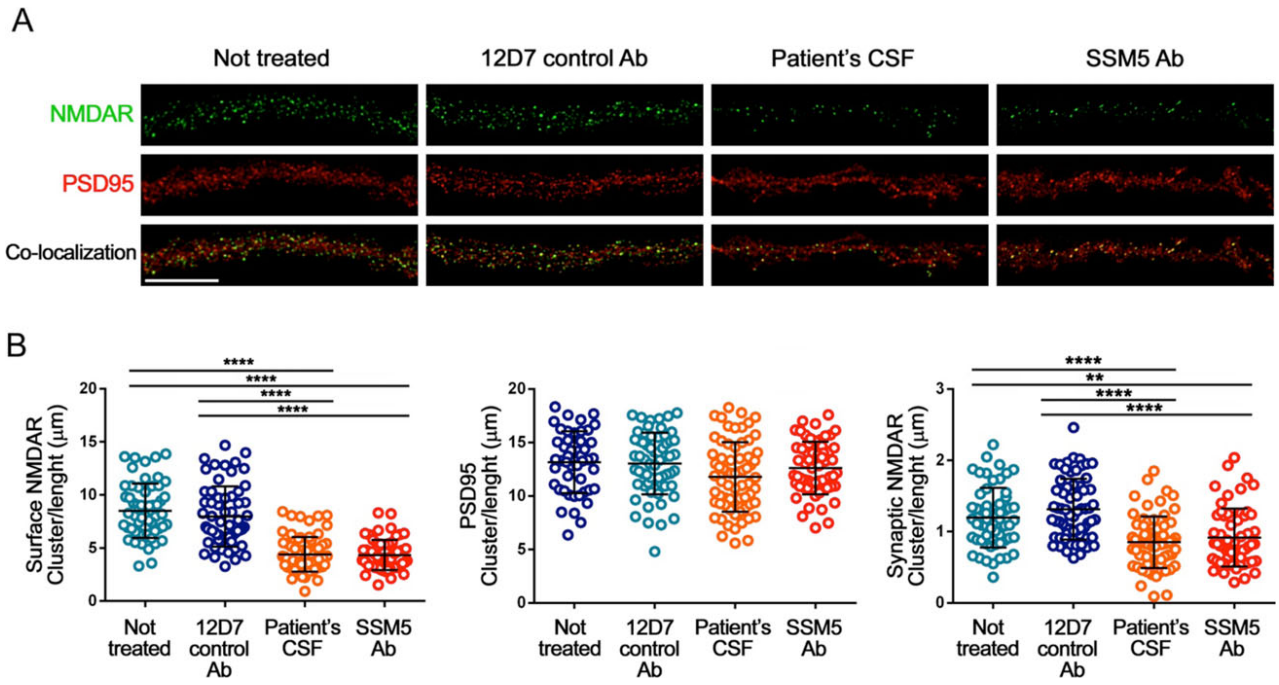

Figure 5. RhuMab SSM5 decreases the density of cell surface and synaptic NMDAR in cultured hippocampal neurons. (A) Representative dendrites from cultures of primary rat hippocampal neurons showing the density of NMDAR clusters (top panels), PSD95, an excitatory postsynaptic protein (middle panels), and synaptic NMDAR (colocalization of NMDAR with PSD95, lower panels) after 24 h treatment with control rhuMab 12D7 (4.5 μg/mL), CSF from a patient with anti-NMDAR encephalitis ("patient's CSF," 1:20 dilution), patient-derived rhuMab SSM5 (4.5 μg/mL) or not treated; scale bar represents 10 mm. The quantification of these effects is shown in (B), demonstrating the density of surface NMDAR (left plot), PSD95 (middle plot) and synaptic NMDAR (right plot). Patient-derived rhuMab SSM5, but not the control rhuMab 12D7 causes a significant reduction of surface and synaptic NMDAR clusters similarly to that of the CSF from a patient with anti-NMDAR encephalitis. No effects occurred on PSD95. All graphs represent mean ± SD, $n = 60$ cells per condition. Significance of treatment effect was assessed by one-way ANOVA ($P < 0.0001$ for NMDAR, synaptic NMDAR) with Bonferroni post hoc correction. $^{**}P < 0.001$, $^{****}P < 0.0001$.

onset anti-NMDAR encephalitis in the current study showed intrathecal B-cell and plasma cell accumulation and intrathecal production of NMDAR-specific IgG. Moreover, using single-cell RT-PCR of FACS-sorted $CD138^+$ CSF plasma cells and recombinant antibody technology,[19,21] we identified expanded clones and were able to obtain seven different rhuMab (SSM1-7) from intrathecal cePc of one of the anti-NMDAR encephalitis patients. Ig sequences showed varying numbers of mutations from published germline sequences, indicating antigen-driven expansion and ongoing somatic hypermutations. RhuMab SSM5 showed reactivity with NMDAR and was used for further studies, whereas the remaining showed no CNS tissue reaction at all.

We confirmed the antigen specificity of rhuMab SSM5 by immunohistochemistry of brain tissue sections and immunoprecipitation from brain membrane fractions.[17] Moreover, this recombinant antibody competed with patients' CSF antibodies for the same restricted epitope on the extracellular amino terminal domain of the GluN1 subunit of the NMDA receptor,[29] decreased the density of cell surface and synaptic NMDAR in cultured neurons, and significantly reduced NMDAR mediated currents in *Xenopus* oocytes expressing GluN1/GluN2B. Importantly, continuous infusion of rhuMab SSM5 into the cerebroventricular system of mice for 14 days resulted in progressive impairment of memory paralleled by accumulation of brain-bound antibody and specific reduction of the density of synaptic NMDAR clusters, as previously reported in a similar model of infusion of patients' CSF.[11,15] Similar to this previously reported model,[15] the impairment of memory was maximal on Day 18 and normalized by Day 25, consistent with a transitory, not structurally damaging effect of rhuMab SSM5. Taken together, using patient-derived rhuMab SSM5 we were able to reproduce most relevant functional aspects previously demonstrated with sera or CSFs from patients with anti-NMDAR encephalitis containing polyclonal antibody mixtures.

By reconstructing functional autoantibodies from CSF cePc in the form of rhuMab, we demonstrate the presence of a CNS-specific antigen-driven humoral immune response in the CSF compartment of patients with anti-NMDAR encephalitis, consistent with studies showing that the sensitivity of NMDA receptor antibody testing is

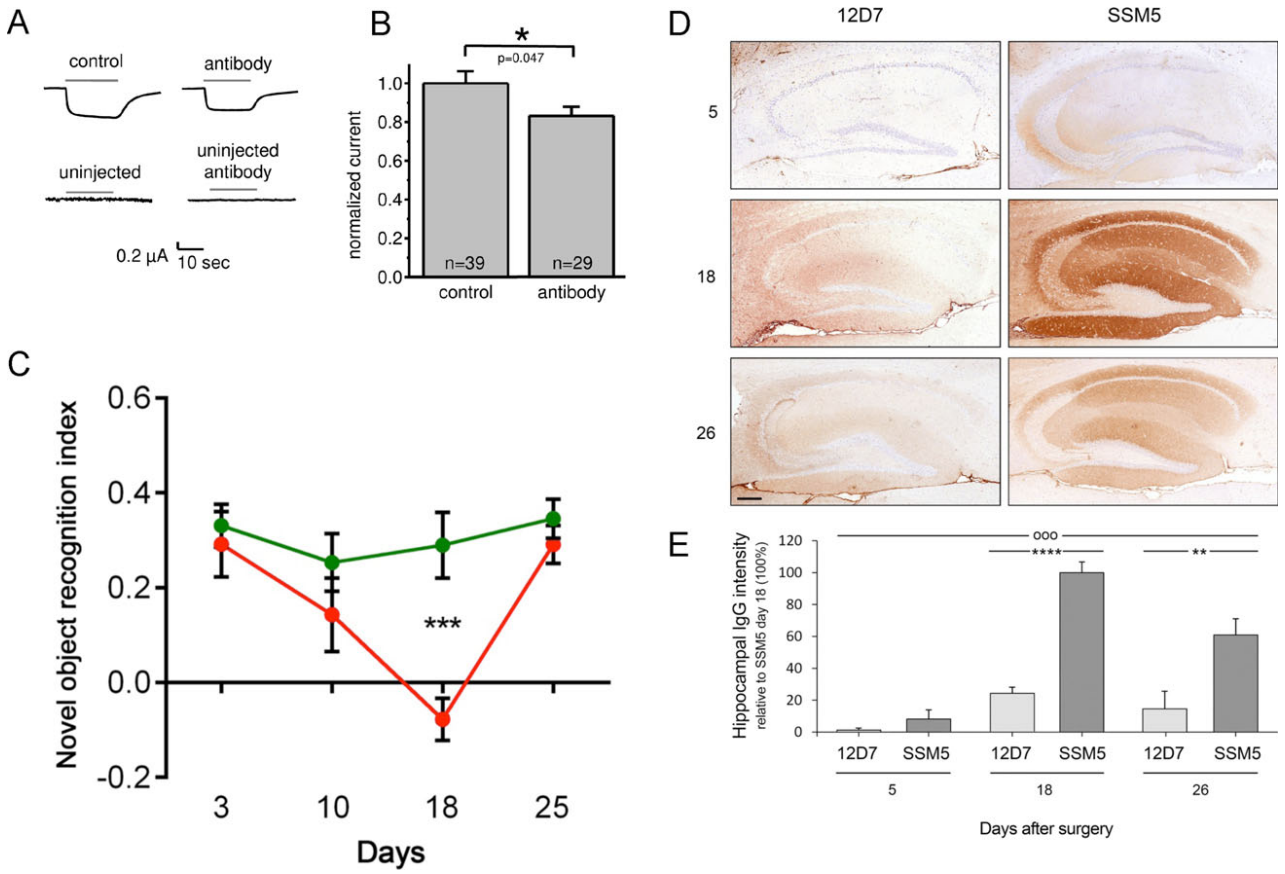

Figure 6. RhuMab SSM5 reduces NMDAR-mediated currents in vitro and induces severe memory deficits in mice. (A, B) RhuMab SSM5 reduces NMDAR-mediated currents in transfected *Xenopus* oocytes. (A) Representative current traces measured in *Xenopus* oocytes expressing GluN1-1a plus GluN2B in response to superfusion with a solution containing 100 μmol/L glutamate plus 10 μmol/L glycine in Ba^{2+} Ringer. All currents were measured at −70 mV. GluN1-1a/GluN2B expressing oocytes were preincubated with 4 μg/mL patient-derived rhuMab in bath medium for 1 h prior to measurement ("antibody"), whereas GluN1-1a/GluN2B expressing control oocytes were not preincubated with antibody ("control"). Control oocytes were treated the same way, either preincubated with patient rhuMab ("uninjected, antibody," $n = 5$) or not preincubated ("uninjected," $n = 7$). Uninjected oocytes revealed no measurable currents. (B) GluN1-1a/GluN2B amplitudes in oocytes either without ("control") or with ("antibody") preincubation with autoantibody were measured and are shown normalized to control currents. Data are given as mean ± SEM. Statistical testing was performed by two-tailed *t*-test with an α error of 0.05. Significant difference is indicated by $*P < 0.05$; *n* indicates number of oocytes measured. (C–E) Cerebroventricular infusion of anti-NMDAR rhuMab SSM5 causes severe reversible memory deficits. (C) Infusion of rhuMab SSM5 into the cerebroventricular system of mice for a total of 14 days causes deficits of memory. Novel object recognition index in mice treated with the patient-derived rhuMab (SSM5, red circles) and the control rhuMab (12D7, green circles) (each at 90 μg/mL in saline solution). A high index indicates better object recognition memory. Note that mice infused with patient-derived rhuMab showed a progressive decrease of memory that was maximal on Day 18. The total time of exploration of both objects was similar in both groups (not shown). Data are presented as mean ± SEM. Number of animals: SSM5: $n = 7$, 12D7: $n = 7$. Significance of treatment effect was assessed by two-way ANOVA with an α error of 0.05 and post hoc testing with Bonferroni adjustment (asterisks). $***P < 0.001$. (D, E) Animals infused with rhuMab SSM5 have a progressive increase of human IgG bound to hippocampus. (D) Immunostaining of human IgG in sagittal brain sections showing the hippocampus of representative animals infused with anti-NMDAR monoclonal antibody (SSM5) (right panels) and control antibody (12D7) (left panels), sacrificed at the indicated experimental days. In animals infused with the SSM5 antibody, a gradual increase of IgG immunostaining until Day 18, followed by decrease of immunostaining is observed. Scale bar represents 200 μm. (E) Quantification of intensity of human IgG immunolabeling in hippocampus of mice infused with SSM5 antibody (dark gray columns) and control CSF (pale gray columns) sacrificed at the indicated time points. Mean intensity of IgG immunostaining in the group with the highest value (animals treated with anti-NMDAR monoclonal antibody (SSM5) and sacrificed at Day 18) was defined as 100%. Data are presented as mean ± SEM. Number of animals: 5 animals per condition and time point. Significance of treatment effect was assessed by two-way ANOVA with an α error of 0.05 (o) and post hoc testing with Bonferroni adjustment (*). $^{ooo}P < 0.001$, $**P < 0.01$, $****P < 0.0001$.

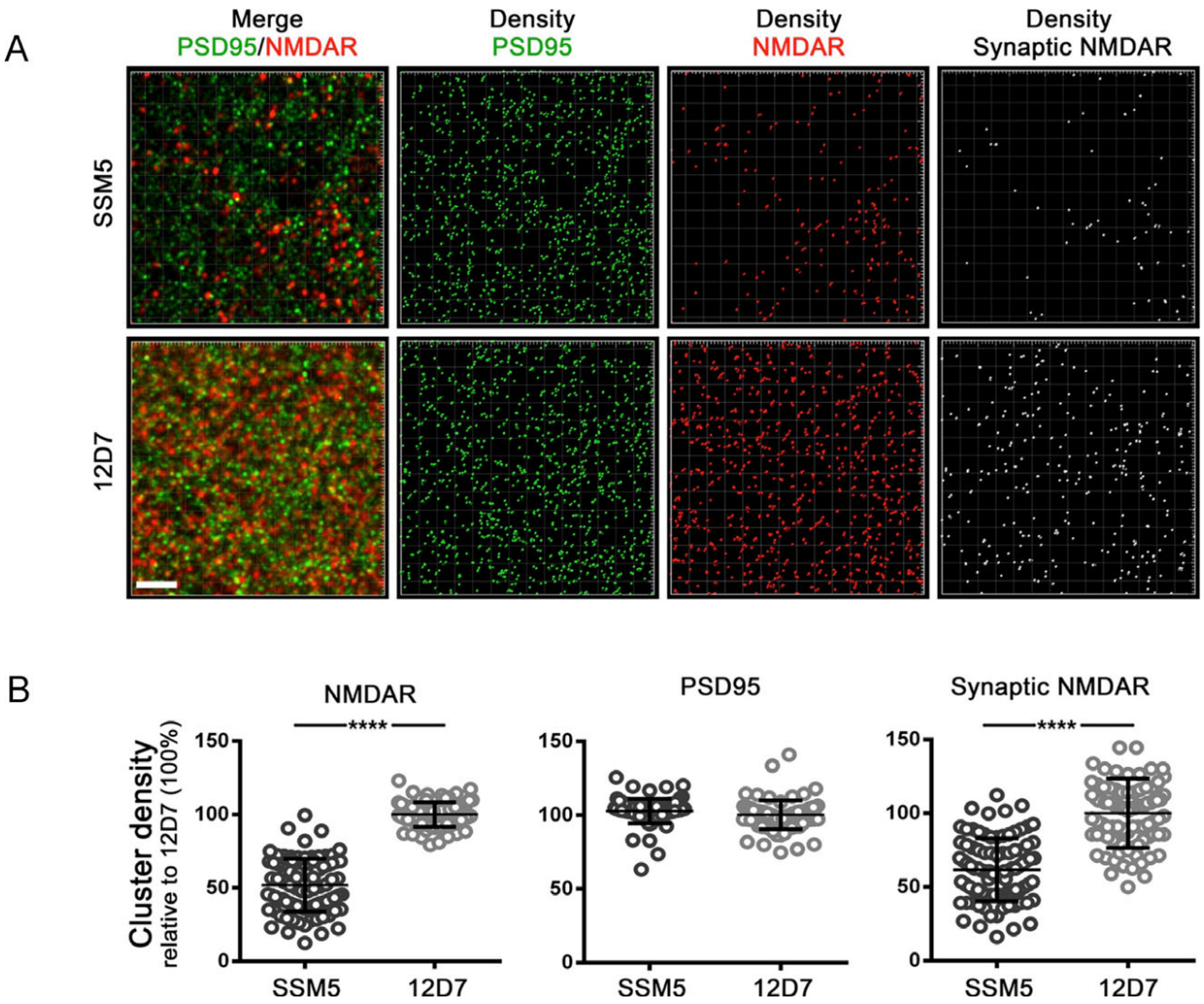

Figure 7. RhuMab SSM5 decreases the density of synaptic NMDAR density in mice hippocampus after intraventricular infusion. (A, B) Anti-NMDAR monoclonal antibody (SSM5) mediates a reduction of total and synaptic NMDAR in mice hippocampus. (A) 3D projection of the density of total clusters of NMDAR, PSD95, and synaptic clusters of NMDAR (defined as NMDAR clusters colocalizing with PSD95) in a hippocampal region from a representative animal of each experimental group. Merged images (merge: PSD95 [green]/NMDAR [red]) were postprocessed and used to calculate the density of clusters (density = spots/μm^3). Scale bar represents 2 μm. (B) Quantification of the density of total NMDAR, total PSD95, and synaptic NMDAR clusters at Day 18 in a pooled analysis of hippocampal areas (CA1, CA2, CA3, and dentate gyrus) in animals treated with anti-NMDAR monoclonal antibody (SSM5; dark gray) and control antibody (12D7; pale gray). Mean density of clusters in control antibody treated animals was defined as 100%. Data are presented as scatterplot *plus* mean ± SD. Number of animals: 5 animals per condition (18 hippocampal areas per animal = 90 hippocampal areas per condition). Significance of treatment effect was assessed by two-tailed *t*-test with an α error of 0.05. ****$P < 0.0001$.

higher in CSF than in serum and CSF antibody levels correlate with the course of the disease.[5] Whether autoreactive B-cell affinity maturation indeed occurs inside the CNS compartment and some of the clonally related B cells migrate to the peripheral system to produce self-reactive antibodies, or CNS-specific B-cell clones transmigrate the BBB and proliferate in the "B-cell friendly" environment of the CNS, remains to be elucidated in further studies.

At this point we cannot answer, to which degree antibody-mediated targeting of the NMDAR also accounts for the variety of other symptoms affecting approximately 75% of patients with anti-NMDAR encephalitis, ranging from mood and psychiatric alterations to seizures and disorders of movements and consciousness.[30,31] It is important to keep in mind that in the human disease the antibodies are synthesized by plasma cells distributed throughout the brain and meninges suggesting a widespread presence of

antibodies (along with inflammatory changes) in the brain parenchyma.[13] In contrast, the passive transfer model used here favors the antibody binding in the hippocampus (due to passive diffusion and close proximity to the ventricular system and CSF) and at a lesser degree in other cortical regions, and lacks inflammatory infiltrates.[11,15] Future studies using other forms of antibody delivery, active immunization, or different mouse strains or additional rodent or non-human primate species may answer whether "host" factors, or additional, so far unidentified intrathecal antibody specificities, contribute to the variety of symptoms observed in anti-NMDAR encephalitis. However, a similar variety of symptoms is observed in models of NMDAR antagonists in which the spectrum of symptoms is dependent of the dose and intensity of effects on the NMDAR.[32]

Taken together, we unambiguously show that intrathecal accumulation of B cells and plasma cells corresponds to the clinical course in patients with anti-NMDAR encephalitis. Moreover, presence of intrathecal cePc with hypermutated antigen receptors indicates an antigen-driven intrathecal immune response in patients with anti-NMDAR encephalitis. Consistently, a single recombinant human GluN1-specific monoclonal antibody, rebuilt from intrathecal cePc by reverse genetics, is sufficient to reproduce NMDAR epitope specificity and key pathogenic features of the human disease in vitro and in vivo.

Having reconstructed pathogenic antineuronal antibody signatures in recombinant form permits further elucidation of disease mechanisms and development of targeted therapies in anti-NMDAR encephalitis and will increase our understanding of the role of NMDAR in synaptic function, cognition and behavior in general.

Acknowledgments

We would like to thank Verena Schütte, Kerstin Gottschalk, and Schumina Säuberlich, Department of Neurology, WWU Münster, Germany, for excellent technical assistance. We are grateful for the complimentary initial screening of rhuMab specificity by Euroimmun, Lübeck, Germany. The expert technical help of Katharina Raba, FACS facility of the HHU Düsseldorf, Germany, and Jason Cline, Department of Neurology, HHU Düsseldorf, Germany is highly appreciated.

Author Contribution

MM, SB, CB, and JS performed FACS sorting, single-cell PCR, sequencing, cloning, expression, and purification and part of IHC characterization of rhuMabs under supervision of NG; FD and SB performed immunoprecipitation (IP) experiments under supervision of NK and NG; JP and FM performed immunohistochemistry with rat brain and immunocompetition assays, and studied the effects of rhuMab on primary cultures of hippocampal neurons and animal behavior under supervision of EMG, RM, and JD. KSG recruited and treated the patients under supervision of NM. KB performed the neuropsychological testing under the supervision of AJ. CCG analyzed flow cytometry data under the supervision of SGM and NM. NSS, GS, SK, NK, and NM performed electrophysiological analysis. KKF performed immunocytochemistry with transfected HEK cells under supervision of FL and KPW. AJB performed histopathological analysis of a former anti-NMDAR encephalitis patient contributed by CEE. CW and CSN performed injection experiments of rhuMabs together with complement in rodent hippocampus for an earlier version of the manuscript. NG, JD, NM, HPH, SGM, and HW designed and supervised the project. NM and NG wrote the first draft of the manuscript. All authors contributed to and approved the final manuscript.

Conflict of Interest

All authors declare no relevant conflicts of interest.

References

1. Dalmau J, Gleichman AJ, Hughes EG, et al. Anti-NMDA-receptor encephalitis: case series and analysis of the effects of antibodies. Lancet Neurol 2008;7:1091–1098.
2. Titulaer MJ, McCracken L, Gabilondo I, et al. Treatment and prognostic factors for long-term outcome in patients with anti-NMDA receptor encephalitis: an observational cohort study. Lancet Neurol 2013;12:157–165.
3. Pruss H, Finke C, Holtje M, et al. N-methyl-D-aspartate receptor antibodies in herpes simplex encephalitis. Ann Neurol 2012;72:902–911.
4. Armangue T, Leypoldt F, Malaga I, et al. Herpes simplex virus encephalitis is a trigger of brain autoimmunity. Ann Neurol 2014;75:317–323.
5. Gresa-Arribas N, Titulaer MJ, Torrents A, et al. Antibody titres at diagnosis and during follow-up of anti-NMDA receptor encephalitis: a retrospective study. Lancet Neurol 2014;13:167–177.
6. Camdessanché J-P, Streichenberger N, Cavillon G, et al. Brain immunohistopathological study in a patient with anti-NMDAR encephalitis. Eur J Neurol 2011;18:929–931.
7. Martinez-Hernandez E, Horvath J, Shiloh-Malawsky Y, et al. Analysis of complement and plasma cells in the brain of patients with anti-NMDAR encephalitis. Neurology 2011;77:589–593.
8. Moscato EH, Peng X, Jain A, et al. Acute mechanisms underlying antibody effects in anti-N-methyl-D-aspartate receptor encephalitis. Ann Neurol 2014;76:108–119.

9. Hughes EG, Peng X, Gleichman AJ, et al. Cellular and synaptic mechanisms of anti-NMDA receptor encephalitis. J Neurosci 2010;30:5866–5875.
10. Mikasova L, De Rossi P, Bouchet D, et al. Disrupted surface cross-talk between NMDA and Ephrin-B2 receptors in anti-NMDA encephalitis. Brain 2012;135 (Pt 5):1606–1621.
11. Planagumà J, Haselmann H, Mannara F, et al. Ephrin-B2 prevents N-methyl-D-aspartate receptor antibody effects on memory and neuroplasticity. Ann Neurol 2016;80:388–400.
12. Vitureira N, Letellier M, Goda Y. Homeostatic synaptic plasticity: from single synapses to neural circuits. Curr Opin Neurobiol 2012;22:516–521.
13. Bien CG, Vincent A, Barnett MH, et al. Immunopathology of autoantibody-associated encephalitides: clues for pathogenesis. Brain 2012;135(Pt 5):1622–1638.
14. Dalmau J, Tüzün E, H-y W, et al. Paraneoplastic anti-N-methyl-D-aspartate receptor encephalitis associated with ovarian teratoma. Ann Neurol 2007;61:25–36.
15. Planagumà J, Leypoldt F, Mannara F, et al. Human N-methyl D-aspartate receptor antibodies alter memory and behaviour in mice. Brain 2015;138(Pt 1):94–109.
16. Dalmau J. NMDA receptor encephalitis and other antibody-mediated disorders of the synapse: The 2016 Cotzias Lecture. Neurology 2016;87:2471–2482.
17. Kreye J, Wenke NK, Chayka M, et al. Human cerebrospinal fluid monoclonal N-methyl-D-aspartate receptor autoantibodies are sufficient for encephalitis pathogenesis. Brain 2016;139(Pt 10):2641–2652.
18. Obermeier B, Mentele R, Malotka J, et al. Matching of oligoclonal immunoglobulin transcriptomes and proteomes of cerebrospinal fluid in multiple sclerosis. Nat Med 2008;14:688–693.
19. von Büdingen H-C, Harrer MD, Kuenzle S, et al. Clonally expanded plasma cells in the cerebrospinal fluid of MS patients produce myelin-specific antibodies. Eur J Immunol 2008;38:2014–2023.
20. Golombeck KS, Bönte K, Mönig C, et al. Evidence of a pathogenic role for CD8(+) T cells in anti-GABAB receptor limbic encephalitis. Neurol Neuroimmunol Neuroinflamm 2016;3:e232.
21. Kuenzle S, von Büdingen H-C, Meier M, et al. Pathogen specificity and autoimmunity are distinct features of antigen-driven immune responses in neuroborreliosis. Infect Immun 2007;75:3842–3847.
22. Tiller T, Meffre E, Yurasov S, et al. Efficient generation of monoclonal antibodies from single human B cells by single cell RT-PCR and expression vector cloning. J Immunol Methods 2008;329(1–2):112–124.
23. Saitou N, Nei M. The neighbor-joining method: a new method for reconstructing phylogenetic trees. Mol Biol Evol 1987;4:406–425.
24. Hillis DM, Bull JJ, White ME, et al. Experimental phylogenetics: generation of a known phylogeny. Science 1992;255:589–592.
25. Raymond C, Tom R, Perret S, et al. A simplified polyethylenimine-mediated transfection process for large-scale and high-throughput applications. Methods 2011;55:44–51.
26. Lai M, Hughes EG, Peng X, et al. AMPA receptor antibodies in limbic encephalitis alter synaptic receptor location. Ann Neurol 2009;65:424–434.
27. Petit-Pedrol M, Armangue T, Peng X, et al. Encephalitis with refractory seizures, status epilepticus, and antibodies to the GABAA receptor: a case series, characterisation of the antigen, and analysis of the effects of antibodies. Lancet Neurol 2014;13:276–86.
28. Seebohm G, Chen J, Strutz N, et al. Molecular determinants of KCNQ1 channel block by a benzodiazepine. Mol Pharmacol 2003;64:70–77.
29. Gleichman AJ, Spruce LA, Dalmau J, et al. Anti-NMDA receptor encephalitis antibody binding is dependent on amino acid identity of a small region within the GluN1 amino terminal domain. J Neurosci 2012;32:11082–11094.
30. Kayser MS, Kohler CG, Dalmau J. Psychiatric manifestations of paraneoplastic disorders. Am J Psychiatry 2010;167:1039–1050.
31. Kayser MS, Dalmau J. Anti-NMDA receptor encephalitis, autoimmunity, and psychosis. Schizophr Res 2016;176:36–40.
32. Masdeu JC, Dalmau J, Berman KF. NMDA Receptor Internalization by Autoantibodies: a Reversible Mechanism Underlying Psychosis? Trends Neurosci 2016;39:300–310.
33. Castillo-Gomez E, Oliveira B, Tapken D, et al. All naturally occurring autoantibodies against the NMDA receptor subunit NR1 have pathogenic potential irrespective of epitope and immunoglobulin class. Mol Psychiatry, advance online publication, 9 August 2016; doi:10.1038/mp.2016.125
34. Levitan IB. It is calmodulin after all! Mediator of the calcium modulation of multiple ion channels. Neuron 1999;22:645–648.

Supporting Information

Additional Supporting Information may be found online in the supporting information tab for this article:

Table S1. Clinical, magnetic resonance imaging, and electroencephalography findings in patients with anti-NMDAR encephalitis.

Table S2. Routine CSF and PB analysis and antibody titers of patients with anti-NMDAR encephalitis.

Table S3. Neuropsychological domains with respective tests applied during neuropsychological testing of patients with anti-NMDAR encephalitis.

Table S4. Results of the different neuropsychological tests in patients with anti-NMDAR encephalitis at initial assessment 1–16 weeks after admission.

Table S5. Results of the different neuropsychological tests in patients with anti-NMDAR encephalitis at follow-up assessment 8–48 months after initial assessment.

Table S6. Baseline characterization of the peripheral and intrathecal autoimmune response in anti-NMDAR encephalitis using multi-parameter flow cytometry before immunotherapy.

Table S7. Follow-up characterization of the peripheral and intrathecal autoimmune response in anti-NMDAR encephalitis using multiparameter flow cytometry at 5–7 months after initiation of immunotherapy.

Figure S1. Cerebral MRI in patients with anti-NMDAR encephalitis.

Supplementary Materials

Supplementary Methods

Patients and rhuMab synthesis

Magnetic Resonance Imaging (MRI)

Standard cerebral MRI was performed on 1.5 Tesla scanners. Diffusion weighted imaging (DWI) with calculation of apparent diffusion coefficient (ADC)-map, axial and coronal T1-SE before and after application of gadolinium, axial and coronal FLAIR-, T2-FFE-, and T2-TSE sequences were performed.

Neuropsychological assessment

A comprehensive neuropsychological test battery conducted by an experienced, certified clinical neuropsychologist assessed all patients. The test battery covers the full range of neuropsychological domains as presented in supplementary table 3 (**Suppl. Tab. 3**). The test scores represent the individual percentile rank in comparison to neurologically healthy adults matched for age and level of education.

Multi-parameter flow cytometry of PB and CSF

Multi-parameter flow cytometry of PB and CSF was performed as previously reported [1, 2]. PB and CSF of healthy controls were obtained from 25 individuals with suspected presence of a neurologic disorder that retrospectively turned out to suffer from somatization disorders. In addition to the clinical classification, patients included in the control group also fulfilled the following laboratory criteria defining a non-inflammatory CSF: <5 cells/µL, <500 mg protein/mL, <2 mM lactate, no disruption of the PB-CSF-barrier (defined by the CSF/serum albumin ratio), no intrathecal immunoglobulin IgG, IgA, or IgM synthesis (Reiber criteria) [3], and no CSF-specific oligoclonal bands on isoelectric focusing. Potential disease-related changes in the cellular composition of both PB and CSF compartment were analyzed using multi-parameter flow cytometry. CSF samples were obtained by lumbar puncture, collected in

polypropylene tubes, and were processed within 30 minutes. Cells were obtained from ethylene-diamine-tetra-acetic acid (EDTA) blood by erythrocyte lysis using VersaLyse buffer (Beckman Coulter, Germany) following the manufacturer's instructions. Cells were obtained from CSF by centrifugation (15 minutes, 290 *g*, 4 °C) and incubation in VersaLyse buffer. Cells were stained using the following fluorochrome-conjugated antibodies: CD14-FITC, CD138-PE, HLA-DR-ECD, CD3-PC5.5, CD56-PC7, CD4-APC, CD19-APCAlexafluor700, CD16-APCAlexafluor750, CD8-PacificBlue, and CD45-KromeOrange (all Beckman Coulter, Germany) and analyzed by two blinded authors (MH, CCG) using the Navios (Beckman Coulter, Germany). The gating strategy to determine leukocyte subsets in PB and CSF cells was performed as described [1].

Anti-neuronal antibody testing

Serum and CSF were tested for the presence of IgG antibodies against intracellular neuronal antigens (ANNA1 (Hu), ANNA2 (Ri), ANNA3, PCA1 (Yo), PCA2, Tr/DNER, Ma1/2, CV2/CRMP5, Amphyphysin, SOX1, GAD65) and neuronal surface membrane antigens (NMDA receptor, AMPA receptor, $GABA_A$ receptor, $GABA_B$ receptor, glycine receptor, CASPR2, LGI1 and VGKC) using established assays [4].

From serum and cerebrospinal fluid antibody titers in cell-based assays, the NMDAR-specific IgG index (AI) was calculated using the following formula [3, 5]:

$$AI = \frac{Q\ NMDA - R}{Q\ IgG} = \frac{(\text{IgNMDA} - \text{R [CSF]}/\text{IgNMDA} - \text{R [serum]})}{(\text{Ig total [CSF]}/\text{Ig total [serum]})}$$

where NMDAR indicates the specific NMDAR IgG titer. In case the specific NMDAR IgG titer was 0 in serum, it was set to 1 to enable AI calculation. Q_{Ig} was replaced by Q_{lim} if $Q_{Ig} > Q_{lim}$, as suggested [3]. Q_{lim} represents the upper limit of the Q_{Ig} under the assumption that the IgG fraction in the CSF originates only from blood. Q_{lim} can be calculated for an individual patient from the CSF/serum quotient of albumin (Q_{Alb}) [3]. AI values ≥ 4 were considered positive [3].

Histopathological analysis

For histopathological analysis, sections from cerebral biopsy specimen of a former patient treated at the Department of Epileptology, University of Bonn, Germany, with later on established anti-NMDAR encephalitis and a newly occurring cerebral lesion on MRI were incubated with antibodies against CD138 antigen using standard methods, counterstained with hematoxylin.

Characterization of rhuMab specificity

Immunoprecipitation (IP)

Homogenization of the frozen brain tissue was performed using buffer containing 320 mM sucrose, 20 mM Tris-HCl pH 7.4, 1 mM IAA (2-Iodoacetamide), 1 mM EDTA, 1 mM PMSF (phenylmethanesulfonylfluoride), complete Roche proteinase inhibitor cocktail tablets (without EDTA) and a glass pestle. Cell debris was removed by a brief centrifugation at 1000g for 10 min at 4°C before total membrane fractions were prepared by ultracentrifugation at 275000g for 20 min at 4°C. Protein concentrations were determined by BC assay kit (Uptima).

Solubilization of membrane proteins was carried out at 4°C for 30 min using 1% dodecanoylsucrose (DDS) and 150 mM NaCl (for NMDAR fraction: 1 % DDS, 1 % deoxycholate and 200 mM NaCl) in 20 mM Tris-HCl pH 7.4, 1 mM IAA, 1 mM EDTA, 1 mM PMSF, complete Roche proteinase inhibitor cocktail tablets without EDTA. Non-solubilized matter was pelleted at 125000g for 15 min at 4°C and the supernatant was prepared for the immunoprecipitations (IPs) by pre-clearing for 2 hr at 4°C with non-coupled Dynabeads (Invitrogen). IP were performed using rhuMab (5 ug, covalently coupled to Dynabeads via DMP) overnight at 4°C under constant agitation, washed 4x 10 min before elution with 1x lithium dodecyl sulfate (LDS) sample buffer.

Western blot

The LDS (lithium dodecyl sulfate) eluted IP samples were supplemented with 100 mM DTT and reduced at 37°C for 15 min. Samples were run on 4-20% reducing SDS-PAGE gels, blotted to PVDF membrane and blocked with 5% BSA. Primary detection antibody (rabbit anti-NR1, Millipore) was incubated overnight at 4°C followed by subsequent PBS-T washes for 1 hr. Bound primary antibody was visualized with goat-anti-rabbit IgG HRP (sc-2004, Santa Cruz) secondary antibody and ECL substrate (GE Healthcare) as recommended by the manufacturers.

Immunohistochemistry with rat brain

For immunohistochemistry assays, adult female Wistar rats were sacrificed without perfusion. Brains were removed, sagittally sectioned in half, fixed by immersion in 4% paraformaldehyde for 1 hour at 4°C, cryopreserved in 40% sucrose for 24 hours at 4°C, embedded in freezing compound media, and snap frozen in isopentane chilled with liquid nitrogen. Seven-micrometer-thick tissue sections of rat brain were sequentially incubated with 0.3% H_2O_2 for 15 minutes, 5% goat serum for 1 hour and patient derived rhuMab (SSM5) or control rhuMab (12D7) (90 µg/ml) at 4°C overnight. After using a biotinylated secondary antibody against human IgG (diluted 1:2000; BA-3000, Vector laboratories) for 1 hour at room temperature (RT), the reactivity was developed with the avidin-biotin-peroxidase method. Results were photographed with an AxioCam MRc colour camera adapted to a confocal microscope (Zeiss LSM710) and analyzed with Zen software (Zen 2012 blue edition 1.1.1.0, Zeiss).

Immunocompetition assay

To determine whether the patient derived rhuMab was directed against epitopes recognized by serum antibodies from patients with anti-NMDAR encephalitis an immunocompetition assay was performed. In brief, sections of rat brain were pre-incubated with serum of a patient with anti-NMDAR encephalitis or a healthy blood donor (diluted 1:2) overnight at 4ºC, washed in PBS, incubated with the biotinylated patient derived rhuMab (SSM5) or a biotinylated control

rhuMab (12D7) (diluted 1:20) for 1 hour at RT. The reactivity was developed with the avidin-biotin-peroxidase method. The patient derived rhuMAb was considered to compete for the epitopes recognized by serum of a patient with anti-NMDAR encephalitis, if pre-incubation of the tissue with the patients' serum abrogated the reactivity of the biotinylated patient derived rhuMAb monoclonal antibody. Pictures were taken under the microscope as described above [6].

Immunocytochemistry with transfected HEK cells

HEK293 cells were transfected with GluN1/N2B in equimolar ratios, or the indicated GluN1 mutants (see below). Cells were grown for 24 hours after transfection before assessment; all cells were routinely grown in the presence of ketamine (500 μM) to prevent cell death after transfection. Transfected cells were then fixed with 4% paraformaldehyde for 10 minutes at 4°C, permeabilized with 0.3% Triton X-100 for 5 minutes at RT, blocked with 1% BSA in PBS for 90 minutes and then incubated with patient's CSF diluted 1:16 or recombinant antibodies (final concentration 4.3 μg/ml) in 1% BSA in PBS and a mouse monoclonal antibody against a non-competing GluN1 epitope located in the extracellular loop at amino acid 660-811 (dilution 1:20000; MAB363, Millipore) overnight at 4°C, followed by the corresponding fluorescent secondary antibodies (Alexa Fluor 488 goat anti-human IgG, A11013, diluted 1:1000; and Alexa Fluor 594 goat anti-mouse IgG, A11032, diluted 1:1000, both from Invitrogen) for 1 hour at RT. Images were acquired with a Zeiss Axioscope with a 62x Plan APO objective. Results were photographed using Zeiss Zen software. The GluN1 mutants have been previously described [7]. In brief, G369I and G369S are single point mutations where glycine 369 was replaced by an isoleucine or serine, respectively. HEK cells transfected with these mutants were used for immunocytochemistry following the same technique and serum dilutions indicated above.

Functional analysis of anti-NMDAR specific rhuMab SSM5 *in vitro* and *in vivo*

Two-electrode voltage-clamp analysis of transfected Xenopus laevis oocytes

Synthesis of cRNA

Rat GluN1-1a/pSGEM and GluN2B/pSGEM cDNAs were used as templates for synthesis of cRNA. cDNAs were linearized with an appropriate restriction enzyme. cRNA was synthesized from 1 µg linearized DNA using an *in vitro* transcription kit (mMessage mMachine T7 kit – Ambion, Life Technologies, Darmstadt, Germany). Concentrations of cRNA were examined by photospectrometry (NanoDrop ND-100) and the quality of the transcript was verified by agarose gel electrophoresis.

Heterologous expression in Xenopus laevis oocytes

cRNA (0.8 ng of each cRNA) was injected into stage V-VI *Xenopus* oocytes, provided by Ecocyte Bioscience (Castrop-Rauxel, Germany). All measurements were performed 5 days after injection of cRNA. Oocytes were incubated at 17-18°C.

Electrophysiological recordings

The two-electrode voltage-clamp technique was used to record whole cell currents in *Xenopus* oocytes. Data were acquired with Gepulse software and data analyses were done with Ana software (http://users.ge.ibf.cnr.it/pusch/programs-mik.htm). For voltage clamp experiments, agonist solutions were prepared in Ba^{2+}- buffer (mM: NaCl 90, $BaCl_2$ 1.5, KCl 2.0, and HEPES–NaOH 10, pH 7.2 with NaOH). Current and voltage electrodes were filled with 3 M KCl and had resistances of 0.5–1.2 MΩ. The oocytes were held at −70 mV and agonists (100 µM glutamate and 10 µM glycine; Sigma-Aldrich, Schnelldorf, Germany) were superfused for 20 s at a flow rate of 10–14 ml min^{-1}. NR1-1a/NR2B expressing oocytes were pre-incubated with 4 µg/ml rhuMaB in bath medium for 1 hour prior measurement. The experiments were repeated with three batches of oocytes; in all repetitions qualitatively similar data were obtained.

Effects of rhuMab on primary cultures of hippocampal neurons

To determine the effects of patient derived rhuMab (SSM5) on cultured neurons, 50 µl of CSF from a patient with anti-NMDAR encephalitis, the patient derived rhuMab (SSM5; 90 µg/ml), or the isotype control rhuMab (12D7; 90 µg/ml) were added to cultures of dissociated rat hippocampal neurons seeded in Corning® 35 mm x 10mm dishes (Sigma-Aldrich, St Louis, MO) containing 1ml of Neurobasal medium + B-27® Supplement (Thermo-Fisher, Waltham, MA). After 24 h, neurons were washed with phosphate buffered saline (PBS), and incubated with CSF containing high titer NMDAR antibodies (used here as reagent, diluted 1:20) for 1h at 4 Cº. Cells were then washed, fixed with 4% paraformaldehyde, permeabilized with 0.3% Triton X-100, blocked for 60 minutes with 1% bovine serum albumin (BSA), and incubated with a PSD95 antibody (1:200, PA1-4667, Thermo-Fisher) for 1 hour at room temperature. Neurons were then washed and incubated for 1 hour at room temperature with the secondary antibodies Alexa Fluor 488 goat anti-human IgG (A-11013, Molecular Probes) and Alexa Fluor 594 goat anti-rabbit IgG (A-11037, Molecular Probes) (all diluted 1:1000). Slides were then mounted with ProlonGold with 4′,6-Diamidino-2-phenylindole dihydrochloride (DAPI, P36935, Molecular Probes) and results scanned at 1024x1024 lateral resolution and Nyquist optimized z-sampling frequency with a confocal microscope (Zeiss LSM710) with EC-Plan NEOFLUAR CS 100x/1.3, oil objective. For cluster analysis the images were deconvolved with AutoQuantX3 software (Bitplane AG, Zurich, Switzerland) followed by automatic segmentation using the spot detection algorithm from Imaris suite 7.6.4 (Bitplane). The density of clusters was expressed as number of spots per µm length of dendrite. For colocalization analysis of clusters to determinate the synaptic NMDAR a spot co-localization algorithm between NMDAR and PSD95 implemented in Imaris suite 7.6.4 was applied.

Effects of rhuMab on animal behaviour

Animals

Fourteen male C57BL6/J mice (Charles River), 8–10 weeks old (25–30 g) were housed in cages of five until 1 week before surgery when they were housed individually. The room was maintained at a controlled temperature (21 ± 1°C) and humidity (55 ± 10%) with illumination at 12-h cycles; food and water were available ad libitum. All experiments were performed during the light phase, and animals were habituated to the experimental room for 1 week before starting the tests. Animal procedures were conducted in accordance with standard ethical guidelines (European Communities Directive 86/609/EU) and approved by the local ethical committees.

Surgery

Surgery was done as we previously reported [8]. Briefly, animals were deeply anaesthetized by intraperitoneal injection of a mixture of ketamine (75 mg/kg) and medetomidine (1 mg/kg). Mice were then placed in a stereotaxic frame, and a bilateral catheter (PlasticsOne, model 3280PD-2.0/SP) was inserted into the ventricles (0.2 mm anterior and 1.00 mm lateral from bregma, depth 2.2 mm) and secured with dental cement. Two osmotic pumps (model 1002, Alzet; volume 100 µl, flow rate 0.25 µl/h, duration 14 days) were then connected to the catheters and subcutaneously implanted on the back of the mice. The effects of the anesthesia were partially reverted by the s.c. injection of Atipamezol (2.5 mg/kg). Appropriate ventricular placement of the catheters was assessed in randomly selected mice injecting methylene blue through the catheters.

Cerebroventricular infusion of CSF or monoclonal antibodies was performed loading each of the osmotic pumps with 100 µl of undiluted patient's CSF or the patient derived rhuMAb (SSM5) or isotype control rhuMab (12D7) (90 µg/ml in saline solution). The pumps were then connected to a 0.28mm IM (internal diameter) polyethylene tube (C314CT, PlasticsOne) and left overnight in sterile PBS at 37°C.

Novel object recognition test

This test was performed in an open field arena (45 x 45 x 40 cm, Panlab). One day before surgery, mice were habituated for 30 minutes in the open field without objects. On days 3, 10, 18 and 25, mice were put back into the open field arena for 9 minutes; two identical objects were presented, and the time the mice spent exploring each object was recorded. After a retention phase of 3 hours, the mice were placed for another 9 minutes into the open field where one of the familiar objects was replaced with a novel object and the total time spent exploring each object (novel and familiar) was registered. During the test phase of the open field paradigm, the objects were positioned in the opposite corners of those used in the training phase and the novel object was presented in 50% of trials on the right and in 50% of trials on the left side. Object exploration was defined as the orientation of the nose to the object at a distance of less than 2 cm. A discrimination index was calculated as the difference of the time spent exploring the novel and the time spent exploring the familiar object divided by the total time exploring both objects. A higher discrimination index is considered to reflect greater memory retention for the familiar object [8].

Immunohistochemistry, confocal microscopy

For determination of rhuMab bound to brain tissue using immunoperoxidase staining, 7 µm-thick tissue sections were sequentially incubated with 0.25% H_2O_2 for 10 minutes at 4°C, 5% goat serum for 15 minutes at room temperature (RT), biotinylated goat anti-human IgG (1:2000, Vector labs, Burlingame, CA, USA) overnight at 4°C, and the reactivity developed using avidin-biotin-peroxidase and diaminobenzidine. Sections were mildly counterstained with hematoxylin, and results photographed under a Leica DMD108 microscope (Mannheim, Germany). Images were prepared creating a mask for diaminobenzidine color, converting the mask to grey scale intensities, and inverting the pixels using Adobe Photoshop CS6 package. Hippocampal and cerebellar regions were manually outlined; intensity and area were quantified using the public domain Fiji ImageJ software (http://fiji.sc/Fiji). Values were

normalized to the group with the highest mean (defined as 100%, animals infused with anti-NMDAR monoclonal antibody (SSM5) sacrificed at day 18).

To quantify the effects of rhuMab on total cell-surface and synaptic NMDAR clusters, PSD95, non-permeabilized 5 µm brain sections were blocked with 5% goat serum, incubated with human CSF antibodies (1:20, used here as primary NMDAR antibody) for 2 hours at room temperature (RT), washed with phosphate buffered saline (PBS), permeabilized with Triton X-100 0.3% for 10 minutes at RT, and serially incubated with rabbit polyclonal anti-PSD95 (1:250, ab18258 Abcam) overnight at 4ºC, and the corresponding secondary antibodies, anti-human IgG Alexa Fluor 594 and goat anti-Rabbit Alexa Fluor 488 (A-11014, A-11008, Molecular Probes) all diluted 1:1000, for 1 hour at RT. Slides were mounted and results scanned with a confocal microscope (Zeiss LSM710). Standardized z-stacks including 50 optical images were acquired from 18 hippocampal regions per animal including CA1, CA2, CA3 and dentate gyrus. For cluster density analysis a spot detection algorithm from Imaris suite 7.6.4 (Bitplane) was used. Density of clusters in each hippocampal region was expressed as spots/mm^3. Synaptic localization was defined as co-localization of NMDAR with post-synaptic PSD95, and synaptic cluster density was expressed as colocalized spots/mm^3. For animals treated with anti-NMDAR monoclonal antibody (SSM5) or control antibody (12D7), the mean densities of all 18 hippocampal regions were calculated for total and synaptic NMDAR, and normalized to the mean density of the 18 hippocampal regions in animals treated with control antibody (12D7) (= 100%).

Pt.	Age at onset, Sex	Core clinical features	Interval between disease onset and diagnosis T1 (weeks) & T1 and follow-up T2 (months)	Modified Rankin Scale	Tumor	MRI	EEG
1	23, f	Psychosis, dysphasia, memory dysfunction, dyskinesia, autonomic dysregulation	3 26	T1: 4 T2: 0	None	T1: Left frontal cortico-subcortical T2-/FLAIR-hyperintense lesion, otherwise normal T2: Regression of left frontal cortico-subcortical T2-/FLAIR-hyperintense lesion	T1: Continuous bilateral frontal and intermittent general slowing in the theta-delta band, no epileptic discharges T2: n.d.
2	28, f	Psychosis, memory dysfunction, dyskinesia	4 13	T1: 3 T2: 0	None	T1: Normal T2: Normal	T1: Continuous bilateral frontal slowing in the delta band, no epileptic discharges T2: Normal
3	21, f	Psychosis, memory dysfunction, dyskinesia, dysphasia	2 14	T1: 3 T2: 0	None	T1: Left temporal cortical T2-/FLAIR-hyperintense lesion and swelling, otherwise normal T2: Almost complete regression of left temporal cortical T2-/FLAIR-hyperintense lesion	T1: Continuous bilateral temporal and intermittent general slowing in the theta-delta band, left temporal sharp-waves and sharp-slow-waves T2: Normal
4	51, f	Psychosis, memory dysfunction, dyskinesia	4 10	T1: 4 T2: 1	SCLC	T1: Bilateral cerebellar post-ischemic lesions, otherwise normal T2: Bilateral cerebellar post-ischemic lesions, otherwise normal	T1: Continuous bilateral temporal slowing in the theta-delta band, no epileptic discharges T2: Normal

Supplementary Table 1: Clinical, magnetic resonance imaging, and electroencephalography findings in patients with anti-NMDAR encephalitis. T1 indicates initial findings upon admission; T2 indicated follow-up findings after 5 to 7 months of immunotherapy.

Pt.	WBC (cells/µl)	Protein (mg/L)	Albumin ratio (x 10^{-3})	Intrathecal IgG synthesis (%)	Isoelectric focusing	NMDAR IgG ab titers in serum/csf	NMDA-R-specific IgG ab index
1	T1: 22 T2: 3	T1: 393 T2: 385	T1: 4.5 T2: 4.3	T1: 17 T2: 0	T1: Type II T2: Type II	T1:1:320/1:3.2 T2: neg/1:10	T1:2.7 T2:3571.4
2	T1: 4 T2: 0	T1: 498 T2: 417	T1: 7.3 T2: 5.6	T1: 0 T2: 0	T1: Type I T2: Type I	T1:1:100/1:100 T2: 1:10/1:1	T1: 277.8 T2: 35.7
3	T1: 7 T2: 1	T1: 177 T2: 304	T1: 2.7 T2: 3.5	T1: 0 T2: 0	T1: Type I T2: Type I	T1: neg./1:32 T2: neg./n.d.	T1: 18.4 T2: n.d.
4	T1: 0 T2:1	T1: 237 T2:733	T1: 4.4 T2: 7.7	T1: 11 T2:0	T1: Type II T2: Type I	T1: 1:320/1:320 T2:1:10/1:32	T1: 294.1 T2:864.9

Supplementary Table 2: Routine CSF and PB analysis and antibody titers of patients with anti-NMDAR encephalitis. T1 indicates initial findings upon admission; T2 indicated follow-up findings after 5 to 7 months of immunotherapy.

Neuropsychological Domain	Test	Test Parameter
Attention:		
Short Term Memory	Auditory Verbal Learning Test (AVLT), German version [9]	AVLT, trial 1, verbal memory span
Working Memory	Wechsler Memory Scale Revised (WMS), German version [10]	WMS-R forward, digit span forward
	Wechsler Memory Scale Revised (WMS), German version [10]	WMS-R backward, digit span backward
Cognitive Speed	Trail Marking Test (TMT) [11]	TMT, trial A
Memory:		
Verbal Learning	Auditory Verbal Learning Test (AVLT), German version [9]	AVLT, trial 5
Verbal Learning (cummulated)	Auditory Verbal Learning Test (AVLT), German version [9]	AVLT, trial 1-5
Short Term Verbal Recall	Auditory Verbal Learning Test (AVLT), German version [9]	AVLT, trial 6, recall after interference
Short Term Verbal Loss	Auditory Verbal Learning Test (AVLT), German version [9]	AVLT, trial 5-6, loss after interference
Long Term Verbal Recall	Auditory Verbal Learning Test (AVLT), German version [9]	AVLT, trial 7, recall after 30 minutes
Long Term Verbal Loss	Auditory Verbal Learning Test (AVLT), German version [9]	AVLT, trial 5-7, loss after 30 minutes
Verbal Recognition	Auditory Verbal Learning Test (AVLT), German version [9]	AVLT, trial 8, recognition
Short Term Figural Recall	Rey Complex Figure Test (RCFT) [12]	RCFT, 3 minutes recall
Executive Functions:		
Visuospatial ability	Rey Complex Figure Test (RCFT) [12]	RCFT copy trial, draw a copy of a complex figure
Set shifting	Trail Marking Test (TMT) [11]	TMT trial B
Verbal Fluency	Regensburger Wortflüssigkeitstest (RWT) [13]	1 minute phonematic verbal fluency letters

Supplementary Table 3: Neuropsychological domains with respective tests applied during neuropsychological testing of patients with anti-NMDAR encephalitis.

		Attention				**Memory**							**Executive Functions**			
Patients	**Time Flow Cytometry – Neuropsychology (weeks)**	Short Term Memory(digit span forward)	Short Term Memory (verbal span)	Working Memory	Cognitive Speed	Verbal Learning	Verbal Learning(cummulated)	Short Term Verbal Recall	Short Term Verbal Loss	Long Term Verbal Recall	Long Term Verbal Loss	Verbal Recognition	Visuospatial Ability	Set Shifting	Verbal Fluency	**Total Percentile Rank Sum**
1	6	71	40	14	9	30	30	5	5	5	5	50	0	9	9	202
2	2	68	60	42	20	45	50	25	10	35	25	50	17	9	16	388
3	1	n. d.	10	2	9	4	4	5	60	10	65	20	1	9	9	199
4	16	n. d.	15	71	70	4	4	4	4	4	4	4	17	70	n. d.	201

Supplementary Table 4: Results of the different neuropsychological tests in patients with anti-NMDAR encephalitis at initial assessment 1 to 16 weeks after admission. All results are given as percentile ranks (PR): far below average: < PR 10, below average: PR 10 – 15.9, average: PR 16-84, above average: PR 85-100. Total percentile rank sums were calculated from all parameters available from all patients at initial and follow-up assessment. Some tests were not determined (n. d.) in individual patients.

		Attention				**Memory**							**Executive Functions**			
Patients	**Time 1st to 2nd Neuropsychological Assessment (months)**	Short Term Memory(digit span forward)	Short Term Memory (verbal span)	Working Memory	Cognitive Speed	Verbal Learning	Verbal Learning (cummulated)	Short Term Verbal Recall	Short Term Verbal Loss	Long Term Verbal Recall	Long Term Verbal Loss	Verbal Recognition	Visuospatial Ability	Set Shifting	Verbal Fluency	**Total Percentile Rank Sum**
1	12	48	40	3	n. d.	45	70	15	5	50	40	20	17	n. d.	n. d.	305
2	48	87	80	92	10	70	90	50	25	90	65	50	17	9	25	648
3	12	84	80	29	70	45	55	50	45	70	65	50	n. d.	10	25	569
4	8	34	30	52	70	4	5	4	20	4	10	5	17	70	16	291

Supplementary Table 5: Results of the different neuropsychological tests in patients with anti-NMDAR encephalitis at follow-up assessment 8 to 48 months after initial assessment. All results are given as percentile ranks (PR): far below average: < PR 10, below average: PR 10 – 15.9, average: PR 16-84, above average: PR 85-100. Total percentile rank sums were calculated from all parameters available from all patients at initial and follow-up assessment. Some tests were not determined (n. d.) in individual patients.

	Peripheral Blood (PB)						**Cerebrospinal Fluid (CSF)**					
	Anti-NMDA-R Encephalitis		**Control**				**Anti-NMDA-R Encephalitis**		**Control**			
Cell type	**Median**	**Interquartile range**	**Median**	**Interquartile range**	**P-value**	**Statistical Test**	**Median**	**Interquartile range**	**Median**	**Interquartile range**	**P-value**	**Statistical Test**
$CD19^+$ B cells (% lymphocytes)	13.7	20.4	12.6	5.5	0.591	WRST	**5.7**	**4.6**	**0.8**	**0.6**	**0.002**	**WRST**
$CD19^+$ B cells (cells/ml)	81098	79075	173176	200569	0.054	**WRST**	**194**	**487**	**5**	**9**	**0.002**	**WRST**
$CD138^+$ $CD19^+$ plasma cells (% lymphocytes)	0.4	0.8	0.05	0.08	0.092	WRST	**1.5**	**5.0**	**0**	**0**	**0.006**	**WRST**
$CD138^+$ $CD19^+$ plasma cells (cells/ml)	1985	3942	646	1537	0.393	WRST	**40**	**1177**	**0**	**0**	**0.009**	**WRST**
$CD4^+$ T cells (% T cells)	77.5	22.3	68.2	14.0	0.200	WRST	79.0	7.6	74.0	8.2	0.251	WRST
$CD4^+$ T cells (cells/ml)	517224	461598	666111	472726	0.121	WRST	1798	13703	530	715	0.054	WRST
$HLADR^+$ $CD4^+$ T cells (% of $CD4^+$ T cells)	**7.3**	**4.9**	**4.7**	**1.8**	**0.046**	**WRST**	7.0	2.8	5.4	3.8	0.137	WRST
$HLADR^+$ $CD4^+$ T cells (cells/ml)	21772	13619	32249	13686	0.166	WRST	**125**	**927**	**24**	**51**	**0.040**	**WRST**
$CD8^+$ T cells (% of T cells)	**17.3**	**6.6**	**26.6**	**7.0**	**0.020**	**WRST**	15.2	6.5	22.3	7.8	0.096	WRST
$CD8^+$ T cells (cells/ml)	**80684**	**1068289**	**279817**	**228059**	**0.005**	**WRST**	296	1414	126	230	0.121	WRST
$HLADR^+$ $CD8^+$ T cells (% of $CD8^+$ T cells)	**12.2**	**1.8**	**7.4**	**4.1**	**0.037**	**WRST**	35.3	9.9	26.8	10.6	0.147	WRST
$HLADR^+$ $CD8^+$ T cells (cells/ml)	**8774**	**9951**	**16821**	**13135**	**0.025**	**WRST**	**87**	**439**	**33**	**57**	**0.040**	**WRST**

Supplementary Table 6: Baseline characterization of the peripheral and intrathecal autoimmune response in anti-NMDAR encephalitis using multi-parameter flow cytometry before immunotherapy. Absolute numbers (in cells/ml) and relative fractions (in %) of lymphocyte subsets in peripheral blood (PB) and cerebrospinal fluid (CSF) in four patients with anti-NMDA-R encephalitis and controls are given as median and interquartile range. Confirmatory statistics was performed using the Wilcoxon rank sum test (WRST) with an α-error of 0.05. Cell types, which were significantly different between patients with anti-NMDA-R encephalitis and controls, are bold.

	Peripheral Blood (PB)						**Cerebrospinal Fluid (CSF)**					
	Anti-NMDA-R Encephalitis		**Control**				**Anti-NMDA-R Encephalitis**		**Control**			
Cell type	**Median**	**Interquartile range**	**Median**	**Interquartile range**	**P-value**	**Statistical Test**	**Median**	**Interquartile range**	**Median**	**Interquartile range**	**P-value**	**Statistical Test**
$CD19^+$ B cells (% lymphocytes)	12.9	18.0	12.6	5.5	0.635	WRST	**2.7**	**5.3**	**0.8**	**0.6**	**0.008**	**WRST**
$CD19^+$ B cells (cells/ml)	73121	721177	173176	200569	0.155	WRST	10	60	5	9	0.137	WRST
$CD138^+$ $CD19^+$ plasma cells (% lymphocytes)	0.1	0.7	0.05	0.08	0.055	WRST	0	0.03	0	0	0.823	WRST
$CD138^+$ $CD19^+$ plasma cells (cells/ml)	1274	6854	646	1537	0.635	WRST	0	0.532	0	0	0.933	WRST
$CD4^+$ T cells (% T cells)	74.4	10.8	68.2	14.0	0.101	WRST	79.4	7.7	74.0	8.2	0.359	WRST
$CD4^+$ T cells (cells/ml)	253043	3235958	666111	472726	0.121	WRST	421	1065	530	715	0.825	WRST
$HLADR^+$ $CD4^+$ T cells (% of $CD4^+$ T cells)	6.5	10.9	4.7	1.8	0.591	WRST	9.2	10.2	5.4	3.8	0.195	WRST
$HLADR^+$ $CD4^+$ T cells (cells/ml)	16616	70986	32249	13686	0.297	WRST	50	62	24	51	0.728	WRST
$CD8^+$ T cells (% of T cells)	**16.4**	**5.9**	**26.6**	**7.0**	**0.011**	**WRST**	17.5	4.3	22.3	7.8	0.240	WRST
$CD8^+$ T cells (cells/ml)	42185	715271	279817	228059	0.137	WRST	76	225	126	230	0.507	WRST
$HLADR^+$ $CD8^+$ T cells (% of $CD8^+$ T cells)	11.7	4.1	7.4	4.1	0.062	WRST	**50.0**	**7.9**	**26.8**	**10.6**	**<0.001**	**WRST**
$HLADR^+$ $CD8^+$ T cells (cells/ml)	4758	51736	16821	13135	0.121	WRST	42	102	33	57	0.681	WRST

Supplementary Table 7: Follow-up characterization of the peripheral and intrathecal autoimmune response in anti-NMDAR encephalitis using multi-parameter flow cytometry at 5 to 7 months after initiation of immunotherapy. Absolute numbers (in cells/ml) and relative fractions (in %) of lymphocyte subsets in peripheral blood (PB) and cerebrospinal fluid (CSF) in four patients with anti-NMDAR encephalitis and controls are given as median and interquartile range. Confirmatory statistics was performed using the Wilcoxon rank sum test (WRST) with an α-error of 0.05. Cell types, which were significantly different between patients with anti-NMDA-R encephalitis and controls, are bold.

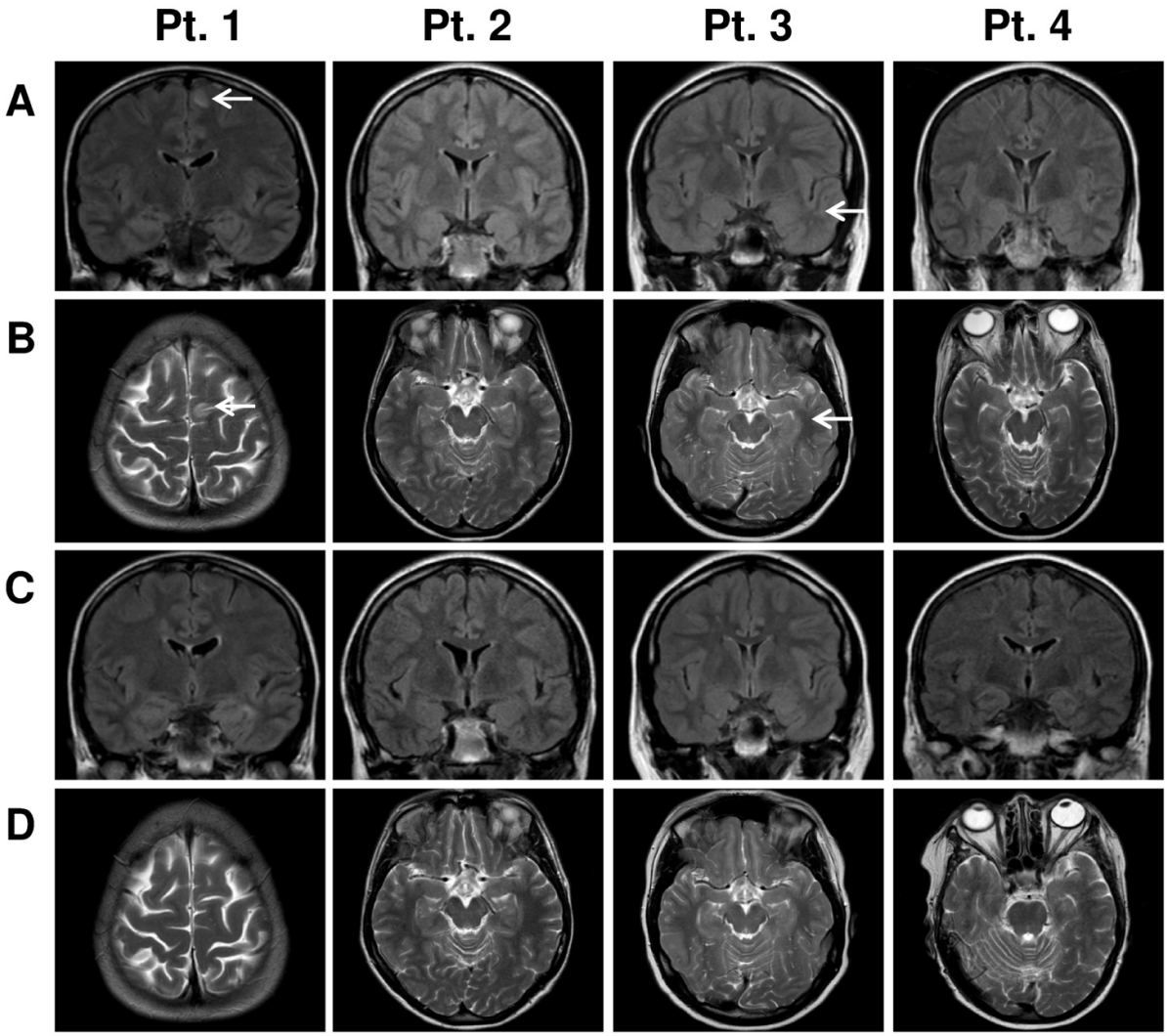

Supplementary Figure 1: Cerebral MRI in patients with anti-NMDAR encephalitis. Coronal FLAIR- (A, C) and axial T2 (B, D) sequences of four patients (Pt.1-4) with anti-NMDAR encephalitis at the time of admission (A, B) and after 5 to 7 months of immunotherapy (C, D). White arrows indicate cortico-subcortical lesions.

Supplemental References

1. Lueg G, Gross CC, Lohmann H, et al. Clinical relevance of specific T-cell activation in the blood and cerebrospinal fluid of patients with mild Alzheimer's disease. Neurobiol Aging. 2015; 36(1):81-9.

2. Golombeck KS, Bönte K, Mönig C, et al. Evidence of a pathogenic role for CD8(+) T cells in anti-GABAB receptor limbic encephalitis. Neurol Neuroimmunol Neuroinflamm. 2016; 3(3):e232.

3. Reiber H, Peter JB. Cerebrospinal fluid analysis: disease-related data patterns and evaluation programs. J Neurol Sci. 2001; 184(2):101-22.

4. Wandinger K-P, Saschenbrecker S, Stoecker W, Dalmau J. Anti-NMDA-receptor encephalitis: a severe, multistage, treatable disorder presenting with psychosis. J Neuroimmunol. 2011; 231(1-2):86-91.

5. Leypoldt F, Höftberger R, Titulaer MJ, et al. Investigations on CXCL13 in anti-N-methyl-D-aspartate receptor encephalitis: a potential biomarker of treatment response. JAMA Neurol. 2015; 72(2):180-6.

6. Dalmau J, Furneaux HM, Cordon-Cardo C, Posner JB. The expression of the Hu (paraneoplastic encephalomyelitis/sensory neuronopathy) antigen in human normal and tumor tissues. Am J Pathol. 1992; 141(4):881-6.

7. Gleichman AJ, Spruce LA, Dalmau J, Seeholzer SH, Lynch DR. Anti-NMDA receptor encephalitis antibody binding is dependent on amino acid identity of a small region within the GluN1 amino terminal domain. J Neurosci. 2012; 32(32):11082-94.

8. Planagumà J, Leypoldt F, Mannara F, et al. Human N-methyl D-aspartate receptor antibodies alter memory and behaviour in mice. Brain. 2015; 138(Pt 1):94-109.

9. Helmstaedter C, Lendt M, Lux S. Verbaler Lern- und Merkfähigkeitstest - VLMT. Göttingen, Beltz Test Verlag. 2001.

10. Härtling C, Markowitsch HJ, Neufeld H. WMS-R Wechsler Gedächtnistest - Revidierte Fassung. Bern, Hans Huber Verlag. 2000.

11. Tombaugh TN. Trail Making Test A and B: normative data stratified by age and education. Arch Clin Neuropsychol. 2004; 19(2):203-14.

12. Shin MS, Park SY, Park SR, Seol SH, Kwon JS. Clinical and empirical applications of the Rey-Osterrieth Complex Figure Test. Nat Protoc. 2006;1(2):892-9.

13. Aschenbrenner A, Tucha O, Lange K. RWT Regensburger Wortflüssigkeits-Test. Hogrefe Verlag, Göttingen. 2000.

Author "Sumanta Barman" performed single-cell PCR, sequencing, cloning, expression and purification of the recombinant human monoclonal antibodies (rhuMabs) in purpose of the development of a recombinant monoclonal antibody from clonally expanded intrathecal plasma cells. He also performed immunoprecipitation (IP) experiments to confirm the antigen specificity of the recombinant human monoclonal antibody. After developing the monoclonal antibody and confirming it's antigen specificity, further characterization of the antibody was done by co-authors. Mr. Barman also contributed to the data acquisition, data analysis, interpretation and drafting the manuscript.

Published scientific article II

An assay to determine mechanisms of rapid autoantibody-induced neurotransmitter receptor endocytosis and vesicular trafficking in autoimmune encephalitis

frontiers in Neurology

ORIGINAL RESEARCH
published: 01 March 2019
doi: 10.3389/fneur.2019.00178

An Assay to Determine Mechanisms of Rapid Autoantibody-Induced Neurotransmitter Receptor Endocytosis and Vesicular Trafficking in Autoimmune Encephalitis

*Elsie Amedonu[1,2], Christoph Brenker[3], Sumanta Barman[4], Julian A. Schreiber[1], Sebastian Becker[1], Stefan Peischard[1], Nathalie Strutz-Seebohm[1], Christine Strippel[2], Andre Dik[2], Hans-Peter Hartung[4], Thomas Budde[5], Heinz Wiendl[2], Timo Strünker[3], Bernhard Wünsch[6], Norbert Goebels[4], Sven G. Meuth[2], Guiscard Seebohm[1] and Nico Melzer[2]**

[1] Myocellular Electrophysiology and Molecular Biology, Institute for Genetics of Heart Diseases, University of Muenster, Muenster, Germany, [2] Department of Neurology, University of Muenster, Muenster, Germany, [3] Centre of Reproductive Medicine and Andrology, University of Muenster, Muenster, Germany, [4] Department of Neurology, Universitätsklinikum and Center for Neurology and Neuropsychiatry LVR Klinikum, Heinrich Heine University Duesseldorf, Duesseldorf, Germany, [5] Institute for Physiology I, University of Muenster, Muenster, Germany, [6] Institute for Pharmaceutical and Medical Chemistry, University of Muenster, Muenster, Germany

OPEN ACCESS

Edited by:
Stefan Bittner,
Johannes Gutenberg University
Mainz, Germany

Reviewed by:
Chiara Cordiglieri,
Istituto Nazionale Genetica Molecolare (INGM), Italy
Christoph Kleinschnitz,
Universität Würzburg, Germany
Erhard Wischmeyer,
Universität Würzburg, Germany

***Correspondence:**
Nico Melzer
nico.melzer@ukmuenster.de

Specialty section:
This article was submitted to Multiple Sclerosis and Neuroimmunology, a section of the journal Frontiers in Neurology

Received: 19 September 2018
Accepted: 11 February 2019
Published: 01 March 2019

Citation:
Amedonu E, Brenker C, Barman S, Schreiber JA, Becker S, Peischard S, Strutz-Seebohm N, Strippel C, Dik A, Hartung H-P, Budde T, Wiendl H, Strünker T, Wünsch B, Goebels N, Meuth SG, Seebohm G and Melzer N (2019) An Assay to Determine Mechanisms of Rapid Autoantibody-Induced Neurotransmitter Receptor Endocytosis and Vesicular Trafficking in Autoimmune Encephalitis. Front. Neurol. 10:178. doi: 10.3389/fneur.2019.00178

N-Methyl-D-aspartate (NMDA) receptors (NMDARs) are among the most important excitatory neurotransmitter receptors in the human brain. Autoantibodies to the human NMDAR cause the most frequent form of autoimmune encephalitis involving autoantibody-mediated receptor cross-linking and subsequent internalization of the antibody-receptor complex. This has been deemed to represent the predominant antibody effector mechanism depleting the NMDAR from the synaptic and extra-synaptic neuronal cell membrane. To assess in detail the molecular mechanisms of autoantibody-induced NMDAR endocytosis, vesicular trafficking, and exocytosis we transiently co-expressed rat GluN1-1a-EGFP and GluN2B-ECFP alone or together with scaffolding postsynaptic density protein 95 (PSD-95), wild-type (WT), or dominant-negative (DN) mutant Ras-related in brain (RAB) proteins (RAB5WT, RAB5DN, RAB11WT, RAB11DN) in HEK 293T cells. The cells were incubated with a pH-rhodamine-labeled human recombinant monoclonal GluN1 IgG1 autoantibody (GluN1-aAb$^{pH-rhod}$) genetically engineered from clonally expanded intrathecal plasma cells from a patient with anti-NMDAR encephalitis, and the pH-rhodamine fluorescence was tracked over time. We show that due to the acidic luminal pH, internalization of the NMDAR-autoantibody complex into endosomes and lysosomes increases the pH-rhodamine fluorescence. The increase in fluorescence allows for mechanistic assessment of endocytosis, vesicular trafficking in these vesicular compartments, and exocytosis of the NMDAR-autoantibody complex under steady state conditions. Using this method, we demonstrate a role for PSD-95 in stabilization of NMDARs in the cell membrane in the presence of GluN1-aAb$^{pH-rhod}$, while RAB proteins did not exert a significant effect on vertical trafficking of

the internalized NMDAR autoantibody complex in this heterologous expression system. This novel assay allows to unravel molecular mechanisms of autoantibody-induced receptor internalization and to study novel small-scale specific molecular-based therapies for autoimmune encephalitis syndromes.

Keywords: autoimmune encephalitis, N-Methyl-D-aspartate receptors, cross-linking, endocytosis, vesicular trafficking, exocytosis, autoantibodies

INTRODUCTION

Most of the glutamatergic signaling mechanisms in the central nervous system (CNS) rely on the binding of this neurotransmitter (NT) to specific glutamate receptors (GluRs). Ionotropic ligand-gated ion channels (iGluRs) and metabotropic G protein-coupled receptors (mGluRs) mediate fast and slow glutamatergic excitatory synaptic transmission at synapses between neuronal axons and dendrites (1). The iGluRs include the slow, modulatory N-Methyl-D-aspartate receptors (NMDARs), the fast α-Amino-3-hydroxy-5-methyl-4-isoxazolepropionic acid receptors (AMPARs) (2), and the Kainate receptors (KARs), which typically do not contribute to baseline synaptic transmission.

Functional adult neuronal NMDARs are hetero-tetrameric complexes, formed predominantly by two GluN1 and two GluN2 subunits (3). The subunits share a similar membrane topology, i.e., four transmembrane domains (M1–M4), a reentrant membrane loop between M3 and M4 domains, and long extracellular N- and intracellular C-termini (relatively short for GluN1) (4). Hallmarks of NMDARs include voltage-sensitive block by extracellular Mg^{2+}, slow current kinetics, and high Ca^{2+} permeability (1). Thereby, NMDARs serve a crucial function in synaptic plasticity (expressed as a change in receptor number and functional properties), learning, and memory. These processes start with the release of glutamate from presynaptic axon terminals and the subsequent binding together with the co-agonist glycine mainly to postsynaptic NMDARs. Postsynaptic NMDARs, in turn, are associated with and regulated by several proteins that together constitute the postsynaptic density (PSD), an elaborate complex of interlinked proteins and elements of the cytoskeleton.

Neuronal glutamate receptor trafficking is a multi-step process that involves protein synthesis at the dendritic tree of the postsynaptic neuron, receptor subunit quality control and assemblage in the endoplasmic reticulum (ER), processing in the Golgi apparatus (GA), vesicular packaging in the Golgi complex (GC), subsequent *vertical trafficking* to the neuronal cell surface membrane and anchorage at the PSD, *lateral trafficking* into and out of the PSD, as well as the internalization (endocytosis), subsequent neuronal surface membrane reinsertion (exocytosis) carried out by endosomes (*vertical trafficking*) or degradation carried out by lysosomes (5). At each step of the trafficking process, NMDARs associate with specific partner proteins that allow for their maturation and/or transportation (4).

Glutamate receptors are major targets in autoimmune encephalitis syndromes (6, 7), in which autoantibodies of the immunoglobulin (Ig) G type target iGluRs like NMDARs (8) and AMPARs (9) as well as mGluRs like metabotropic glutamate receptor 1 (mGluR1) (10) and 5 (mGluR5) (11). These autoantibodies disrupt receptor function, cross-link receptors leading to internalization of the antibody-receptor complex (9, 12–15), and activate complement depending on the autoantibody, its IgG subclass, and the complement concentration in the cerebrospinal fluid.

NMDAR autoantibodies are of the IgG 1 or 3 subtypes and can directly affect the gating of the receptor (16). Residues N^{368}/G^{369} in the extracellular domain of the GluN1 subunit of NMDARs may form part of the immunodominant binding region for IgG on the receptor molecule. In single-channel recordings, antibody binding to the receptor instantly caused more frequent openings and prolonged open times of the receptor (16). Moreover, NMDAR autoantibodies caused selective and reversible decrease in postsynaptic surface density and synaptic anchoring of NMDAR in both glutamatergic and GABAergic rat hippocampal neurons by disrupting the interaction of NMDAR with Ephrin-B2 receptors (17), followed by selective NMDAR cross-linking and internalization (13, 14). Consistently, NMDAR antibodies selectively decreased NMDAR-mediated miniature excitatory post-synaptic currents (mEPSCs) without affecting AMPAR-mediated mEPSCs in cultured rat hippocampal neurons (13).

In cultured rat hippocampal neurons, once internalized, antibody-bound NMDAR traffic through recycling endosomes and lysosomes, but do not induce compensatory changes in glutamate receptor gene expression (14). The internalized antibody-receptor complexes co-localize rather with RAB11-positive recycling endosomes than with Lamp1-positive lysosomes suggesting subsequent recycling and exocytosis (14). The process of NMDAR internalization plateaus after 12 h, reaching a steady state that persists throughout the duration of the antibody treatment (14), likely reflecting a state of equilibrium between the rate of receptor internalization and the

Abbreviations: AMPA, α-Amino-3-hydroxy-5-methyl-4-isoxazolepropionic acid; AMPAR, α-Amino-3-hydroxy-5-methyl-4-isoxazolepropionic acid receptor; CNS, central nervous system; DMEM, Dulbecco's modified Eagle's medium; DN, dominant-negative; ECFP, enhanced cyan fluorescent protein; EE, early endosomes; EGFP, enhanced green fluorescent protein; ER, endoplasmic reticulum; FBS, fetal bovine serum; GluN1-aAb$^{pH-rhod}$, pH-rhodamine-labeled human recombinant monoclonal GluN1 IgG1 autoantibody; GA, Golgi apparatus; GC, Golgi complex; GluR, glutamate receptors; Ig, immunoglobulin; iGluR, ionotropic glutamate receptor; KAR, kainate receptor; NEAA, non-essential amino acids; NMDA, N-Methyl-D-aspartate; NMDAR, N-Methyl-D-aspartate receptor; NT, neurotransmitter; mEPSCs, miniature excitatory post-synaptic currents; mGluR, metabotropic G-protein coupled receptor; PSD-95, postsynaptic density protein 95; RAB, Ras-related in brain; RE, recycling endosomes; RV, recycling vesicle; WT, wild-type.

rate of receptor (re-)insertion from different compartments into the surface membrane (14).

Probably due to the lack of blood-brain barrier disruption in NMDAR encephalitis and subsequent lack of relevant complement concentrations in the cerebrospinal fluid, as well as internalization of NMDAR together with the autoantibodies, no complement depositions or major neuronal loss could be detected in biopsy specimens of patients with NMDAR encephalitis, despite large numbers of intracerebral autoantibody-secreting plasma cells (18, 19). Indeed, fully reversible impairment of behavior and memory occurs in mice receiving passive intrathecal transfer of NMDAR autoantibodies (20, 21) that is prevented by co-application of ephrin (22).

The effects on receptor-mediated currents are rather small in heterologous expression systems and do not allow for mechanistic studies on autoantibody-induced neurotransmitter receptor internalization and trafficking in anti-NMDAR encephalitis and other forms of autoimmune encephalitis (21). Thus, the aim of this study was to develop an assay suitable to study in molecular detail the mechanism of autoantibody-induced NMDAR endocytosis, vesicular trafficking, and exocytosis and potentially to study novel small-scale specific molecular-based therapies for autoimmune encephalitis syndromes.

MATERIALS AND METHODS

Construction of NMDAR Expression Vectors

NMDAR constructs were kindly provided by Prof. Michael Hollmann, Receptor Biochemistry, Faculty of Chemistry and Biochemistry, Ruhr University Bochum, Germany. cDNAs encoding the rat GluN1-1a and GluN2B NMDAR subunits were sub-cloned into the pEGFP-N1 and pECFP-N1 mammalian expression vectors, respectively. To allow for the visualization of the subunits, enhanced cyan fluorescent protein (ECFP), and enhanced green fluorescent protein (EGFP) were inserted in-frame at the N-terminus of the subunits. The subunit-containing plasmids were amplified via growth in *E. coli* followed by purification based on a modified alkaline lysis procedure (QIAGEN Miniprep kit).

The generation of PSD-95 as well as WT and DN RAB5 and RAB11 expression vector constructs has been described elsewhere (5, 23).

HEK 293T Cell Co-transfection

HEK 293T cells were cultured in growth media comprising high-glucose Dulbecco's modified Eagle's medium (DMEM) supplemented with 10% fetal bovine serum (FBS), non-essential amino acids (NEAA), Pen-Strep, and 2 mM glutamine. Two days prior to transfection, exponentially growing cells were seeded on poly-D-lysine-coated glass bottom 96-well-plates to a density of approximately 5.0–8.0 $\times$ 10^5/well. Two hours prior to co-transfection, the culture medium was replaced with fresh culture medium. HEK 293T cells were then transiently co-transfected with the cDNAs (0.25 μg GluN1-1a-EGFP and 0.25 μg GluN2B-ECFP) encoding the NMDAR subunits as well as PSD-95, or WT, or DN RAB proteins using the FuGene HD (Promega Corporations) transfection technique according to manufacturer's instructions or left untransfected. 24 h post co-transfection, cells were seeded onto poly-D-lysine-coated glass bottom 96-well-plates. Confocal laser-scanning microscopy was used to quantify cell-surface NMDAR density ($\times$63 glycerol objective; TCS-SP5 Leica- Microsystems, Germany).

pH-rhodamine Labeling of a Human Recombinant Monoclonal GluN1 Autoantibody

Generation of a recombinant human monoclonal GluN1 autoantibody (GluN1-aAb) engineered from clonally expanded intrathecal plasma cells of a patient with anti-NMDAR encephalitis has recently been described (21). Labeling of GluN1-aAb was performed using a pHrodo™ Red Microscale Labeling Kit (Thermofisher Scientific) according to the recommendations of the supplier. Briefly, 100 μL of GluN1-aAb solution (1 mg/mL in PBS) were transferred to a "component D" containing reaction tube and supplemented with 10 μL of 1M sodium bicarbonate. pHrodo red succinimidyl ester was dissolved in 10 μL of DMSO. From the resulting solution, 0.70 μL (as calculated according to the equation 1 of the labeling kit's protocol) was added to the reaction tube containing the pH-adjusted GluN1-aAb. This reaction mixture was incubated for 15 min at RT to allow conjugation. For separation from unbound dye, the reaction mix was spun through a resin-containing column (provided with the kit) at 1,000 g for 5 min. The purified pH-rhodo red labeled GluN1-aAb (GluN1-aAb$^{pH-rhod}$) was recovered from the collection tube and stored aliquoted at −20°C, while unbound dye remained in the resin.

Co-incubation of GluN1-aAb$^{pH\text{-}rhod}$ With HEK 293T Cells Expressing GluN1-1a-EGFP/GluN2B-ECFP NMDARs and Fluorescence Intensity Analysis

The rhodamine fluorophore possesses a well-known pH- and temperature-dependent fluorescence quantum yield (24), which decreases linearly as pH and temperature increases (25). These physicochemical properties needed to be considered in our experimental setting.

Untransfected or co-transfected HEK 293T cells from the same 96-well-plate were incubated with GluN1-aAb$^{pH-rhod}$ at a concentration of 4 μg/ml in phosphate-buffered saline (PBS, pH 7.4) for 2 min. After that, unbound GluN1-aAb$^{pH-rhod}$ was washed-out by superfusing 96-wells with PBS to yield cell-bound GluN1-aAb$^{pH-rhod}$ fluorescence. Wells on the same 96-well-plate without cells incubated with GluN1-aAb$^{pH-rhod}$ at a concentration of 4 μg/ml in PBS without wash-off served as control. All incubations were conducted at 4°C on ice to prevent endocytosis prior to recordings.

Subsequently, fluorescence of GluN1-EGFP and GluN1-aAb$^{pH-rhod}$ was excited at 480 and 520 nm and detected at 510 nm (confocal imaging) and 580 nm (plate reader), respectively, verifying GluN1-1a-EGFP expression and

presence of the GluN1-aAb-bound rhodamine fluorescence (GluN1-aAb$^{pH-rhod}$).

Subsequently, the temperature was increased rapidly from 4 to 30°C to allow for endocytosis, and pH-rhodamine-fluorescence was repetitively excited at 520 nm and the emission was detected at 580 nm. The overall pH-rhodamine fluorescence decreased exponentially with time reaching a steady state after approximately 500 s mainly reflecting the known temperature-dependent fluorescence quantum yield of rhodamine under all experimental conditions.

The steady state pH-rhodamine-fluorescence intensity at 580 nm after 500 s of HEK 293T cells expressing GluN1-1a-EGFP/GluN2B-ECFP NMDARs was significantly higher compared to untransfected HEK 293T cells and served as a cumulative measure of endocytosis of GluN1-aAb$^{pH-rhod}$ bound to the NMDAR with subsequent acidification within endosomes and/or lysosomes and exocytosis. This allowed for mechanistic studies in HEK 293T cells expressing GluN1-1a-EGFP/GluN2B-ECFP NMDARs co-transfected with scaffolding protein PSD-95 as well as RAB5WT and RAB5DN (mediating vesicle endocytosis) and RAB11WT or RAB11DN (mediating vesicle exocytosis).

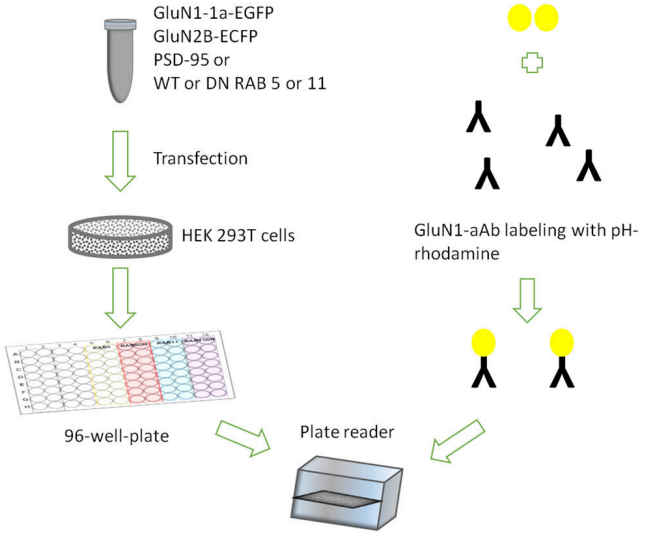

FIGURE 1 | Assay design showing HEK 293T cells transiently expressing rat GluN1-1a-EGFP/GluN2B-ECFP incubated with GluN1-aAb$^{pH-rhod}$ in 96-well-plates under variable conditions in parallel.

Statistical Analysis

Data was analyzed using Origin 9 (OriginLab Corporation). One-way ANOVA followed by multiple pair-wise comparisons with Bonferroni's *post-hoc* correction was used to statistically analyze differences in fluorescence intensity; $p \leq 0.05$ were considered as significant; data in figures were expressed as mean ± SEM. All experiments were performed in triplicates.

RESULTS

To assess in detail the molecular mechanisms of NMDAR autoantibody-induced NMDAR endocytosis, vesicular trafficking, and exocytosis we transiently expressed rat GluN1-1a-EGFP and GluN2B-ECFP alone or together with PSD-95 or with WT- or DN-mutant RAB proteins (RAB5WT, RAB5DN, RAB11WT, RAB11DN) in HEK 293T cells. As a control, HEK 293T cells were left untransfected.

The cells were incubated with a pH-rhodamine-labeled human recombinant monoclonal GluN1 IgG1 autoantibody [GluN1-aAb$^{pH-rhod}$, (21)].

We surmised that the pH-rhodamine fluorescence is increased during the ensuing internalization of the NMDAR-autoantibody complex, due to the acidic luminal pH of endosomes and lysosomes. This might allow for mechanistic assessment of endocytosis, vesicular trafficking in both vesicular compartments and exocytosis of the NMDAR-autoantibody complex (for assay design see **Figure 1**).

In a first set of experiments, HEK 293T cells were transiently co-transfected only with rat GluN1-1a-EGFP and GluN2B-ECFP or left untransfected. After 2 days, expression of fluorescently labeled NMDARs was verified using confocal laser-scanning microscopy. About 70–80% of the cells expressed GluN1-1a-EGFP as subunit putatively targeted by the GluN1-aAb$^{pH-rhod}$ (**Figure 2A**) and GluN2B-ECFP (data not shown). Longer expression times or higher amounts of NMDAR-cDNA for transfections decreased expression levels, supposedly due to cytotoxic effects of pronounced overexpression of NMDARs.

Next, GluN1-1a-EGFP- and GluN2B-ECFP-transfected and untransfected cultured cells were incubated with GluN1-aAb$^{pH-rhod}$. The incubation was performed at 4°C to stop ongoing endocytosis. After that, unbound GluN1-aAb$^{pH-rhod}$ was washed-off. As a control, wells without cells were incubated with GluN1-aAb$^{pH-rhod}$ without wash-off.

Subsequently, GluN1-1a-EGFP and GluN1-aAb$^{pH-rhod}$ fluorescence was excited at 480 nm and 520 nm and measured at 510 and 580 nm, respectively, verifying GluN1-1a-EGFP expression of transfected but not untransfected cells and presence of the GluN1-aAb-bound rhodamine fluorescence (GluN1-aAb$^{pH-rhod}$, **Figure 2B**).

The plate was subsequently transferred to a fluorescence plate reader for time-resolved detection of the pH-rhodamine fluorescence intensity at 30°C. The temperature was increased rapidly from 4–30°C to start endocytosis, and pH-rhodamine-fluorescence was repetitively excited at 520 nm and the emission was detected at 580 nm. The overall rhodamine fluorescence at 580 nm decreased exponentially with time, reaching a steady state after approximately 500 s (**Figure 3B**) mainly reflecting the known temperature-dependent fluorescence quantum yield of rhodamine (24–26) under all experimental conditions.

Of note, the fluorescence-spectrum did not change over time (**Figure 3A**), illustrating that pH-rhodamine fluorescence was detected throughout the experiments. Moreover, steady-state fluorescence intensities of empty wells without wash-off of GluN1-aAb$^{pH-rhod}$ were much larger than those of wells with HEK 293T cells illustrating the known background fluorescence of pH rhodamine at neutral pH of 7.4 in PBS (roughly 1/3 of the maximal fluorescence at acidic pH of 4.0) and thus the necessity of the washing step (**Figure 3B**).

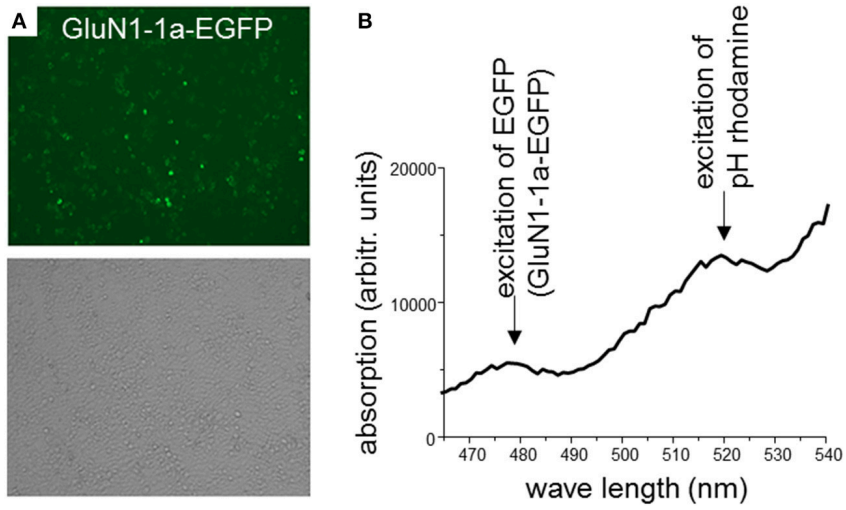

FIGURE 2 | (A) HEK 293T cells co-expressing rat GluN1-1a-EGFP and GluN2B-ECFP. 2 days after transfection, expression of fluorescently labeled NMDARs was verified using confocal laser-scanning microscopy. About 70–80% of the cells expressed GluN1-1a-EGFP as subunit putatively targeted by the GluN1-aAb$^{pH-rhod}$ (upper panel) and GluN2B-ECFP (data not shown). Light microscopy demonstrates typical cell densities (lower panel). **(B)** Binding of GluN1-aAb$^{pH-rhod}$ to the NMDAR subunits as determined by the plate reader experiment. HEK 293T cells expressing GluN1-1a-EGFP/GluN2B-ECFP were incubated with GluN1-aAb$^{pH-rhod}$ on ice in 96-well-plates. GluN1-1a-EGFP and GluN1-aAb$^{pH-rhod}$ fluorescence was excited at wavelengths of 480 nm and 520 nm and emission measured at wavelengths of 510 and 580 nm, respectively, verifying the GluN1-1a-EGFP expression and the binding of GluN1-aAb$^{pH-rhod}$.

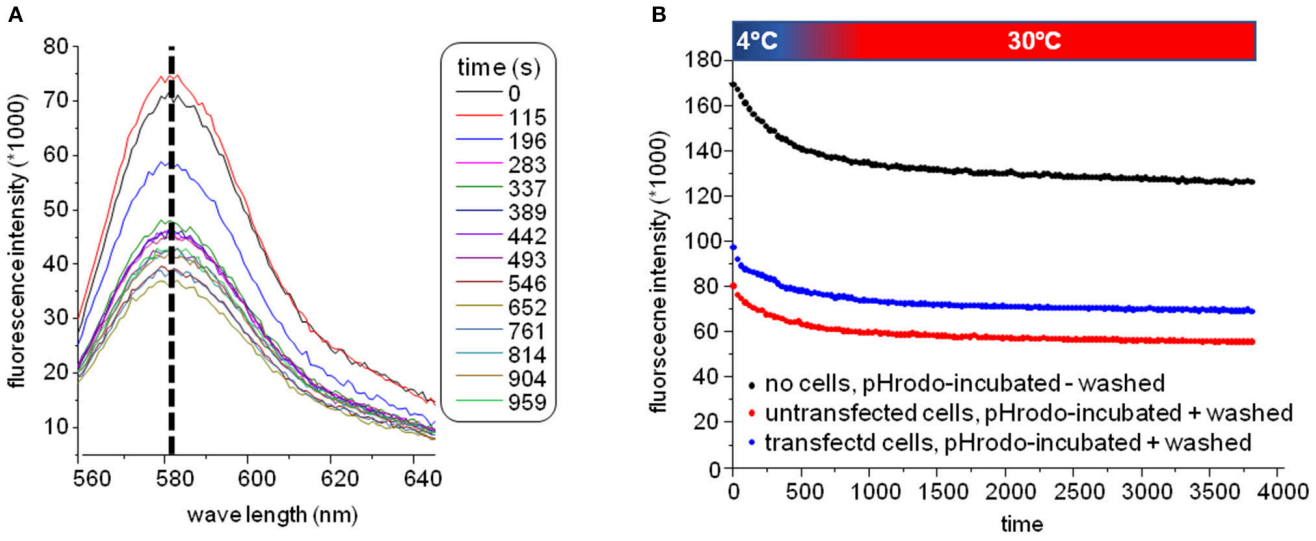

FIGURE 3 | (A) Spectra of the GluN1-aAb$^{pH-rhod}$ fluorescence. The overall fluorescence at 580 nm decreased over time reaching a steady state after approximately 500 s mainly reflecting the known temperature-dependent fluorescence quantum yield of rhodamine (24–26) elicited by elevating the temperature for 4–30°C at the beginning of the experiment under all experimental conditions. During this decay, the excitation spectrum did not shift/change indicating that indeed pH-rhodamine-fluorescence was detected throughout the whole experiment. **(B)** Representative time-dependent traces of the GluN1-aAb$^{pH-rhod}$ fluorescence without wash-off of the unbound GluN1-aAb$^{pH-rhod}$ in PBS at pH 7.4 (black trace) and after wash-off of unbound GluN1-aAb$^{pH-rhod}$ in wells seeded with HEK 293T cells expressing GluN1-1a-EGFP/GluN2B-ECFP (blue trace) or untransfected HEK 293T cells (red trace). The steady state pH-rhodamine-fluorescence intensity at 580 nm after 500 s of HEK 293T cells expressing GluN1-1a-EGFP/GluN2B-ECFP NMDARs was significantly higher compared to the background fluorescence of untransfected HEK 293T cells and served as a cumulative measure of endocytosis of GluN1-aAb$^{pH-rhod}$ bound to the NMDAR with subsequent acidification within endosomes and/or lysosomes and exocytosis.

The steady state pH-rhodamine-fluorescence intensity at 580 nm after 500 s of HEK 293T cells expressing GluN1-1a-EGFP/GluN2B-ECFP NMDARs was significantly higher compared to the background fluorescence of untransfected HEK 293T cells (**Figure 4**) and served as a cumulative measure of endocytosis of GluN1-aAb$^{pH-rhod}$ bound to the NMDAR with

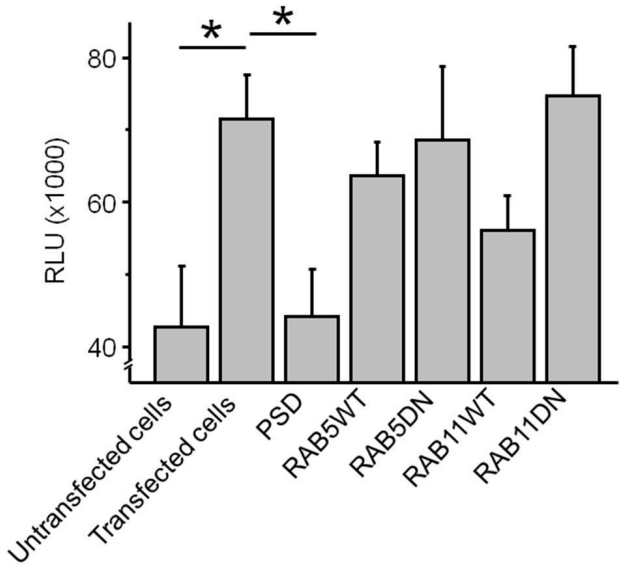

FIGURE 4 | The co-expression of GluN1-1a-EGFP/GluN2B-ECFP NMDARs with the scaffolding protein PSD-95 significantly reduced the cumulative steady state pH-rhodamine-fluorescence intensity at 580 nm after 500 s toward background levels of untransfected HEK 293T cells. In contrast, co-transfection with RAB5WT or RAB5DN (mediating/inhibiting endocytosis) or RAB11 WT or RABDN (mediating/inhibiting exocytosis) did not significantly affect the cumulative steady state pH-rhodamine-fluorescence intensity at 580 nm after 500 s in this heterologous expression system. One-way ANOVA followed by multiple pair-wise comparisons with Bonferroni's *post-hoc* correction was used to statistically analyze differences in fluorescence intensity; $p \leq 0.05$ were considered as significant (*); data are expressed as mean ± SEM. All experiments were performed in triplicates.

subsequent acidification within endosomes and/or lysosomes and exocytosis. This allowed for mechanistic studies in HEK 293T cells expressing GluN1-1a-EGFP/GluN2B-ECFP NMDARs co-transfected with scaffolding protein PSD-95 as well as WT and DN RAB5 (mediating vesicle endocytosis) and RAB11 (mediating vesicle exocytosis).

The co-expression of GluN1-1a-EGFP/GluN2B-ECFP NMDARs with the scaffolding protein PSD-95 significantly reduced the cumulative steady state pH-rhodamine-fluorescence intensity at 580 nm after 500 s toward background levels of untransfected HEK 293T cells (**Figure 4**). In contrast, co-transfection with RAB5WT or RAB5DN (mediating/inhibiting endocytosis) or RAB11 WT or RABDN (mediating/inhibiting exocytosis) did not significantly affect the cumulative steady state pH-rhodamine-fluorescence intensity at 580 nm after 500 s in this heterologous expression system (**Figure 4**).

DISCUSSION

NMDARs are among the most important excitatory receptors in the human brain. NMDAR autoantibodies cause encephalitis by binding to NMDARs, transducing conformational changes and subsequent endocytosis (21, 27). Recently, we showed that pre-incubation for an hour of a recombinant human monoclonal GluN1 autoantibody engineered from clonally expanded intrathecal plasma cells of a patient with anti-NMDAR encephalitis reduced NMDAR-mediated currents recorded from *Xenopus laevis* oocytes by about 20% (21). This result is similar to previous results in *Xenopus laevis* oocytes, showing a time-dependent inhibition of steady-state NMDAR-mediated currents of about 30% within 16 min upon exposure to dialysed sera of patients with anti-NMDAR encephalitis (28). To record NMDAR-mediated currents *in Xenopus laevis* oocytes (and other heterologous expression systems), it is required to use Ca^{2+}-free media to block current inactivation (29). This might explain the rather small antibody-mediated action in oocytes (and probably other heterologous expression systems) compared to the pronounced effects on NMDAR expression on neuronal cell surface *in vitro*, *ex vivo*, and on memory impairment *in vivo* in mice. The Ca^{2+}-free recording conditions may cause conformational changes of the NMDAR induced by binding of the antibody or modulate antibody binding itself and thus diminish subsequent receptor cross-linking and internalization.

These effects on receptor-mediated currents in *Xenopus laevis* oocytes (and other heterologous expression systems) do not allow for further mechanistic studies on autoantibody-induced neurotransmitter receptor internalization and trafficking in anti-NMDAR encephalitis and other forms of autoimmune encephalitis (30). Thus, the aim of this study was to develop an assay suitable for this kind of study.

We used a pH-rhodamine labeled single recombinant human GluN1 IgG1 autoantibody [GluN1-aAb$^{pH-rhod}$, (21)]. This monoclonal autoantibody has previously been shown to evoke all effects of natural NMDAR autoantibodies contained in cerebrospinal fluid of patients with anti-NMDAR encephalitis *in vitro* and *in vivo* (21).

We tested the effects of GluN1-aAb$^{pH-rhod}$ incubation on NMDAR endocytosis, trafficking, and exocytosis mechanisms in HEK 293T cells co-transfected with EGFP-tagged GluN1-1a and ECFP-tagged GluN2B subunits alone or together with PSD-95 or WT- or DN-mutant RAB 5 (mediating endocytosis) and 11 (mediating exocytosis) proteins.

Endocytosis, intracellular trafficking, and exocytosis of the antibody-receptor complex is mediated by transporting vesicles with acidic luminal pH. Thus, we took advantage of this fact, as we found that the use of the steady state GluN1-aAb$^{pH-rhod}$ fluorescence in HEK 293T cells expressing GluN1-1a-EGFP/GluN2B-ECFP NMDARs was significantly higher compared to the background fluorescence of untransfected HEK 293T cells. Thus, this steady state fluorescence served as a cumulative measure of endocytosis of GluN1-aAb$^{pH-rhod}$ bound to the NMDAR with subsequent acidification within endosomes and/or lysosomes and exocytosis.

Using this approach we could demonstrate a role for PSD-95 for stabilization of NMDAR in the cell membrane in the presence of NMDAR autoantibodies. This suggests that autoantibody-induced depletion from the cell membrane predominantly affects extra-synaptic NMDARs not associated with PSD-95 and to a lesser extent synaptic NMDARs. This finding is consistent with the notion that autoantibodies through dissociation from clustering ephrinB2 receptors lead to lateral diffusion of synaptic NMDARs within the neuronal cell membrane out to the synapse where they become cross-linked and internalized as extra-synaptic NMDARs (17, 31). Cell membrane stabilization of

synaptic NMDARs [displaying pro-survival functions (32)] and internalization of extra-synaptic NMDARs [displaying cell-death promoting functions (32)] is further consistent with the lack of overt neurodegeneration in NMDAR encephalitis despite excitotoxic excessive extracellular levels of glutamate (33–35).

Endocytosis, intracellular trafficking and exocytosis are under the guidance of small G-proteins of the RAB type. The use of functional WT and DN mutants has been previously successful in identification of intracellular trafficking pathways of glutamate receptors (36). We found that co-transfection with WT or DN RAB5 (mediating/inhibiting endocytosis) did not affect the cumulative steady state GluN1-aAb$^{pH-rhod}$ fluorescence intensity, whereas the cumulative steady state GluN1-aAb$^{pH-rhod}$ fluorescence intensity was tentatively lowered by co-transfection with WT RAB11 (mediating exocytosis) and tentatively augmented by co-transfection with RAB11DN (inhibiting exocytosis) compared to expression of NMDARs alone. This lack of overt effects of RAB proteins on endocytosis, trafficking and exocytosis of the antibody-receptor complex in our assay is probably due to the overlay by the temperature-dependent fluorescence decrease the amplitude of which is roughly as large as the steady state amplitude of the pH-dependent fluorescence increase upon internalization of the antibody-receptor complex. These opposing effects hinder detailed kinetic analysis of the autoantibody-induced vertical trafficking of the NMDAR performed here.

Hence, given the necessity of washing-off unbound GluN1-aAb$^{pH-rhod}$ and halting trafficking during that time by lowering the temperature due to the residual rhodamie fluorescence at pH 7.4 in PBS, the use of fluorophores (that inevitably are also concordantly temperature-sensitive) with an optimized pH-dependence i.e., no fluorescence at physiological pH of 7.4 might be better suited for our assay. They would enable synchronic adding of the labeled antibody to the cells cultured in PBS at pH 7.4 at constant temperature of 30°C and thus time-resolved tracking of fluorescence increase upon antibody-receptor internalization.

Taken together, we demonstrate a role for PSD-95 for stabilization of NMDAR in the cell membrane of HEK 293T cells in the presence of NMDAR autoantibodies, while RAB proteins did not exert a significant effect on vertical trafficking of the internalized NMDAR autoantibody complex in this heterologous expression system.

Our assay should be sensitive enough to study novel small-scale specific molecular-based therapies for autoimmune encephalitis that may become feasible as follows:

1) Autoantibody binding to the GluN1 subunit and subsequent induction of conformational changes in the NMDAR could be blocked by antibody fragments, for example. However, with existence of a multitude of autoantibody epitopes within the NMDAR, this approach may not be successful.
2) The autoantibody binding-induced conformational changes within the NMDAR. Small molecule allosteric modulators have recently been developed (5, 37, 38). Potentially, these compounds may be used to block the conformational changes induced by GluN1-aAb$^{pH-rhod}$ binding and thus inhibit internalization.
3) Inhibition of the GluN1-aAb$^{pH-rhod}$-induced internalization. To achieve this, general cellular trafficking pathways have to be blocked. It is questionable if such an approach can be tolerated by patients and would not cause severe side effects.

Taking these considerations into account, development and use of small molecule allosteric modulators may represent a group of drug candidates for anti-NMDAR encephalitis and other forms of autoimmune encephalitis. Evidenced by the relatively robust novel assay, they may be used to screen for compounds that block autoantibody-induced NMDAR cross-linking and internalization. This should always be accompanied by NMDAR stabilization within the synapse to avoid accumulation of NMDAR at extra-synaptic sides of the cell membrane potentially promoting excitotoxic cell death in NMDAR encephalitis.

Therefore, screening results obtained with our assay in HEK 293T overexpressing NMDAR should always be validated using super-resolution microscopy in cultured living neurons and brain slices exhibiting physiological expression levels and subcellular localization of NMDARs.

CONCLUSION

This novel assay allows to unravel molecular mechanisms of autoantibody-induced receptor internalization and to study novel small-scale specific molecular-based therapies for autoimmune encephalitis syndromes.

DATA AVAILABILITY

The dataset obtained and analyzed in the current study is available from the corresponding author on a reasonable request.

AUTHOR CONTRIBUTIONS

CS and AD: collected patient samples under the supervision of HW, SM, and NM; SBa and NG: performed the synthesis and pH-rhodamine labeling of GluN1-aAb$^{pH-rhod}$; EA, SBe, SP, and JS: performed the transfection, immunocytochemistry, and confocal microscopy with the HEK 293T cells; EA, CB, and TS: together with TB, NS-S, GS, and NM performed incubation of transfected HEK 293T cells with GluN1-aAb$^{pH-rhod}$ and data analysis; H-PH, BW, SM, GS, and NM: designed and supervised the project; EA, SM, GS, and NM: wrote the first draft of the manuscript. All authors contributed to and approved the final version of the manuscript.

FUNDING

This work was supported by the German Research Foundation (DFG, INST 2105/27-1 to SM), the German Academic Exchange Service (DAAD-MoE postgraduate scholarship to EA), the Walter und Ilse-Rose-Stiftung (to H-PH), the Forschungskommission of the Heinrich-Heine-University Düsseldorf, Germany (to NG) and the Bundesministerium für Bildung und Forschung (BMBF 031A232 to NG).

ACKNOWLEDGMENTS

We thank Prof. Michael Hollmann, Receptor Biochemistry, Faculty of Chemistry and Biochemistry, Ruhr University Bochum, Germany for providing the NMDAR constructs used in this study, and Christina Burhoi, Institute for Genetics of Heart Diseases (IfGH), University of Muenster, Germany, for excellent technical assistance.

REFERENCES

1. Traynelis SF, Wollmuth LP, Mcbain CJ, Menniti FS, Vance KM, Ogden KK, et al. Glutamate receptor ion channels: structure, regulation, and function. *Pharmacol Rev*. (2010) 62:405–96. doi: 10.1124/pr.109.002451
2. Hollmann M, Heinemann S. Cloned glutamate receptors. *Annu Rev Neurosci*. (1994) 17:31–108. doi: 10.1146/annurev.ne.17.030194.000335
3. Dingledine R, Borges K, Bowie D, Traynelis SF. The glutamate receptor ion channels. *Pharmacol Rev*. (1999) 51:7–61.
4. Petralia RS, Al-Hallaq RA, Wenthold RJ. Trafficking and targeting of NMDA receptors. In: Van Dongen AM, editor. *Biology of the NMDA Receptor*. Boca Raton, FL: CRC Press/Taylor & Francis (2009).
5. Seebohm G, Neumann S, Theiss C, Novkovic T, Hill EV, Tavare JM, et al. Identification of a novel signaling pathway and its relevance for GluA1 recycling. *PLoS ONE*. (2012) 7:e33889. doi: 10.1371/journal.pone.0033889
6. Melzer N, Meuth SG, Wiendl H. Paraneoplastic and non-paraneoplastic autoimmunity to neurons in the central nervous system. *J Neurol*. (2013) 260:1215–33. doi: 10.1007/s00415-012-6657-5
7. Graus F, Titulaer MJ, Balu R, Benseler S, Bien CG, Cellucci T, et al. A clinical approach to diagnosis of autoimmune encephalitis. *Lancet Neurol*. (2016) 15:391–404. doi: 10.1016/S1474-4422(15)00401-9
8. Dalmau J, Gleichman AJ, Hughes EG, Rossi JE, Peng X, Lai M, et al. Anti-NMDA-receptor encephalitis: case series and analysis of the effects of antibodies. *Lancet Neurol*. (2008) 7:1091–8. doi: 10.1016/S1474-4422(08)70224-2
9. Lai M, Hughes EG, Peng X, Zhou L, Gleichman AJ, Shu H, et al. AMPA receptor antibodies in limbic encephalitis alter synaptic receptor location. *Ann Neurol*. (2009) 65:424–34. doi: 10.1002/ana.21589
10. Sillevis Smitt P, Kinoshita A, De Leeuw B, Moll W, Coesmans M, Jaarsma D, et al. Paraneoplastic cerebellar ataxia due to autoantibodies against a glutamate receptor. *N Engl J Med*. (2000) 342:21–7. doi: 10.1056/NEJM200001063420104
11. Lancaster E, Martinez-Hernandez E, Titulaer MJ, Boulos M, Weaver S, Antoine JC, et al. Antibodies to metabotropic glutamate receptor 5 in the Ophelia syndrome. *Neurology*. (2011) 77:1698–701. doi: 10.1212/WNL.0b013e3182364a44
12. Coesmans M, Smitt PA, Linden DJ, Shigemoto R, Hirano T, Yamakawa Y, et al. Mechanisms underlying cerebellar motor deficits due to mGluR1-autoantibodies. *Ann Neurol*. (2003) 53:325–36. doi: 10.1002/ana.10451
13. Hughes EG, Peng X, Gleichman AJ, Lai M, Zhou L, Tsou R, et al. Cellular and synaptic mechanisms of anti-NMDA receptor encephalitis. *J Neurosci*. (2010) 30:5866–75. doi: 10.1523/JNEUROSCI.0167-10.2010
14. Moscato EH, Peng X, Jain A, Parsons TD, Dalmau J, Balice-Gordon RJ. Acute mechanisms underlying antibody effects in anti-N-methyl-D-aspartate receptor encephalitis. *Ann Neurol*. (2014) 76:108–19. doi: 10.1002/ana.24195
15. Peng X, Hughes EG, Moscato EH, Parsons TD, Dalmau J, Balice-Gordon RJ. Cellular plasticity induced by anti-alpha-amino-3-hydroxy-5-methyl-4-isoxazolepropionic acid (AMPA) receptor encephalitis antibodies. *Ann Neurol*. (2015) 77:381–98. doi: 10.1002/ana.24293
16. Gleichman AJ, Spruce LA, Dalmau J, Seeholzer SH, Lynch DR. Anti-NMDA receptor encephalitis antibody binding is dependent on amino acid identity of a small region within the GluN1 amino terminal domain. *J Neurosci*. (2012) 32:11082–94. doi: 10.1523/JNEUROSCI.0064-12.2012
17. Mikasova L, De Rossi P, Bouchet D, Georges F, Rogemond V, Didelot A, et al. Disrupted surface cross-talk between NMDA and Ephrin-B2 receptors in anti-NMDA encephalitis. *Brain*. (2012) 135:1606–21. doi: 10.1093/brain/aws092
18. Martinez-Hernandez E, Horvath J, Shiloh-Malawsky Y, Sangha N, Martinez-Lage M, Dalmau J. Analysis of complement and plasma cells in the brain of patients with anti-NMDAR encephalitis. *Neurology*. (2011) 77:589–93. doi: 10.1212/WNL.0b013e318228c136
19. Bien CG, Vincent A, Barnett MH, Becker AJ, Blumcke I, Graus F, et al. Immunopathology of autoantibody-associated encephalitides: clues for pathogenesis. *Brain*. (2012) 135:1622–38. doi: 10.1093/brain/aws082
20. Planaguma J, Leypoldt F, Mannara F, Gutierrez-Cuesta J, Martin-Garcia E, Aguilar E, et al. Human N-methyl D-aspartate receptor antibodies alter memory and behaviour in mice. *Brain*. (2015) 138:94–109. doi: 10.1093/brain/awu310
21. Malviya M, Barman S, Golombeck KS, Planaguma J, Mannara F, Strutz-Seebohm N, et al. NMDAR encephalitis: passive transfer from man to mouse by a recombinant antibody. *Ann Clin Transl Neurol*. (2017) 4:768–83. doi: 10.1002/acn3.444
22. Planaguma J, Haselmann H, Mannara F, Petit-Pedrol M, Grunewald B, Aguilar E, et al. Ephrin-B2 prevents N-methyl-D-aspartate receptor antibody effects on memory and neuroplasticity. *Ann Neurol*. (2016) 80:388–400. doi: 10.1002/ana.24721
23. Seebohm G, Strutz-Seebohm N, Birkin R, Dell G, Bucci C, Spinosa MR, et al. Regulation of endocytic recycling of KCNQ1/KCNE1 potassium channels. *Circ Res*. (2007) 100:686–92. doi: 10.1161/01.RES.0000260250.83824.8f
24. Ferguson J, Mau AWH. Spontaneous and stimulated emission from dyes. Spectroscopy of the neutral molecules of acridine orange, proflavine, and rhodamine B. *Aust J Chem*. (1973) 26:1617–24. doi: 10.1071/CH9731617
25. Kubin RF, Fletcher AN. Fluorescence quantum yields of some rhodamine dyes. *J Lumin*. (1982) 27:455–62. doi: 10.1016/0022-2313(82)90045-X
26. Moreau D, Lefort C, Burke R, Leveque P, O'connor RP. Rhodamine B as an optical thermometer in cells focally exposed to infrared laser light or nanosecond pulsed electric fields. *Biomed Opt Express*. (2015) 6:4105–17. doi: 10.1364/BOE.6.004105
27. Kreye J, Wenke NK, Chayka M, Leubner J, Murugan R, Maier N, et al. Human cerebrospinal fluid monoclonal N-methyl-D-aspartate receptor autoantibodies are sufficient for encephalitis pathogenesis. *Brain*. (2016) 139:2641–52. doi: 10.1093/brain/aww208
28. Castillo-Gomez E, Oliveira B, Tapken D, Bertrand S, Klein-Schmidt C, Pan H, et al. All naturally occurring autoantibodies against the NMDA receptor subunit NR1 have pathogenic potential irrespective of epitope and immunoglobulin class. *Mol Psychiatry*. (2017) 22:1776–84. doi: 10.1038/mp.2016.125
29. Levitan IB. It is calmodulin after all! Mediator of the calcium modulation of multiple ion channels. *Neuron*. (1999) 22:645–8. doi: 10.1016/S0896-6273(00)80722-9
30. Crisp SJ, Kullmann DM, Vincent A. Autoimmune synaptopathies. *Nat Rev Neurosci*. (2016) 17:103–17. doi: 10.1038/nrn.2015.27
31. Jezequel J, Johansson EM, Dupuis JP, Rogemond V, Grea H, Kellermayer B, et al. Dynamic disorganization of synaptic NMDA receptors triggered by autoantibodies from psychotic patients. *Nat Commun*. (2017) 8:1791. doi: 10.1038/s41467-017-01700-3
32. Hardingham GE, Bading H. Synaptic versus extrasynaptic NMDA receptor signalling: implications for neurodegenerative disorders. *Nat Rev Neurosci*. (2010) 11:682–96. doi: 10.1038/nrn2911
33. Melzer N, Biela A, Fahlke C. Glutamate modifies ion conduction and voltage-dependent gating of excitatory amino acid transporter-associated anion channels. *J Biol Chem*. (2003) 278:50112–9. doi: 10.1074/jbc.M307990200
34. Melzer N, Torres-Salazar D, Fahlke C. A dynamic switch between inhibitory and excitatory currents in a neuronal glutamate transporter. *Proc Natl Acad Sci USA*. (2005) 102:19214–8. doi: 10.1073/pnas.0508837103
35. Manto M, Dalmau J, Didelot A, Rogemond V, Honnorat J. *In vivo* effects of antibodies from patients with anti-NMDA receptor encephalitis: further evidence of synaptic glutamatergic dysfunction. *Orphanet J Rare Dis*. (2010) 5:31. doi: 10.1186/1750-1172-5-31

36. Seebohm G, Piccini I, Strutz-Seebohm N. Paving the way to understand autoantibody-mediated epilepsy on the molecular level. *Front Neurol*. (2015) 6:149. doi: 10.3389/fneur.2015.00149
37. Dey S, Temme L, Schreiber JA, Schepmann D, Frehland B, Lehmkuhl K, et al. Deconstruction - reconstruction approach to analyze the essential structural elements of tetrahydro-3-benzazepine-based antagonists of GluN2B subunit containing NMDA receptors. *Eur J Med Chem*. (2017) 138:552–64. doi: 10.1016/j.ejmech.2017.06.068
38. Gawaskar S, Temme L, Schreiber JA, Schepmann D, Bonifazi A, Robaa D, et al. Design, synthesis, pharmacological evaluation and docking studies of GluN2B-selective NMDA receptor antagonists with a Benzo[7]annulen-7-amine Scaffold. *Chem Med Chem*. (2017) 12:1212–22. doi: 10.1002/cmdc.201700311

Conflict of Interest Statement: The authors declare that the research was conducted in the absence of any commercial or financial relationships that could be construed as a potential conflict of interest.

Author "Sumanta Barman" produced recombinant human monoclonal (rhuMab) NMDAR antibody, carried out pH-rhodamine labelling of human recombinant monoclonal GluN1 IgG1 autoantibody (GluN1-aAb$^{pH-rhod}$). Co-authors used the monoclonal antibody and pH-rhodamine labelled GluN1-aAb$^{pH-rhod}$ to perform further experiments to assess the molecular mechanisms of autoantibody-induced NMDAR endocytosis, vesicular trafficking, and exocytosis. He also contributed to the acquisition, analysis and interpretation of data and to write the manuscript.

Published scientific article III

N-Methyl-D-Aspartate receptor antibodies in autoimmune encephalopathy alter oligodendrocyte function

N-Methyl-D-Aspartate Receptor Antibodies in Autoimmune Encephalopathy Alter Oligodendrocyte Function

Carlos Matute, PhD,[1] Ana Palma, MSc,[1] María Paz Serrano-Regal, MSc,[1] Estibaliz Maudes, MSc,[2] Sumanta Barman, MSc,[3] María Victoria Sánchez-Gómez, PhD,[1] María Domercq, PhD,[1] Norbert Goebels, MD,[3] and Josep Dalmau, MD, PhD[2,4,5]

Objective: Antibodies against neuronal N-methyl-D-aspartate receptors (NMDARs) in patients with anti-NMDAR encephalitis alter neuronal synaptic function and plasticity, but the effects on other cells of the nervous system are unknown.

Methods: Cerebrospinal fluid (CSF) of patients with anti-NMDAR encephalitis (preabsorbed or not with GluN1) and a human NMDAR-specific monoclonal antibody (SSM5) derived from plasma cells of a patient, along the corresponding controls, were used in the studies. To evaluate the activity of oligodendrocyte NMDARs and α-amino-3-hydroxy-5-methyl-4-isoxazolepropionic acid (AMPA) receptors in vitro after exposure to patients' CSF antibodies or SSM5, we used a functional assay based on cytosolic Ca^{2+} imaging. Expression of the glucose transporter (GLUT1) in oligodendrocytes was assessed by immunocytochemistry.

Results: NMDAR agonist responses were robustly reduced after preincubation of oligodendrocytes with patients' CSF or SSM5 but remained largely unaltered with the corresponding controls. These effects were NMDAR specific, as patients' CSF did not alter responses to AMPA receptor agonists and was abrogated by preabsorption of CSF with HEK cells expressing GluN1 subunit. Patients' CSF also reduced oligodendrocyte expression of glucose transporter GLUT1 induced by NMDAR activity.

Interpretation: Antibodies from patients with anti-NMDAR encephalitis specifically alter the function of NMDARs in oligodendrocytes, causing a decrease of expression of GLUT1. Considering that normal GLUT1 expression in oligodendrocytes and myelin is needed to metabolically support axonal function, the findings suggest a link between antibody-mediated dysfunction of NMDARs in oligodendrocytes and the white matter alterations reported in patients with this disorder.

ANN NEUROL 2020;00:1–7

Recent studies have identified a group of human disorders in which synaptic receptors are directly targeted by autoantibodies.[1] In particular, autoantibodies to the GluN1 subunit of the N-methyl-D-aspartate receptor (NMDAR) cause receptor internalization and reduced surface expression in neurons, leading to encephalitis symptoms that include psychosis, cognitive decline, seizures, and coma.[2] An intriguing feature of this disease is the dissociation between the severity of symptoms of most patients and the low frequency (~32%) of magnetic resonance imaging (MRI) abnormalities using standard clinical sequences.[3] Yet studies with diffusion tensor imaging

View this article online at wileyonlinelibrary.com. DOI: 10.1002/ana.25699

Received Apr 9, 2019, and in revised form Jan 15, 2020. Accepted for publication Feb 6, 2020.

Address correspondence to Dr Matute, Achucarro Basque Center for Neuroscience, E-48940 Leioa, Spain, E-mail: carlos.matute@ehu.es; and Dr Dalmau, Institut d'Investigacions Biomèdiques August Pi i Sunyer, Hospital Clínic, Universitat de Barcelona, Barcelona, Spain. E-mail: jdalmau@clinic.cat

From the [1]Achucarro Basque Center for Neuroscience, Biomedical Research Networking Center on Neurodegenerative Diseases and Department of Neurosciences, University of the Basque Country, Leioa, Spain; [2]August Pi i Sunyer Biomedical Research Institute, Hospital Clinic, University of Barcelona, Barcelona, Spain; [3]Department of Neurology, Medical Faculty, Heinrich Heine University Düsseldorf, Düsseldorf, Germany; [4]Department of Neurology, University of Pennsylvania, Philadelphia, PA; and [5]Catalan Institution for Research and Advanced Studies (ICREA), Barcelona, Spain

(DTI) and superficial white matter mean diffusivity show extensive changes in white matter integrity in most patients.[4,5]

Oligodendrocytes make myelin and support axons metabolically with lactate.[6] Like neurons, oligodendrocytes express NMDARs, which plays a critical role in supplying lactate to axons to sustain proper propagation of action potentials.[7] Thus, stimulation of NMDARs by glutamate released from axons results in a translocation of the glucose transporter GLUT1 into the oligodendrocyte plasma membrane and myelin compartment, enhancing glucose uptake and glycolytic support of fast spiking axons.[7]

Here, we tested the hypothesis that the function of NMDARs in oligodendrocytes may also be impaired in patients with anti-NMDAR encephalitis. We provide proof-of-principle evidence that the activity of those receptors is robustly reduced in patients with anti-NMDAR encephalitis and that these changes affect the expression of GLUT1.

Patients and Methods

Patients, Control Cerebrospinal Fluid Samples, and Monoclonal Antibodies

The 7 patients included in the study were selected from a previously reported cohort of cases with anti-NMDAR encephalitis.[3] All 7 patients fulfilled criteria of anti-NMDAR encephalitis,[8] and their random selection was based on the amount of cerebrospinal fluid (CSF) available for the current studies. The median age was 16 years (range = 10–25 years), and 4 were female. In all cases, the CSF was obtained during the acute stage of the disease, and all were negative for glial autoantibodies such as aquaporin-4, myelin oligodendrocyte glycoprotein, and glial fibrillary acidic protein. By the time of diagnosis (in all cases within 4 weeks of disease onset), 6 patients had normal clinical MRI studies, and 1 had a 0.2mm abnormality on fluid-attenuated inversion-recovery (FLAIR)/T2 sequences in the right temporal lobe. NMDAR antibody titers were determined by serial dilutions of CSF using a cell-based assay (median = 1/160, range = 1/20–1/640). For controls, we used the CSF of 3 patients with noninflammatory mild cognitive decline and 4 patients with normal pressure hydrocephalus who were negative for NMDAR antibodies. The effect of the same patients' CSF antibodies (and lack of effect of control CSF) had been previously reported in investigations using cultured neurons and cerebroventricular transfer of CSF antibodies to mice, resulting in robust NMDAR internalization, impairment of hippocampal long-term potentiation, and memory deficits.[9] In all instances, the CSF samples had been dialyzed against phosphate-buffered saline and the exclusion of other antibodies confirmed with tissue immunohistochemistry and NMDAR immunoabsorption experiments.[9]

Pooled CSF from the 3 patients with the highest NMDAR antibody titers (all >1:80) was immunoabsorbed with HEK293T cells expressing the GluN1 subunit of the NMDAR or cells not expressing this subunit, as previously reported.[10] A recombinant monoclonal human antibody (SSM5) derived from intrathecal plasma cells of a patient with anti-NMDAR encephalitis and a control isotype against an irrelevant antigen (12D7) were used in some assays. The high specificity of SSM5 and its effects on mice behavior and synaptic NMDARs (which were similar to those caused by pooled CSF from patients) and the lack of effect of 12D7 have been previously reported.[11]

Animal Ethics Statement

This study was carried out in accordance with the recommendations and approval of the internal animal ethics committee of the University of the Basque Country (UPV/EHU), in accordance with the European Communities Council Directive. Rats of both sexes were used for all experiments.

Oligodendrocyte Culture

Highly enriched cultures of oligodendrocytes were prepared from mixed glial cultures obtained from newborn Sprague–Dawley rat forebrain cortices as previously described.[12] Briefly, after detaching from mixed cultures, oligodendrocyte progenitor cells were seeded onto poly-D-lysine-coated coverslips and cultured at 37°C and 5% CO_2 in SATO differentiation medium containing the following: 1mg/ml bovine serum albumin, 100μg/ml transferrin, 16μg/ml putrescine, 40ng/ml thyroxine, 30ng/ml tri-iodothyronine, 60ng/ml progesterone, 40ng/ml sodium selenite, 63μg/ml N-acetyl-cysteine, 5μg/ml insulin (all from Sigma-Aldrich, St Louis, MO); and 2mM L-glutamine plus 10ng/ml CNTF and 1ng/ml NT3 (both from PeproTech, Rocky Hill, NJ) to induce oligodendrocyte maturation for 6 days. At this stage, the majority of cells expressed myelin basic protein, a marker of mature oligodendrocytes (Fig 1A).

Cytosolic Ca^{2+} Imaging

Oligodendrocytes were incubated with each individual patient or control CSF sample (diluted 1:50) at 37°C for 4 hours, and the effect on NMDA-mediated cytosolic [Ca^{2+}] was measured as reported.[13] In brief, after incubation with patient or control CSF, oligodendrocytes were loaded with Fluo-4 AM (1mM; Molecular Probes;

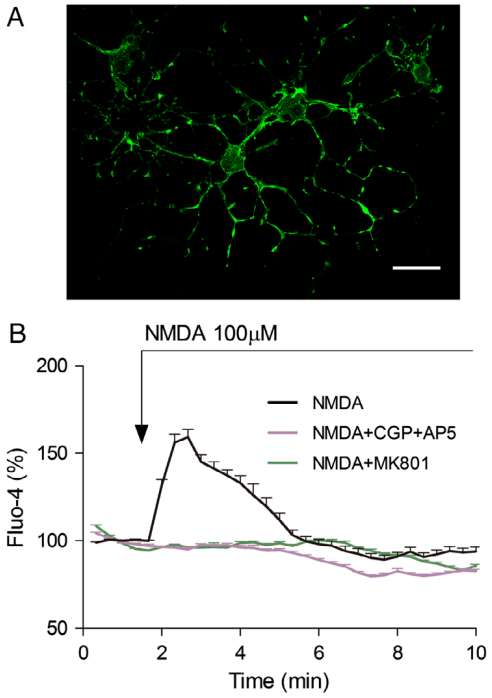

FIGURE 1: Functional assay of N-methyl-D-aspartate (NMDA) receptor (NMDAR) responses in oligodendrocyte cultures derived from the rat forebrain. (A) Myelin basic protein staining showing the typical branched appearance of oligodendrocytes in these cultures. Bar = 30μm. (B) Recordings of Ca^{2+} responses following application of NMDA plus glycine (both at 100μM; *arrow*) using Fluo-4. Responses are blocked in the presence of NMDAR antagonists CGP39551 (1μM) and AP5 (100μM; NMDA + CGP + AP5) and MK801 (50μM; NMDA + MK801). In all instances, data represent the average ± standard error of the mean of values obtained from at least 2 to 3 different cultures and analyzed using one-way analysis of variance with Tukey post-test (NMDA alone vs NMDA plus antagonists, $p < 0.001$).

Invitrogen, Barcelona, Spain) in incubation buffer for 30 minutes at 37°C followed by 20 minutes wash to allow de-esterification. Oligodendrocytes were then exposed to NMDA applied together with glycine (both at 100μM), and the Ca^{2+} images were acquired through a 40X objective by an inverted LCS SP8 confocal microscope (Leica, Wetzlar, Germany) at an acquisition rate of 1 frame/10 seconds during 5 minutes. For data analysis, a homogeneous population of 15 to 25 cells per coverslip was selected in the field of view, and oligodendrocyte somata were selected as region of interest. Background values were always subtracted and data expressed as F/F0 ± standard error of the mean (SEM; %), in which F represents the fluorescence value for a given time point and F0 represents the mean of the resting fluorescence level. For each individual patients' CSF or control CSF, this experiment was repeated 3 times in oligodendrocyte cultures grown in identical conditions.

To confirm that the effects were related to NMDAR-specific antibodies, we ran similar experiments where oligodendrocytes were incubated with the indicated pooled patients' CSF preabsorbed with HEK293 cells expressing or not expressing GluN1 or with the monoclonal human anti-GluN1 (SSM5) or the corresponding isotype control (12D7) as reported.[11]

Immunofluorescence Staining

Cultured oligodendrocytes were processed for immunostaining as described previously.[14] Briefly, cells were fixed in 4% paraformaldehyde in phosphate-buffered saline and incubated with mouse antimyelin basic protein antibodies (1:500; BioLegend, San Diego, CA) or anti-GLUT 1 (1:250; Santa Cruz Biotechnology, Dallas, TX) followed by goat antimouse IgG Alexa Fluor-488 (1:400; Invitrogen) secondary antibody. Both 4′,6-diamidino-2-phenylindole (DAPI) and calcein-AM (Molecular Probes) staining were used to identify nuclei and cells, respectively. Cells were visualized with a laser scanning confocal microscope (LCS SP8) at the Analytic and High-Resolution Microscopy Facility in the Achucarro Basque Center for Neuroscience.

Statistical Analysis

CSF samples from each of the patients and controls (n = 7 each) were used to treat 3 different cultures at identical conditions. To analyze NMDA responses, calcium recordings were obtained from 15 to 25 cells for each sample and culture, and the mean of the responses for each sample was used for analysis. Data obtained with α-amino-3-hydroxy-5-methyl-4-isoxazolepropionic acid (AMPA) responses and with human monoclonal antibodies and isotype control were analyzed in a similar way. Statistical analysis for comparisons between multiple experimental groups was made using 1-way analysis of variance (ANOVA) with Tukey post hoc test. For comparisons among individual control and patients' CSF samples (n = 7 each), we normalized by the naive response to minimize the potential variability on NMDA response between cultures and analyzed the data using 2-tailed Student t test. To analyze GLUT1 expression, fluorescence intensity was recorded from 15 to 20 cells for each sample and culture. The mean of 3 different cultures was obtained for each condition. Statistical analysis was made using one-way ANOVA with Tukey post hoc test. All data are shown as mean ± SEM. In all cases, statistical analyses were performed using Prism version 5.0 (GraphPad Software, San Diego, CA). Differences were considered statistically significant where $p < 0.05$.

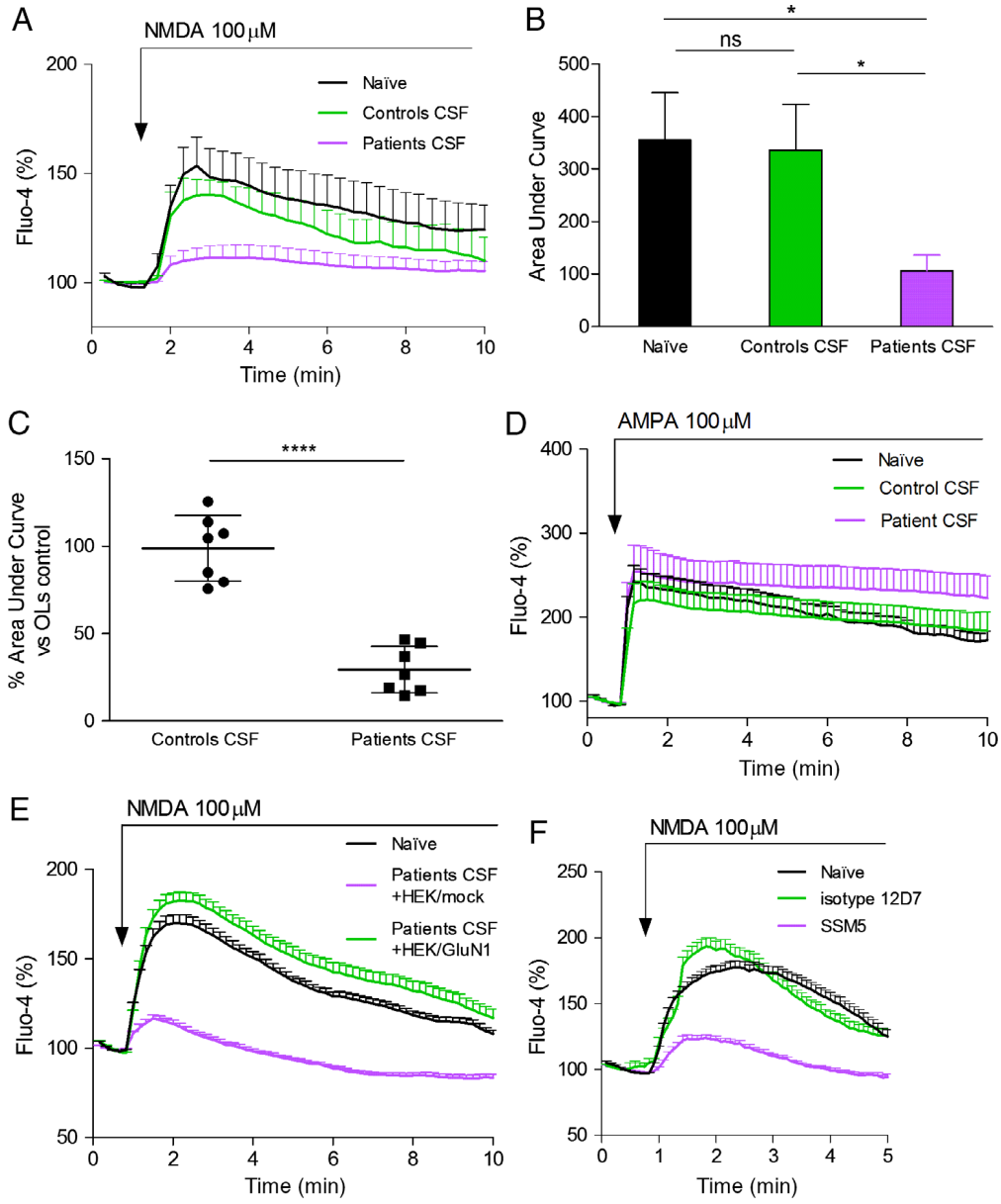

FIGURE 2: Specific N-methyl-D-aspartate (NMDA) receptor (NMDAR) responses in oligodendrocytes (OLs) in response to agonist application after incubation with patient and control cerebrospinal fluid (CSF). (A) Recordings of the basal Ca^{2+} responses in naive OLs (black trace, naive) were not significantly modified after incubation with CSF from control subjects (green trace, mean value of 7 control CSF samples in 3 different experiments) but were significantly reduced following exposure to patients' CSF (magenta trace, mean value of 7 patients' CSF samples in 3 different experiments); $p < 0.001$, one-way analysis of variance (ANOVA) with Tukey post-test. (B) Histogram depicting the area under the curve displayed by the recordings in (A). Note that the values after preincubation with CSFs from patients are lower than in control naive OLs or after preincubation with control CSF; *$p < 0.05$, one-way ANOVA with Tukey post-test. (C) Graph showing the effects of each individual CSF from controls or patients on the NMDAR responses in naive OLs (100%); ****$p < 0.001$, unpaired 2-tailed Student *t* test. (D) The α-amino-3-hydroxy-5-methyl-4-isoxazolepropionic acid (AMPA) receptor responses are similar in OLs not preincubated with CSF (naive, black) and those preincubated with control CSF (green) or patients' CSF (magenta). (E) Preabsorption of pooled patients' CSF in HEK cells transfected with GluN1 (green), but not with HEK cells mock transfected (magenta), results in NMDA responses similar to those of naive (black) OLs (naive vs patients' CSF + HEK/mock, $p < 0.001$; patients' CSF + HEK/GluN1 vs patients' CSF + HEK/mock, $p < 0.001$; one-way ANOVA with Tukey post-test). (F) Pretreatment of OLs with the human monoclonal NMDAR antibody SSM5, but not isotype control 12D7, abolishes the NMDA response (naive vs SSM5, $p < 0.001$; 12D7 isotype vs SSM5, $p < 0.001$; one-way ANOVA with Tukey post-test). In all graphs, data of each sample represent the average ± standard error of the mean of values obtained from 3 different cultures. n.s. = not significant.

Results

NMDARs are highly permeable to Ca^{2+} upon activation by their endogenous ligands. Because of that, we set an assay to evaluate whether patients' antibodies were able to alter NMDAR function using Fluo-4, a calcium indicator that exhibits an increased fluorescence upon binding Ca^{2+}, and time-lapse fluorescence microscopy. Cultured oligodendrocytes exposed to NMDA applied together with glycine induced a robust and fast increase in cytosolic Ca^{2+} with a peak amplitude of 159 ± 4% compared with resting levels (100%) that progressively decreased to baseline by around 5 to 10 minutes of stimulation (see Fig 1B). To assess the specificity of the responses triggered by NMDA and glycine, we used CGP39551 (1μM) and AP5 (100μM), 2 potent, selective and competitive NMDAR antagonists, as well as MK801 (50μM), a noncompetitive antagonist that binds to a site located within the NMDAR-associated ion channel and thus prevents Ca^{2+} flux. In all instances, the responses to NMDA and glycine were abolished in the presence of these antagonists (see Fig 1B).

The profile and amplitude of agonist responses were not significantly altered by preincubation of oligodendrocytes for 4 hours with CSF obtained from controls (peak response = 140 ± 7% vs 154 ± 13% for naive oligodendrocytes; Fig 2A). Instead, after preincubation with CSF from patients with anti-NMDAR encephalitis, the cytosolic Ca^{2+} responses to NMDA plus glycine exhibited a sharp reduction (maximal amplitude = 111 ± 5%), indicative of a strong reduction in the number of receptors being available to the agonists in the oligodendrocyte plasma membrane (see Fig 2A).

To further analyze the changes in the responses during the whole period of recording, we calculated the area under the curve to compare the levels of Ca^{2+} accumulated over the time window examined. This analysis revealed that CSF from healthy donors on average did not significantly alter Ca^{2+} cytosolic load over time after incubation with the agonists (336 ± 87% vs 355 ± 91% in naive cells). In contrast, CSF from patients with anti-NMDAR encephalitis nearly abolished the response (106 ± 30% vs agonists alone or control CSF, $p < 0.05$, in both instances; see Fig 2B). An individual analysis of the effects of CSF from patients showed different levels of NMDAR remaining functionality ranging from 15 to 47% (see Fig 2C), whereas CSF from controls had little or no effect (>76% or higher functionality preserved). The intensity of effects of patients' CSF antibodies correlated with CSF antibody titers in 6 of 7 patients (data not shown).

As AMPA receptors (AMPARs) are highly expressed in oligodendrocytes,[15] we tested whether activation of these receptors with AMPA applied together with cyclothiazide (both at 100μM) was affected by patients' CSF. Contrary to the robust effect of patients' CSF on the

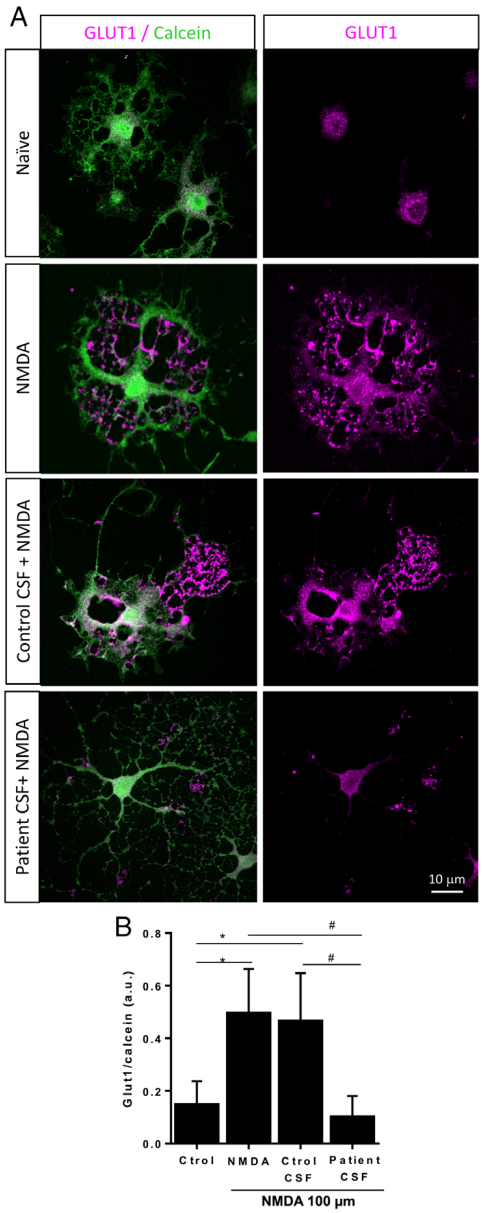

FIGURE 3: Effects of patients' cerebrospinal fluid (CSF) on the GLUT1 expression (magenta) in oligodendrocytes (green) after N-methyl-D-aspartate receptor (NMDA) receptor (NMDAR) activation. (A) First row (naive) shows minimal expression of GLUT1 (magenta) by oligodendrocytes (green) without NMDAR activation. Second row shows that the application of NMDA induces extensive expression of GLUT1. This NMDA-induced expression of GLUT1 is not affected if oligodendrocytes are preincubated with controls' CSF (third row) but is dramatically reduced if oligodendrocytes are preincubated with patients' CSF (fourth row). (B) Quantitation of results described in (A); *$p < 0.05$; #$p < 0.05$ using one-way analysis of variance with Tukey post-test. Oligodendrocytes are counterstained with calcein (green). Data represent the average ± standard error of the mean of values obtained from oligodendrocytes in 2 coverslips from 3 different cultures.

NMDAR-mediated responses, no effects were observed on the profile of AMPAR-mediated responses (see Fig 2D), strongly suggesting the specific blockade of NMDARs by patients' CSF.

The specificity of the changes in NMDAR-mediated responses caused by patients' CSF antibodies was further assessed with 2 different approaches. First, we used pooled patients' CSF samples preabsorbed with HEK293 cells expressing GluN1 or with cells not expressing this subunit (mock transfected cells). These experiments showed that the effect of patients' CSF antibodies were abrogated when CSF samples were preabsorbed with HEK293 cells expressing GluN1 but not with samples preabsorbed with HEK293 mock transfected cells (see Fig 2E). Second, we assessed the changes in oligodendrocyte NMDAR-mediated responses using a previously reported monoclonal human GluN1 antibody (SSM5) and the corresponding isotype control (12D7).[11] We found that pretreatment of oligodendrocytes with SSM5, but not 12D7, efficiently blocked the NMDAR-mediated responses (see Fig 2F). Taken together, these 2 sets of experiments provide robust evidence that the reduction of NMDAR-mediated responses in oligodendrocytes is mediated by patients' GluN1 antibodies.

NMDAR activity in oligodendrocytes mediates the translocation of GLUT1 to the membrane and myelin compartment, a feature that has structural consequences for the white matter.[7] Therefore, having shown that patients' CSF antibodies impaired NMDAR activation, we next determined whether they affected the NMDAR-dependent peripheral expression of GLUT1. These studies showed that the levels of GLUT1 were substantially reduced in secondary and tertiary processes of oligodendrocytes pretreated with patients' CSF antibodies but not controls' CSF (Fig 3). Overall, these findings provide a potential link between anti-NMDAR encephalitis and white matter alterations described in patients with this disorder.

Discussion

In this study, we show that treatment of oligodendrocytes with CSF from patients with anti-NMDAR encephalitis or a recombinant monoclonal antibody derived from plasma cells of a patient, but not the corresponding controls, decreased receptor activation by NMDA. These pathogenic effects were abrogated when patients' CSF was preabsorbed in NMDAR-expressing HEK293 cells, confirming the pathogenic role of the antibodies. Moreover, patients' CSF antibodies did not alter AMPAR function, suggesting a specific impairment in NMDAR activation. These antibody-mediated effects were associated with a reduced expression of GLUT1 in the distal processes of oligodendrocytes. Because expression of GLUT1 is important for axonal function, the findings suggest a novel pathogenic mechanism beyond the reported antibody effects on neuronal synaptic receptors and plasticity.

In oligodendrocytes, NMDARs control the supply of energy substrates to support the proper function of axons via GLUT1 translocation to the oligodendrocyte membrane.[7] Studies have shown that the amplitude of the action potentials in axons during high-frequency stimulation decreases in the absence of NMDAR in oligodendrocytes and recovers more slowly when returning at low frequency stimuli.[7] Prolonged loss of NMDAR function in oligodendroglia leads to axonal pathology and neuroinflammation in white matter tracts, resulting in neurological symptoms and motor dysfunction.[7] Although astrocytes can also support axonal function by releasing lactate in the white matter,[16] the direct oligodendrocyte–axon interaction is needed to adjust energy demands and prevent long-term structural damage.[7]

In a series of 577 patients with anti-NMDAR encephalitis, 67% had normal clinical MRI studies, and for the most part the other patients had mild or transient cortical-subcortical FLAIR abnormalities.[3] The high frequency of normal findings using standard MRI sequences was also indicated in a systematic review of the literature that included 1,167 patients, showing that 62% had normal MRI. Moreover, among the 38% of patients with abnormal findings, the subcortical white matter was as frequently involved as the gray matter.[17] In contrast, when a cohort of 24 patients was examined using MRI DTI sequences, all patients had widespread changes in white matter integrity that correlated with disease severity. Interestingly, 17 (71%) of these patients had normal standard clinical MRIs.[18] In another study of 46 patients with anti-NMDAR encephalitis (36 recovered and 10 unrecovered from the disease), the unrecovered patients showed widespread superficial white matter damage compared with the recovered patients and healthy controls who had normal findings.[4] Thus, anti-NMDAR encephalitis is associated with characteristic alterations of functional connectivity and widespread changes of white matter integrity, despite normal findings in routine clinical MRI.[18]

Based on the current findings and previously reported clinical and pathological studies in which cellular inflammatory infiltrates are usually mild without clear involvement of the white matter,[19] we postulate that the indicated MRI white matter changes may be directly mediated by NMDAR antibodies. The white matter effects, along with the previously reported impairment of synaptic function and plasticity,[9,20] would help explain the dissociation between symptom severity and frequently normal MRI clinical sequences (despite almost constant

DTI changes). A future task is to determine whether patients' antibodies alter white matter integrity in an existing animal model of passive transfer of antibodies,[21] examining changes in expression of GLUT1, how these changes correlate with white matter abnormalities (using rodent MRI studies), and the degree of reversibility of these alterations. These studies are important because there are currently no biomarkers of the course of the disease[22]; therefore, a better understanding of the white matter changes during the disease may lead to a potentially useful biomarker.

Acknowledgment

This study was supported by Biomedical Research Networking Center on Neurodegenerative Diseases (CB06/05/0076; C.M.) and by grants from the Ministry of Economy and Competitiveness (SAF2016-75292-R; C.M.), Basque Government (IT702-13 and PIBA2016; C.M. and M.D., respectively), Forschungskommission of Heinrich Heine University Düsseldorf, Germany (N.G.), Instituto de Salud Carlos III/FEDER (FIS 17/00234 and PIE 16/00014; J.D.), CIBERER CB15/00010 (J.D.), La Caixa Foundation Health Research Award (J.D.), AGAUR Generalitat de Catalunya (J.D.), Safra Foundation, and Fundació CELLEX (J.D.). A.P. and M.P.S.-R. hold fellowships from the University of the Basque Country and the Ministry of Economy and Competitiveness, respectively.

We thank S. Marcos for her expert assistance with tissue culture, Dr L. Escobar for her support with Leica TCS STED SP8 laser scanning confocal microscope, Dr J. Ballesteros, F. Soria, and T. Armangué for advice in statistics analysis, and the Animal Facility (SGIker) of the University of the Basque Country (UPV/EHU).

Author Contributions

C.M. and J.D. contributed to the conception and design of the study. All authors contributed to the acquisition and analysis of data. C.M. and J.D. contributed to drafting the text and preparing the figures.

Potential Conflicts of Interest

J.D.: royalties, Athena Diagnostics, Euroimmun; research project, SAGE Therapeutics.

References

1. Dalmau J, Geis C, Graus F. Autoantibodies to synaptic receptors and neuronal cell surface proteins in autoimmune diseases of the central nervous system. Physiol Rev 2017;97:839–887.
2. Dalmau J, Gleichman AJ, Hughes EG, et al. Anti-NMDA-receptor encephalitis: case series and analysis of the effects of antibodies. Lancet Neurol 2008;7:1091–1098.
3. Titulaer MJ, McCracken L, Gabilondo I, et al. Late-onset anti-NMDA receptor encephalitis. Neurology 2013;81:1058–1063.
4. Phillips OR, Joshi SH, Narr KL, et al. Superficial white matter damage in anti-NMDA receptor encephalitis. J Neurol Neurosurg Psychiatry 2018;89:518–525.
5. Peer M, Prüss H, Ben-Dayan I, et al. Functional connectivity of large-scale brain networks in patients with anti-NMDA receptor encephalitis: an observational study. Lancet Psychiatry 2017;4:768–774.
6. Nave KA, Werner HB. Myelination of the nervous system: mechanisms and functions. Annu Rev Cell Dev Biol 2014;30:503–533.
7. Saab AS, Tzvetavona ID, Trevisiol A, et al. Oligodendroglial NMDA receptors regulate glucose import and axonal energy metabolism. Neuron 2016;91:119–132.
8. Graus F, Titulaer MJ, Balu R, et al. A clinical approach to diagnosis of autoimmune encephalitis. Lancet Neurol 2016;15:391–404.
9. Planagumà J, Haselmann H, Mannara F, et al. Ephrin-B2 prevents N-methyl-D-aspartate receptor antibody effects on memory and neuroplasticity. Ann Neurol 2016;80:388–400.
10. Höftberger R, Sepulveda M, Armangue T, et al. Antibodies to MOG and AQP4 in adults with neuromyelitis optica and suspected limited forms of the disease. Mult Scler 2015;21:866–874.
11. Malviya M, Barman S, Golombeck KS, et al. NMDAR encephalitis: passive transfer from man to mouse by a recombinant antibody. Ann Clin Transl Neurol 2017;4:768–783.
12. Sánchez-Gómez MV, Serrano MP, Alberdi E, et al. Isolation, expansion, and maturation of oligodendrocyte lineage cells obtained from rat neonatal brain and optic nerve. Methods Mol Biol 2018;1791: 95–113.
13. Ruiz A, Alberdi E, Matute C. Cgp37157, an inhibitor of the mitochondrial na+/ca2+ exchanger, protects neurons from excitotoxicity by blocking voltage-gated ca2+ channels. Cell Death Dis 2014;5:e1156.
14. Arellano RO, Sánchez-Gómez MV, Alberdi E, et al. Axon-to-glia interaction regulates GABAA receptor expression in oligodendrocytes. Mol Pharmacol 2016;89:63–74.
15. Butt AM, Fern RF, Matute C. Neurotransmitter signaling in white matter. Glia 2014;62:1762–1779.
16. Brown AM, Ransom BR. Astrocyte glycogen and brain energy metabolism. Glia 2007;55:1263–1271.
17. Bacchi S, Franke K, Wewegama D, et al. Magnetic resonance imaging and positron emission tomography in anti-NMDA receptor encephalitis: a systematic review. J Clin Neurosci 2018;52:54–59.
18. Finke C, Kopp UA, Scheel M, et al. Functional and structural brain changes in anti-N-methyl-D-aspartate receptor encephalitis. Ann Neurol 2013;74:284–296.
19. Dalmau J, Tüzün E, Wu HY, et al. Paraneoplastic anti-N-methyl-D-aspartate receptor encephalitis associated with ovarian teratoma. Ann Neurol 2007;61:25–36.
20. Moscato EH, Peng X, Jain A, et al. Acute mechanisms underlying antibody effects in anti-N-methyl-D-aspartate receptor encephalitis. Ann Neurol 2014;76:108–119.
21. Planagumà J, Leypoldt F, Mannara F, et al. Human N-methyl D-aspartate receptor antibodies alter memory and behaviour in mice. Brain 2015;138:94–109.
22. Dalmau J, Armangué T, Planagumà J, et al. An update on anti-NMDA receptor encephalitis for neurologists and psychiatrists: mechanisms and models. Lancet Neurol 2019;18:1045–1057.

Author "Sumanta Barman" performed the synthesis of recombinant human monoclonal (rhuMab) NMDAR and isotype control antibodies. Co-authors used the monoclonal antibodies to evaluate the changes of NMDAR-mediated responses in oligodendrocyte. He also contributed to the acquisition, analysis and interpretation of data.

Published scientific article IV

Dose-dependent inhibition of demyelination and microglia activation by IVIG

ANNALS of Clinical and Translational Neurology
Open Access
ANA American Neurological Association since 1875

RESEARCH ARTICLE

Dose-dependent inhibition of demyelination and microglia activation by IVIG

Meike Winter[1,a], Christine Baksmeier[1,a], Julia Steckel[1], Sumanta Barman[1], Manish Malviya[1,b], Melanie Harrer-Kuster[2,c], Hans-Peter Hartung[1] & Norbert Goebels[1]

[1]Department of Neurology, Medical Faculty, Heinrich-Heine-University Duesseldorf, Moorenstr. 5, D-40225 Duesseldorf, Germany
[2]University of Zuerich, Clinical Neuroimmunology, Zuerich, Switzerland

Correspondence
Norbert Goebels, Department of Neurology, Medical Faculty, Heinrich-Heine-University Duesseldorf, Moorenstr. 5, D-40225 Duesseldorf, Germany. Tel: +49 211 810.4594;
Fax: +49 211 810.4597;
E-mail: norbert.goebels@uni-duesseldorf.de

Present addresses
[b]CPTP, Centre Physiopathologie de Toulouse-Purpan, INSERM U1043 - CNRS UMR5282-Université Toulouse III, Toulouse, France
[c]AbbVie AG, Baar, Switzerland

Funding Information
Grants of the German Ministry for Education and Research (BMBF) (31P7398, to NG) and the Forschungskommission of the Medical Faculty of the Heinrich-Heine-University Duesseldorf (HHU) funded this study.

Received: 13 August 2015; Revised: 25 April 2016; Accepted: 9 May 2016

Annals of Clinical and Translational Neurology **2016; 3(11): 828–843**

doi: 10.1002/acn3.326

[a]These authors contributed equally.

Abstract

Objective: Intravenous immunoglobulin (IVIG) is an established treatment for numerous autoimmune conditions. Clinical trials of IVIG for multiple sclerosis, using diverse dose regimens, yielded controversial results. The aim of this study is to dissect IVIG effector mechanisms on demyelination in an *ex vivo* model of the central nervous system (CNS)-immune interface. **Methods**: Using organotypic cerebellar slice cultures (OSC) from transgenic mice expressing green fluorescent protein (GFP) in oligodendrocytes/myelin, we induced extensive immune-mediated demyelination and oligodendrocyte loss with an antibody specific for myelin oligodendrocyte glycoprotein (MOG) and complement. Protective IVIG effects were assessed by live imaging of GFP expression, confocal microscopy, immunohistochemistry, gene expression analysis and flow cytometry. **Results**: IVIG protected OSC from demyelination in a dose-dependent manner, which was at least partly attributed to interference with complement-mediated oligodendroglia damage, while binding of the anti-MOG antibody was not prevented. Staining with anti-CD68 antibodies and flow cytometry confirmed that IVIG prevented microglia activation and oligodendrocyte death, respectively. Equimolar IVIG-derived Fab fragments or monoclonal IgG did not protect OSC, while Fc fragments derived from a polyclonal mixture of human IgG were at least as potent as intact IVIG. **Interpretation**: Both intact IVIG and Fc fragments exert a dose-dependent protective effect on antibody-mediated CNS demyelination and microglia activation by interfering with the complement cascade and, presumably, interacting with local immune cells. Although this experimental model lacks blood–brain barrier and peripheral immune components, our findings warrant further studies on optimal dose finding and alternative modes of application to enhance local IVIG concentrations at the site of tissue damage.

Introduction

Clinical trials have established Intravenous immunoglobulin (IVIG) as a well-tolerated, effective drug for the treatment of a wide variety of diseases, ranging from immunodeficiency to autoimmunity (for review see[1–4]). In neurology, IVIG serves as a mainstay therapy in immune-mediated neuropathies[5–8] and has been shown to be equally effective as plasmapheresis in Guillain-Barré Syndrome[9] and myasthenic crisis.[10,11] In multiple sclerosis, clinical trials applying different dose regimens and study designs (for review see[12–16]), yielded inconclusive results. More recently, IVIG has gained some attention as a treatment option for special forms of inflammatory CNS conditions, which are characterized by pathognomonic autoantibody signatures such as neuromyelitis optica,[16,17] yet larger controlled trials are still lacking.

Mechanistically, a plethora of therapeutic modes of action have been attributed to IVIG (for review see[3,4,18–21]). While a number of reports described effects of IVIG on

various cellular immune components, ranging from T cells,[22–27] B cells,[28,29] NK cells[30] and dendritic cells,[31] other authors stress the influence of IVIG on humoral autoimmunity, suggesting anti-idiotypic antibodies in IVIG, FcR engagement, inhibition of complement deposition and others (for review see[3,4,19,32]).

This study focused on IVIG effects on antibody-mediated immune mechanisms. We utilized murine organotypic cerebellar slice cultures (OSC) as an *ex vivo* model of the immune-CNS interface. As compared to primary cell cultures on the one hand and animal models on the other, the use of OSC has the advantage that the complex spatial microarchitecture of the CNS is maintained and effector mechanisms of CNS damage can be clearly defined, unobscured by the blood-brain barrier (BBB) and peripheral immune components.

Using transgenic mice, which express green fluorescent protein (GFP) in oligodendrocytes and myelin, allowed us to directly monitor demyelination in living OSC. Previously, we had demonstrated the usefulness of this model for the live imaging analysis of different immune effector mechanisms deemed relevant in CNS inflammation[33,34] as well as the process of CNS myelination itself.[35] Now we systematically evaluated - in a "checkerboard" fashion - multiple variables potentially influencing IVIG-mediated therapeutic effects on demyelination induced by a myelin-specific antibody and complement.

We demonstrated that the addition of IVIG efficiently inhibits antibody-mediated demyelination and microglia activation in OSC of the CNS. This effect clearly depended on the Fc part rather than the antigen-binding Fab fragment, since IVIG-derived Fab fragments could neither protect OSC from demyelination nor prevent microglia activation, suggesting a possible direct effect on microglia via binding to SIGN-R1. Interestingly, monoclonal IgG was incapable of exerting protection in a demyelinating environment. While IVIG did not substantially inhibit the binding of the demyelinating antibody to target structures, IVIG-mediated protection was overruled by increasing concentrations of complement. Our data argue for a direct effect of IVIG on cells of the CNS and on the complement cascade, thereby protecting oligodendrocytes in an inflammatory environment.

Material and Methods

Animal husbandry

Mice were bred at the animal facility of the Heinrich-Heine-University Duesseldorf under specific pathogen-free conditions. B. Zalc kindly provided PLP-GFP mice.[36,37] In these mice, GFP is expressed under regulatory elements of the PLP gene in oligodendrocytes and located in the cytosol as well as in the myelin sheath (B. Zalc, personal communication).

Media

Dissecting medium

A dissecting medium was used to dissociate the chopped cerebellar OSC from each other and consisted of Hank's Balanced Salt Solution with calcium and magnesium (HBSS, Invitrogen, Darmstadt, Germany), 100 U/mL penicillin, 100 μg/mL streptomycin (P/S, both Invitrogen), 5 mg/mL glucose (Sigma-Aldrich, Seelze, Germany) and 1 mmol/L kynurenic acid (Sigma-Aldrich). The pH was adjusted to 7.2-7.4.

Washing medium

A quantity of 50% HBSS, 50% MEM (Life-Technologies, Darmstadt, Germany), supplemented with P/S and 25 mmol/L HEPES (Sigma-Aldrich).

Culture medium

A quantity of 50% MEM supplemented with P/S, 25% HBSS supplemented with P/S, 25% horse serum (Sigma-Aldrich), 5 mg/mL glucose and 2 mmol/L glutamine.

OSC

OSC were prepared according to a modified protocol published by Stoppini *et al.*[38] Shortly, P9-P11 pubs were anesthetized, killed, the cerebellum was removed and cut into 400 μm thick slices using a McIllwain tissue chopper. OSC were then dissected manually in ice-cold dissecting medium and transferred to washing medium for 10 min on ice. OSC were cultured on cell culture inserts with a pore diameter of 0.4 μm (Millipore, Billerica, Massachsetts, USA) at 37°C and 5% CO_2 for 3–5 days and subsequently at 33°C and 5% CO_2 for the duration of the experiment.

Fab fragment preparation

Fab fragments were generated from whole IVIG by papain cleavage using a Fab Preparation Kit (Thermo Fisher Scientific GmbH, Darmstadt, Germany), according to the manufacturer's instructions. Fab fragments and IVIG were dialyzed against HBSS using a dialysis cassette (Thermo Fisher Scientific GmbH) prior to use.

Demyelination

Pooled, lyophilized normal baby rabbit serum (BRS) reconstituted in 1 mL of water was used as a source of complement (Cedarlane, Ontario, Canada). For clarity of this manuscript, BRS is referred to as "complement". Three to twelve percent (vol/vol) of complement were used together with 5-40 μg/mL recombinant humanized 8-18c5 (hu8-18c5 IgG1, kappa[39,40]), directed against MOG, for the duration indicated to induce demyelination.[33] IVIG (Privigen®, CSL-Behring, Hattersheim, Germany; 1-12 mg/mL), monoclonal IgG (Rituximab®, Roche, Basel, Switzerland; 6 or 12 mg/mL), IVIG-derived Fab fragments (4 mg/mL), bovine serum albumin (BSA, Sigma; 6-12 mg/mL) or human serum albumin (HSA, CSL-Behring; 12 mg/mL) were added at the beginning of demyelination for the duration of the experiment as indicated. Prior to use, Fc fragments, IVIG, HSA, Rituximab, and Fab fragments were dialyzed against HBSS. BSA was dissolved in HBSS.

Flow cytometry

To better quantify the fraction of living oligodendrocytes and microglia, single-cell suspensions were prepared by enzymatic digestion of OSC in HBSS + 0.5% BSA using the Neural Tissue Dissociation Kit-Postnatal Neurons (Miltenyi Biotec, Bergisch Gladbach, Germany) according to the manufacturer's recommendations, stained with Fixable Viability Dye (eFluor 450, eBioscience, San Diego, California, USA) and anti-CD11b PerCP-Cy™5.5 (eBioscience), fixed with 4% PFA/PBS and analyzed by flow cytometry (BD FACS Canto ™ II). GFP positive cells not stained by eFluor 450 were quantified as "living oligodendrocytes". CD11b positive cells not stained by eFluor 450 were quantified as "living microglia". Living oligodendrocytes and living microglia were expressed in percent of all living and gated cells.

Quantification of fluorescence

For the quantification of the relative myelin content of OSC during demyelination, we assessed the intensity of GFP expression in living OSC at different time points during each experiment: Using ImageJ software, we assessed the area of fluorescence signal exceeding a defined threshold in digital images acquired with an Olympus BX51 microscope (Hicksville, NY) at 4× magnification. The threshold was chosen according to the background intensity, and only the specific GFP expression was quantified. For each individual OSC, results are depicted relative to time point 0, prior to the beginning of the experiment.

Immunostaining of OSC

OSC were fixed in 4% paraformaldehyde (PFA, Sigma-Aldrich) dissolved in PBS (Life-Technologies) for 1 h at room temperature, permeabilized with 1% Triton X-100 (Thermo-Scientific) in PBS for 30-45 min and blocked with 10% normal goat serum (Sigma-Aldrich) in 0.2% Triton X-100 in PBS for 1 h after 3 washes with PBS. Primary antibodies (anti-NF200, N52, Millipore; anti-CD68, FA-II, BioLegend, San Diego, CA) were diluted in PBS supplemented with 1% goat serum and 0.2% Triton X-100, according to the manufacturer's instructions and were incubated for 2-3 days at 4°C. After three consecutive washes in PBS, OSC were incubated overnight with secondary antibodies (goat α mouse-Cy5 and goat α rabbit-Cy3, both Millipore), diluted in PBS, supplemented with 1% goat serum and 0-2% Triton X-100 according to the manufacturer's instructions at 4°C in the dark. Images were acquired using an LSM500 confocal laser-scanning microscope (Zeiss, Oberkochen, Germany) and analyzed with Zen black software (Zeiss), ImageJ, and Photoshop. Some images were contrast enhanced to facilitate visibility in composite figures.

Quantitative RT-PCR

RNA was isolated from a single OSC following a standard TRIZOL protocol. cDNA was synthesized using Super-Script III Reverse Transcriptase (Invitrogen) and oligo-dT (Invitrogen). Quantitative PCR was performed according to the manufacturer's instructions, using the SensiFAST™ Probe Lo-ROX Kit from Bioline (London, UK). Primer-Probe sets specific for glyceraldehyde 3-phosphate dehydrogenase (GAPDH, Mm99999915_g1), myelin basic protein (MPB, Mm01266402_m1), CNPase (Cnp, Mm01306640_m1), Iba1 (Mm00479862_g1), NG2 (Mm00507257) and NF200 (Mm01191456_m1) were purchased from Life Technologies. PCR was performed in an ABI Prism 7500 (Applied Biosystems, Darmstadt, Germany) with 45 cycles. Gene expression was normalized to GAPDH and the untreated control.

Results

IVIG inhibits immune-mediated demyelination in a dose-dependent manner

We induced demyelination in OSC with 5 μg/mL recombinant humanized MOG-specific antibody and 6% complement as described previously.[33] This treatment induces rapid and pronounced demyelination, which can be monitored by the quantification of the GFP fluorescence emitted by intact myelin/oligodendrocytes (as described in

Material and Methods) before and during treatment. In untreated OSC, GFP-fluorescence remained stable (or slightly increased due to still ongoing myelination) during the observation period of several days, while demyelinated OSC showed a progressive decrease in GFP-fluorescence over time. IVIG itself, with or without complement, had no effect on myelin integrity (Fig. S2), whereas the addition of IVIG significantly reduced the decrease of GFP-fluorescence in OSC treated with anti-MOG antibody and complement (Fig. 1B) in a dose-dependent fashion. The addition of BSA (12 mg/mL) as a control protein had no effect on demyelination (Fig. 1A and B). Likewise, HSA (12 mg/mL) did not inhibit demyelination (Fig. S1). In Figure 1 A representative images of the GFP-expression are depicted. For confocal microscopy, fixed OSC were counterstained with an antibody specific for the axonal protein NF200. As we have shown previously,[33] anti-MOG antibody and complement efficiently caused demyelination, while axons remained largely intact (Fig. 1C). Whereas axons in the anti-MOG/complement-treated group were demyelinated, myelin was well preserved at the two highest concentrations of IVIG (6 and 12 mg/mL). Additionally, we analyzed gene expression in OSC one and 2 days after the beginning of demyelination, when antibody and complement were still on the slices (Fig. 2A). The kinetics of mRNA-expression of the myelin genes MBP and CNPase paralleled the degradation of GFP in demyelinating OSC (Fig. 2B and C), supporting that the time course and extent of demyelination is adequately represented by the quantification of GFP-fluorescence. On the level of gene transcription, IVIG at a concentration of 6 mg/mL ameliorated the reduction of myelin-associated gene-expression. Interestingly, the expression of Iba1, a marker for microglia, was also reduced in demyelinating

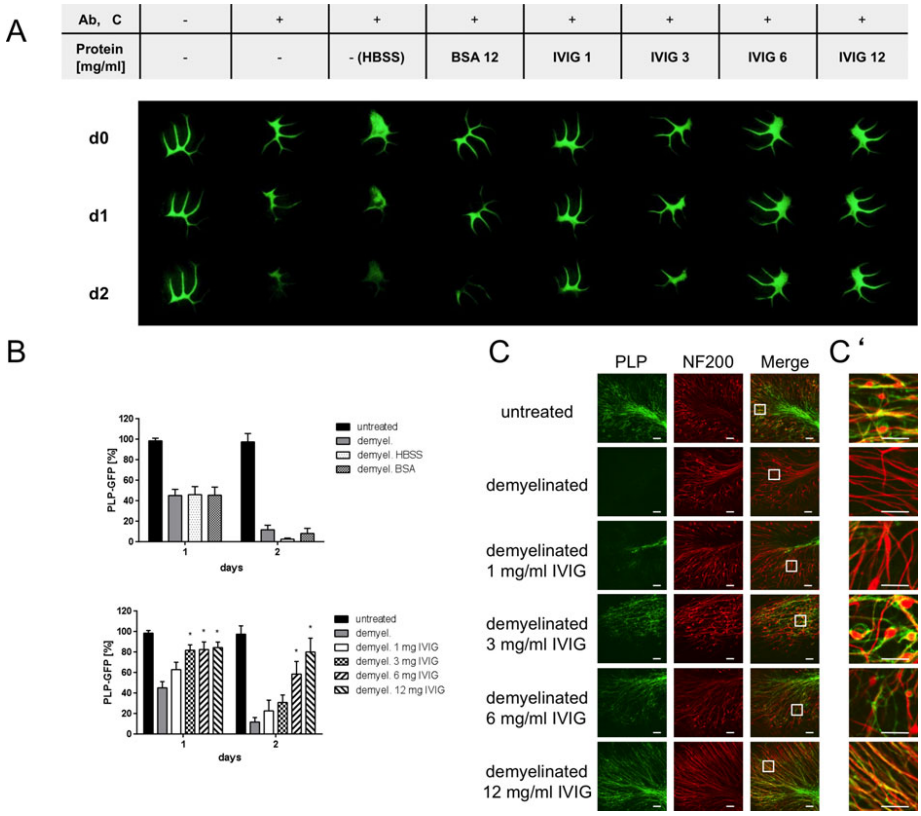

Figure 1. Intravenous immunoglobulin (IVIG) inhibits immune-mediated demyelination in organotypic cerebellar slice culture (OSC). OSC were treated as indicated and green fluorescent protein (GFP)-expression was assessed in living OSC using a fluorescence microscope 1 and 2 days after the induction of demyelination. Quantification was performed with Image J Software. After 2 days, OSC were fixed, stained with anti-NF200 antibody and analyzed via confocal microscopy. (A) Representative images (40× magnification) of PLP-GFP-expression: IVIG suppresses immune-mediated demyelination in a dose-dependent fashion. (B) Quantification of the GFP^+ area relative to day 0 (n = 6 OSC per group); Upper graph: Addition of irrelevant protein bovine serum albumin (12 mg/mL) or solvent (HBSS) does not inhibit demyelination. Lower graph: IVIG inhibits demyelination in a concentration-dependent manner. (C) Representative confocal images: IVIG preserves the myelin sheath around axons. (C′) Magnification of boxed area. Scale bars (C) 50 μm (C′) 25 μm. Significances were calculated in respect to the demyelinated control using one-way analysis of variance and Dunnett's post hoc test. $^*P \leq 0.05$. Values are depicted as mean ± SEM.

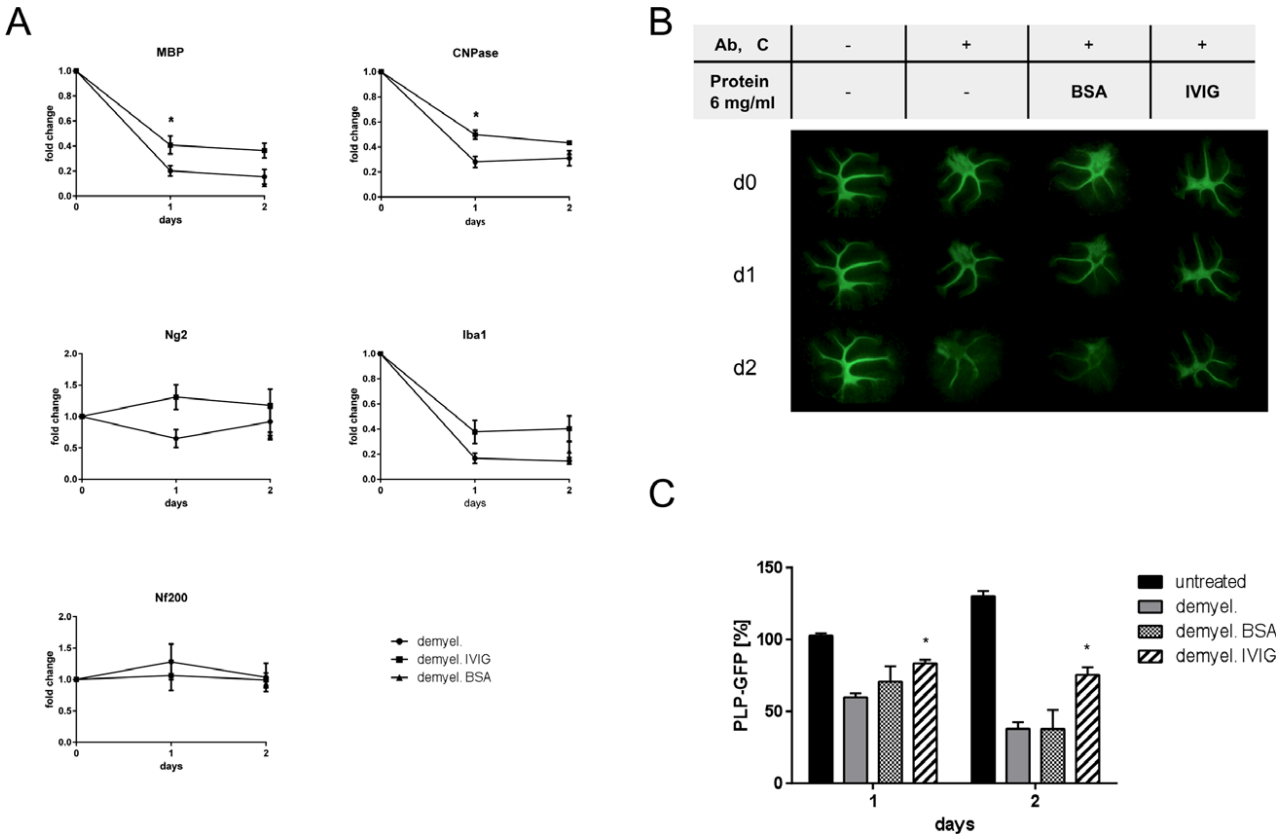

Figure 2. Intravenous immunoglobulin (IVIG)-mediated protection of oligodendrocytes in demyelinated organotypic cerebellar slice culture (OSC) is reflected on the level of gene expression. OSC were demyelinated with 5 μg/mL anti-MOG antibody and 6% complement alone (circles), with additional 6 mg/mL IVIG (squares) or with additional 6 mg/mL bovine serum albumin (BSA) (triangles). The expression of indicated genes was assessed 1 and 2 days after the onset of demyelination via quantitative rtPCR. Values for BSA treated controls (triangles) were determined for day two only. (A) Expression of indicated genes normalized to GAPDH, relative to the untreated control: While gene expression of axonal (neurofilament N200) and oligodendrocyte progenitor cell (NG2) markers is hardly affected by demyelination/IVIG treatment, IVIG treatment protects against demyelination-induced reduction in gene expression of myelin (MBP, CNPase) and microglial (Iba1) gene expression. Significances were calculated with the student's *t*-test. (B) Representative images of PLP- green fluorescent protein (GFP) expression of OSC used for RT-PCR on days 1 and 2. (C) Quantification of the GFP$^+$ area (n = 3–6 OSC per group): IVIG but not BSA inhibits demyelination of OSC. Significances were calculated in respect to the demyelinated control using one-way analysis of variance and Dunnett's post hoc test. *$P \leq 0.05$. Values are depicted as mean ± SEM.

OSC. This effect was partially inhibited by IVIG (Fig. 2A). Corresponding to our results from confocal microscopy, mRNA expression of the axonal marker NF200 was not affected by either demyelination or IVIG treatment. Similarly, NG2 expression remained relatively stable, indicating that neither the demyelination-treatment, nor IVIG had a strong influence on the population of oligodendrocyte precursor cells (Fig. 2A).

IVIG prevents immune-mediated oligodendrocyte death in anti-MOG antibody and complement-treated OSC

For a better quantification of this protective effect, we additionally analyzed oligodendrocyte and microglia survival by flow cytometry: Single cell suspensions, prepared from untreated and treated OSC following enzymatic dissociation, were stained with Fixable Viability Dye eFluor 450 and CD11b (both eBioscience) before flow cytometry. GFP+ cells not stained by eFluor 450 were quantified as "living oligodendrocytes" and expressed in percent of all gated living cells (Fig. 3). As expected, the percentage of living oligodendrocytes was significantly decreased in demyelinated OSC with or without the presence of BSA, while IVIG clearly promoted oligodendrocyte survival (Fig. 3). No significant effects were observed in the microglia population.

IVIG does not neutralize the binding of anti-MOG antibody

To further characterize the mechanisms underlying the IVIG-mediated inhibition of demyelination and cell

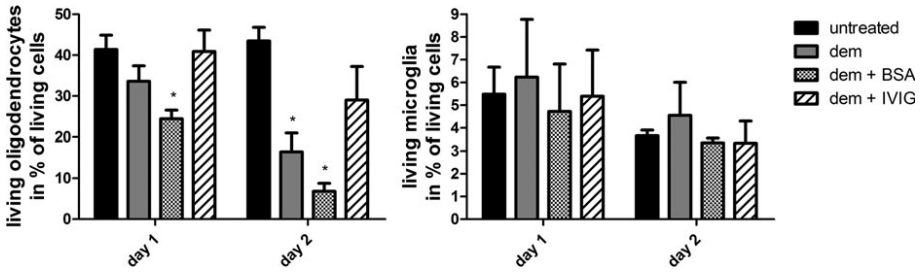

Figure 3. Intravenous immunoglobulin (IVIG) inhibits oligodendrocyte death in antibody-mediated demyelination. Organotypic cerebellar slice cultures (OSC) were demyelinated with 5 μg/mL anti-MOG antibody and 5% complement with or without 6 mg/mL IVIG or 6 mg/mL bovine serum albumin (BSA). One and two days after the onset of demyelination, single cell suspensions of OSC were stained for viability and microglia (CD11b), fixed and analyzed by flow cytometry (4 OSC per condition, oligodendrocytes $n = 4$, microglia $n = 3$). Green fluorescent protein (GFP) positive cells not stained by eFluor 450 were quantified as "living oligodendrocytes". CD11b positive cells not stained by eFluor 450 were quantified as "living microglia". Living oligodendrocytes and living microglia were expressed in percent of all living and gated cells. Demyelination in the absence or presence of BSA significantly reduced the percentage of viable oligodendrocytes, while the addition of IVIG prevented a significant relative reduction of viable oligodendrocytes. No significant effects on the viability of microglia cells were detected. Significances were calculated in respect to the untreated control using one-way analysis of variance and Dunnett's post hoc test. $*P \leq 0.05$. Values are depicted as mean $\pm$ SEM.

death, we analyzed whether IVIG interferes with the binding of the anti-MOG antibody to its cognate targets, e.g. by anti-idiotypic neutralization of anti-MOG antibodies. If that were the case, we would expect that increasing concentrations of pathogenic antibody counteract the protective effect of IVIG. To test this hypothesis, we stepwise raised anti-MOG antibody concentrations from 5 to 40 μg/mL. Yet, IVIG-mediated inhibition of demyelination was unaffected by increasing antibody concentrations as assessed by the quantification of GFP expression (Fig. 4A and B). Confocal micrographs confirmed that even at the highest anti-MOG antibody concentration (40 μg/mL), the integrity of myelin and axons were maintained by IVIG (Fig. 4B and B').

Furthermore, we investigated whether IVIG could possibly supplant anti-MOG antibodies from binding to their epitope on the myelin sheath. To this end, OSC were preincubated with 6 mg/mL IVIG for 3 days prior to fixation and IHC with the biotinylated anti-MOG antibody. Confocal colocalization of PLP-GFP-fluorescence (green) and anti-MOG staining (red) (Fig. 5) clearly indicates that binding of the anti-MOG antibody to its target structures was not affected by IVIG pretreatment. It therefore seems unlikely that IVIG exerts "anti-idiotypic" effects by IgG specific for the MOG epitope of the hu8-18c5 antibody or for the antibody used in the experiments itself.

IVIG-mediated protection is overruled by rising complement concentrations

To determine whether IVIG exerts its effects on demyelination by interfering with complement deposition and/or activation, we induced demyelination with 5 μg/mL anti-MOG antibody and varied the concentration of complement from 3% to 12%. As shown in Figure 6, at a complement concentration of 3%, only very mild demyelination occurred. Yet, raising the concentration of complement to 6%, 9% and 12% clearly led to increasing demyelination (Fig. 6A). While IVIG (6 mg/mL) significantly protected from demyelination at a complement concentration of 6%, this protection was overruled at complement concentrations of 9% and 12% (Fig. 6A and B), and demyelination occurred irrespectively of the presence of IVIG. These findings clearly support that IVIG interferes with complement deposition and/or activation in a dose-dependent fashion.

Interestingly, these effects were paralleled by morphological changes of tissue resident microglia cells: Confocal images revealed that in untreated slices and slices treated with anti-MOG antibody and 3% complement, $CD68^+$ microglia cells were small, ramified and evenly distributed within the tissue, resembling an inactivated state, irrespective of the presence of IVIG. In contrast, in slices treated with anti-MOG antibody and 6%, 9% or 12% complement, microglia cells displayed a typical activated phenotype and appeared rounded up, swollen, mainly being located at the sites of myelin destruction. In OSC demyelinated with anti-MOG antibody and 6% complement, IVIG prevented these morphological changes typical for microglia activation. Similar to demyelination, IVIG failed to prevent microglia activation when OSC were demyelinated with 9% and 12% complement, indicating that IVIG inhibits the activation of microglia cells by either direct or indirect interaction but can be overruled by excess concentrations of complement.

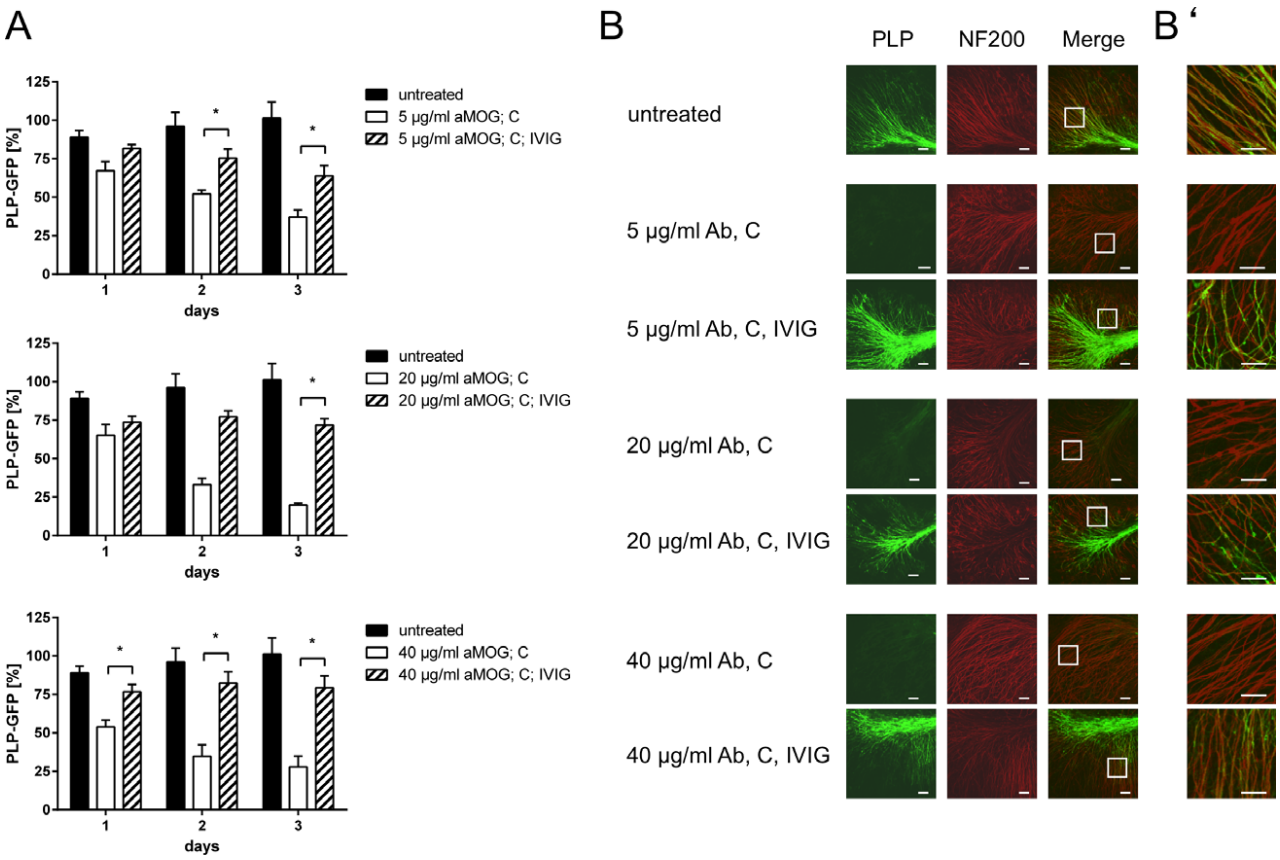

Figure 4. Intravenous immunoglobulin (IVIG)-mediated inhibition of demyelination is independent of the anti-MOG antibody concentration. Organotypic cerebellar slice cultures (OSC) were demyelinated with varying concentrations of anti-MOG antibody and 6% complement with or without 6 mg/mL IVIG. Green fluorescent protein (GFP)-expression in living OSC was assessed with a fluorescence microscope at days 1, 2 and 3. Quantification of GFP-fluorescence was performed with Image J Software. After 3 days, OSC were fixed, stained with anti-NF200 antibody and analyzed by confocal microscopy. (A) Quantification of the GFP^+ area ($n = 4$–6 OSC per group) showed that IVIG-mediated inhibition of demyelination was not overruled by increasing concentrations of the anti-MOG antibody. (B) Representative confocal images illustrate that 6 mg/mL IVIG preserved the integrity of myelin sheaths around axons at all concentrations of the anti-MOG antibody. (B′) Magnification of boxed area. Scale bars (B) 50 μm, (B′) 25 μm. Significances between the demyelinated condition with and without IVIG were calculated with the student's *t*-test. Control bars were included for better comparability. $*P \leq 0.05$. Values are depicted as mean ± SEM.

Myelin protection by IVIG depends on the Fc terminus, not the variable region

In order to elucidate which part of the immunoglobulin molecules present in IVIG is responsible for the observed effects, we cleaved IVIG to obtain pure Fab fragments via papain digestion. Figure 7A shows the purified denatured and native Fab fragments in lanes 2 and 4, respectively. OSC were demyelinated with 5 μg/mL anti-MOG antibody and 6% complement in the presence or absence of either 6 mg/mL IVIG or equimolar IVIG-derived Fab fragments. As control protein, 6 mg/mL BSA was added to demyelinating OSC. In contrast to intact IVIG, neither the Fab fragments nor BSA effectively suppressed demyelination (Fig. 7B and C). Confocal images revealed that only OSC, which were treated with intact IVIG, were still myelinated after 3 days. We additionally stained phagocytizing microglia with an anti-CD68 antibody. In untreated OSC, microglia appeared small, ramified and evenly distributed within the tissue, while microglia in demyelinated OSC had an activated phenotype and strongly expressed CD68. IVIG reduced microglial activation to control levels.

Additionally, we studied the effect of Fc fragments derived from a polyclonal preparation of human IgG. Interestingly, Fc fragments protected axons from demyelination even more efficiently than equimolar concentrations of IVIG: Both 1 and 2 mg/mL huFc protected myelin to about 75-90%, while 6 mg/mL IVIG inhibited myelin degradation only to about 60% (Fig. 8A). Confocal imaging confirmed that the addition of IVIG or equimolar amounts of huFc both inhibited microglia

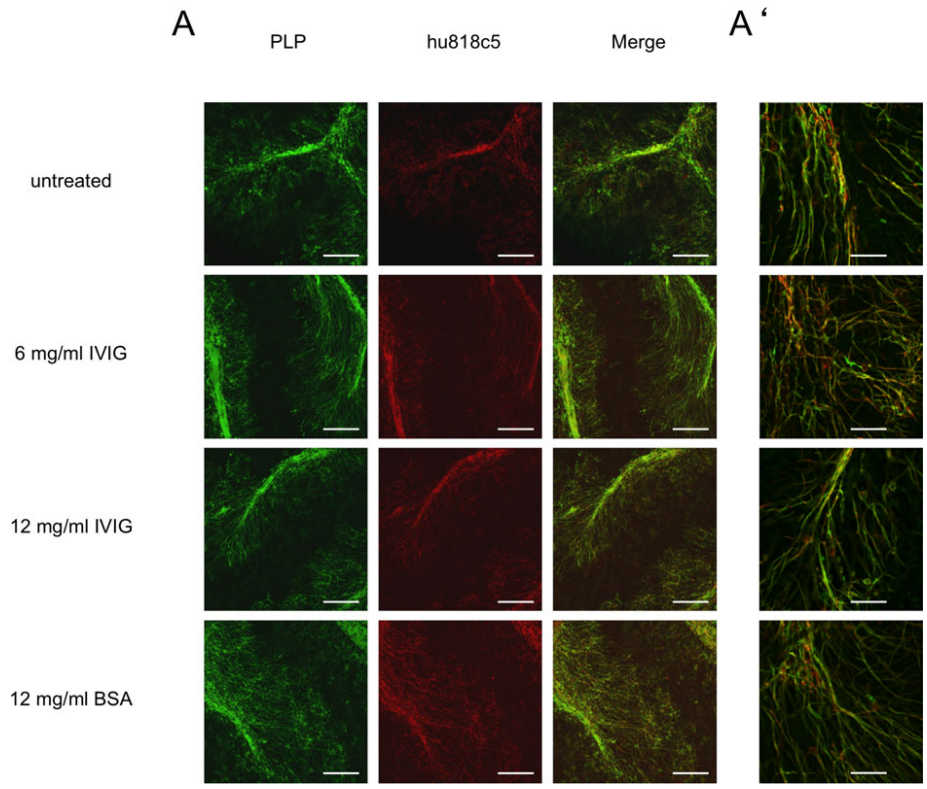

Figure 5. Intravenous immunoglobulin (IVIG) does not compete with the binding of anti-MOG antibody during demyelination. Organotypic cerebellar slice cultures were incubated with or without IVIG or bovine serum albumin (BSA) as indicated for 3 days and subsequently fixed and stained with a biotinylated hu8-18C5 anti-MOG antibody: The anti-MOG antibody used for demyelination in our experiments bound strongly to myelin irrespective of pretreatment with IVIG or BSA. Scale bars (A) 100 μm, (A') 50 μm.

activation and severe demyelination in anti-MOG antibody and complement-treated OSC (Fig. 8B).

IVIG-mediated protection seems to depend on specific modifications of the Fc terminus or the composition of isotypes

Since the great variety of IgG-specificities within the IVIG preparation apparently was dispensable for the observed protective effects, the question remained open, whether equal concentrations of a monoclonal IgG would suffice to inhibit demyelination in our model system. We therefore assessed whether the monoclonal antibody Rituximab® also inhibits immune-mediated demyelination in OSC. While 6 and 12 mg/mL IVIG clearly protected OSC from myelin degradation, Rituximab had no significant protective effect at either concentration (Fig. 9A and B). Likewise, while microglia activation was inhibited in IVIG-treated demyelinating OSC, microglia was highly activated in demyelinated OSC, which was not altered by the addition of Rituximab (Fig. 9B), arguing for the necessity of specific modifications of the Fc terminus of IgG antibodies.

Discussion

In this study, we aimed to assess direct protective effects of IVIG on CNS tissue during demyelination, a damage characteristic for multiple sclerosis.[41] As compared to animal models on the one hand and primary cell cultures on the other, the use of OSC as an *ex vivo* model of the CNS–immune interface has the advantage that effector mechanisms of CNS damage can be clearly defined while the complex spatial microarchitecture of the CNS is maintained.

To mimic immune-mediated demyelination, OSC were incubated with a humanized recombinant anti-MOG antibody together with complement for 2–3 days. At the concentrations of anti-MOG antibody and complement tested, this treatment resulted in rapid and severe demyelination and damage of oligodendrocytes, while axons remained largely intact for the duration of the experiment as shown before.[33] The addition of IVIG blocked this immune-mediated demyelination in a concentration-dependent manner, arguing for IVIG-dependent actions within the CNS that exceed the modulation of peripheral

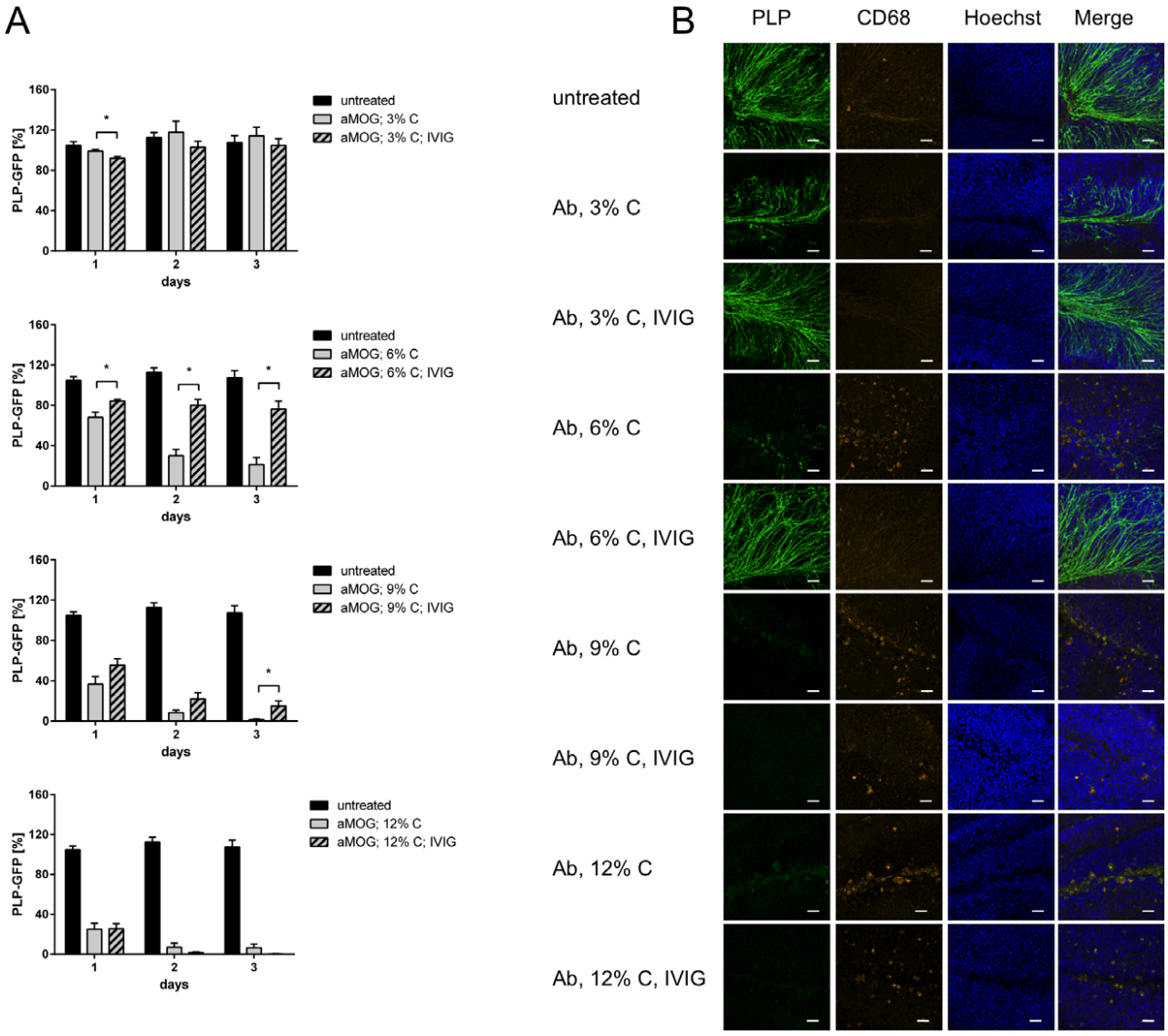

Figure 6. Intravenous immunoglobulin (IVIG)-mediated inhibition of demyelination is overruled by increasing concentrations of complement. Organotypic cerebellar slice cultures (OSC) were demyelinated with 5 μg/mL anti-MOG antibody and varying concentrations of complement with or without 6 mg/mL IVIG. Green fluorescent protein (GFP)-expression in living OSC was assessed with a fluorescence microscope at days 1, 2 and 3. Quantification was performed with Image J Software. After 3 days, OSC were fixed, stained with anti-CD68 antibody and Hoechst dye and analyzed by confocal microscopy. (A) Quantification of the GFP^+ area (n = 7–8 OSC per group): At the higher concentrations of complement, the protective effect of IVIG is abrogated. (B) Representative confocal images: At complement concentrations above 6%, IVIG does not preserve the myelin sheaths or prevent microglial activation. (B′) Magnification of boxed area. Scale bars (B) 50 μm, (B′) 25 μm. Significances between the demyelinated condition with and without IVIG were calculated with the student's t-test. Control bars were included for better comparability. $^*P \leq 0.05$. Values are depicted as mean ± SEM.

immune mechanisms. IVIG clearly reduced demyelination of axons as depicted in Figure 1, while albumin at the same concentrations did not affect demyelination, excluding effects merely due to a higher protein-concentration in the IVIG-treated cultures. This protective effect of IVIG was reproducible both by flow cytometry and on the level of gene expression: flow cytometry of single cell suspensions prepared from OSC confirmed a significant reduction of living oligodendrocytes induced by anti-MOG antibody and complement, irrespective of the presence of BSA, while in IVIG-treated OSC, the fraction of viable oligodendrocytes was not significantly reduced (Fig. 3). No significant effect on the viability of microglia cells was observed. Correspondingly, mRNA levels of the myelin genes MBP and CNPase were both lowered in demyelinating OSC, an effect which was reduced by IVIG.

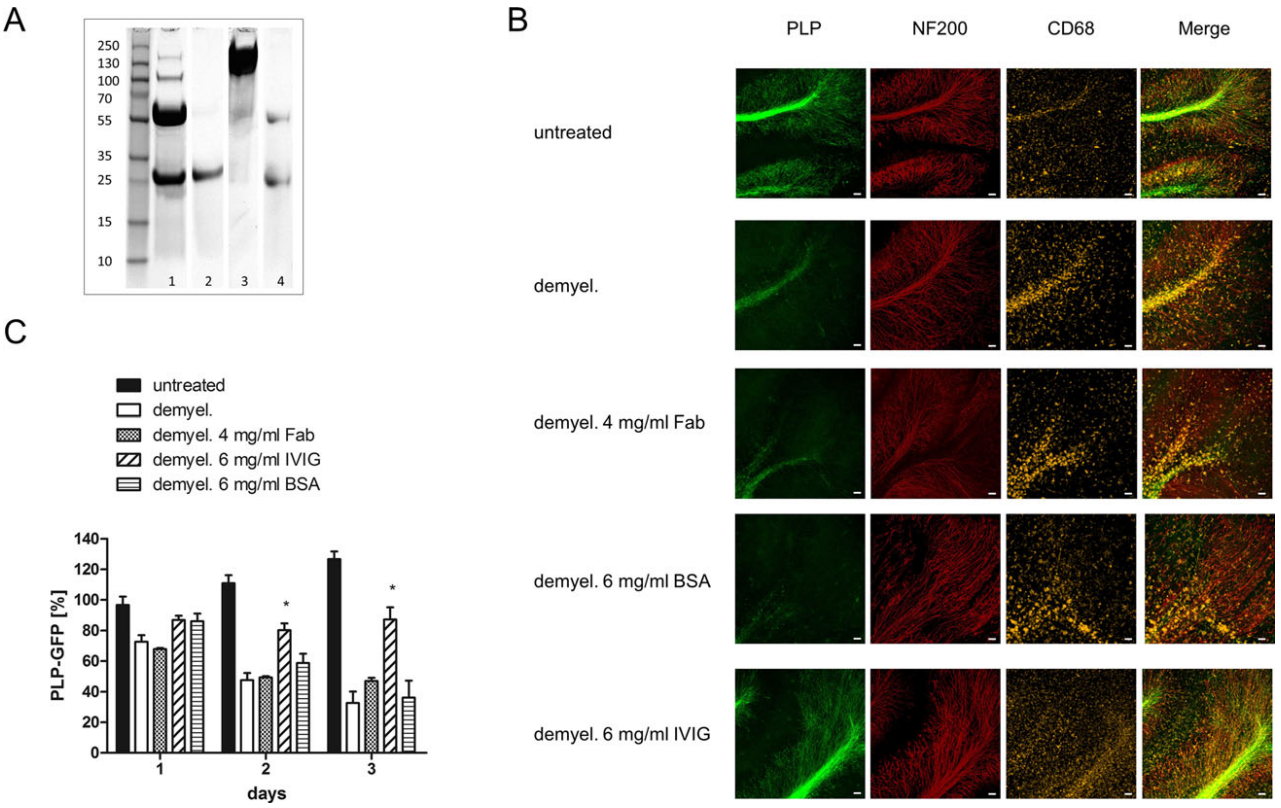

Figure 7. Ig-variable regions do not mediate intravenous immunoglobulin (IVIG)-mediated inhibition of demyelination. Polyclonal Fab fragments were generated from whole IVIG by papain cleavage (see material and methods). (A) To verify the purity of the preparation, Fab fragments were separated on a 12% SDS-gel under denaturing (lanes 1 and 2) or native (lanes 3 and 4) conditions. Lanes 1 and 3 show whole IgG, while lanes 2 and 4 show purified Fab fragments. (B, C) organotypic cerebellar slice culture (OSC) was demyelinated with 5 μg/mL anti-MOG antibody and 6% complement with or without 6 mg/mL IVIG, 4 mg/mL Fab fragment or 6 mg/mL bovine serum albumin (BSA) or were left untreated. Green fluorescent protein (GFP) expression in living OSC was assessed by fluorescence microscopy at days 1, 2 and 3. Quantification was performed with Image J Software. After 3 days, OSC was fixed, stained with anti-NF200 and anti-CD68 antibody and analyzed via confocal microscopy. (B) Representative confocal images: IVIG but not Fab fragments or BSA inhibit demyelination of axons and microglia activation. (C) Quantification of the GFP^+ area (n = 3 OSC per group): IVIG but not Fab fragments or BSA inhibit immune-mediated demyelination in OSC. Scale bar 50 μm. Significances were calculated in respect to the demyelinated control using one-way analysis of variance and Dunnett's post hoc test. $^*P \leq 0.05$. Values are depicted as mean ± SEM.

Paralleling microglia activation, mRNA expression of the microglia marker Iba1 was reduced in demyelinated OSC (Fig. 2A), in line with findings by Silverman and colleagues in a different experimental model.[42] Microglia cells in demyelinated OSC, when compared to the untreated controls, appeared swollen and rounded, resembling the morphology of highly activated, phagocytizing microglia. In untreated OSC, microglia appeared ramified and small, reflecting the phenotype of resting microglia (Figs. 6-9). As visualized by immunohistochemistry, IVIG strongly reduced microglia activation (Figs. 6-9) in demyelinating OSC, whereas BSA added instead of IVIG at the same concentration did not visibly modulate microglia (Fig. 7). Previously, it was demonstrated that IVIG influences microglia activation by different mechanisms, involving both Fc- and Fab-dependent pathways: Stangel and collegues showed, that IVIG activates matrix-metalloproteinase (MMP-9) in cultured microglia in vitro,[43] while earlier, the same group demonstrated that IVIG down regulates endocytosis via $F(ab')_2$-, and receptor-mediated phagocytosis by Fc-dependent mechanisms.[44] Additionally, IVIG was described to activate TNFα-secretion and NO-production in isolated microglia cells via Fc receptors.[45,46] These findings suggest that IVIG may influence both activating and silencing mechanisms in microglia, fine-tuning the activation status of these cells. Our data implicate that IVIG modulates microglia activation within the CNS tissue, which is likely to contribute to the preservation of myelin in OSC. Nevertheless, the question remains open whether modulation of microglia activation is a primary, direct effect of IVIG treatment or a result of IVIG-mediated reduction of oligodendrocyte/myelin damage in

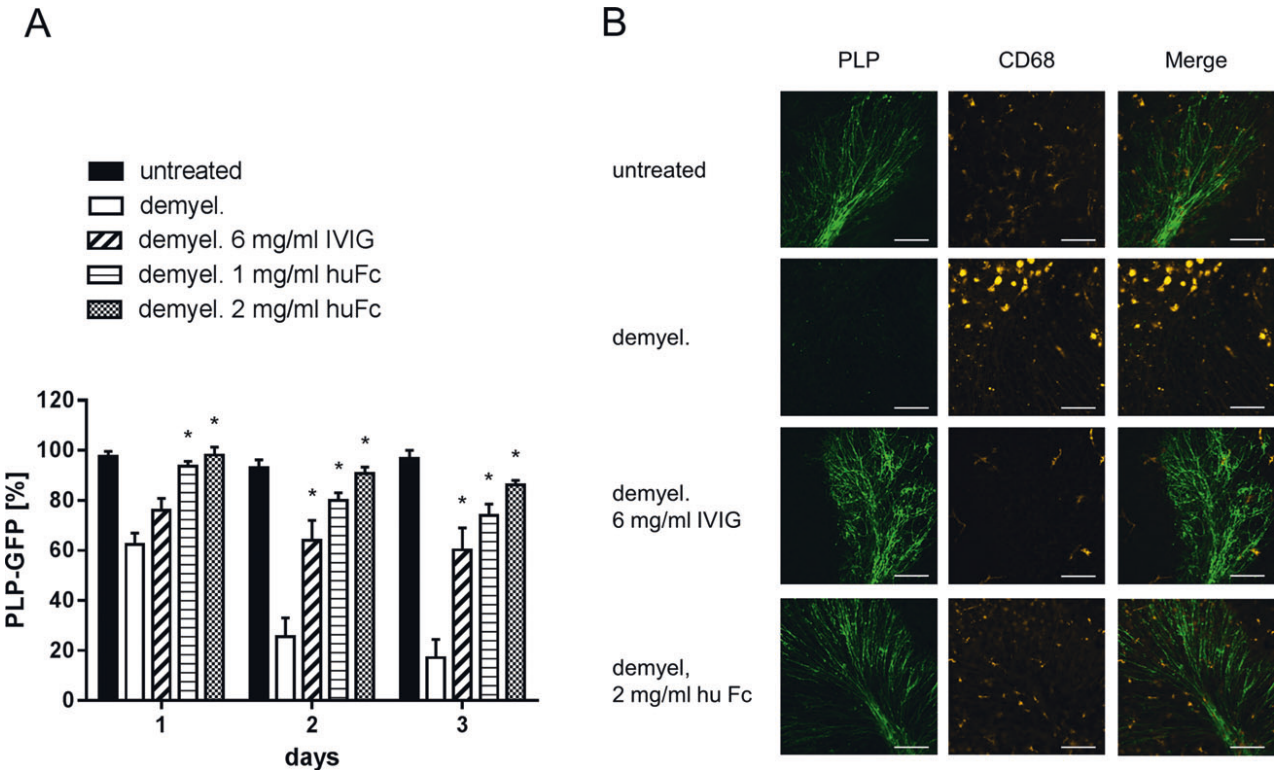

Figure 8. Intravenous immunoglobulin (IVIG) induced protection from demyelination is Fc-mediated. Organotypic cerebellar slice cultures (OSC) were demyelinated with 5 μg/mL anti-MOG antibody and 6% complement with or without 6 mg/mL IVIG or 2 mg/mL human polyclonal Fc fragment or were left untreated. Green fluorescent protein (GFP)-expression was assessed in living OSC under a fluorescence microscope 1, 2 and 3 days after the induction of demyelination. Quantification was performed with Image J Software. After 3 days, OSC were fixed, stained with an anti-CD68 antibody and analyzed via confocal microscopy. (A) Quantification of the GFP^+ area (n = 3-12 OSC per group): Fc fragments suppress demyelination even more potently than whole IVIG at an equimolar concentration. (B) Representative confocal images. Scale bars 100 μm. Significances were calculated in respect to the demyelinated control using one-way analysis of variance and Dunnett's post hoc test. $^*P \leq 0.05$. Values are depicted as mean ± SEM.

demyelinating OSC, leading to a secondary decrease of activation stimuli in the microenvironment of the inflamed brain tissue.

In line with our previously published data[33] axons were not affected by demyelination or by IVIG treatment, as shown by immunohistochemical staining and RT-PCR analysis of the axonal marker NF-200. At least within the time frame observed, oligodendrogenesis also did not seem to be influenced by IVIG, since IVIG did not alter NG2-expression in demyelinating OSC. BSA again had no effect on the expression of any gene assessed, excluding artifacts due to a higher concentration of protein in the culture medium.

Others and we have demonstrated that IVIG itself together with complement does not result in demyelination (Fig. S2,[47]), indicating that IVIG does not contain proportions of naturally occurring oligodendrocyte/myelin-specific antibodies sufficient to cause demyelination in the presence of complement. Alternatively, oligodendrocyte/myelin-specific antibodies contained in IVIG preparations may be of isotypes unsuited for complement-mediated lysis, e.g. IgG4, but sufficient to compete with "pathogenic" autoantibodies in patients with demyelinating diseases. To further address this point, we assessed, whether IVIG competes with the anti-MOG antibody for binding to its target epitope within the tissue, a prerequisite for efficient assembly of anti-MOG-C3b complexes at the oligodendrocyte surface. Confocal images show that preincubation of OSC with IVIG for 3 days does not reduce staining of myelinated structures with the anti-MOG antibody by immunohistochemistry (Fig. 5). Therefore, it seems unlikely that IVIG reduces demyelination by masking target epitopes of the anti-MOG antibody used for demyelination.

To further elucidate the mode of action of IVIG in our model, we varied concentrations of anti-MOG antibody or complement in separate experiments to dissect, whether IVIG interferes with either component. The

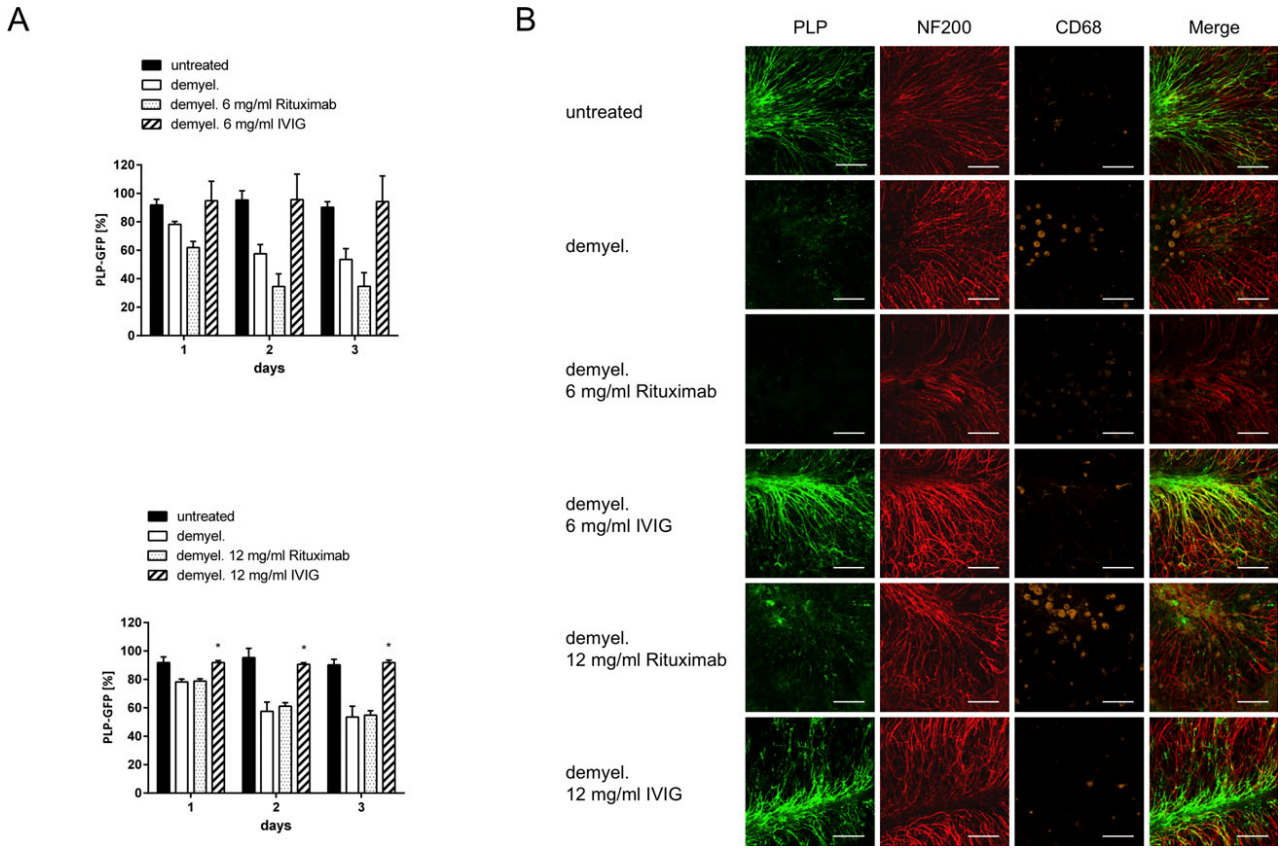

Figure 9. Monoclonal IgG does not protect organotypic cerebellar slice cultures (OSC) from immune-mediated demyelination. OSC were demyelinated with 5 μg/mL anti-MOG antibody and 6% complement with or without intravenous immunoglobulin (IVIG) or Rituximab or were left untreated as indicated. Green fluorescent protein (GFP)-expression in living OSC was assessed by fluorescence microscopy at day 1, 2 and 3. (A) Quantification of the GFP^+ area (n = 4–5 OSC per group) was performed with Image J Software: IVIG but not Rituximab suppresses demyelination in OSC. (B) Representative confocal images: IVIG but not the recombinant monoclonal antibody Rituximab prevents demyelination of axons and microglial activation. Significances were calculated in respect to the demyelinated control using one-way analysis of variance and Dunnett's post hoc test. $^*P \leq 0.05$. Values are depicted as mean ± SEM.

results were remarkably clear: While elevating the concentration of the anti-MOG antibody had no influence on IVIG-mediated protection of myelin, increasing the concentration of complement gradually overruled IVIG protection. This finding strongly argues for an interference of IVIG with the complement cascade, rather than anti-idiotypic blocking of anti-MOG-antibodies. This is partially congruent with the literature. Using FcRγ-/- and C1q-/- mice in a model of anti-MOG antibody enhanced experimental autoimmune encephalomyelitis (EAE), Becher and collegues demonstrated that - while the functional expression of FcRγ on systemic accessory cells appeared to be vital for the *development* of CNS inflammation - the *demyelinating* capacity of such autoAb *in vivo* relies on complement activation and is FcR-independent.[48] Since the 1990s, it is known that IVIG acts as acceptor for complement components like C3b and C4b, thereby scavenging them from cell-bound immune complexes.[49] However, the formation of soluble $C3b_2$-IgG complexes results in amplification of complement activation, rather than in attenuation, since these soluble complexes are even more effective in cleaving C3 and thereby amplifying the complement cascade than cell-bound complexes. IVIG however was shown to additionally lower the half-life of soluble $C3b_n$-IgG complexes both *in vitro* and *in vivo*, which reduces the concentration of C3-convertase and by that the nascence of reactive complement-factors and the proceeding of the complement-cascade.[50,51]

Since IVIG presumably interferes with the complement reaction, we asked the question, whether autoantibodies against complement components may scavenge complement factors from the medium, preventing the formation of membrane-bound C3b2-IgG complexes and subsequent lysis of oligodendrocytes. To this end we tested the effects of IVIG-derived Fab fragments versus human Fc fragments from a polyclonal preparation of IgG on

demyelination in our model. IVIG-derived Fab fragments could not provide protection from anti-MOG antibody and complement-mediated demyelination or microglia-activation, while Fc fragments were even more potent than complete IVIG in inhibiting demyelination (Figs. 7 and 8).

Several autoantibodies against complement factors have been described and in other studies anti-idiotypic effects of IVIG were found to be responsible for the scavenging of complement in various model systems.[52,53] We clearly show that blocking of complement by IVIG does not involve specific antigen binding via the variable antigen-binding regions (Fab fragments) of the IgG molecules contained in IVIG. Instead, our findings confirm that the Fc part of IVIG can interfere with the complement cascade, in line with Yuki *et al.*[54]

Both animal experiments and clinical evidence suggest that the modification pattern of the Fc terminus by sugar residues is crucial for the Fc-mediated therapeutic effects of IVIG. Ravetch and colleagues showed that sialyl-residues bound to the Fc region seem to be indispensable for certain effects.[55,56] Sialylated IgG preferably interacts with C-type lectins like the human DC-Sign (Dendritic Cell-Specific Intercellular adhesion molecule-3-Grabbing Non-integrin) or the murine homolog SignR1.[57] Park *et al.*[58]demonstrated mSign-R1 expressed on microglial cells in the cerebellum, identifying microglia as a likely target for IVIG-interference. The lack of sialyl residues in the monoclonal antibody Rituximab[59] may also be an explanation for its inability to protect from demyelination in our experimental system. In a recent study however, Campbell *et al.* showed that the therapeutic effects of IVIG in two antibody and complement-dependent models of arthritis are dependent on the Fc part but are independent of the sialylation pattern, putting the importance of Fc modifications up for debate.[60] We propose that in the complex microenvironment of the CNS, Fc-mediated effector-mechanisms of IVIG may play a pivotal role, possibly acting on both microglia and complement factors in parallel by distinct or cumulative mechanisms.

In summary we demonstrate that IVIG modulates immune-CNS interactions in a multimodal fashion: In our model of immune (antibody/complement)-mediated demyelination, the preservation of myelin seems to largely depend on the inhibition of the complement cascade by IVIG. Additionally, IVIG-mediated suppression of microglia activation may be an important effect of IVIG, even though this hypothesis is yet to be addressed. Our data clearly shows that in this model system the observed effects entirely depend on Fc-dependent mechanisms, while the variable Fab fragment is not needed to convey protection.

Taken together our findings raise a number of potential clinical considerations:

- On the one hand, the applied dose of IVIG needs to be sufficient to counteract complement factors. While in most "autoimmune" conditions an empirical standard dose of 2 g IVIG/kg bodyweight is applied, clinical trials in the past have used a variety of dosing regimens, possibly offering an explanation for controversial effects. Since complement factors seem to be a major target of IVIG at least in diseases with clear "antibody/complement" mediated effector mechanisms (such as myasthenia gravis and many others), measurements of serum complement activity or derivatives thereof may be helpful for "personalized" treatment regimens both with regard to dosage and frequency of application.
- While this is a relatively obvious conclusion from this study, it is also tempting to speculate on the potential beneficial direct effects of IVIG on a variety of CNS diseases. At first glance, the lack of a BBB in our experimental model seems to limit the interpretation of our findings with regards to a therapeutic *in vivo* situation. We found few data on the actual amount of systemically administered IVIG reaching the CNS compartment: van Engelen detected a mean increase of 44% in cerebrospinal fluid (CSF) IgG concentration in epilepsy patients after systemic IVIG delivery, with the extent of increase correlating with Q albumin, a measure of blood CSF permeability.[61] Wurster and Haas measured an intrathecal Ig concentration reaching close to 1% of the serum Ig concentration (0.317 g/L vs. 32.1 g/L) in a patient with polyradiculitis after infusion of 30 g IVIG.[62] More recent studies in rodents by Sha Mi and colleagues established that systemically applied therapeutic antibodies could reach the CSF in therapeutic concentrations.[63] Likewise, IVIG was detected "throughout the brain of injected mice, in capillaries, brain parenchyma and brain cells".[64] While these studies support that immunoglobulin may reach the mammalian CNS in spite of an intact BBB, this is expected to be even more the case in inflammatory CNS conditions characterized by (an at least partial) BBB breakdown: Hawkins and collegues described a partial enhancement of CNS lesions in chronic relapsing experimental encephalomyelitis by immunoglobulin added to gadolinium-DTPA (diethylenetriaminepentaacetic acid).[65]

  In spite of these promising reports, lacking systematic studies, we can currently not answer which proportion of systemically applied IVIG reaches the CNS compartment, nor can we estimate which local IVIG concentrations would be needed to achieve therapeutic effects. Nevertheless, in debilitating immune-mediated diseases namely MS, also an intrathecal application suitable to

deliver high local IVIG concentrations to the CNS may be worth considering.

- Since our study confirms that solely the Fc part of IVIG conveys protection from immune-mediated demyelination, future trials with recombinant forms of Fc fragments may be considered, for which Ravetch and collegues elegantly demonstrated anti-inflammatory activity if adequately sialylated.[56]
- In our study, we did not touch on the issue whether IVIG has an influence on remyelination in the OSC model of immune-induced demyelination, but it will be interesting to assess direct effects of IVIG within the CNS on remyelination processes in OSC in the future.[66]

Acknowledgments

Grants of the German Ministry for Education and Research (BMBF 31P7398, to NG) and the Forschungskommission of the Medical Faculty of the Heinrich-Heine-University Duesseldorf (HHU) funded this study. CB received a PhD stipend of the iBrain graduate school of the HHU. The support of the Biomedical Research Center of the HHU is gratefully acknowledged. The Multiple Sclerosis Center at the Department of Neurology, HHU, is supported in part by the Walter-and-Ilse-Rose Stiftung. HPH is a member of the "German Competence Network Multiple Sclerosis" (KKNMS), supported by the BMBF.

Author Contributions

M. W., C. B., N. G. conceived and designed the experiments. M. W., C. B., J. S., S. B., M. M., M. H.-K. performed the experiments. M. W., C. B., J. S., N. G. analyzed the data and M. W., C.B., H.-P. H., N. G. wrote the paper.

Conflict of Interest

NG received, with approval by the Rector of the Heinrich-Heine-University, travel support to scientific conferences from Bayer, Biogen, Genzyme, Novartis; research support (unrelated to this manuscript) from Novartis; honoraries for lectures (unrelated to this manuscript) from Biogen. HPH received fees for consulting and serving on steering committees from CSL Behring, Baxter, Novartis, Octapharma, with approval by the Rector of Heinrich-Heine-University.

References

1. Hartung HP, Mouthon L, Ahmed R, *et al*. Clinical applications of intravenous immunoglobulins (IVIg)–beyond immunodeficiencies and neurology. Clin Exp Immunol 2009;158(Suppl 1):23–33.
2. Schwartz-Albiez R, Monteiro RC, Rodriguez M, *et al*. Natural antibodies, intravenous immunoglobulin and their role in autoimmunity, cancer and inflammation. Clin Exp Immunol 2009;158(Suppl 1):43–50.
3. Gelfand EW. Intravenous immune globulin in autoimmune and inflammatory diseases. N Engl J Med 2012;367:2015–2025.
4. Lünemann JD, Nimmerjahn F, Dalakas MC. Intravenous immunoglobulin in neurology-mode of action and clinical efficacy. Nat Rev Neurol 2015;11:80–89.
5. Dalakas MC. Advances in the diagnosis, pathogenesis and treatment of CIDP. Nat Rev Neurol 2011;7:507–517.
6. Nimmerjahn F, Lünemann JD. Expression and function of the inhibitory Fcγ-receptor in CIDP. J Peripher Nerv Syst 2011;16(Suppl 1):41–44.
7. Eftimov F, Winer JB, Vermeulen M, *et al*. Intravenous immunoglobulin for chronic inflammatory demyelinating polyradiculoneuropathy. Cochrane Database Syst Rev 2013;12:CD001797.
8. Lehmann HC, Hughes RA, Hartung HP. Treatment of chronic inflammatory demyelinating polyradiculoneuropathy. Handb Clin Neurol 2013;115:415–427.
9. Yuki N, Hartung HP. Guillain-Barré syndrome. N Engl J Med 2012;366:2294–2304.
10. Gilhus NE, Owe JF, Hoff JM, *et al*. Myasthenia gravis: a review of available treatment approaches. Autoimmune Dis 2011;2011:847393.
11. Hughes RA, Swan AV, van Doorn PA. Intravenous immunoglobulin for Guillain-Barré syndrome. Cochrane Database Syst Rev 2014;9:CD002063.
12. Stangel M, Gold R. Intravenous immunoglobulins in MS. Int MS J 2005;12:4.
13. Hohlfeld R. Intravenous immunoglobulins in MS: a panacea lacking approval? Int MS J 2005;12:1–2.
14. Fazekas F, Lublin FD, Li D, *et al*. Intravenous immunoglobulin in relapsing-remitting multiple sclerosis: a dose-finding trial. Neurology 2008;71:265–271.
15. Cohen JA. How effective is intravenous immunoglobulin for the treatment of relapsing-remitting multiple sclerosis? Nat Clin Pract Neurol 2008;4:588–589.
16. Buttmann M, Kaveri S, Hartung HP. Polyclonal immunoglobulin G for autoimmune demyelinating nervous system disorders. Trends Pharmacol Sci 2013;34:445–457.
17. Elsone L, Panicker J, Mutch K, *et al*. Role of intravenous immunoglobulin in the treatment of acute relapses of neuromyelitis optica: experience in 10 patients. Mult Scler 2014;20:501–504.
18. Nimmerjahn F, Ravetch JV. The antiinflammatory activity of IgG: the intravenous IgG paradox. J Exp Med 2007;204:11–15.

19. Hartung HP. Advances in the understanding of the mechanism of action of IVIg. J Neurol 2008;255(Suppl 3):3–6.
20. Ballow M. The IgG molecule as a biological immune response modifier: mechanisms of action of intravenous immune serum globulin in autoimmune and inflammatory disorders. J Allergy Clin Immunol 2011;127:315–323; quiz 324-5.
21. Schwab I, Nimmerjahn F. Intravenous immunoglobulin therapy: how does IgG modulate the immune system? Nat Rev Immunol 2013;13:176–189.
22. Aktas O, Waiczies S, Grieger U, *et al*. Polyspecific immunoglobulins (IVIg) suppress proliferation of human (auto)antigen-specific T cells without inducing apoptosis. J Neuroimmunol 2001;114:160–167.
23. Janke AD, Giuliani F, Yong VW. IVIg attenuates T cell-mediated killing of human neurons. J Neuroimmunol 2006;177:181–188.
24. Ephrem A, Chamat S, Miquel C, *et al*. Expansion of CD4 + CD25 + regulatory T cells by intravenous immunoglobulin: a critical factor in controlling experimental autoimmune encephalomyelitis. Blood 2008;111:715–722.
25. Maddur MS, Janakiraman V, Hegde P, *et al*. Inhibition of differentiation, amplification, and function of human T(H) 17 cells by intravenous immunoglobulin. J Allergy Clin Immunol 2011;127:823–30.
26. Mausberg AK, Dorok M, Stettner M, *et al*. Recovery of the T-cell repertoire in CIDP by IV immunoglobulins. Neurology 2013;80:296–303.
27. Othy S, Hegde P, Topçu S, *et al*. Intravenous gammaglobulin inhibits encephalitogenic potential of pathogenic T cells and interferes with their trafficking to the central nervous system, implicating sphingosine-1 phosphate receptor 1-mammalian target of rapamycin axis. J Immunol 2013;190:4535–4541.
28. Tackenberg B, Jelcic I, Baerenwaldt A, *et al*. Impaired inhibitory Fcgamma receptor IIB expression on B cells in chronic inflammatory demyelinating polyneuropathy. Proc Natl Acad Sci USA 2009;106:4788–4792.
29. Kessel A, Peri R, Haj T, *et al*. IVIg attenuates TLR-9 activation in B cells from SLE patients. J Clin Immunol 2011;31:30–8.
30. Jacobi C, Claus M, Wildemann B, *et al*. Exposure of NK cells to intravenous immunoglobulin induces IFN gamma release and degranulation but inhibits their cytotoxic activity. Clin Immunol 2009;133:393–401.
31. Crow AR, Brinc D, Lazarus AH. New insight into the mechanism of action of IVIg: the role of dendritic cells. J Thromb Haemost 2009;7(Suppl 1):245–248.
32. Pincetic A, Bournazos S, DiLillo DJ, *et al.* Type I and type II Fc receptors regulate innate and adaptive immunity. Nat Immunol 2014;15:707–716.
33. Harrer MD, von Büdingen HC, Stoppini L, *et al*. Live imaging of remyelination after antibody-mediated demyelination in an *ex-vivo* model for immune mediated CNS damage. Exp Neurol 2009;216:431–438.
34. Sobottka B, Harrer MD, Ziegler U, *et al*. Collateral bystander damage by myelin-directed CD8 + T cells causes axonal loss. Am J Pathol 2009;175:1160–1166.
35. Sobottka B, Ziegler U, Kaech A, *et al*. CNS live imaging reveals a new mechanism of myelination: the liquid croissant model. Glia 2011;59:1841–1849.
36. Spassky N, Goujet-Zalc C, Parmantier E, *et al*. Multiple restricted origin of oligodendrocytes. J Neurosci 1998;18:8331–8343.
37. Le Bras B, Chatzopoulou E, Heydon K, *et al*. Oligodendrocyte development in the embryonic brain: the contribution of the plp lineage. Int J Dev Biol 2005;49:209–220.
38. Stoppini L, Buchs PA, Muller D. A simple method for organotypic cultures of nervous tissue. J Neurosci Methods 1991;37:173–182.
39. Kuenzle S, von Büdingen HC, Meier M, *et al*. Pathogen specificity and autoimmunity are distinct features of antigen-driven immune responses in neuroborreliosis. Infect Immun 2007;75:3842–3847.
40. von Büdingen HC, Harrer MD, Kuenzle S, *et al*. Clonally expanded plasma cells in the cerebrospinal fluid of MS patients produce myelin-specific antibodies. Eur J Immunol 2008;38:2014–2023.
41. Lubetzki C, Stankoff B. Demyelination in multiple sclerosis. Handb Clin Neurol 2014;122:89–99.
42. Silverman HA, Dancho M, Regnier-Golanov A, *et al*. Brain region-specific alterations in the gene expression of cytokines, immune cell markers and cholinergic system components during peripheral endotoxin-induced inflammation. Mol Med 2014;20:601–611.
43. Pul R, Kopadze T, Skripuletz T, *et al*. Polyclonal immunoglobulins (IVIg) induce expression of MMP-9 in microglia. J Neuroimmunol 2009;217:46–50.
44. Stangel M, Joly E, Scolding NJ, Compston DA. Normal polyclonal immunoglobulins ('IVIg') inhibit microglial phagocytosis in vitro. J Neuroimmunol 2000;106:137–144.
45. Stangel M, Compston A. Polyclonal immunoglobulins (IVIg) modulate nitric oxide production and microglial functions in vitro via Fc receptors. J Neuroimmunol 2001;112:63–71.
46. Pul R, Nguyen D, Schmitz U, *et al*. Comparison of intravenous immunoglobulin preparations on microglial function in vitro: more potent immunomodulatory capacity of an IgM/IgA-enriched preparation. Clin Neuropharmacol 2002;25:254–259.
47. Stangel M, Compston A, Scolding NJ. Oligodendroglia are protected from antibody-mediated complement injury by normal immunoglobulins ("IVIg"). J Neuroimmunol 2000;103:195–201.
48. Urich E, Gutcher I, Prinz M, Becher B. Autoantibody-mediated demyelination depends on complement

activation but not activatory Fc-receptors. Proc Natl Acad Sci USA 2006;103:18697–18702.
49. Frank MM, Miletic VD, Jiang H. Immunoglobulin in the control of complement action. Immunol Res 2000;22:137–146.
50. Lutz HU, Stammler P, Jelezarova E, *et al*. High doses of immunoglobulin G attenuate immune aggregate-mediated complement activation by enhancing physiologic cleavage of C3b in C3bn-IgG complexes. Blood 1996;88:184–193.
51. Lutz HU, Stammler P, Bianchi V, *et al*. Intravenously applied IgG stimulates complement attenuation in a complement-dependent autoimmune disease at the amplifying C3 convertase level. Blood 2004;103:465–472.
52. Basta M, Van Goor F, Luccioli S, *et al*. F(ab)'2-mediated neutralization of C3a and C5a anaphylatoxins: a novel effector function of immunoglobulins. Nat Med 2003;9:431–438.
53. Lutz HU, Späth PJ. Anti-inflammatory effect of intravenous immunoglobulin mediated through modulation of complement activation. Clin Rev Allergy Immunol 2005;29:207–212.
54. Yuki N, Watanabe H, Nakajima T, Späth PJ. IVIG blocks complement deposition mediated by anti-GM1 antibodies in multifocal motor neuropathy. J Neurol Neurosurg Psychiatry 2011;82:87–91.
55. Kaneko Y, Nimmerjahn F, Ravetch JV. Anti-inflammatory activity of immunoglobulin G resulting from Fc sialylation. Science 2006;313:670–673.
56. Anthony RM, Nimmerjahn F, Ashline DJ, *et al*. Recapitulation of IVIG anti-inflammatory activity with a recombinant IgG Fc. Science 2008;320:373–376.
57. Anthony RM, Wermeling F, Karlsson MC, Ravetch JV. Identification of a receptor required for the anti-inflammatory activity of IVIG. Proc Natl Acad Sci USA 2008;105:19571–19578.
58. Park JY, Choi HJ, Prabagar MG, *et al*. The C-type lectin CD209b is expressed on microglia and it mediates the uptake of capsular polysaccharides of Streptococcus pneumoniae. Neurosci Lett 2009;450:246–251.
59. Huang W, Giddens J, Fan SQ, *et al*. Chemoenzymatic glycoengineering of intact IgG antibodies for gain of functions. J Am Chem Soc 2012;134:12308–12318.
60. Campbell IK, Miescher S, Branch DR, *et al*. Therapeutic effect of IVIG on inflammatory arthritis in mice is dependent on the Fc portion and independent of sialylation or basophils. J Immunol 2014;192:5031–5038.
61. van Engelen BG, Renier WO, Weemaes CM, *et al*. Cerebrospinal fluid examinations in cryptogenic West and Lennox-Gastaut syndrome before and after intravenous immunoglobulin administration. Epilepsy Res 1994;18:139–147.
62. Wurster U, Haas J. Passage of intravenous immunoglobulin and interaction with the CNS. J Neurol Neurosurg Psychiatry 1994;57:21–25.
63. Pepinsky RB, Shao Z, Ji B, *et al*. Exposure levels of anti-LINGO-1 Li81 antibody in the central nervous system and dose-efficacy relationships in rat spinal cord remyelination models after systemic administration. J Pharmacol Exp Ther 2011;339:519–529.
64. St-Amour I, Paré I, Alata W, *et al*. Brain bioavailability of human intravenous immunoglobulin and its transport through the murine blood-brain barrier. J Cereb Blood Flow Metab 2013;33:1983–1992.
65. Hawkins CP, Munro PM, MacKenzie F, *et al*. Duration and selectivity of blood-brain barrier breakdown in chronic relapsing experimental allergic encephalomyelitis studied by gadolinium-DTPA and protein markers. Brain 1990;113(Pt 2):365–378.
66. Watzlawik JO, Wootla B, Painter MM, *et al*. Cellular targets and mechanistic strategies of remyelination-promoting IgMs as part of the naturally occurring autoantibody repertoire. Expert Rev Neurother 2013;13:1017–1029.

Supporting Information

Additional Supporting Information may be found online in the supporting information tab for this article:

Figure S1. Human serum albumin does not protect organotypic cerebellar slice cultures (OSC) from immune-mediated demyelination. OSC were demyelinated with 5 μg/mL anti-MOG antibody and 4% complement with or without 6 mg/mL IVIG (6 mg/mL) or HSA (12 mg/mL) or were left untreated. GFP expression in living OSC was assessed by fluorescence microscopy at days 1-3 and quantified relative to day 0 with Image J Software (n = 4 OSC per group). Treatment with the irrelevant protein (HSA, 12 mg/mL) does not inhibit demyelination. Significances were calculated in respect to the demyelinated control using one-way analysis of variance and Dunnett's post hoc test. $^*P \leq 0.05$. Values are depicted as mean ± SEM.

Figure S2. IVIG ± complement does not initiate demyelination in organotypic cerebellar slice culture (OSC). OSC were treated as indicated. For demyelination the slices were incubated with 5 μg/mL anti-MOG antibody and 6% complement. GFP expression in living OSC was assessed by fluorescence microscopy at days 1-3 and quantified relative to day 0 with Image J Software (n = 6-8 OSC per group). Neither IVIG alone nor IVIG with complement lead to demyelination in OSC. Significances were calculated in respect to the untreated control using one-way analysis of variance and Dunnett's post hoc test. $^*P \leq 0.05$. Values are depicted as mean ± SEM.

Figure S1. Human serum albumin does not protect organotypic cerebellar slice cultures (OSC) from immune-mediated demyelination. OSC were demyelinated with 5 *μ*g/mL anti-MOG antibody and 4% complement with or without 6 mg/mL IVIG (6 mg/mL) or HSA (12 mg/mL) or were left untreated. GFP expression in living OSC was assessed by fluorescence microscopy at days 1-3 and quantified relative to day 0 with Image J Software (*n* = 4 OSC per group). Treatment with the irrelevant protein (HSA, 12 mg/mL) does not inhibit demyelination. Significances were calculated in respect to the demyelinated control using one-way analysis of variance and Dunnett's post hoc test. *$P \leq 0.05$. Values are depicted as mean ± SEM.

Figure S2. IVIG ± complement does not initiate demyelination in organotypic cerebellar slice culture (OSC). OSC were treated as indicated. For demyelination the slices were incubated with 5 *μ*g/mL anti-MOG antibody and 6% complement. GFP expression in living OSC was assessed by fluorescence microscopy at days 1-3 and quantified relative to day 0 with Image J Software (*n* = 6-8 OSC per group). Neither IVIG alone nor IVIG with complement lead to demyelination in OSC. Significances were calculated in respect to the untreated control using one-way analysis of variance and Dunnett's post hoc test. *$P \leq 0.05$. Values are depicted as mean ± SEM.

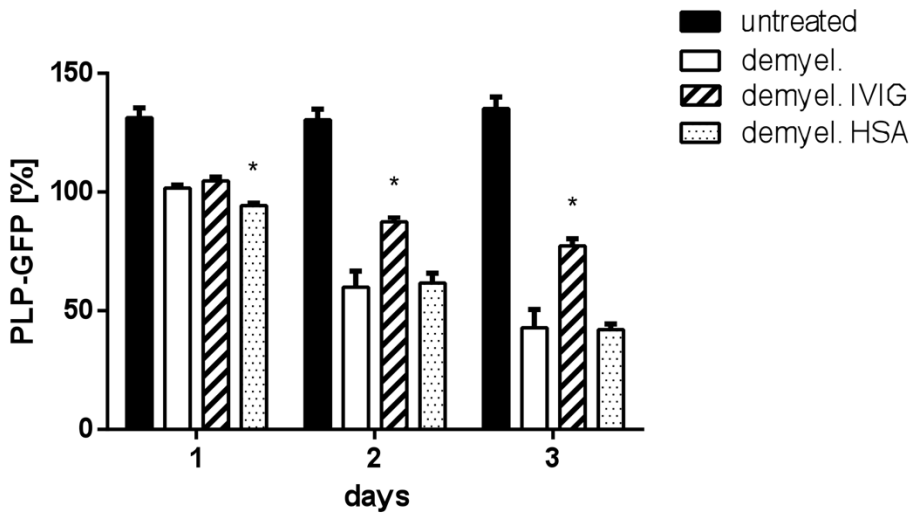

Winter et al., Supplementary Figure 1: ***HSA does not protect OSC from immune-mediated demyelination***.

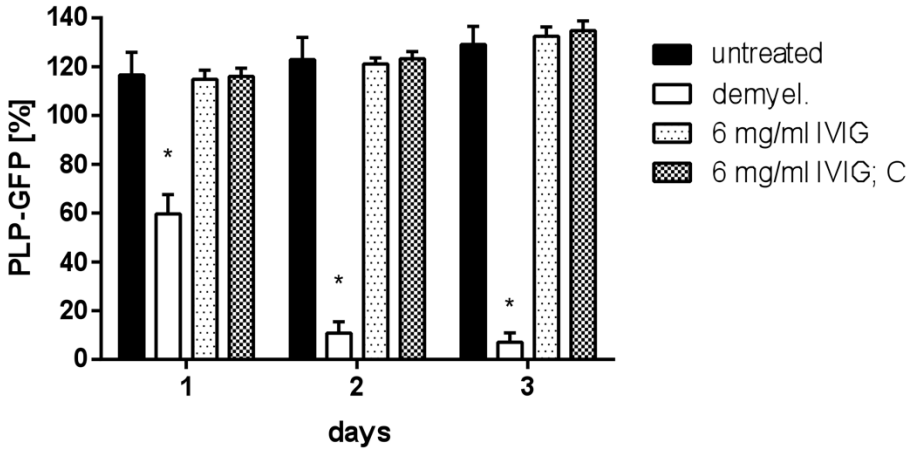

Winter et al., Supplementary Figure 2: ***IVIG +/- complement do not initiate demyelination in OSC.***

Author "Sumanta Barman" produced recombinant humanized MOG-specific monoclonal antibody for inducing demyelination in living organotypic cerebellar slice cultures (OSC).

7 Curriculum Vitae

For reasons of data protection, the curriculum vitae is not published in the online version.

8 Financial support

This work was funded by grants provided to Professor Norbert Goebels by the Forschungskommission of the Medical Faculty of the Heinrich-Heine-University Düsseldorf (HHU), the German Ministry for Education and Research (BMBF), Novartis and Sanofi-Genzyme. The Forschungskommission of the Medical Faculty of the Heinrich-Heine-University Düsseldorf (HHU) and Sanofi-Genzyme, to which I would like to express my special gratitude, funded my position.

9 Acknowledgements

First of all, my heartfelt gratitude to Professor Dr. Norbert Goebels, my supervisor, for his constant encouragement and guidance to complete my PhD thesis in the field of neuroimmunology. I appreciated the freedom of action and independency during my PhD thesis. I would like to express my deepest gratitude to my co-supervisors Professor Dr. Philipp Lang for supporting my work with helpful discussions. I would like to thank Dr. Manish Malviya and Jason Cline for helping with single cell PCR and antibody purification experiments. I also would like to thank Armin Scheffler, Pia Sporkmann and Anna Coordt for helping next generation sequencing experiments. My thanks would go to Dr. Vera Balz, Nora Hinssen, Katharina Raba and Lena Schünemann for excellent technical assistance. I also thank all our collaborators, especially Dr. Tobias Ruck, Dr. Nico Melzer and Professor Dr. Josep Dalmau. I owe my sincere thankfulness to all of my colleagues at my lab for their help, exciting discussions and relaxing chats. Not but least my thanks would go to my beloved family for their loving consideration, inspiration and great confidence in me all through these years.

10 Declaration

"I declare under oath that I have produced my thesis independently and without any undue assistance by third parties under consideration of the 'Principles for the Safeguarding of Good Scientific Practice at Heinrich Heine University Düsseldorf"

Sumanta Barman